T.C.
DOKUZ EYLUL UNIVERSITY
IZMIR INTERNATIONAL BIOMEDICINE AND GENOME INSTITUTE

DETERMINATION AND VERIFICATION OF NEW TARGETS IN LIVER CANCER

UMUT EKİN

DEPARTMENT OF MOLECULAR BIOLOGY AND GENETICS

DOCTOR OF PHILOSOPHY THESIS

İZMİR-2022

THESIS CODE:DEU.HSI.PhD-2016850046

T.C.
DOKUZ EYLUL UNIVERSITY
IZMIR INTERNATIONAL BIOMEDICINE AND GENOME INSTITUTE

DETERMINATION AND VERIFICATION OF NEW TARGETS IN LIVER CANCER

DEPARTMENT OF MOLECULAR BIOLOGY AND GENETICS

DOCTOR OF PHILOSOPHY THESIS

UMUT EKİN

Advisor: Asst. Prof. Yavuz Oktay
Co-Advisor: Prof. Dr. Mehmet Öztürk

(Part of this thesis was supported by Türkiye Bilimsel ve Teknolojik Araştırma Kurumu, Araştırma Destek Programları with the Project code 113S389)

THESIS CODE: DEU.HSI.PhD-2016850046

Dokuz Eylül University Izmir International Biomedicine and Genome Institute Department of Genomics and Molecular Biotechnology, Molecular Biology and Genetics graduate program Doctor of Philosophy student Umut Ekin has successfully completed his Doctor of Philosophy thesis titled "**DETERMINATION AND VERIFICATION OF NEW TARGETS IN LIVER CANCER**" on the date of

19/01/2022

Asst. Prof. Dr. Yavuz OKTAY
Dokuz Eylül University
CHAIR

Assoc. Prof. Dr. Özden Yalçın ÖZUYSAL
Izmir Institute of Technology
MEMBER

Asst. Prof. Hani ALOTAİBİ
Dokuz Eylül University
MEMBER

Prof. Dr. Petek BALLAR KIRMIZIBAYRAK
Ege University
MEMBER

Assoc. Prof. Gökhan KARAKÜLAH
Dokuz Eylül University
MEMBER

Prof. Dr. Safiye Neşe ATABEY
Tınaztepe University
SUBSTITUTE MEMBER

Assoc. Prof. Dr. Şerif ŞENTÜRK
Dokuz Eylül University
SUBSTITUTE MEMBER

Dokuz Eylül Üniversitesi İzmir Uluslararası Biyotıp ve Genom Enstitüsü Genom Bilimleri ve Moleküler Biyoteknoloji Anabilim Dalı,
Moleküler Biyoloji ve Genetik Doktora programı öğrencisi Umut Ekin, **'KARACİĞER KANSERİNDE YENİ HEDEFLERİN BELİRLENMESİ VE DOĞRULANMASI'** konulu Doktora tezini 19.01.2022 tarihinde başarılı olarak tamamlamıştır.

Dr. Öğr. Üyesi Yavuz OKTAY
Dokuz Eylül Üniversitesi
BAŞKAN

Doç. Dr. Özden YALÇIN ÖZUYSAL
İzmir Yüksek Teknoloji Enstitüsü
ÜYE

Dr. Öğr. Üyesi Hani ALOTAİBİ
Dokuz Eylül Üniversitesi
ÜYE

Prof. Dr. Petek BALLAR KIRMIZIBAYRAK
Ege Üniversitesi
ÜYE

Doç.Dr. Gökhan KARAKÜLAH
Dokuz Eylül Üniversitesi
ÜYE

Prof. Dr. Safiye Neşe ATABEY
Tınaztepe Üniversitesi
YEDEK ÜYE

Doç.Dr.Şerif ŞENTÜRK
Dokuz Eylül Üniversitesi
YEDEK ÜYE

TABLE OF CONTENTS

LIST OF TABLES

LIST OF FIGURES

ABBREVIATIONS

Dox	Doxycycline
DS	Dataset
ECD	Extracellular domain
ECM	Extracellular matrix
EDTA	Ethylene Diamine Tetra Acetic Acid
ERAD	Endoplasmic-reticulum-associated protein degradation
FC	Fold Change
FDR	False discovery rate
FNH	Focal nodular hyperplasia
g	Gram
GAIN	G-protein-coupled receptor autoproteolysis-inducing
GPS	GPCR proteolysis site
GPR133	G-protein coupled receptor 133
GSEA	Gene Set Enrichment Analysis
HBV	hepatitis B virus
HCA	hepatocellular adenoma
HCV	hepatitis C virus
HDV	hepatitis D virus
HSC	hepatic stellate cells
IMM	İmmortal
kDa	kilodalton
LB	Luria Bertani
mA	miliamper
MetS	Metabolic syndrome
ml	milliliter
mM	milimolar
NAFLD	Non-alcoholic fatty liver disease
NASH	Non-alcoholic steatohepatitis
ng	nanogram
NGS	Next-Generation Sequencing
NTF	N-terminal fragment

PS	Pre-senescence
RIN	RNA integrity number
RMA	Robust Multichip Average
RNA	Ribonucleic acid
ROS	Reactive oxygen species
RPM	Revolutions per minute
SAHF	Senescence-associated heterochromatic foci
SAM	sterile α-motif
SASP	senescence-associated secretory phenotype
SiRNA	Small interfering RNA
SNP	Single nucleotide polymorphism
TAD	transactivation domain
TCA	Trichloroacetic Acid
TCGA	The Cancer Genome Atlas
TSVdb	TCGA Splice Variant database
ul	microliter
UPR	unfolded protein response
WHO	World Health Organization
TPM	Transcript per million
cDNA	complementary DNA
qPCR	quantitative polymerase chain reaction
BCA	Bicinchoninic Acid
BSA	Bovine serum albumin
RIPA	Radioimmunoprecipitation assay
SDS-	Sodium Dodecyl Sulfate
PAGE	Polyacrylamide Gel Electrophoresis
TEMED	Tetramethylethylenediamine
PVDF	Poly(vinylidene fluoride)
TBS	Tris-buffered saline
HRP	Horseradish peroxidase

ACKNOWLEDGEMENTS

First and foremost, I am grateful to my supervisor, Prof. Mehmet Öztürk for his continuous support, patience, and invaluable advice during my Ph.D. studies. His immense knowledge, plentiful experience, and wide personal network have encouraged me during my academic research.

I would like to thank all Öztürk Lab. members that our paths crossed during this long journey: Umur Keleş, Evin İşcan, Tuğçe Batur, Aybike Erdoğan, Çiğdem Özen, Erhan Bal, Sıla Kahyaoğlu, Özden Öz, Zeynep Mutlu, Seval Kılıç, Huriye Erbak Yılmaz, Özgün Teksoy and Zehra Zeynep Kaplan. They were always generous in sharing and helping. We've always been more than just friends.

I would like to thank Yavuz Oktay, Hani Alotaibi, Gökhan Karakülah, Petek Ballar, and Özden Yalçın for their guidance and suggestions throughout the study.

I would like to thank all research laboratories in İBG especially Atabey lab and Erdal lab. which were always generous to us. Besides the knowledge and lab material we shared, also formed wonderful friendships and experienced memories.

I would like to thank again Peyda Korhan and Evin İşcan for their support and encouragement during thesis progress.

I would like to thank all core facilities in İBG; Melek Üçüncü and Didem Çimtay from imaging core, and Ahmet Bursalı from bioinformatics core. They were always willing to help me.

Last but not least, I would like to thank my family for their hearted support and patience in this long, tough achievement.

DETERMINATION AND VERIFICATION OF NEW TARGETS IN LIVER CANCER

Umut Ekin, Dokuz Eylül University Izmir International Biomedicine and Genome Institute
umut.ekin@ibg.edu.tr

ABSTRACT

Hepatocellular carcinoma (HCC) is one of the most common cancers around the world, with poor prognosis and high mortality rates. The diagnosis and effective treatment of HCC at early stages is challenging with few treatment options including surgical resection or liver transplantation. At late stages, restricted options of chemotherapy become one of the most important treatment modalities for advanced hepatocellular carcinoma, although patient survival can be enhanced by just several months. Thus, understanding the mechanisms in progression will shed light on novel therapeutic approaches that are urgently needed to increase patient survival in HCC. In our studies, we aimed to determine and identify new targets in liver cancer and evaluate them as potential therapeutic targets.

Firstly, we evaluated ATAD2 (ATPase Family AAA Domain Containing 2) which was found one of the hepatocellular immortality signature gene increases in senescence escape, as a therapeutic target in HCC. The bioinformatics analysis from clinical data demonstrated the elevation of ATAD2 in HCC patients' tumors compared to non-tumors and in correlation with well-known proliferation marker Ki-67. This significant correlation was not only in HCC patient samples but also observed in the time course of rat liver regeneration. Additionally, ATAD2 was dysregulated in response to drug treatments, especially inhibition with Tunicamycin-induced apoptosis. Our in vitro findings with ATAD2 knockdown demonstrated that gene expression responses to ATAD2 inactivation in different HCC cell lines were highly heterogeneous.

Secondly, the information previously gained from pre-senescent and immortal phenotypes of the HCC cell clones was used to find new therapeutic candidate genes. The integration of patient survival data with previously collected data of the genes overexpressed in immortal phenotype of the HCC cell clones revealed some candidate genes, and GPR133 (G-protein coupled receptor 133) was selected for further functional analysis. In line with poor prognosis, we showed the elevation of GPR133 in HCC cell lines and patient samples at the transcriptional level. Our preliminary functional studies with ectopic expression of GPR133 in HepG2 cell line showed decreased spheroid formation with altered morphology.

Lastly, we focused on transcription factor p73, which is the member of the tumor suppressor p53 family. The complex structure of the p73 gene generates different isoforms with its alternative promoters and C-terminal splicing variants. These alternative isoforms were not fully elucidated in terms of their expression and specific targets in HCC. At this part of our studies, we determined the differential expression of varying isoforms at transcriptional and protein levels in different HCC cell lines. Our findings showed that overexpression of TAp73beta caused cell cycle arrest and inhibition of colony formation abilities in a cell line-dependent manner. Our findings by bioinformatics analysis with the ectopic expression of TAp73beta in Hep3B cells revealed that TAp73beta expression is in association with cell cycle, development, growth signaling, metabolism, immune response, and stress response pathways.

In conclusion, we tried to find new candidate genes that may be targeted for HCC treatment. With additional studies, the exact mechanisms of candidate genes in HCC progression can be identified and their potentials can be revealed for therapeutic applications.

Key Words: Hepatocellular Carcinoma, p73, ATAD2, GPR133, Gene expression profiles

KARACİĞER KANSERİNDE YENİ HEDEFLERİN BELİRLENMESİ VE DOĞRULANMASI

Umut Ekin, Dokuz Eylül Üniversitesi İzmir Uluslararası Biyotıp ve Genom Enstitüsü
umut.ekin@ibg.edu.tr

ÖZET

Hepatosellüler karsinom (HSK), kötü prognoz ve yüksek ölüm oranları ile dünya çapında en yaygın kanserlerden biridir. HSK'nın erken evrelerde teşhisi ve etkili tedavisi zor olup cerrahi rezeksiyon veya karaciğer transplantasyonu dahil olmak üzere birkaç tedavi seçeneği ile sınırlıdır. İleri seviyelerde, sınırlı kemoterapi seçenekleri, hastanın sağkalımını sadece birkaç ay artırabilmesine rağmen, ilerlemiş hepatoselüler karsinom için en önemli tedavi yöntemlerinden biri haline gelmektedir. Bu nedenle, hastalığın ilerlemesindeki mekanizmaları anlamak, HSK'da hasta sağ kalımını artırmak için acilen ihtiyaç duyulan yeni terapötik yaklaşımlara ışık tutacaktır. Çalışmalarımızda karaciğer kanserinde yeni hedefleri belirleyerek potansiyel terapötik hedefler olarak değerlendirmeyi amaçladık..

İlk olarak senesensten kaçışta artış gösteren hepatoselüler imza genlerinden ATAD2 geni terapötik bir hedef olarak değerlendirildi. Topladığımız klinik data ile yaptığımız biyoinformatik analiz, hastaların tümör dokularında, tümör olmayanlara göre daha çok ATAD2 ekspresyonu olduğunu ve aynı artış korelasyonunun iyi bilinen proliferasyon belirteci Ki-67 için de geçerli olduğunu gördük. Bu anlamlı korelasyon sadece HSK hasta örneklerinde olmayıp, zamana bağlı sıçan karaciğeri yenilenmesi sürecinde de olduğunu gözlemledik. Ek olarak, ATAD2, ilaç ile muameleye, özellikle Tunikamisin kaynaklı apoptoza yanıt olarak inhibisyon göstermiştir. Yaptığımız ATAD2 silinmesine bağlı in vitro çalışmalar, ATAD2'nin inactive edilmesinin HSK hücrelerinde hetorejen yanıtlara yol açtığını göstermiştir.

İkincisi, senesens öncesi ve ölümsüz fenotip gösteren HSK hücre klonlarından daha önce elde ettiğimiz bilgileri kullanarak yeni ilaç adayı genler aradık. Ölümsüz fenotipte artış gösteren genlerle hasta sağkalım datalarını entegre ederek aday genler ortaya koyduk ve bu genlerden GPR133/ADGRD1 genini sonraki fonksiyonel analizlerde kullanmak üzere belirledik. Kötü prognozla ilişkili olarak, HSK hücre hatlarında ve hasta numunelerinde transkripsiyonel seviyede GPR133 seviyesinin yükseldiğini gösterdik. HepG2 hücre hatlarında GPR133ün ektopik ifadesiyle yaptığımız öncül çalışmalar neticesinde hücrelerin küresel yapı oluşturarak büyümesinde azalma ve oluşan kürelerin morfolojisinde değişiklikler gösterilmiştir.

Son olarak, p53 ailesinin bir üyesi olan p73 transkripsiyon faktörüne odaklandık. Bu genin sahip olduğu karmaşık yapı nedeniyle alternatif promotör kullanımı ve alternatif C-ucu birleştirmesi birçok farklı izoform oluşturmasını sağlamaktadır. Bu alternatif izoformların HSK'daki ekspresyonları ve özgün hedefleri tam olarak aydınlatılmamıştır. Çalışmamızın bu bölümünde, HSK'nın farklı hücre hatlarında, alternatif izoformların değişken ekspresyonlarını transkript ve protein seviyesinde inceledik. Özellikle bazı HSK hücre hatlarında TAp73beta izoformuyla yaptığımız çalışmalar, hücre hattına bağlı olarak hücre döngüsünde durma ve koloni oluşturabilme yeteneklerinde azalma olduğunu göstermiştir. Biyoinformatik analizlerle TAp73beta'nın Hep3B hücrelerindeki ektopik ekspresyonundan elde ettiğimiz bulgular, TAp73beta ekspresyonunun hücre döngüsü, gelişim, büyüme sinyali, metabolizma, bağışıklık yanıtı ve stres yanıtı yolaklarıyla ilişki içinde olduğunu göstermiştir.

Sonuç olarak, HSK tedavi sürecinde kullanılabilecek yeni aday genler belirlemeye çalıştık. Yapılacak ek çalışmalarla, bu aday genlerin HSK gelişiminde aldıkları roller belirlenebilir ve tedavi uygulamalarındaki potansiyelleri ortaya çıkartılabilir.

Anahtar Kelimeler: Hepatoselüler Karsinom, p73, ATAD2, GPR133, Gen ekspresyon profilleri

1 INTRODUCTION AND AIM

Liver cancer is one of the leading causes of cancer-related death worldwide with an increasing incidence that is estimated to reach one million cases in several years. The most prevalent form of liver cancer is hepatocellular carcinoma (HCC) and represents approximately 90% of all liver cancer cases [1]. Unfortunately, HCC is usually detected late in its progression. The insufficient effective systemic chemotherapy results in poor patient survival; after two years is less than 50%, while survival after five years is barely 10% [2]. The progression of HCC occurs as a multistage with well-defined etiological factors, and the majority of HCC patients are diagnosed with pre-existing cirrhosis [3]. In the advancement of cirrhosis, chronic hepatocyte turnover is one of the major predisposing factors and leads to telomere shortening and senescence [4]. However, during liver malignancy, senescent cells may escape from this stationary state and gain immortal phenotype with inactivating growth control genes that sustain proliferation and reactivate telomerase reverse transcriptase [5].

The replicative senescence has previously been studied in our group, and phenotypically different clones of Huh7 have been distinguished under senescence and immortal features [6]. The comparison of these Huh7 clones which reflects senescence and immortal phenotypes and integration of patient samples of cirrhosis and HCC data resulted in the signature gene set composed of 15 genes that discriminate HCC from cirrhosis [7]. Furthermore, this gene set was extensively studied by our group, and expression of ATAD2, which is one of the signature genes increased in HCC, was shown in HCC cell lines while absent in normal hepatocytes. Furthermore, ATAD2 was gradually elevated from the early to late stages of HCC progression. ATAD2 knockdown caused apoptosis and reduced cell survival, as well as lowered tumor development in some HCC cell lines [8]. Based on these previous findings, we aimed to further evaluate the potential of ATAD2 as a therapeutic target as well as a biomarker for proliferation. With different methodologies, we intended to understand the cell-dependent mechanism of ATAD2 in HCC. In addition to this, we sought to find new drug targets in HCC by analyzing the upregulated genes in the immortal phenotype to the pre-senescent phenotype of Huh7 clones previously described above. In line with the main goal of the research, we sought targetable proteins with high potential by applying different criteria including significance in patient survival, localization in a cell, and expression in vital organs, to the gene sets we compared. In analysis, GPR133 (ADGRD1) came forward with restricted information and obscurity in the literature with high potential since GPCRs are targeted by about 35% of approved drugs [9].

Furthermore, Its poor prognosis was only studied in glioblastoma, and increased expression was linked to hypoxic conditions and CD133 positivity in the tumor [10,11]. Thus, we studied this gene as a potential drug target in HCC.

The p73 gene has been thoroughly studied for its significance in cancer because of its close relationship and homology with tumor suppressor gene p53 [12–14]. While p53 was found frequently mutated in many cancers, p73 mutations are rarely reported [15]. The p73 has complicated biology because of the varying transcription of isoforms and antagonized functions of translated proteins. Thus, TAp73 isoforms act as tumor suppressors, while DNp73 isoforms exhibit proto-oncogene characteristics, and unlike opposite functions of these N-terminal isoforms, the implications of C-terminal changes are not clear [16,17]. In this part of our study, we tried to determine the role of different p73 isoforms in HCC. We evaluated the importance of the TAp73 isoform which has a trans-activating domain, with different C-terminal variations. The isoform-specific regulatory functions were studied to understand the downstream pathways with HCC progression.

2 BACKGROUND INFORMATION & LITERATURE

2.1 Liver Malignancy

The liver is the largest solid internal organ that accounts for approximately 2.5% of average body weight. It consists of mainly 4 lobes: right, left, caudate, and quadrate. Roughly hexagonal-shaped liver lobules are the basic functional unit of the liver and the bulk of the lobules are formed by single-cell thick plates of hepatocytes. These cells constitute 60 % of the liver cells population that accounts for 80% of cell mass and play a pivotal role in the production and secretion of bile, and metabolism of lipids, carbohydrates, and proteins as well. Besides hepatocytes, endothelial cells, Kupffer cells that can be called liver resident macrophages, and liver fat-storing stellate cells take part in the liver organization. In general, the functions of the liver can be summarized as the storage and metabolism of vitamins and nutrients, the secretion of bile, metabolism of bilirubin, and metabolic detoxification of toxins as well as hormones and drugs [18].

Like a most normal functioning organ, the liver may also progress cancer. Liver cancers divide into two main categories as primary and secondary. Hepatocellular carcinoma (HCC) is the most common type of primary liver cancer. The rest of the primary liver cancers include cholangiocarcinoma, hepatoblastoma, angiosarcoma, fibrolamellar carcinoma, and other mesenchymal cancers of the liver. The secondary liver cancers originated from different metastatic tumors like breast, lung, pancreas, and colorectal cancers [19].

The most common type of liver cancer, HCC, predominantly occurs in patients with underlying chronic liver diseases and cirrhosis. Globally, most cases of primary hepatocellular carcinoma develop in the setting of cirrhotic livers. Thus, the primary causes of HCC are considered as chronic hepatitis B or C virus infections, alcoholic cirrhosis, and non-alcoholic steatohepatitis (NASH). Secondarily, heavy alcohol consumption, nonalcoholic fatty liver disease, aflatoxins intake, obesity, type 2 diabetes, and smoking count as other risk factors [20]. In addition, Focal nodular hyperplasia (FNH) and hepatocellular adenoma (HCA) that defined as the benign formation of proliferative hepatocytes, may undergo a malignant transformation in patients without existing liver diseases and cirrhosis [21].

Hepatocarcinogenesis, the malignancy that drives the nonmalignant liver cells into HCC, is a progressive and complex mechanism that includes the accumulation of epigenetic and genetic changes at the molecular and cellular levels. This progression of malignancy is characterized by alterations in cell physiology from early cancerous to overtly malignant lesions

at the histologic level as well. The development of HCC starts with chronic liver injury by different etiological factors that lead to the turnover of liver cells. This chronic necrosis/proliferation cycle leads to cirrhosis and the formation of abnormal liver nodules. Further progression converts these nodules to dysplastic nodules and HCC [22].

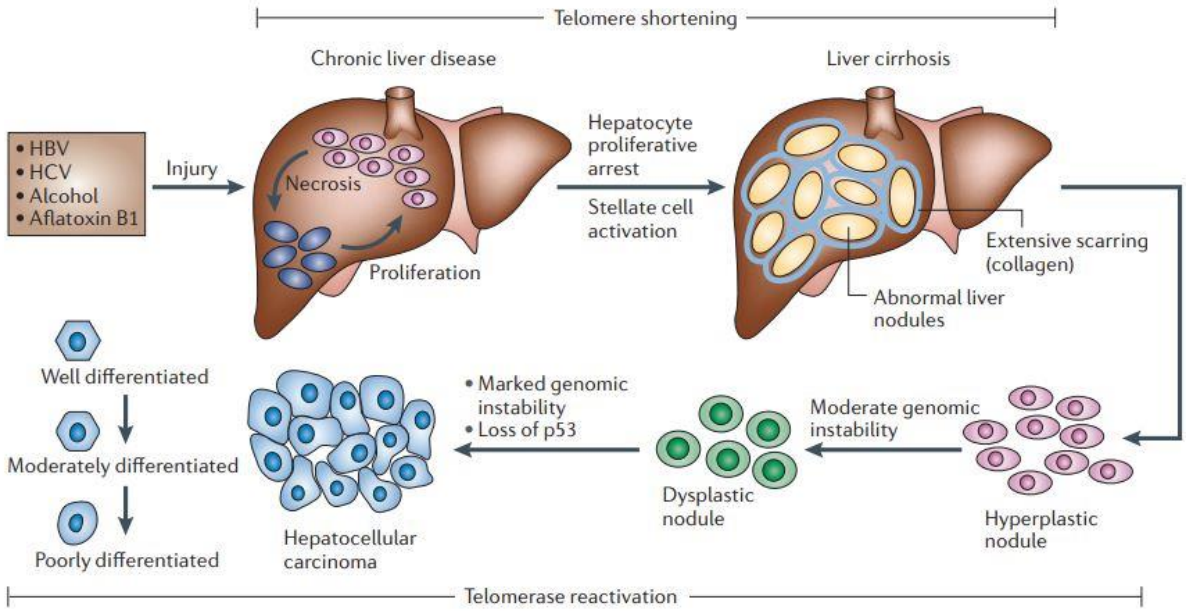

Figure 1**:** Multistep progression of Hepatocellular Carcinoma [22].

2.1.1 Epidemiology of Hepatocellular Carcinoma

Liver cancer is a serious public health problem with ascending new cases over 900.000. Worldwide, liver cancer ranks seventh in cancer incidences, and third in mortality rates after lung and colorectum cancers according to cases of World Health Organization (WHO) in 2021 (https://gco.iarc.fr/today/home). Among primary liver cancers, hepatocellular carcinoma accounts for the most common form with a coverage rate over 80% of all cases while cholangiocarcinoma is between 10–20% and angiosarcoma approximately 1% [23]. Although the incidence and mortality rates are highest in the regions of East Asia and Africa, increasing rates of cases are observed in different locations of the USA and Europe [24].

2.1.2 Etiological Factors in Hepatocellular Carcinoma Progression

The etiology of hepatocellular carcinoma is complex and multifactorial. The progression of HCC starts with a hepatic injury that causes inflammation and leads to necrosis of hepatocytes and regeneration. Then, in most cases, the condition switches to chronic liver

disease and gives rise to fibrosis, cirrhosis, and finally HCC sequentially. The catastrophic environment is formed under the influence of many risk factors described below.

2.1.2.1 The virus-associated mechanisms driving hepatocarcinogenesis

One of the major risk factors of HCC is the infection with hepatitis B virus (HBV) and hepatitis C virus (HCV). About 80 % of HCC occurs in the cirrhotic liver. Hence, approximately 30% of the patients with a chronic infection between 20 to 30 years develop cirrhosis. The risk of HCC may arise up to 15 and 17 fold in chronic HBV carriers and patients with HCV infections, respectively [25,26].

The main viral actor, HBV, is a member of the Hepadnavirus family with partially double-stranded circular DNA. The open reading frame of the virus encodes four proteins: the three viral envelope surface proteins (pre-S/S), core antigens (pre-C/C), viral polymerase (P), and X proteins. Basically, the virus enters the cell by endocytosis after receptor recognition. After nucleocapsids are transported to the nucleus where the circular DNA is converted to covalently closed circular DNA (cccDNA). This stable form acts as the template for further viral RNA transcription. The viral DNA can integrate itself into the host genome with 90% frequency and oxidative stress or DNA damage can also promote this integration [27,28]. Furthermore, elevated DNA damage and replication during chronic inflammation also increase the capability of the virus to integrate the host genome. In the genome, these integrations may result in genomic instabilities with translocations, chromosomal deletions, and DNA amplification. Additionally, many of these integration-related events occur closely around fragile or cancer-associated regions [29,30]. Besides integration to the genome, the presence of viral protein such as x protein (HBx) may associate with the cell cycle regulation, signaling pathways, and DNA repair by interacting directly or indirectly [28].

Unlike HBV, HCV is a member of the Flaviviridae family with a linear positive RNA genome. It is not capable to integrate itself into the host cell, but viral oncogenic actions mostly resulted from its viral proteins and their activated host responses. The oncogenic actions of core protein: interaction with tumor suppressor proteins like p53, p73, and pRB, upregulation of TGFbeta, or activation of RAF/MAPK, resulting in increased cell growth, proliferation, or decreased apoptosis [31]. Another RNA virus, Hepatitis D virus (HDV) which needs HBV surface antigens to replicate, is also associated with an increased risk of HCC [32].

2.1.2.2 Alcohol-associated mechanisms in hepatocarcinogenesis

Non-alcoholic fatty liver disease (NAFLD) and alcoholic liver disease (ALD) are multifactorial diseases that occur because of a combination of environmental (dietary) and genetic variables with fatty liver disease (steatosis) at the initial stage. In ALD, the excessive consumption of alcohol is considered as the major actor. On the contrary, obesity and metabolic syndrome are linked to NAFLD. In both cases, the progress of the disease may result in cirrhosis and further hepatocellular carcinoma [33].

Alcohol is classified as a carcinogen and daily chronic consumption of alcohol exceeding 80 grams for 10 years or higher raises the HCC risk by 5 fold [26]. The presence of excess alcohol can interfere with lipid metabolism and induce fat deposition in the liver altering the functions of metabolic enzymes. These malfunctions may result in the accumulation of triglycerides, phospholipids, and cholesterol esters through inhibition of mitochondrial β-oxidation and elevation of fatty acid synthesis [34]. The ALD spectrum starts from alcoholic steatosis to steatohepatitis, fibrosis, cirrhosis, and then hepatocellular carcinoma (HCC). In the earliest stage of ALD, steatosis may develop in 90% of heavy drinkers with elevated AST, ALT, and gamma-glutamyl transferase levels in the blood. The histology also shows different sized lipid droplets in the cytosol of hepatocytes [35].

NAFL is characterized as hepatic steatosis (fatty liver) with varying liver conditions that continue as injury and fibrosis. The progression of NAFL may evolve more serious form called nonalcoholic steatohepatitis (NASH) with inflammation and hepatocyte damage to fibrosis and cirrhosis [36]. Metabolic syndrome (MetS) which covers obesity, hyperglycemia, dyslipidemia, and systemic hypertension is considered as the main risk factor for NAFLD and NASH. The risk factors, arbiters in the pathogenicity of NAFLD and NASH, are mainly due to the accumulation of toxic lipid species that are generated with an overloaded liver capacity which cannot cope with the metabolism of energy substrates. These toxic metabolites cause hepatocellular stress and injury. At this point, cirrhosis and hepatocellular carcinoma may be progressed in the lead of fibrogenesis and genomic instability [37].

2.1.2.3 Aflatoxin-B1-associated mechanism in hepatocarcinogenesis

The toxic fungal metabolites, aflatoxins, are produced by the Aspergillus family of fungus and are recognized as a global food safety concern. The consumption of contaminated food with aflatoxins, especially aflatoxin B1 (AFB1) is the most common and toxic of the four types, is one of the risk factors for liver cancer [38]. The conversion of aflatoxins into its intermediates

with cytochrome p450 family enzymes brings in mutagenic and carcinogenic properties. The intermediate, aflatoxin-8,9-exo-epoxide has a high affinity to react with DNA and proteins, critically with tumor suppressor p53. This interaction causes transversion of guanine into thymidine at codon 249 [39,40]. This 249Ser mutation accounts for 90% of p53 mutations in AFB1-related HCC and generates mutant p53 protein unable to bind to responsive genes. The interaction of AflatoxinB1 and HBV favors hepatocarcinogenesis synergistically. The high consumption of AFB1 among HCC patients with HBV increases mortality 10 times [41,42].

2.1.3 Genetic and epigenetic factors in Hepatocellular Carcinoma

Hepatocellular carcinoma is a progressive disease with different steps characterized by the accumulation of various abnormalities at various phases of the progression events. Especially, initiation and progression of carcinogenesis are mostly associated with altered genetic and epigenetic mechanisms. These irreversible genetic defects accumulate in hepatocytes, causing altered gene expression and, eventually, malignant transformation as summarized in Figure 2 [43]. The aberrations in the chromosome, frequently induced by errors in mitosis or interruptions in DNA replication and repair result in loss or gains of chromosomal fragments.

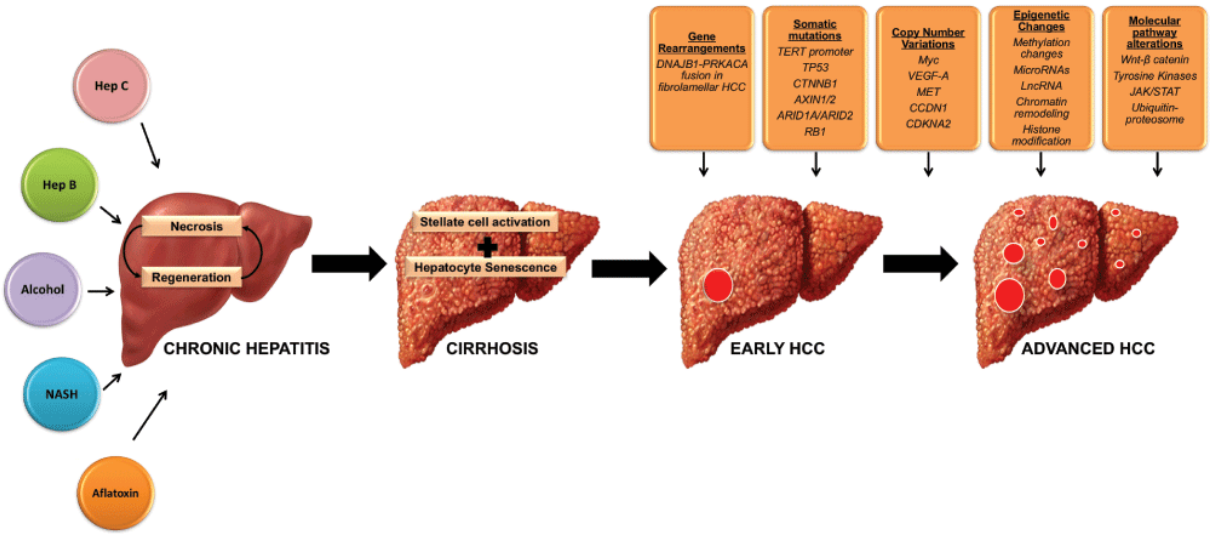

Figure 2: Hepatocellular Carcinoma Pathogenesis with progression factors.
The etiological factors initiate chronic hepatitis that leads to cirrhosis. The progressive accumulation of genetic and epigenetic events with altered molecular pathways leads to HCC [43].

The studies achieved with comparative arrays as genome hybridization, high-density single-nucleotide polymorphism or whole-genome analysis revealed that chromosomal regions show gains in chromosomes 1q, 5p, 6p, 7q, 8q, 17q, and 20q. The analysis also showed losses in 1p, 4q, 6q, 8p, 9p, 13q, 14q,16p-q, 17p, 21p-q, and 22q [44–50]. Among these regions, the most common chromosome abnormalities in HCC is chromosome 1q amplification, especially the region 1q21 was discovered to be amplified in more than half of HCC patients. Chromodomain Helicase DNA Binding Protein 1 Like (CHD1L), a well-known oncogene, is found in that location [51,52]. Furthermore, the association of gain in 1q21-23 was observed in the early development of HCC [53]. Another common amplification was seen in 8q, especially 8q24 that includes well-known oncogenes cMYC and PTK2 [54,55]. Besides gains, loss of chromosome segments was also frequently observed in HCC. More than 50% of HCC patients have deleted region of 1p35-36 that contains tumor suppressors like 14-3-3 σ and Rb-interacting zinc finger 1 (RIZ1) [56]. Additionally, 8p21-22 which includes deleted in liver cancer 1(DLC1) was found to be frequently deleted in HCC [57]. Cell adhesion molecule E-cadherin that takes the role in the inhibition of proliferation and metastasis locates in 16q22 which is also one of the frequently deleted regions [58].

Integration of HBV into the host genome that causes genetic damage and chromosomal instability is frequently seen in HBV-related HCC patients [59]. The deregulation of host gene expression and re-arranged integrations play critical roles in HCC development [60]. Studies carried out with PCR-based methods or deep sequencing suggested that the insertional sites are random and no preferential genome location for HBV stated but studies with recurrent HBV integration showed controversy that there may be preferential integration sites that alter telomerase reverse transcriptase gene (hTERT), mixed-lineage leukemia 4 (MLL4) and cyclin E-1 (CCNE1) [61,62].

After years of chronic liver disease, HCC may occur with the accumulation of mutations in the genome. These mutations act as drivers mostly at the cirrhotic stage and HCC develops with the accumulation of progressive mutations. These mutations may divide into constitutional mutations such as germline mutations and single nucleotide polymorphisms (SNP), or somatic mutations. The predisposition of germline mutations can be exampled as HFE mutation with iron-related Haemochromatosis, ATF7B mutation with copper overload as Wilson disease, SERPIN1 mutation with Alpha-1 antitrypsin deficiency, and FAH mutation with Tyrosinemia that roles in the development of cirrhosis/HCC [63,64]. Furthermore, the potential of SNPs as the risk of HCC arises with its participation in many genes associated with biological pathways. The genes that belong to inflammation as TNFA, IL1B, IL10, TGFB, and STAT4, or oxidative stress-related genes like GSTM1, SOD2, and MPO. Additionally, cell cycle and DNA repair genes: MDM2, TP53, MTHFR, and XRCC3 genes were also included [65,66]. However, few of them were validated such as Patatin-like phospholipase domain-containing 3 (PNPLA3) and Transmembrane 6 superfamily member 2 (TM6SF2) are the genes involved in lipid metabolism and composition of lipid droplets [63].

The mutational studies in HCC leaped forward with the light of technological improvements. Studies with next genome sequencing (NGS) shed light on the landscape of HCC genetics. Besides viral integrations or focal amplifications, promoter mutations in telomerase reverse transcriptase that result in abnormal activation are one of the most prevalent somatic alterations detected in HCC [67]. After TERT alterations, beta-catenin gene CTNNB1 and tumor protein TP53 are the second frequently mutated genes. With varying mutation rates, less frequently mutated genes can be listed as ARID1A, ARID2, AXIN1, RPS6KA, NFE2L2, KEAP1, RB1, VEGFA, and FGF19. Lastly there are rare mutations KRAS, MLL4 ,SF3B1 and many others with low frequency rates [44,50,68–74]. These mutations influence important

pathways that take a role in hepatocarcinogenesis, especially cell cycle control, epigenetic regulation, telomere maintenance, oxidative stress, Wnt/ß-catenin, AKT/mTOR, and MAP kinase pathways [66].

The comprehensive large-scale genome-wide studies not only increased the understanding of hepatocellular cancer genetics but also reshaped the view of the role of epigenetic alterations in HCC. These epigenetic alterations are mainly collected under the dysregulation of DNA methylation, non-coding RNAs, chromatin modifiers, and histone deacetylation, which affect cell proliferation, metastasis, progression, and development of HCC.

DNA methylation is characterized as the transfer of methyl groups to cytosine bases located at the promoter and regulatory regions of genes, mostly including cytosine-phosphate-guanine (CpG) rich regions or CpG islands [75]. In the early events of HCC progression, the specific promoter hypermethylation and global hypomethylation have a key role [76]. The study performed with single hepatocyte cells derived from hepatitis B positive HCC and its respective paired tissues and normal liver showed hypermethylation of EMILIN2, TRIM58, GRASP, WNK2, TM6SF1, TLX3, and HIST1H4F genes [77]. Another study that aims to find biomarker genes from plasma DNA in comparison of HCC patients tumor and non-tumor samples showed hypermethylation in CDKL2, CDKN2A, HIST1H3G, STEAP4, and ZNF154 genes in 63% of the patients, and hypomethylation in genes such as CCL20, AKT3, SCGB1D1, WFDC6, PAX4, GCET2, CD300E and CD1B [78].

Other epigenetic regulators that take part in HCC progression are the chromatin modifiers or remodelers. In HCC, there are some well-studied chromatin remodelers such as AT-Rich Interaction Domain 1A (ARID1A), AT-Rich Interaction Domain 1B (ARID1B), and AT-rich interactive domain 2 (ARID2). These genes take part in SWItch/Sucrose Non-Fermentable (SWI/SNF) chromatin remodeling complexes which ease promoter-transcriptional machinery access. These genes were observed as the third most often mutated ones in HCC [50]. Besides AT-Rich Interaction Domain genes, some components of SWI/SNF complex genes also mutated in HCC, especially alcohol-related cases, such as SMARCC2, SMARCC1, SMARCB1, SMARCA4, and SMARCA2 [69].

Histone modifications are another component of epigenetic regulation via altering chromatin structure. These structural changes occur with acetylation, methylation, phosphorylation, and ubiquitination reactions at histone proteins. The interaction between

histones and DNA regulates the expression profiles of genes that participated in the repair and replication of DNA or gene transcription [79]. Enhancer of zeste homolog 2 (EZH2), a methyltransferase is frequently upregulated in HCC, catalyzes histone H3-K27 triMe [80]. MLL1–5 enzymes that catalyze H3KYMe reactions are also inactivated in HCC [69]. Besides these, correlation of decrease in histone H2A ubiquitination [81] or overexpression of Histone deacetylase 3 (HDAC3) was also linked to HCC [82].

Non-coding RNAs and their correlation with cancer are one of the hot topics in the field. With the identification of new long non-coding RNAs or miRNAs, new epigenetic regulators were identified which correlates with HCC progression. These non-coding RNAs can regulate genes in a way of oncogenic or tumor suppressors. Oncogenic miRNA21 is one of the upregulated miRNAs in HCC that take a role in the regulation of tumor suppressor phosphatase and tensin homolog (PTEN) takes a role in cell proliferation, migration, and invasiveness. In addition, mitogen-activated protein kinase kinase 3 (MAP2K3) is another target that is repressed in HCC [83,84]. Other upregulated miRNAs can be exampled as miR-221 and miR-222 that accompanied in decreased expression of PTEN and TIMP3 [85]. Correlation between downregulation of miR-26 and expression of vascular endothelial growth factor A (VEGFA) shows the tumor suppressor property of miR-26 in HCC, especially in angiogenesis [86]. Well-known long coding RNA, HOTAIR, is found to be upregulated in HCC to mediate specific gene silencing by H3K27me3. Attenuation of HOTAIR showed accordance in reduced proliferation [87,88].

2.1.4 Liver Fibrosis and Cirrhosis

Liver fibrosis is caused by persistent liver injury along with the buildup of extracellular matrix (ECM) proteins, which is a common feature of most chronic liver disorders. Chronic HCV infection, alcohol addiction, and nonalcoholic steatohepatitis (fatty liver disease) are the leading causes of liver fibrosis. Thus, cirrhosis is a terminal stage of progressive hepatic fibrosis in chronic diffuse liver disease and is defined by the formation of nodules of regenerated hepatocytes after an accumulation of ECM proteins disrupts the hepatic architecture by establishing a fibrous scar. Cirrhosis causes hepatic insufficiency and portal hypertension due to hepatocellular dysfunction and increased intrahepatic resistance to blood flow [89].

Fibrosis is a key pathogenic step in the progression of all chronic liver disorders to cirrhosis [90]. Chronic inflammation is linked to long-term liver damage and regeneration, which can lead to fibrosis and cirrhosis, as well as the development of HCC. In liver

inflammation, necrosis and apoptosis of hepatocytes have an important role in the sequence of events that leads to the progression of hepatic fibrosis. The damage response released from hepatocytes awakens dormant hepatic stellate cells (HSC) and Kupffer cells, triggering inflammatory and fibrogenic responses in these activated cell types [91–93]. This complex stimulation leads to fibrosis orchestrated by a complex network of cytokine-induced signaling pathways: Transforming Growth Factor Beta (TGF-β), Platelet-Derived Growth Factor (PDGF), and the inflammasome (NLRP3)-Caspase1 pathway, as well as WNT/beta-catenin signaling, have all been linked to HSC activation and fibrosis development [94–96]. After activation, HSCs transdifferentiate to myofibroblasts that switch from dormant non-proliferative state characterized as star-like morphology with high amounts of lipid droplets in the cytoplasm to proliferative and contractile myofibroblast phenotype. They gradually lose their star-like shape and lipid droplets, while producing different ECM components including collagens, fibronectin, laminin, alpha Smooth Muscle Actin (α-SMA), and Tissue Inhibitor of Metalloproteinase 1 (TIMP1) [91,97,98]. In addition to this, signaling pathways that affect the epithelial to mesenchymal cell transition (EMT), such as Notch and Hedgehog, are involved in the transition between hepatic stellate cells and myofibroblasts. This transition can be reverted from myofibroblast to deactivated hepatic stellate cells by a mesenchymal to epithelial cell transition (MET) [99]. In normal injury with tissue repair, myofibroblasts may quickly be eliminated by apoptosis or inactivation but disorganization of equilibrium between synthesis and degradation of the ECM triggering progressive liver fibrosis [100,101]. Additionally, macrophages, especially the major population of hepatic macrophages: Kupffer cells play a central role in liver inflammation and fibrosis. The activated Kupffer cells, mostly in response to secreted Danger-Associated-Molecular-Pattern molecules (DAMPs) by damaged hepatocytes or cholangiocytes, quickly secrete pro-inflamatory signals including IL-1β, TNFα, chemokine (C-C motif) ligand 2 (CCL2), and CCL5 that activates HSCs and other immune cells [102]. Activated HSCs influence the recruitment of immune cells by secreting pro-inflammatory and chemoattractant chemicals, as well as ECM [103].

To sum up, hepatic fibrosis develops in response to injury to hepatocytes or cholangiocytes in different etiologies by dysregulated inflammatory processes. As a result of the robust immune responses triggered by a persistent viral infection and liver disease, chronic inflammation and hepatocyte death occur. In addition to viral infection, fat accumulation in the liver leads to hepatocyte apoptosis and oxidative stress. As a result, under repetitive

inflammation followed by reparative anti-inflammatory immune responses, excessive buildup of ECM occurs [104].

2.1.5 Histopathological progression of Hepatocellular Carcinoma

In hepatocellular malignancy, premalignant lesions such as dysplastic foci, low-grade dysplastic nodules, and high-grade dysplastic nodules are found most commonly in cirrhotic livers and chronic liver diseases. Dysplastic foci consist of several hepatocyte clusters under < 1 mm diameter in size with non-invasive growth. They were segmented as small and large cells dysplasia based on nuclear to cytoplasmic ratio and cellular atypia that differs them from surrounding tissue. Dysplastic nodules (DN) are under < 15 mm diameter in size but larger than surrounding cirrhotic nodules and subdivided into Low and High grades. Low-grade dysplastic nodules have distinct borders with minimal atypia, a slight increase in nuclear to cytoplasmic ratio, no mitosis, and preserved single-cell thickness in liver plates. In high-grade dysplastic nodules, considered mostly precursor of HCC, cells remain uniform, minimal nuclear atypia, a slight increase in nuclear to cytoplasmic ratio, occasional mitoses, and rise to 3 cell thickness in liver plates. Hepatocellular carcinoma can be classified into two main groups from a pathological perspective as early HCCs and progressed HCCs. Early HCC indicated as well-differentiated, lower than 2cm in diameter, and ill-defined edges with a faintly nodular appearance while progressed HCC should be larger than 2cm in diameter or lower than 2cm in diameter with moderate differentiation with clear nodular type [105,106]. In the early stages of cirrhosis, regenerative nodules in the liver produce dysplastic nodules. Then, over time in the progression of HCC, DNs transform into well-differentiated, moderately-differentiated, and poorly-differentiated HCCs [107].

Intertumor and intratumor heterogeneity are two types of tumor heterogeneity in the liver. While intertumor refers to tumors from different patients exhibiting profound differences in both morphology and histology, intratumors reflect the heterogeneity of nodular HCCs in the same liver with variations gained by tumor cell evolution [108]. The heterogeneity for intratumors stemmed from the development of different clones or single clones that metastasized intrahepatically. The natural selection of tumors and clonal development with microenvironmental conditions drive the clonal difference within the tissue [109] and TERT promoter, p53, and CTNNB1 mutations were identified founder driver mutations since they present across all sections of the same tumor, as well as across primary and metastatic tumors [110].

The liver is a vital metabolic center in the body, and its processes are carried out by a highly coordinated arrangement of different cell types. The main structure consists of parenchymal (hepatocytes and cholangiocytes) and nonparenchymal cells (fibroblasts, stellate cells, Kupffer cells, and endothelial cells) [111]. In normal liver, hepatocytes constitute most of the liver mass and are at a quiescent state. Upon injury or loss of liver mass, they gain proliferative capacity for regeneration. The turnover of the hepatocytes is predominantly caused by the replication of remaining hepatocytes instead of stem cells [112]. However, the replicative potential of the hepatocytes can be substantially compromised in acute liver failure or chronic hepatitis and inturn hepatic progenitor cells (oval cells), a bipotential progenitor that can differentiate to hepatocytes and cholangiocytes, appear in the canals of Hering and restore the liver mass loss [112–114].

In the progression of HCC, the cell of origin in the tumor can be stemmed from hepatic progenitor cells and mature hepatocytes. Hepatoblasts as the liver progenitor cells can differentiate into hepatocytes and cholangiocytes [115]. The alterations in the Hippo-WW45 pathway [116] and deletion of neurofibromatosis type 2 (NF2) tumor suppressor gene may amplify the number of progenitor cells [117], and subsequently, cause the development of hepatocellular carcinoma and cholangiocarcinoma. In contrast, a study in genotoxic and genetic murine models with a fate-tracing system shows that Hepatocellular carcinomas developed only from hepatocytes, never from the progenitor/biliary compartment [118]. In parallel, cells that express progenitor markers including EPCAM, SOX9, and PROM1 were not associated with HCC tumorgenesis in the DEN/CCl_4 mouse model [119]. The expression of p62 enhances c-Myc and mTORC1 activation, specifically in hepatocytes, resulting in HCC carcinogenesis [120]. Additionally, the plasticity of the hepatocytes that refers to the capacity to dedifferentiate into precursor cells with progenitor-like characteristics, may lead to HCC carcinogenesis. The absence of functional tumor suppressor TP53 can lead the hepatocytes to differentiate and further mutations in WNT or NOTCH progress to liver cancers [121]. In line with plasticity, the transdifferentiation of adult hepatocytes to biliary-like cells may also lead to intrahepatic cholangiocarcinoma [122]. Finally, as the cell of origin in HCC, cancer stem cells were also implied in carcinogenesis. Although no consensus has been established for an ideal marker, several hepatic progenitor markers including epithelial cell adhesion molecule (EpCAM), CD90, and CD133 were mostly accepted [123].

2.2 Senescence in liver

In normal cells, cellular senescence is a persistent cell cycle arrest that may be influenced by multiple internal and external stimuli, as well as developmental signals. Senescence is thought to be a multi-step, highly dynamic process in which senescent cells' characteristics develop and diversify in response to their environment.

2.2.1 Characteristics and biomarkers of senescent cells

Several cellular and molecular alterations, in other words, morphological and molecular biomarkers of senescent cells, separate senescent cells from other non-dividing cells (like quiescent or terminally differentiated cells). The most apparent macroscopic biomarkers in senescence are multiple or enlarged nuclei and expanded cytoplasm with a higher number of lysosomes and Golgi apparatus [124]. Senescent cells show resistance to apoptosis via expressing anti-apoptotic B cell lymphoma proteins which weakens the permeability of mitochondrial outer membrane results in a decrease in apoptosis-inducing factors release [125]. The absence of proliferation indicators like Ki67, lower phosphorylated Rb levels and 5-bromodeoxyuridine (BrdU) incorporation [124], and elevated expression of cell cycle inhibitors (such as $p16^{INK4a}$, $p21^{CIP1}$, and p27) and tumor suppressors (such as p53 and $p19^{ARF}$) were also considered as indicators of senescence. In addition to these, positive staining for senescence-associated beta-galactosidase (SA-β-GAL) or lipofuscin in response to abnormal lysosomal activity were widely used markers [126,127]. The chromatin in the nucleus of the senescent cells is subject to remodeling upon formation of domains of facultative heterochromatin called formation senescence-associated heterochromatic foci (SAHF) which show the characteristics of transcriptionally silent heterochromatin by histone modifications (H3K9me3) and protein associations (heterochromatin protein 1 homologue-γ (HP1γ) and macroH2A) [128]. Another well-known factor that leads to senescence is the shortening of telomeres which leads to the end-replication problem [129]. Additionally, the capacity of senescent cells to express and secrete a plethora of extracellular modulators such as cytokines, chemokines, proteases, growth factors, and bioactive lipids, is referred to as the senescence-associated secretory phenotype (SASP) and implicated as important biomarkers of senescence [130].

2.2.2 Mechanisms leading to senescence

Senescence can be alerted in many ways by oxidative stress, DNA damage, telomere erosion, chromatin disarrangements, oncogene activation, epigenetic dysregulation, and

inflammation [131]. As a result of multiple stresses and damaging agents, signaling pathways are activated which results in the activation of cell cycle inhibitors and tumor suppressors. Pieces of evidence from multiple sources show that the p53/p21^{CIP1} and retinoblastoma protein (pRb)/p16^{INK4A} tumor suppressor pathways are responsible for the development and establishment of irreversible senescence arrest as summarized in Figure 3 [126,132].

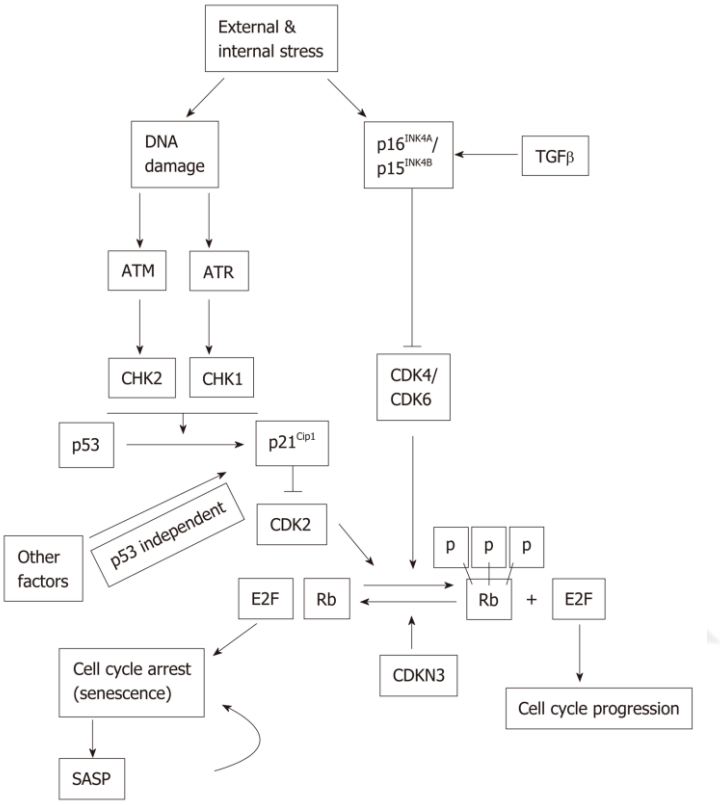

Figure 3**:** The pathways responsible for senescence after induction by multiple sources of stresses [132].

One of the forms of cellular senescence is replicative senescence. It is controlled by a series of molecular processes that are dependent on telomere biology. Telomeres are DNA repeats located at the terminal of the chromosomes. These repeats mainly protect the length of the chromosome with the help of an enzyme called telomerase. The activity of this enzyme preserves the telomere length by adding bases to the ends and protects chromosomes from end-to-end fusions and degradations in replication events [133]. When the telomeres lack a maintenance mechanism, they become increasingly short and eventually unable to sustain the stable formation of the shelterin protein complexes that protect them against DNA damage surveillance mechanisms [134]. When the telomerase activity cannot compensate for the telomere shortening in cell proliferation, this insufficiency results in telomere erosion with

double-strand break signal as DNA damage response (DDR). The DNA damage response triggers a signaling pathway in which ataxia-telangiectasia mutated (ATM) or ATM- and Rad3-related (ATR) kinases are recruited and activated. The recruitment of these apical kinases leads to local phosphorylation of the histone H2AX (γH2AX) with an accumulation of mediator of DNA-damage checkpoint 1 (MDC1) and p53-binding protein 1 (53BP1). Following activation of the checkpoint serine/threonine kinase CHK1 and CHK2, the p53/$p21^{CIP1}$ axis is subsequently triggered. The stabilized and activated p53 protein induces cell-cycle arrest at G1 phase by regulating p21, an inhibitor of Cyclin E/CDK2 and Cyclin D/CDK4 complexes [135,136].

Besides telomere attrition induction, senescence can be induced by oncogenes or tumor suppressors. The oncogene-induced senescence phenomenon was first observed when an oncogenic Harvey rat sarcoma $(HRAS)^{G12V}$ allele was transduced to fibroblasts [137]. The findings were extended to several other oncogenes, $N\text{-}RAS^{Q61R}$ and $B\text{-}RAF^{V600E}$ in RAS pathway [138] as well as $PIK3CA^{E545K}$, AKT, E2F1/3, Cyclin E, MOS, and CDC6 overexpression [139]. Similarly, loss of function mutations in tumor suppressors such as PTEN, NF1, and von Hippel-Lindau disease tumor suppressor (VHL) can induce senescence [140]. These oncogenic changes associate with DNA damage by hyper-replication which results in premature or aberrant DNA replication. Prematurely terminated DNA replication forks and DNA double-strand breaks trigger DNA damage response and lead to phosphorylation of p53 by DNA damage response kinases [141,142]. In addition to these, the CDKN2A locus (also known as INK4A and ARF) encodes two important tumor suppressors, $p16^{INK4A}$ and $p19^{ARF}$, which are connected to replicative senescence. $p19^{ARF}$ controls p53 stability by inactivating the p53-degrading E3 ubiquitin protein ligase (MDM2), whereas $p16^{INK4A}$ inhibits CDK4 and CDK6 [143,144]. In normal cells, this locus is inactivated by the polycomb repressive complexes PRC1 and PRC2. The dissociation of components in this complex activates $p16^{INK4A}$ and induces senescence [145]. The oncogene *Ras* can also elevate reactive oxygen species (ROS) which leads to senescence by hyper-proliferation resulting in DDR [146]. Additionally, the triggered Ras pathway cascade eventually activates p38 MAPK and its substrate p38-regulated/activated protein kinase (PRAK) that directly phosphorylates p53 [147].

2.2.3 Senescence against liver carcinogenesis

Hepatocytes in the adult healthy liver have a very low rate of proliferation since they reside in a dormant state before an action occurs, causing them to enter the cell cycle [148,149].

Thus, the liver has the great regenerative capacity to complete the loss of liver mass. However, the morphology, as well as the response to injury of hepatocytes changes with age. And the full hepatic repair occurs at a slower rate in older animals than young ones after hepatectomy [150,151]. Liver regeneration is a complicated process that varies greatly depending on the kind of trauma, but it usually entails a multicellular response, the recovery of the innate immune milieu, and the revascularization of injured regions. In this complicated process, senescence is considered to involve a key part in the mechanisms which decide the achievement of regeneration [152]. Senescent cells that display markers including $p16^{Ink4a}$, $p19^{Arf}$, and p21, as well as secrete inflammatory components of the senescence-associated secretory phenotype (SASP), maybe accumulate abnormally and in turn, contribute to the loss of tissue function seen in aging and many diseases [126,153,154].

Under normal physiological conditions, the liver is a largely quiescent organ and adult hepatocytes show minimal proliferative action [155]. In the presence of chronic damage to the liver, the accumulation of extracellular matrix proteins (ECM), which include type I collagen produced excessively by activated hepatic stellate cells, results in fibrosis. This accumulation of ECM disrupts the hepatic architecture by establishing a fibrous scar formation. The progressive substitution of liver parenchyma by fibrous scar formation results in cirrhosis [89,156]. The pathogenesis of cirrhosis may be initiated with activation of Kupffer cells by injurious factors such as viral infection, alcohol, and a high-fat diet. These cells attack hepatocytes and damaged hepatocyte cells stimulate the activation of hepatic stellate cells by releasing reactive oxygen species (ROS) and fibrogenic mediators. Therefore, iteration of apoptosis and regeneration of hepatocytes participates in the pathogenesis of cirrhosis [90]. Chronic liver injury results in the buildup of shortened telomeres in hepatocytes because of persistent and recurrent liver damage and regeneration which in turn outcomes cirrhosis [157]. Regardless of the underlying etiology and the age of the patients, telomeres were considerably shorter in cirrhotic samples compared to noncirrhotic samples [4].

Senescence can be considered as an anti-tumor mechanism in hepatocellular carcinoma. In a certain hepatic milieu, hepatocellular senescence has an anti-HCC impact. In hepatoma cells, the induction of senescence with decreasing tumorigenicity is observed by inhibition of Sirtuin 6 (SIRT6) expression that elevates the p21 and p16 expressions. SIRT6 helped to the inhibitory impact of the ERK pathway on cellular senescence by altering the influence of the Smad and p38 MAPK pathways on cellular senescence [158]. The induction of senescence by

chemical agents was also tested against HCC. The HCC cell lines treated with 5-aza-2-deoxycytidine showed upregulation in p16 ^{INK4A} and subsequently pRB dephosphorylation, and G1 arrest associated with positive SABG staining observed [159]. DUSP16 was shown to be increased in HCC and silencing caused cellular senescence, suggesting that it might help HCC cells avoid senescence by blocking the p53/p21-RB and p16^{INK4a}-RB pathways, allowing them to proliferate [160]. In addition, our group previously reported that immortal HCC cells can be reverted spontaneously to a replicative senescence phenotype. The HCC cell line generated three distinct progenies one of which showed lacked telomerase activity due to TERT repression probably in association with the SIP1 gene. The inactivation of SIP1 recovered the cells from senescence arrest [6].

2.3 The role of ATAD2

ATPase family AAA domain-containing protein 2 (ATAD2), also known as AAA+ nuclear coregulatory cancer-associated protein (ANCCA), which is strongly conserved from yeast to human, is composed of two AAA+ domains and a bromodomain [161]. The ATPase domain facilitates protein multimerization by ATP hydrolysis while the bromodomain recognizes acetylated residues in histones. The bromodomain function of ATAD2 is dependent on multimerization via its ATPase domain [162,163]. The normal high expression of ATAD2 is shown in male germ cells [162] as well as in embryonic stem cells [164]. The expression of ATAD2 in dynamic environments like embryonic stem cells and the presence of ATAD2 at acetylated chromatin regions refer to transcriptionally active genes, making ATAD2 in association with chromatin remodeling, DNA replication, and DNA repair. ATAD2 recruitment to chromatin with histone acetylation rises the chromatin accessibility and histone dynamics, which let it be referred to as "generalist facilitator of chromatin dynamics"[164]. Based on structural studies, the hexameric complex of Abo1, known as ATAD2 homolog in yeast, localizes histone H3–H4 onto DNA in an ATP-dependent way by anchoring to histone tails [165]. The association of ATAD2 bromodomain and newly synthesized histones following DNA replication with di-acetylation at K5 and K12 was also shown [166]. With the aid of HJURP homolog (Scm3), the yeast homolog of ATAD2 (Yta7) acts as a deposition factor for CENP-A homolog (Cse4), functioning as a co-chaperon for centrosome formation [167].

In addition to chromatin remodeling, ATAD2 has been observed as a transcriptional co-regulator working on cancer/proliferation-promoting factors such as estrogen and androgen receptors [168], E2F transcription factors [169], and Myc [163,170]. Subsequently, it was

reported that ATAD2 was associated with poor prognosis, and over-expressed in various cancers including breast cancer [169], lung cancer [162,171], ovarian cancer [172,173], colorectal cancer [174,175], cervical cancer [176], gastric cancer [177] and hepatocellular carcinoma [178]. Moreover, a meta-analysis of thirteen studies of nine cancers, some of which aforementioned above, showed that overexpression of ATAD2 was significantly linked to a reduction in overall survival, disease-free survival, recurrence-free survival, and disease-specific survival [179]. The exact mechanisms of ATAD2 overexpression in tumor cells were not identified totally. However, functional studies based on RNA interference have revealed that ATAD2 is implicated in proliferation, invasion, and migration processes in cancers like ovarian [172], cervical cancer [176], and hepatocellular carcinoma [180,181].

2.4 The association of GPR133 with cancers

GPCRs (G-protein coupled receptors) are the largest membrane protein family, mediating the majority of cellular responses to hormones, growth factors, and neurotransmitters as well as responsible for vision, olfaction, and taste in response to light and odors. GPCRs possess seven transmembrane a-helices that traverse the membrane with alternating intracellular and extracellular loop regions. Rhodopsin, secretin, glutamate, adhesion, and Frizzled/Taste2 are the five families of GPCRs found in vertebrates, based on their sequence and structural similarity. The signaling with activating ligands or agonists, the receptor attaches to a heterotrimeric G protein partner and facilitates GTP-to-GDP exchange, causing the G protein to dissociate into its subunits α and βγ, which then regulate downstream signals. Individual GPCRs contain distinct combinations of signal-transduction activities involving numerous G-protein subtypes, as well as G-protein-independent signaling pathways and complicated regulation processes [182,183].

The adhesion GPCRs (aGPCRs) have nine distinct subfamilies that are classified with proposed new names as ADGRL (latrophilins), ADGRA, ADGRB, ADGRC (CELSRs), ADGRD, ADGRE (EGF-TM7), ADGRF, ADGRG, and ADGRV (GPR98) [184]. The aGPCR family includes 33 mammalian homologs that have roles in a variety of developmental and physiological processes. The extracellular domain (ECD), the seven-transmembrane-spanning (7TM) domain, and the intracellular domain make up the modular architecture of aGPCRs. Their ECDs are very large and complex, owing to the presence of numerous adhesive structural folds that enhance interactions with ECM components and receptors in neighboring cells [185]. Most aGPCRs include a GPCR autoproteolysis-inducing (GAIN) domain in their ECDs, which

generally includes a canonical GPCR proteolysis site (GPS) that catalyzes receptor self-cleavage. When the N- and C-terminal fragments (NTF and CTF) are transported to the cell surface, they form heterodimeric receptor molecules through a non-covalent interaction [186].

Recently two main mechanisms of aGPCR modulation were supported: orthosteric agonism (i.e. tethered peptide agonism), which necessitates NTF/CTF dissociation, and allosteric regulation, commonly known as the tunable model, which does not necessitate receptor subunit dissociation. In orthosteric agonism, activation relies on the aGPCR tethered agonist's activity. The seven residues immediately C-terminal to the GPS are the most critical residues or the core of the tethered agonist. The NTF and CTF stay coupled in allosteric types of adhesion GPCR activation, and signaling alterations may be produced by receptor structural changes induced by ligand binding to the NTF, rather than orthosteric interaction by the tethered-peptide agonist [187].

As most of the aGPCRs, GPR133/ADGRD1 has long N termini including a pentraxin-like (PTX) domain and GAIN domain. In the GAIN domain, GPS that catalyzes receptor self-cleavage results in an extracellular N-terminal fragment and a C-terminal fragment which contains the seven-transmembrane region and intracellular C-terminal tail [185,188]. Structural and functional studies revealed that GPR133 couples to the Gs protein/adenylyl cyclase signaling pathway. The ectopic expression resulted in increased cell surface receptors, elevated cyclic adenosine monophosphate (cAMP) levels [189]. The receptor can be activated by tethered agonist called the *Stachel* sequence near the C terminal of GPS. [190]. The H543R mutation in GPR133 that results in uncleavable form causes decreased cAMP levels in respect to wild type. However, the prevention of cleavage still produces cAMP so this phenomenon suggests autoproteolytic cleavage is not the only factor that promotes receptor activation [191].

GPR133 (ADGRD1), one of the adhesion GPCRs family members, were previously linked with different physiological phenomena as adult height by genome-wide association study in Sorbian samples [192], two SNPs for heart rate (the RR interval duration) in electrocardiograms [193], body weight in mice [194] and infertility in female mice because of embryo retention within ampulla [195]. In addition, the association of this orphan receptor with a few cancers has been reported in glioblastoma (GBM) [10], acute myeloid leukemia [196], and human gastric adenocarcinoma [197]. In glioblastoma, the expression of GPR133 was elevated in CD133 positive stem cells and hypoxic parts of human GBM biospecimens. The knockdown of GPR133 *in vitro* reduced tumorsphere formation and cellular proliferation. In

addition, the knockdown of GPR133 in GBM cells reduced tumor formation of the cells *in vivo* [10]. Additionally, besides parallel results were shown in GBM as in Bayin N. S. et. al 2016 [10], it was also shown that GPR133 expression was regulated by hypoxia and Hif1α [11]. According to the publically available genomic data of acute myeloid leukemia (AML), GPR133 (ADGRD1) was found one of eight upregulated aGPCRs in association with poor clinical outcomes [196]. The study in human gastric adenocarcinoma declared that ADGRD1 was regulated by the LINC02407-miR-6845-5p/miR-4455-ADGRD1 pathways [197].

2.5 The role of p73

p73 is identified as a tumor suppressor that belongs to the p53 transcription factor family. It is located at the 1p36 chromosomal location where a region is frequently deleted in tumors [198]. The complexity of the family is enhanced by alternative promoters, alternative splicing, and diverse translation initiation sites. The gene is composed of 15 exons and has two promoters that generate alternative transactivating isoforms: the canonical promoter P1 located upstream of exon 1 that generates TAp73 and the alternative promoter P2 located in intron 3 that give rise to DNp73 isoforms. Besides promoters, alternative splicing of C-terminus generates at least seven potential isoforms (α, β, γ, δ, ε, ζ, and η). Collectively, transcription under two promoters in combination with alternative splicing theoretically produces at least 35 mRNA variants that could encode 29 different p73 protein isoforms [15,199]. The structure of p73 protein consists of functional protein domains and shows diversity based on the generation of alternative isoforms. Structurally, the full-length form, TAp73α, include transactivation domain (TAD), a proline-rich domain (PRD), a DNA-binding domain (DBD), a nuclear-localization signal (NLS), an oligomerization domain (OD), a sterile α-motif (SAM), and an inhibitory domain (ID). The capacity to transactivate distinct genes is determined by the presence or lack of the TAD [200]. As the transcriptional factor, p73 binds to responsive elements of more than two hundred genes that take part in various cellular processes such as apoptosis, DNA repair, and neuronal and epidermal differentiation by its DNA-binding domain (DBD) [201]. The OD domain is responsible for the tetramerization of p73 that is crucial for its transcriptional factorial activity [202]. The SAM domain is encoded with exons 11-13 and is known as the modulator of p73 transcriptional activity since it is localized at a profound alternative splicing site of the C terminus region [203]. The detailed human p73 gene structure and possible isoforms of p73 with functional domains were summarized in Figure 4 [200].

The expression and activity of p73 can be modulated at multiple levels because of its structural complexity. The usage of multiple promoters, alternative splicing, and interaction with other proteins was considered as main regulators. In response to many stimuli including DNA damage, viral oncogenes, proliferative signals, and epigenetic alterations, its expression can be transcriptionally regulated [204–206]. In the transcription of TAp73 from P1 promoter, E2F-1 induces the expression of TAp73 and apoptosis as well in absence of functional p53 without any regulation of p14ARF or MDM2 [207,208], and stabilization of E2F-1 by histone acetyltransferase PCAF or also elevates the TAp73 expression [209]. The

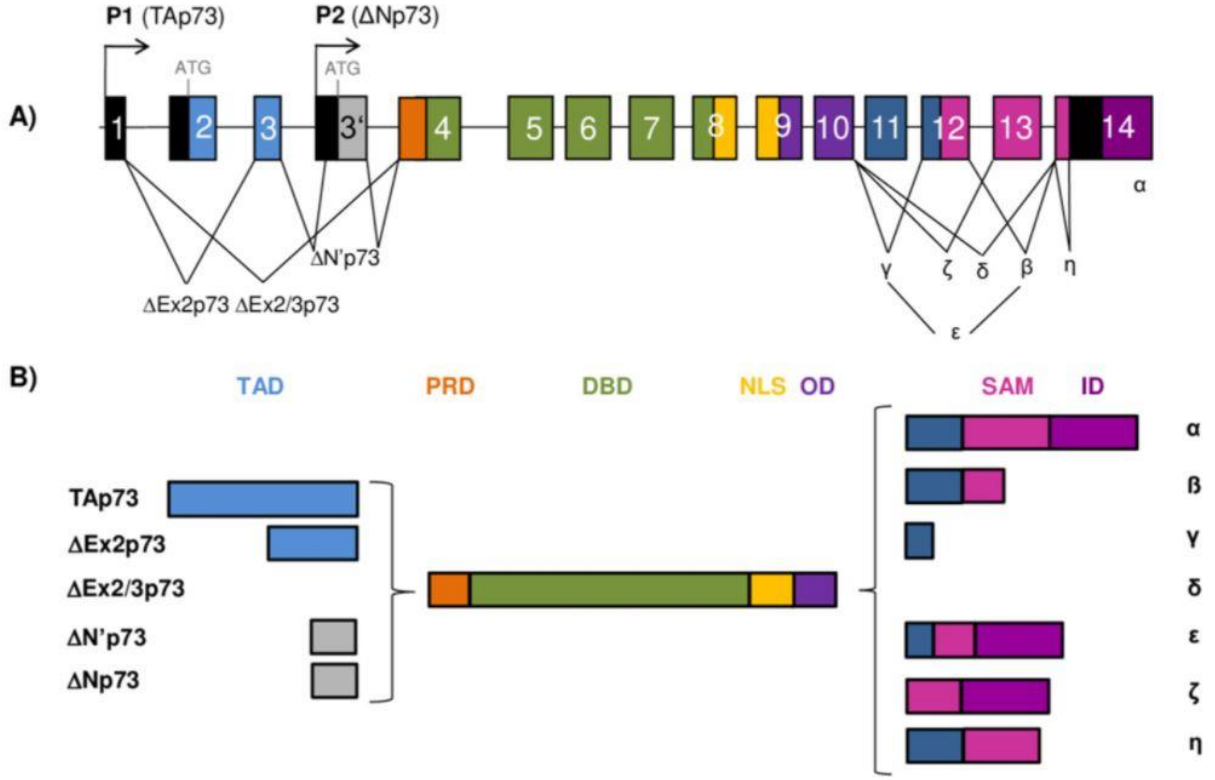

Figure 4**:** The scheme of gene architecture and isoforms of human p73
A) Human p73 gene architecture with promoters and alternative splice sites B) Possible p73 isoforms with their functional domains [200].

TAp73 transactivation by E2F-1 may be hindered with the binding of C-EBPα and ZEB to p73 promoter sites [206,210]. Another transcription factor Early Growth Response-1(EGR1) is also shown as capable of inducing TAp73 [211]. Likely, the promoter activity of p73 was also induced with a member of an important protein complex: geminin coiled-coil domain-containing protein 1(GemC1) [212]. In addition to these, regulation of p73 by the attachment of nuclear factor erythroid 2-related factor 2 (Nrf-2) to both p73 promoters was shown in breast

cancer [213]. In posttranslational regulation of p73, DNA damage-induced p73 phosphorylation via c-Abl results in stabilization and activation of TAp73 and leads to apoptotic response [214]. In contrast, cyclin/CDK complexes can phosphorylate p73 that inhibiting its activity in a cell cycle-dependent manner [215]. Different processes, mostly involving the ubiquitin-proteasome system, keep relatively stable levels of the p73 protein minimal under normal physiological settings. The control of p73 protein stability and degradation has been linked to some ubiquitin E3 ligases like MDM2, ITCH, and TRIM32 [216]. However, the degradation of p73 by Itch can be prevented with the binding of Nedd4-binding partner-1(N4BP1) to Itch [217] or Yes-associated protein 1(Yap1) to p73 [218].

The interpretation of the biological and functional activity of p73 and its isoforms started with *in vivo* knockout experiments in mice. The absence of p73 in p73-knockout (Trp73−/−) mice showed profound defects and revealed its importance in neurogenesis, sensory pathways, and homeostatic control. Besides, the susceptibility to spontaneous tumorigenesis in these mice not increased in comparison to p53 knockout ones [219]. Then heterozygous Trp73+/ mutant mice revealed an increased frequency of a variety of spontaneous tumors under loss of heterozygosity and heterozygous p73 and p53 mutant mice showed more aggressive phenotype compared to mice including only heterozygous p53 [198]. These findings suggested that p73 may have a role in tumor suppression and complicated interrelations among the p53 family members. Furthermore, TAp73-knockout (TAp73−/−) mice generated with deletion of exon 2 and 3 in TAD that result in TAp73 deletion, not DNp73 showed an increase in genomic instability and incidence of spontaneous tumors [220]. The primary embryo fibroblasts (MEFs) derived from p73 knockout mice showed induced polyploidy and aneuploidy in the absence of p53 which suggests the importance of p73 in genomic instability [221].

The expression of p73 isoforms was also implicated in different molecular processes. As transcriptional factors, TAp73 isoforms take part in the regulation of cell cycle checkpoints. The induction of p21 and p57/Kip2 via TAp73 can cause cell cycle arrest in G1 while DNp73 isoforms counteract and promote cell cycle progression. G2/M regulators such as CDC25B, CDC25C, Cyclin B1, Cyclin B2, cdc 2, and Topoisomerase II are likewise repressed by TAp73 [222]. The regulatory role of TAp73 in the cell cycle is also shown in MCF-7 cells. The levels of TAp73 peaked at the S phase of the cell cycle and silencing of TAp73 inhibited cell proliferation. Furthermore, the interaction of TAp73 with p53 responsive elements in the regulatory region of cell cycle progression genes was also observed during cycling [223]. The

genome-wide analysis in p53 mutant cell lines with stimulating DNA damage showed that p73 can regulate over a hundred genes, especially direct targets including BRCA2, Rad51, and mre11. In addition, DNA repair is hampered in cells lacking p73 [224]. Additionally, DNA damage caused by bile acids activated p73 in a c-Abl kinase-dependent manner and activation stimulated DNA repair including the genes SMUG1 and MUTYH that engaged in base excision repair [225]. TAp73 can transactivate pro-apoptotic genes in intrinsic apoptotic pathways including PUMA, Bax, and GRAMD4, and extrinsic apoptotic pathways such as CD95 [226]. Oppositely, the effect of DNp73 isoforms was mostly reported by their dominant-negative role on TAp73 and wild-type p53. The knock-out mice of DNp73 do not show tumor formation compared to TAp73 which supports its oncogenic potential [227]. In support of this, the upregulation of DNp73 with tumor progression in different cancers was observed as increased resistance to therapy and drugs, in other words, chemoresistance [228], inhibition of well-known tumor suppressors: p53 and RB [229], collaboration with oncogenes like Ras [230] and promoting angiogenesis [231].

While TAp73 has been shown to have tumor-suppressing properties, DNp73 acts as an anti-apoptotic protein that is linked to cancer progression. Both variants, however, are overexpressed in a variety of human malignancies including HCC [16,232]. The expression of both TAp73 and DNp73 transcripts was observed in HCC cell lines and patient samples [233]. Aside from expression, the ratio of TAp73 to DNp73 was found to be a critical determinant in apoptotic response, therapeutic responsiveness, and HCC prognosis [17]. In the evaluation of p73 in HCC treatment, recently, the activation of the p73 pathway by stress-inducible nuclear protein 1 (NUPR1) knock-down enhanced sorafenib-induced anti-tumor activities in HCC cells [234].

3 MATERIALS AND METHODS

3.1 Type of the study

The study was conducted completely based on scientific experimental methods.

3.2 Place and time of the conducted study

The study was carried out at the laboratories of Dokuz Eylul University and İzmir Biomedicine and Genome Center between February 2014 and June 2021.

3.3 Test systems

HCC cell lines were used as the test system and stocks of Prof. Mehmet Öztürk's group were used in the experiments.

3.4 Variables of the study

In the study, TAp73 isoforms, GPR133 (ADGRD1), and ATAD2 were considered as variables based on the context. Knock out of ATAD2, overexpression of TAp73beta and ADGRD1 were examined in the context of function at cellular or physiological levels. The treatment of HCC cell lines with different drugs and their cellular responses were also considered as variables for ATAD2 protein expression.

3.5 Materials

3.5.1 Common Reagents

The common chemicals and buffers used in the study are listed in Table 1 and Table 2

Table 1: The list of common chemicals

Reagent Name	**Brand**	**Catalog No**	**Storing temperature**
2-propanol	Sigma	24137	RT
Acetic Acid	Sigma	27225	RT
Acrylamide	Sigma	A3553	RT
Agarose	BioShop	AGA002	RT
Ammonium Persulfate	Sigma	A3678	RT
Bisacrylamide	Sigma	294381	RT
Bovine Serum Albumin	GoldBio	A-420-500	+4°C
Dimethyl Sulfoxide (DMSO)	Sigma	276855	RT
EDTA	Bioshop	EDT001.500	RT
Ethanol	Sigma	32221	RT
Formaldehyde	Sigma	15512	RT

Glycine	BioShop	GLN001.1	RT
Methanol	Milipore	1060092511	RT
NaCl	BioShop	SOD001.1	RT
Non-Fat Milk Powder	BioShop	SKI400.250	RT
Nonidet P-40 Substitute	Amresco	E109	RT
Propidium Iodide	Sigma	p4864	+4°C
Safe View	ABM	G108	+4°C
Saponin	Amresco	0163-100G	RT
Sodium Dodecyl Sulfate (SDS)	BioShop	SDS001.1	RT
TEMED	Sigma	T7024	RT
Tris	Amresco	826	RT
Tris-HCl	BioShop	TRS002.500	RT
Tryptone	Amresco	J859	RT
Tunicamycin	Sigma	T7765	-20°C
Tween-20	Amresco	777	RT

Table 2: Common buffers and their chemical formulations

Name	**Formulation**
RIPA protein lysis buffer	150mM NaCl, 1% Nonidet P-40, 0.1% SDS , 0.5% Sodium deoxycholate and 25mM pH7.4 Tris
Laemmli sample buffer (4x)	0.25M Tris base, 0.28M SDS, 40% Glycerol, 20% 2-mercapto ethanol and 2mg/ml Bromophenol Blue
Run Buffer	14.4g Glycine, 3.02g Tris and 1% SDS in 1L ddH_2O
Transfer Buffer	14.4g Glycine, 3,02g Tris, 0.2% SDS, 20% MetOH and ddH_2O in 1L
TAE buffer (50x)	242g Tris base, 57.1ml Acetic Acid and 100ml of 0.5M EDTA dissolved in 1L ddH_2O pH:8.5
TBS-T (1X)	50mM Tris-HCl, pH 7.5, 150mM NaCl, 0.5% Tween-20
LB (Luria-Bertani) medium	10g BactoTryptone, 5 g yeast extract, 5g NaCl dissolved in 1L ddH_2O
LB (Luria-Bertani) agar	10 BactoTryptone, 5 g yeast extract, 5g NaCl, 15g bacto agar dissolved in 1L ddH_2O

PBS (1X)	137mM NaCl, 2.7mM KCl, 8mM Na_2HPO_4, and 2mMKH_2PO_4, pH 7.4
PBS-T (1X)	1X PBS with 0.1% Tween-20
SRB staining solution	0.04% SRB powder dissolved in 1% Acetic acid

3.5.2 General Laboratory Solutions and Kits

Various chemical solutions and kits used in the study were purchased from different suppliers. Plasmid isolation and total RNA isolation kits were purchased from Machery-Nagel (Düren, Germany). For DNA isolation from agarose gel, the gel extraction kit was purchased from Qiagen (Valencia, CA, USA). For mounting in immunofluorescence, Prolong Gold Antifade Mountant was purchased from Invitrogen (Carlsbad, CA, USA). Apoptosis Assay was performed by Annexin V: PE Apoptosis Detection Kit I (Cat. 559763, Becton Dickinson, Franklin Lakes, NJ, USA).

3.5.3 Cell Culture Media, Supplements, and Reagents

Cell lines used in the study were cultured with basal Roswell Park Memorial Institute-1640 (RPMI-1640) media, supplemented with 10% GIBCO Fetal Bovine Serum, 1x Penicillin/Streptomycin (100U/ml), and 1x MEM non-essential amino acids. Basal media, its supplements, and trypsin-EDTA 0.25% were obtained from ThermoFisher Scientific (Waltham, MA, USA). Cell culture grade 1X PBS without calcium or magnesium was purchased from Serox GmbH (Mannheim, Germany). Tunicamycin, adriamycin, and thapsigargin were obtained from Sigma-Aldrich (St. Louis, MO, USA). For plasmid transfection to mammalian cells, FuGENE HD was purchased from Promega (Medison, WI, USA) and serum-free Gibco OPTIMEM was purchased from Invitrogen (Carlsbad, CA, USA). For siRNA transfection, Lipofectamine RNAiMax solution was purchased from Thermofisher (Waltham, MA, USA).

3.5.4 PCR Reagents

For PCR and cloning experiments, MyTaq DNA polymerase kit was obtained from Bioline (London, England). RevertAid First Strand cDNA synthesis kit and Phusion High-Fidelity polymerase were purchased from ThermoFisher Scientific (Waltham, MA, USA). The gel extraction kit was purchased from Qiagen. DyNAmo HS SYBR Green qPCR Kit F410 was

purchased from Finnzymes. DNA ladders 1kb and 100bp were purchased from ThermoFisher Scientific (Waltham, MA, USA).

3.5.5 Western Blot Reagents

In western blot workflow, Bio-Rad mini-PROTEAN Tetra Cell system (Hercules, CA, USA) was used for gel casting, protein running, and wet transfer. To determine protein concentrations, Bicinchoninic Acid (BCA) kit was purchased from ThermoFisher (Waltham, MA, USA). PVDF membranes were purchased from Millipore (Burlington, MA, USA) and Nitrocellulose membranes were purchased from GE Healthcare (Chicago, IL, USA). For visualization of proteins with Enhanced Chemiluminescence (ECL), SuperSignal West Dura Extended Duration Substrate and SuperSignal West Pico Plus Chemiluminescent Substrate were purchased from ThermoFisher Scientific (Waltham, MA, USA). PageRuler Plus Prestained Protein Ladder, 10 to 250 kDa was purchased from ThermoFisher Scientific (Waltham, MA, USA).

3.5.6 Antibodies

Antibodies used in the study are listed in Table 3

Table 3: Primary and secondary antibodies used in biological assays

Name	**Host**	**Brand**	**Catalog No.**	**Western**	**IF**
ADGRD1_N_term	Rabbit	Covalab	-	1:150	1:250
ADGRD1_C_term	Rabbit	Covalab	-	-	1:150
α-FLAG	Mouse	Sigma	F3165	-	1:250
ATAD2_Purified_1	Rabbit	Covalab	C1257	1:2000	1:250
Ki-67	Mouse	Santa Cruz	Sc-23900	-	1:250
HRD1	Rabbit	Cell Signaling	12925	1:1000	-
CHOP	Mouse	Cell Signaling	2895	1:1000	-
FLp73	Rabbit	Sayan A.E, 2005	-	1:2000	-
DNp73	Mouse	Abcam	ab38C674	1:500	-
p21	Mouse	Abcam	Ab7903	1:1000	-
PARP	Rabbit	Cell Signaling	9542	1:1000	-
α-β-Actin	Rabbit	Abcam	ab6276	1:5000	-
α-Mouse-HRP	Horse	Cell Signaling	7076S	1:5000	-
α-Rabbit-HRP	Goat	Invitrogen	31360	1:5000	-

α-Mouse-Alexa488	Goat	Invitrogen	A11029	-	1:5000
α-Mouse-Alexa594	Goat	Invitrogen	A11005	-	1:5000
α-Rabbit-Alexa488	Goat	Invitrogen	A11008	-	1:5000
α-Rabbit-Alexa594	Goat	Sigma	77671	-	1:5000

3.5.7 Oligonucleotides

Primers used in PCR applications were listed in table 4 and On-TARGETplus Human ATAD2 set of 4 siRNAs used in knock out experiments were listed in Table 5

Table 4: Primers used in expression analysis and cloning

Primer	**Sequence 5'-3'**	**Applications**
Adgrd1_Ex22R	GTGGCAAACATGTACTGGAAA	RT-PCR
Adgrd1_Ex21F	GTCAACATTGGCATCCTCATC	RT-PCR
G133_R	GGTGGTATCGATCCCACGGCTGACAGGTCGAC	Cloning
G133_F	GGTGGTAAGCTTATGGAAAAGCTGCTGCGG	Cloning
GAPDH_R_	CAGCCTTCTCCATGGTGGTGAAGA	qRT/RT-PCR
GAPDH_F_	GGCTGAGAACGGGAAGCTTGTCAT	qRT/RT-PCR
ATAD2_R	TGCGATGCCGATAAATACA	qRT-PCR
ATAD2_F	TGAAAAGGCTTTGGCAATTC	qRT-PCR
TAp73_F	GGCTGCGACGGCTGCAGA	RT-PCR
TAp73_R	GCTCAGCAGATTGAACTGGGCCATG	RT-PCR
DNp73_F	GCCCGCATGTTCCCCAG	RT-PCR
DNp73_R	TTGAACTGGGCCGTGGC	RT-PCR
DN'p73_F	TCGACCTTCCCCAGTCAAGC	RT-PCR
DN'p73_R	TGGGACGAGGCATGGATCTG	RT-PCR
TAp73Δex2_F	GGCTGCGACGGCTGCAGGGA	RT-PCR
TAp73Δex2_R	CAGGCGCCGGCGACATGG	RT-PCR
TAp73Δex2/3_F	GGCTGCGACGGCTGCAGGCC	RT-PCR
TAp73Δex2/3_R	CAGGCGCCGGCGACATGG	RT-PCR

Table 5: siRNAs used in the suppression of ATAD2 expression experiments

Name	**Sequence**
siRNA-1 J-017603-05	CCACAGAUCUAUACCACUA
siRNA-2 J-017603-06	GUAAUCAGCCAAUGUAUUU
siRNA-2 J-017603-07	CGUCGAAGUUGUAGGAUUA
siRNA-2 J-017603-08	CUGAUGAGGUUCCUGAUUA

3.5.8 Plasmids

Plasmids were used in expression and confirmation studies listed in Table 6

Table 6: Plasmids used in the studies

Name	**Bacterial Selection**	**Mammalian Selection**	**Tag**
pCR4-TOPO-GPR133	Ampicillin	NA	-
p3xFLAG-CMV-14_GPR133	Ampicillin	G418	C terminal Flag
pcDNA4TO-GPR133	Ampicillin	Zeocin	-
pcDNA6/TR	Ampicillin	Blasticidin	-
pT-REx-DEST30-TAp73beta	Ampicillin	G418	-

3.6 Methods

3.6.1 Cell culture

All cell line manipulations were performed under Class II type A biosafety cabinets with aseptic cell culture techniques.

Frozen cell vials were taken from liquid nitrogen and immediately thawed in a 37˚C water bath. Cells in freezing medium were directly transferred onto 9ml of the complete medium in 15ml falcon tubes. Tubes were centrifuged for 5 minutes at 1500 RPM and the supernatant discarded. Cells were resuspended in fresh complete media and transferred to a 25cm^2 flask for incubation. All cell incubations were performed in 5% CO_2 incubators at 37˚C

In general, cell manipulation was performed based on the confluency of the cells. When cells were reached 70-90 % confluency, the medium of the cells aspirated and washed with pre-

warmed Calcium or Magnesium free PBS. After PBS was discarded, cells were incubated with 0.25 % Trypsin-EDTA at 37˚C in a CO_2 incubator for cell dissociation. Trypsin inactivation was performed with the addition of a fresh medium with a ratio of 1:9. The cell concentration of cell suspension was determined with trypan blue. A small volume of suspension mixed with trypan blue with a ratio of 1:1 and counted on a hemocytometer. The cell suspension was used for further manipulations.

Cryopreservation of the cells was performed with cell suspension described above. The cell suspension was centrifuged for 5 minutes at 1500 RPM and the supernatant discarded. Pellet was dissolved in a determined amount of freezing medium composed of 10% DMSO and 90% FBS and dispensed as 1ml to screw capped-cryotubes. Vials were kept in a shuttle containing isopropanol at -80°C for a few days and transferred into liquid nitrogen.

3.6.2 Total protein extraction and quantification

The 1xRIPA buffer freshly supplemented with 25x protease inhibitor cocktail (cOmplete, ROCHE), 1mM NaF (Sodium Floride), and 1mM Na_3VO_4 (Sodium Orthovanadate) (1mM) before protein isolation. Cell pellets from 60mm dishes were dissolved with approximately 100ul of RIPA. Homogenates were vortexed vigorously every 5 minutes for 30 minutes and kept on ice. Homogenates were then centrifuged at 17.000xg for 30 minutes at +4°C. Supernatants were transferred to new Eppendorf tubes without disturbing the pellets.

To determine the protein concentrations, BCA assay reagents were freshly mixed as 1:49 volume according to the number of samples and 100ul loaded to each well. BSA stock (2mg/ml) used to prepare linear standard as 0, 1, 2, 4 and 8ug/well. Protein samples were loaded to each well as 2ul/well. Plate incubated at dark on 37˚C for 30 minutes. Absorbance values of each well were obtained at 562nm using MultiSkanGo (ThermoScientific). After blank subtraction, the linear regression curve was plotted. Based on the formula, protein concentrations were calculated. Protein samples were equalized with RIPA buffer concerning the final volume and 4xLoading Dye (with 20 % beta-mercaptoethanol). Samples were boiled at 95˚C for 5 minutes and stored at -80 ˚C until use.

3.6.3 SDS-PAGE and western blot

Polyacrylamide gels were cast according to gel concentration for 10% gel. Resolving Gel (10ml) prepared with 4ml H_2O, 3.3ml 30% Acrylamide mix, 2.5ml 1.5M Tris (pH:8.8), 0.1ml 10% SDS, 0.1ml 10% ammonium persulfate and 4ul TEMED. After approximately 30 minutes of polymerization, stacking gel (3ml) prepared with 2.1ml H_2O, 0.5ml 30% acrylamide mix,

0.38ml 1.0 M Tris (pH:6.8), 0,02ml 10% SDS, 0.02ml 10 % ammonium persulfate and 3ul TEMED. The gels were kept at +4 ˚C in the run buffer before use. Before sample loading to gels, protein samples thawed on ice and boiled again at 95˚C for 5 minutes. Gels were run at 80V for 30 minutes and 120V for approximately 2 hours depending on the size of the interested protein and marker.

PVDF membranes were activated in methanol, and proteins were wet transferred from the gel to membranes as in the standard sandwich model. Transfer performed in 400mA for 2 hours. After transfer, the blocking solution is prepared as 5% Non-Fat Milk Powder which is dissolved in Tris Buffer Saline with 0.5% Tween (TBS-T) and membranes blocked with it for 1 hour at room temperature. Primary antibodies were diluted in a 3% blocking solution and incubated with membranes for 1 hour at room temperature or overnight at +4˚C. Membranes were washed 3 times with TBS-T and incubated with HRP conjugated secondary antibody which dissolved in 3% blocking solution for 1 hour at room temperature and membrane washed as previously mentioned.

Enhanced chemiluminescence solution, composed of peroxidase buffer and enhancer buffer was prepared freshly and used immediately to visualize the protein bands on the PVDF membrane. Images were taken under different exposure times at dark. To visualize and merge the protein ladder, an image of the membrane was also taken with visible light.

3.6.4 Polymerase chain reactions (PCR)

Expression of ADGRD1 transcript levels was evaluated with primers designed based on consensus sequence at C terminal end. PCR reactions were carried by Adgrd1_Ex21F and Adgrd1_Ex22R primers for expression levels of ADGRD1 transcripts in patient samples, cDNA collection of normal tissues, and HCC cell line samples. GAPDH_F and GAPDH_R primers were used as a control in the reactions. The conditions of PCR reactions were 1 cycle of initial denaturation for 1 minute at 95°C, 35 cycles of denaturation for 15 seconds at 95°C, annealing for 30 seconds at 58°C, and extension for 30 seconds at 72°C. The reaction mixtures were prepared with the MyTaq DNA polymerase kit (Bioline)

In cloning of ADGRD1 gene for Flag tag, PCR reaction was set up by Phusion High-Fidelity polymerase (Thermo). G133_R and G133_F primers were used for amplification of the construct. PCR conditions were performed as 1 cycle of initial denaturation for 30 seconds at 98°C, 25 cycles of denaturation for 15 seconds at 98°C, annealing for 30 seconds at 58°C, and extension for 60 seconds at 72°C.

The expression of p73 isoforms was determined with specific primers listed in Table 4. The conditions of PCR reactions were set up as 1 cycle of initial denaturation for 5 minutes at 95°C, 33 cycles of denaturation for 30 seconds at 95°C, annealing for 15 seconds at 60°C, extension for 20 seconds at 72°C, and 1 cycle of final extension for 5 min at 72°C.

3.6.5 Molecular cloning of plasmids

The Human ADGRD1 gene was already cloned commercially into pCR4-TOPO vector and gifted to us by Dr. Demet Saraç. As Tet inducible expression vector, pcDNA4/TO was selected. Based on the orientation and sequence information, the pCR4-TOPO vector was digested with SpeI and NotI for cDNA insert. Target expression vector pcDNA4/TO was digested with NotI and XbaI for compatible ends and correct orientation. Both digestion products were run on 1.5% agarose gel and purified with the gel purification kit (Qiagen) following the instructions of the manufacturer. Ligation reactions were set in three different vector/insert ratios with T4 Ligase at 16°C overnight. For transformation, competent cells prepared with the competent cell kit (Zymo) were used. Competent cells were kept on ice for 5 minutes and 2ul of ligation reaction mix from different vector/insert ratios were put on Eppendorf tubes. The Bacteria-ligation mixture was mixed by gentle pipetting and kept on ice for 10 min. After 10 min, 1/5 of transformation suspension was spread on LB agar plates supplemented with ampicillin. LB agar plates were left at 37°C overnight for incubation. Colonies were picked up by sterile pipette tip into liquid LB media supplemented with ampicillin and incubated for shaking. Confirmation of selected colonies was performed by mini prep DNA isolation kit (MN) followed by restriction with ApaI and NotI. The confirmed colony was inoculated on a large scale for a maxi prep plasmid isolation kit (MN).

Additionally, the ADGRD1 gene was also cloned to the p3XFLAG-CMV-14 vector that has a flag protein tag at its C-terminal end. Two specific primers were designed as G133_F-5’ GGTGGTAAGCTTATGGAAAAGCTGCTGCGG ’3 and G133_R-5’ GGTGGTATCGATC CCACGGCTGACAGGTCGAC ‘3. Insert sequence was amplified with Phusion High-Fidelity (Thermo). As a template, 5ng of the pCR4-TOPO vector was used. Digestion of PCR product and p3XFLAG-CMV-14 vector were performed with HindIII and ClaI. After confirmation of digestions on agarose gel, the same methodology was applied for ligation, transformation, and confirmation steps as indicated above.

3.6.6 Cell viability assay with Sulforhodamine B

Inducible HepG2_ADGRD1, Hep3BTAp73beta, or HepG2TAp73beta clones were seeded at a density of 5000/well in 96 well plates. Experimental setups were designed as control and induced groups in triplicates. After 24 hours from seeding, media was refreshed with fresh media (Dox-) or fresh media supplemented with 1µg/ml Doxycycline (Dox +). At the end of an additional 48h, media was discarded, and wells were washed with PBS gently. Ice cold 100µl of 10 % Trichloroacetic Acid (TCA) was added and incubated at -20°C for 20 minutes. Wells were washed with tap water and air-dried. After air dry, Sulforhodamine B solution (0,4 %, w/v) was added and incubated at RT for 20 minutes. Solution discarded and wells were washed three times with 1% acetic acid solution to remove excess and unbound dye. Wells were air-dried, and stain dissolved by adding 50µl of Tris buffer with pH 10.5 for 20 minutes with gentle shaking. In the end, plates were analyzed at 510nm using MultiSkanGo (ThermoScientific) spectrophotometer.

3.6.7 Immunofluorescence

In the experiments of ADGRD1, sterile circular glass cover slips were placed in 24 well plates, and cells were seeded on them. Cells were transfected with plasmids by FuGENE HD Transfection Reagent (Promega). After incubation of cells for the experiment was finalized, media was discarded, and cells were washed gently with PBS. Cell fixation was performed with 4% formaldehyde for 15 minutes at room temperature. Formaldehyde was discarded and washed with PBS with gentle shaking. Cells were blocked by blocking buffer containing 5% FBS and 0.1% Saponin in PBS for 60 minutes at room temperature. All primary and secondary antibody dilutions were prepared in antibody dilution buffer (1x PBS, 1% BSA, and 0.1% Saponin). Blocking solution was aspirated and slides were incubated overnight at +4˚C with diluted primary antibody. The antibody solution was discarded and washed with PBS 3 times. Appropriate secondary antibodies with fluorescence tags were incubated for 1 hour at room temp with gentle shaking. Wells were aspirated and washed 3 times with PBS. After the final wash, DAPI with the concentration of 100ng/ml was added to wells for 1 min then rinsed. Cover slips were mounted on a drop of mounting media on slides and kept on dark until fluorescence microscopy imaging.

At the beginning of ATAD2 experiments, the pool of ATAD2 siRNAs or control siRNAs were prepared in serum-free RPMI and mixed with Lipofectamine RNAiMax solution (Thermofisher) as suggested in the manufacturer’s instructions. The mixture was incubated at

room temperature for 10 minutes in 24-well plates containing coverslips. Cell suspension (5000 cells/well in RPMI) was added to wells. Cells were then incubated for 48h. At the end of incubation, cells on coverslips were washed with PBS in wells and fixed ice-cold Acetone-Methanol mixture (1:1) for 10 minutes at -20˚C. The fixative mixture was discarded and wells washed with PBS. As a blocking step, cells were incubated with 1% BSA prepared in PBS-T (PBS and 0.1% Triton-X). Primary antibodies against Ki-67 and ATAD2 were diluted in PBS-T containing 0.5% BSA and incubated with cells for 2 hours at room temperature with gentle shaking. Primary antibodies were discarded and wells were washed with PBS-T. Cells were then co-probed with fluorescence tagged anti-mouse and anti-rabbit secondary antibodies diluted in PBS-T containing 0.5% BSA for 90 minutes. Cells were washed, incubated with DAPI, rinsed with dH_2O, and mounted on slides with mounting media as previously described above.

3.6.8 Cell cycle analysis with propidium iodide staining

Hep3B and Huh7 cells were seeded to 60mm^2 dishes with 400k cells in 3ml. After 48 hours, the media was discarded. New media with 0mg/ml, 0.1ug/ml, and 1ug/ml adriamycin were added to cells and incubated for 24 hours. At the end of the 24 hours, all cells were collected. Firstly, the old media of the dishes were transferred to 15ml falcon tubes. Cells were washed with PBS and PBS with detached cells was also collected onto the same falcon tube. Finally, adherent cells were incubated with 0.25 % Trypsin-EDTA, harvested with complete media, and collected to the same falcon tubes. After all cells were collected, falcon tubes were centrifuged at 2500 RPM for 10 minutes. Supernatants were aspirated and pellets were washed with PBS. Falcons centrifuged again and PBS discarded. Cell pellets were resuspended in 1.5ml PBS and kept on ice. To fix the cells, absolute ice-cold ethanol was added dropwise onto cells to reach the final volume of 5ml (70% EtOH) with gentle vortexing. Tubes were kept 15 min on ice and stored -20˚C until analysis day. On the day of flow cytometry analysis, tubes were centrifuged, and ethanol was discarded. Pellets were washed with PBS. Pellets were stained with 100ul PI solution consisting of PI, RNAseA, and Tritonx100 in PBS and transferred to round-bottom polystyrene test tubes. Samples were analyzed by LSR FORTESSA (BD). Similarly, in the analysis of HepG2-GPR133 clones, they were induced with doxycycline for 48h. All control and induced cells were collected and analyzed as described above.

In cell cycle analysis of p73, Hep3B, HepG2, and SNU449TAp73beta clones were seeded to 6 well plates with a density of 100k/well. After 24 hours, cells were treated with or without

doxycycline (1 μg/mL) for 72 h. Samples were collected after trypsinization and subsequently followed the process outlined above for analysis.

3.6.9 Apoptosis assay

Hep3BTAp73beta and SNU449TAp73beta cells were seeded into 6 well plate and after 24h, media refreshed with/without media including doxycycline. Cells were incubated for 72h and collected. The PE Annexin V Apoptosis Detection Kit I (Becton Dickinson) instructions were applied to cells and analyzed by BD FACSCanto II (Becton Dickinson).

3.6.10 Generation of rabbit polyclonal antibody against ADGRD1

The lack of efficient commercially available antibodies against ADGRD1 forced us to generate new antibodies against ADGRD1. The company called Covalab (France) designed antigen peptides and generated antibodies against the N and C terminal of human ADGRD1 protein. Briefly, 4 peptide fragments were designed in which peptide 1 and 2 were located at the N terminal, peptide 3 and 4 were located at the C terminal. The aminoacid sequence and location of the peptides are as follow Peptide 1 (27-44): YSRSQDHPGFQVLASASH and Peptide 2 (484-500): TVHLKHRLTRKQHSEAT, Peptide 3 (817-833): FKHKTKVWSLTS SSART and Peptide 4 (853-868): STKLSPWDKSSHSAHR. Rabbits were immunized with the peptides and immunoreactivity of the animals measured with ELISA at Day 0, 53, and 74. Final bleedings of the rabbits were collected. The amino and carboxyl-terminal antibodies were pooled in separate columns in the purification step respectively. As a result, we had 2 antibodies: Amino (N-terminal) and Carboxy (C-terminal) antibodies in which each of them recognizes 2 different epitopes respectively.

3.6.11 Colony formation assay

Tet inducible TAp73beta or ADGRD1 clones were seeded 500-1000/well in 6 well plates with replicates. After 24 hours, media was refreshed with fresh media (Dox-) or fresh media supplemented with 1μg/ml Doxycycline (Dox +). Media refreshed every three days and colonies were cultured for 15 days. At the end of 15 days, wells were washed with PBS, and colonies were fixed with ice-cold absolute methanol for 10 minutes at -20˚C. After methanol was discarded, colonies were stained with 0.5% Crystal Violet staining solution for 10 minutes at RT. The staining solution was discarded and wells were washed three times with water. Plates were air-dried and photographed. Colonies were quantified with the colony counter plugin of ImageJ.

3.6.12 Spheroid formation

To force cells to grow in suspension, the bottom of 24 well plates were covered with 1% agarose. The HepG2_ADGRD1_15-1 clone was seeded 500/well in media with or without 1µg/ml Doxycycline. Growth of the cells was monitored for 12 days, and bright-field images of the wells were taken at 4-day intervals. At the end of 12 days, six replicates were collected in one tube for each condition. Each tube was centrifuged and pelleted. Pellets were paraffin-embedded to blocks and hematoxylin-eosin staining was performed.

3.6.13 qRT-PCR for microarray analysis

Total RNAs of cell lines (Hep3B, SNU449, and PLC/PRF/5) used in microarray analysis were isolated with NucleoSpin RNA II Kit (MN Machete-Nagel, Duren, Germany). Total RNAs were converted to cDNA using the RevertAid First Strand cDNA synthesis kit (MBI Fermantas, Germany). Reactions for quantitative expression analyses were set up with DyNAmo HS SYBR Green qPCR Kit F410 (Finnzymes). The reaction mix per well contained 10 µl Sybergreen, 0.8 µl of 10 pmol forward and reverse primers, 7.4 µl ddH_2O and 1 µl cDNA were used. After adding mineral oil onto each well as 1:1, the reaction was carried out in the Mx3005p PCR machine (Stratagene). The housekeeping gene, Glyceraldehyde-3-phosphate dehydrogenase (GAPDH) was used as the internal control. These analyses were performed by Dr. Çiğdem Özen.

3.6.14 Statistical analysis of ADGRD1 isoforms in cancers

Two main isoforms of ADGRD1 were examined in TCGA datasets of different patient samples. Datasets were downloaded from the TSDV platform and analyzed. In the statistical analysis of the data, descriptive statistics for the continuous variables were calculated separately for the "Primary Solid Tumor" and "Solid Tissue Normal" groups. Shapiro-Wilk normality test was used to examine whether the continuous variables were normally distributed. Since the data were not normally distributed, two independent Mann-Whitney U test was used to compare the median values of the continuous variables "isoform_uc001uit" and "isoform_uc010tbm" groups. The significance level was taken as $p \geq 0.05$ in all group comparisons. IBM SPSS Version 25.0 statistical package program was used for statistical analysis. These analyses were performed under the supervision of Dr. Aslı Suner Karakülah.

3.6.15 Chemical transfection of cells and generation of stable cell line

Cells were seeded one day before transfection to reach approximately 70-80 % confluent on the day of transfection. After one day, cells were transfected with FuGENE HD (Promega,

USA). Briefly, the medium of the cells was refreshed. Then, expression plasmids were diluted in a serum-free Gibco OPTIMEM (Invitrogen) medium. Based on the amount of expression plasmid, transfection reagent was added at the 1:3 ratio. After mixing with brief vortexing, the mixture was incubated at room temp for 15 minutes. The total transfection mixture was added dropwise on cells and incubated until selection. After 48h of transfection, the media refreshed with selection media. The selection of cells was performed with the following antibiotic concentrations: 10ug/ml and 100ug/ml of zeocin used in the selection of Hep3B and HepG2 cells respectively, 300ug/ml of neomycin used for maintenance of tet inducible system. Cell media supplemented with indicated antibiotics was refreshed every three days. The selection was carried out approximately for 2 weeks. To produce single-cell clones, cells were either seeded to 100mm dishes at very low density or single-cell sorted into 98 well plates by FACS Aria III device (Becton and Dickinson, Franklin Lakes, NJ, USA) with the help of İBG-Flow Cytometry core facility. Firstly, Low-density seeded clones were marked with a pen from the bottom of the dish under the light microscope. Then, the media was discarded, and the plate was washed with PBS. All liquid on the plate was sucked out. Marked colonies were picked up by a 200ul pipette tip with gentle pipetting of the small amount of trypsin in and out. Every clone was immediately seeded to 96 well plates with complete selection media. All collected colonies were tested for their expression profile by western-blot or immunofluorescence.

3.6.16 Gene expression profiling by microarrays

Quality control of total RNAs collected from ATAD2siRNA-transfected or control cells was first tested with the Agilent Bioanalyzer 2100. Based on RNA integrity number values (RIN), samples greater than 9 were used in microarray experiments. As previously described [7], an Affymetrix microarray system was used. In microarray analysis, the Affymetrix platform with GeneChip Human Genome U133 Plus 2.0 arrays was used and analyzed according to manufacturer instructions. Operating Software (Affymetrix) was used to collect and store data. R statistical computing environment (v3.6.1) was used in the analysis of microarray data. The expresso function of the Bioconductor affy package (v1.68.0) was used to perform robust multichip average normalization (RMA) on raw probe intensities in CEL files [235]. To measure significant changes in gene expressions across pairwise comparisons, differential expression analysis was performed with the Limma package (v3.46.0) [236]. The “lmFit” function was used to fit a linear model and the “contrasts.fit” function was used to compute estimated coefficients and standard errors. The “eBayes” function was used for Empirical Bayes

statistics. Differentially expressed genes were determined using a fold change cutoff ≥2. The Gene Ontology (GO) enrichment analysis of differentially expressed genes was performed with clusterProfiler package (v3.14.3) [237] and the GO terms with FDR ≤ 0.05 were considered as significant. Array data was uploaded and can be accessible with GSE178243 number in Gene Expression Omnibus (GEO).

A similar procedure was followed in the analysis of Hep3BTAp73beta induced samples. Briefly, the quality of isolated RNA samples for 12h, 24h, and 48h groups was assessed by Agilent Bioanalyzer (Agilent), and analysis was performed with Affymetrix GeneChip Human Genome U133 Plus 2.0 arrays. The gathering and storage of microarray data utilized with Gene-Chip Operating Software. The quality of CEL files was evaluated with RMAExpress software. The dataset's quality was assessed using AffyPLM. BRB-ArrayTools V4.5.0 was used to perform RMA normalization and class comparison studies. Array data uploaded to Gene Expression Omnibus (GEO) database and can be reached with GSE162860 accession number.

3.6.17 Gene set enrichment analysis

Gene set enrichment analyses (GSEA) were performed using the GSEA tool (v4.0.1) of Broad Institute [238] with default parameters. For the pairwise comparisons, we utilized C5 Gene Ontology biological process gene sets of molecular signature database (MSigDB) release 7.0. We removed gene sets with fewer than 15 genes and more than 500, and 3943 gene sets were included in the GSEA analysis of ATAD2. A similar approach was applied in the analysis of TAp73beta induced/uninduced samples of Hep3B for 12h, 24h, and 48h.

3.6.18 Comparative analysis of ATAD2 and Ki-67 expression

With publically accessible microarray gene expression data (GEO Accession: GSE63742) collected from rat liver during regeneration following two-third hepatectomy, we investigated the association between ATAD2 and Ki-67 expression in the liver. We used the web-based interactive program GEO2R (https://www.ncbi.nlm.nih.gov/geo/geo2r/) to examine the expression data. The highest expression levels for Mki-67 and Atad2 genes were obtained using the “Probe Set 1374775 at” for Mki-67 and “Probe Set 1376599 at” for Atad2 genes, respectively. At reporting, the means and standard deviations (SD) expression values for each time point were used. The TCGA LIHC tumor dataset, which is available at UCSC Xena Browser [239], was used to investigate the relationship between ATAD2 and Ki-67 expression in hepatocellular carcinoma. The data from recurrent tumor samples were not included in the subsequent analysis. In 50 normal solid tissues and 371 primary solid tumors of the liver, the

expression of ATAD2 and MKi67 was examined. Pearson's correlation approach is used to determine the relationship between ATAD2 and MKi67. The R packages dplyr (v1.0.4), ggplot2 (v3.3.3), and ggpubr (v0.4.0) were utilized in the comparative analysis of expression data and the generation of graphics.

3.6.19 Studies of ATAD2 response to different cell stresses

Hep3B, HepG2, and SKBR3 cells were seeded at 500k cell density on 60 mm dishes and incubated for 48h. After they reach 70% confluency, media were replaced with fresh media containing Tunicamycin (5µg/ml and 10µg/ml), Adriamycin (0.1µg/ml and 1µg/ml), or Thapsigargin (1µM and 2µM) per vehicle with their corresponding controls. After drug treatments for 12h and 24h, samples were collected for further analysis.

3.6.20 Immunoprecipitation

HEK293 cells were transiently transfected with or without the vector expressing GPR133 with the flag tag. After cells were collected, they were homogenized with a 5 ml homogenization buffer containing 0,25M Sucrose, 50mM Tris-HCl pH 7.6, 25mM KCl, 10mM MgCl2, 1x PI with 1% Triton X-100 by motor homogenizer (Stuart). Homogenates were centrifuged at 14.000xg for 10 minutes at 4°C. Supernatants were transferred to new tubes. Three different conditions were set up with mouse Flag, rabbit N-Terminal GPR133, and rabbit C-Terminal GPR133 primary antibodies. These primary antibodies (5ug of each) were added to 300ul of transfected and untransfected supernatants respectively. Samples were incubated at 4°C for 1h with gentle agitation. Next, 30 uL of Protein G-Agarose bead suspension (Roche) was added to samples and incubated overnight at 4°C with gentle agitation. Samples were collected by centrifugation for 20 seconds at 12.000 g. Supernatants were collected and indicated as flow through. The remaining pellets (beads) were resuspended in 1 ml Wash Buffer 1 (50mM Tris-HCl pH 7.5, 150 mM NaCl, 1% Nonidet P40, 0.5% Sodium deoxycholate, 1X PI) and incubated 20 min at 4 °C. Samples were collected by centrifugation for 20 seconds at 12.000 g, pellets were dissolved in Wash Buffer 2 (High Salt; 50 mM Tris-HCl pH 7.5, 500 mM NaCl, 0.1% Nonidet P40, 0.05% Sodium deoxycholate) and incubated 20 min at 4 °C. At last, pellets were resuspended with Wash Buffer 2 (Low Salt; 50 mM Tris-HCl pH 7.5, 0.1% Nonidet P40, 0.05% Sodium deoxycholate), incubated 20 min at 4 °C and pelleted. Final pellet dissolved in 50ul of 1x gel-loading buffer. Proteins were boiled for denaturing for 5 minutes at 95°C and beads were removed by centrifugation for 20 sec at 12.000 g at room temp. In western-blot analysis, unprocessed homogenates were loaded as inputs. Detection of the blot

was performed with rabbit N-terminal GPR133 antibody and rabbit HRP-conjugated secondary antibody sequentially.

4 RESULTS

4.1 The role of ATAD2 in HCC

4.1.1 ATAD2 is overexpressed in HCC tumors and correlated with Ki-67 expression

The elevation of ATAD2 expression in HCC was detected previously by our group and correlated with the poor prognosis. This correlation may be due to the increased proliferation rate of tumor cells during progression. To evaluate the clinical importance of ATAD2 in HCC, its expression and correlation with proliferation were tested with Ki-67(encoded with MKI-67 gene) that is a well-known cell proliferation marker widely used in the clinical course of cancer. The expressions of ATAD2 and Ki-67 were analyzed in The Cancer Genome Atlas (TCGA) data available at UCSC Xena Browser [239]. As shown in Figure (5A) left panel, the expression of transcripts was upregulated significantly ($p<0.001$) in HCC samples ($n=371$) in comparison to non-tumor liver samples ($n=50$). Similarly, the proliferation marker, Ki-67 expression was also significantly elevated in HCC tumors in respect to non-tumors as in figure (1A) right panel. To assess the similarity pattern of ATAD2 and Ki-67 in patient samples, Pearson correlation analysis was performed. The analysis as in Figure (5B) demonstrated a significant correlation between ATAD2 and Ki-67 expression ($R=0.61$, $p<2.2e-16$) in HCC.

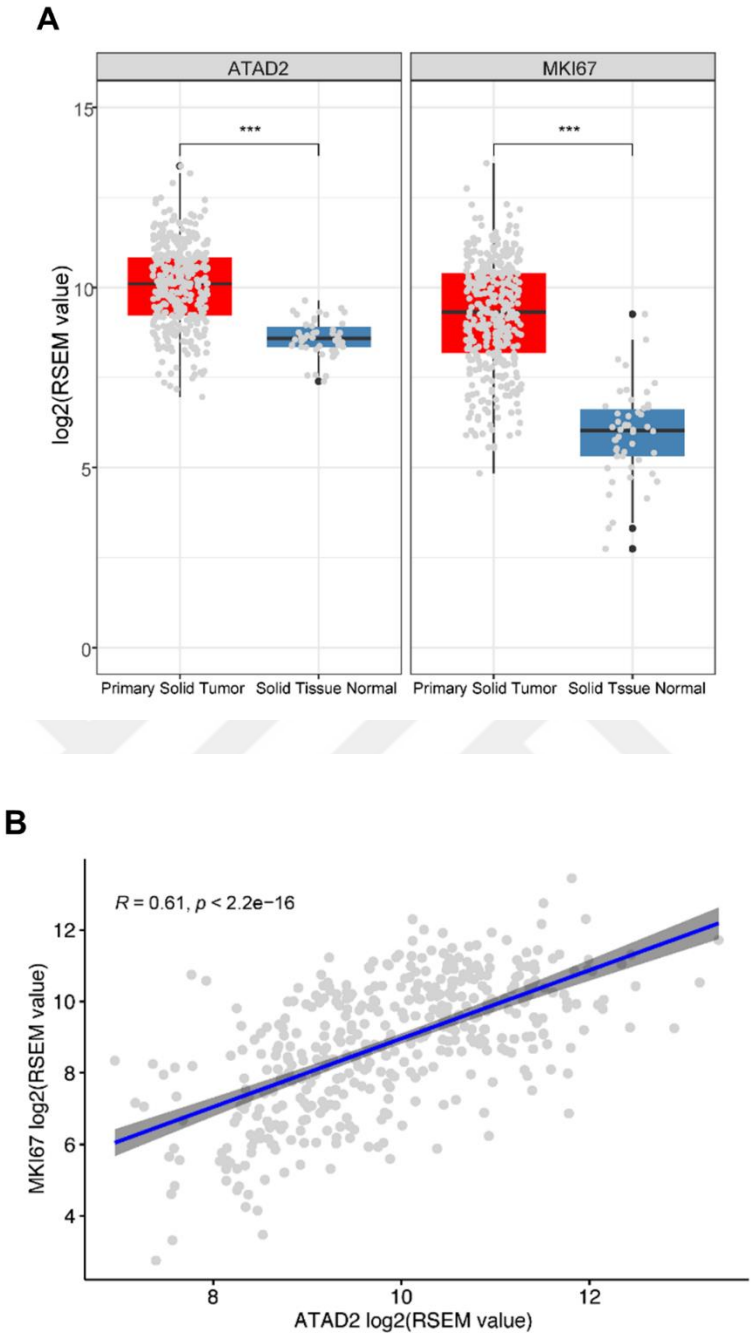

Figure 5: ATAD2 expression is induced in human HCC in correlation with Ki-67.
(A) Both ATAD2 and Ki-67 transcripts are induced significantly in normal liver and HCC samples in TCGA collection expression levels. (B) Highly significant correlation between ATAD2 and Ki-67 expression in HCC. MKI67: Human gene encoding Ki-67 [240].

4.1.2 ATAD2 and Ki-67 expression correlated in rat liver regeneration

The data obtained from HCC samples suggested that the elevation of ATAD2 expression is in correlation with Ki-67 in the liver, maybe due to normal cell proliferation. We further investigated this phenomenon with a microarray expression dataset (GEO Accession: GSE63742) to compare ATAD2 expression with the expression of two cell proliferation markers, Cyclin D1 and Ki-67, during liver regeneration induced in rats by partial hepatectomy. According to the expression of transcripts in time-course as in Figure 6, all transcripts showed low expression at the initial stage of regeneration up to 12 hours. Then, their expression reached maximum levels between 24h-36h. Following that, the levels of Atad2, Ki-67, and Cyclin D1 transcripts gradually decreased and reached starting values after 168 hours. Interestingly, Cyclin D1 showed another increase at 72h.

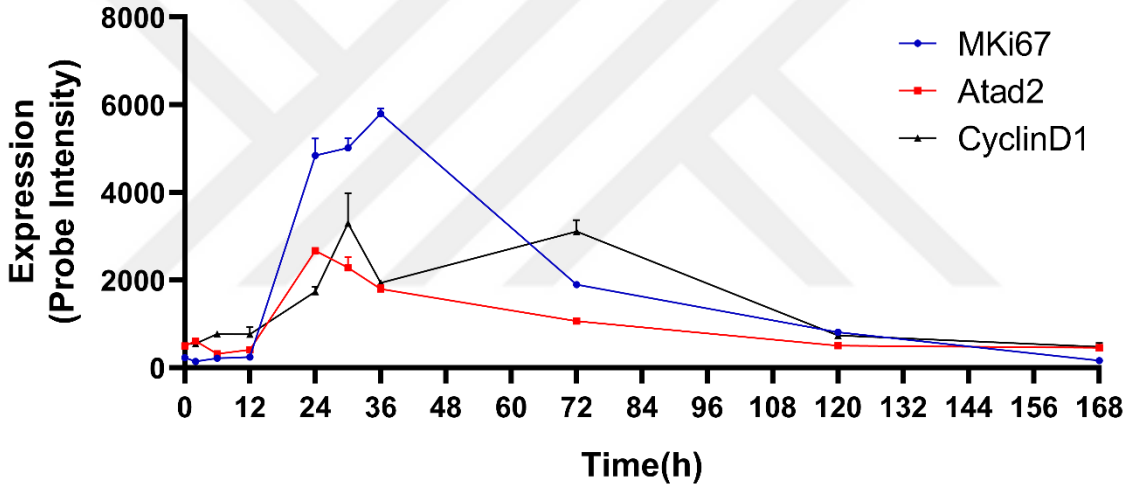

Figure 6: ATAD2 expression profile during rat liver regeneration with proliferation biomarkers Cyclin D1 and Ki-67.

MKi67: Rat gene encoding Ki-67 [240]

4.1.3 ATAD2 is highly expressed in proliferating HCC cell lines.

As previously reported in Yildiz et al. 2013, ATAD2 expression was not observed in freshly isolated human hepatocytes at the protein level by western blot analysis. However, HCC cell lines showed consistent expression with varying intensities. Here, we complemented the HCC cell line data with immunofluorescence studies. We showed the specificity of the nuclear presence of ATAD2 by attenuating its expression with siRNAs. In addition, ATAD2 staining displayed a good correlation with nuclear Ki-67 staining which is a well-known proliferation

marker largely used for tumor pathology (Figure 7). The combination of previous and recent data reveals that ATAD2 expression in the liver should not be just related to liver malignancy and may correlate with the proliferation state of liver tissue.

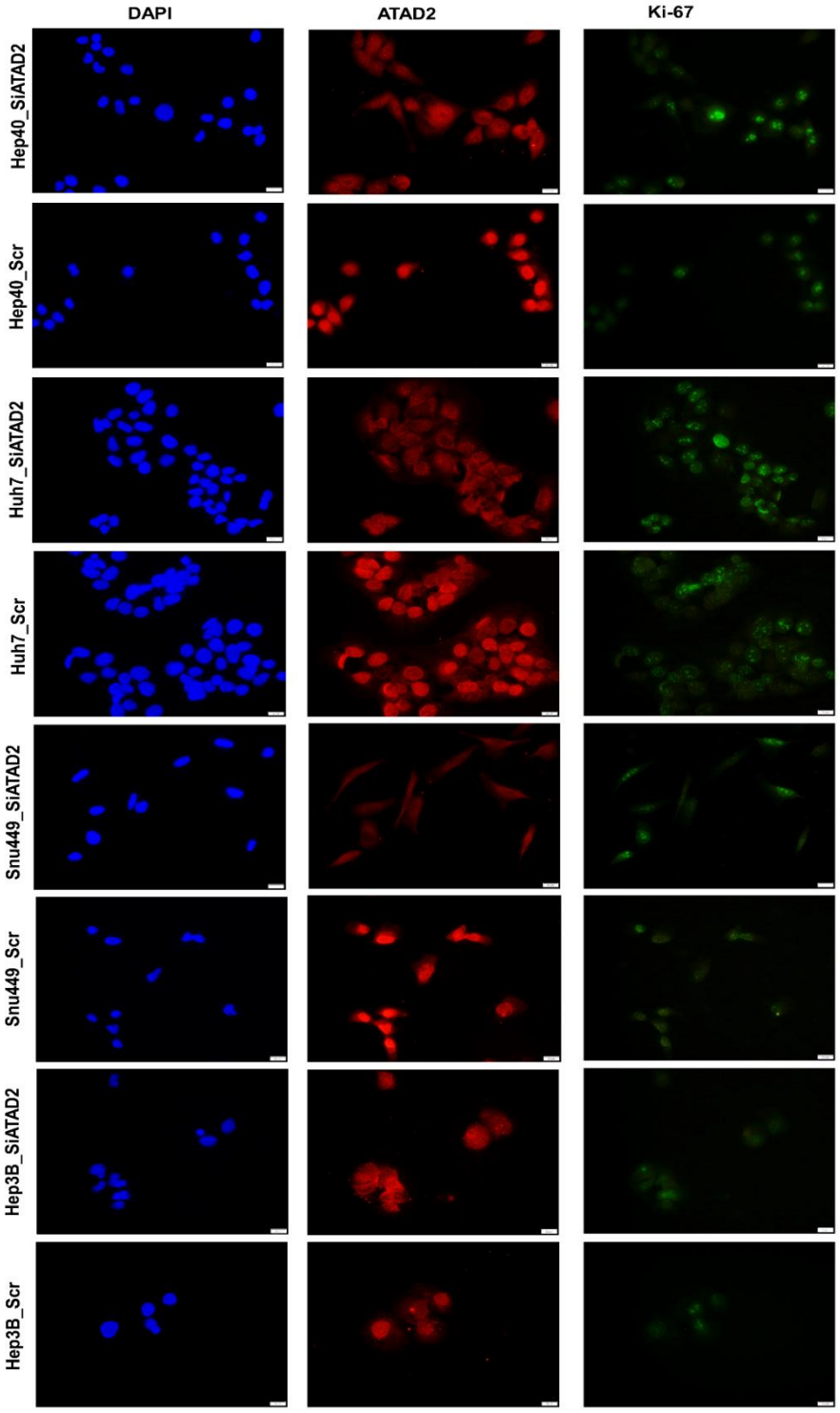

Figure 7: Immunofluorescence imaging of HCC cells indicating nuclear staining of ATAD2 mirroring Ki-67 staining [240].

4.1.4 Gene expression response of HCC cells to ATAD2 depletion

Before the gene expression analysis with microarray, we determined the efficiency of ATAD2 depletion in Hep3B, PLC/PRF/5, and SNU449 cell lines. Samples transfected with siRNA pool and control were evaluated at mRNA and protein level. The real-time PCR analysis showed that the siRNA pool significantly decreased the expression of ATAD2 transcripts as in Figure 8A. Besides transcripts, transfection of siATAD2 efficiently abolished the ATAD2 protein expression in both SNU449 and Hep3B cell lines (Figure 8B).

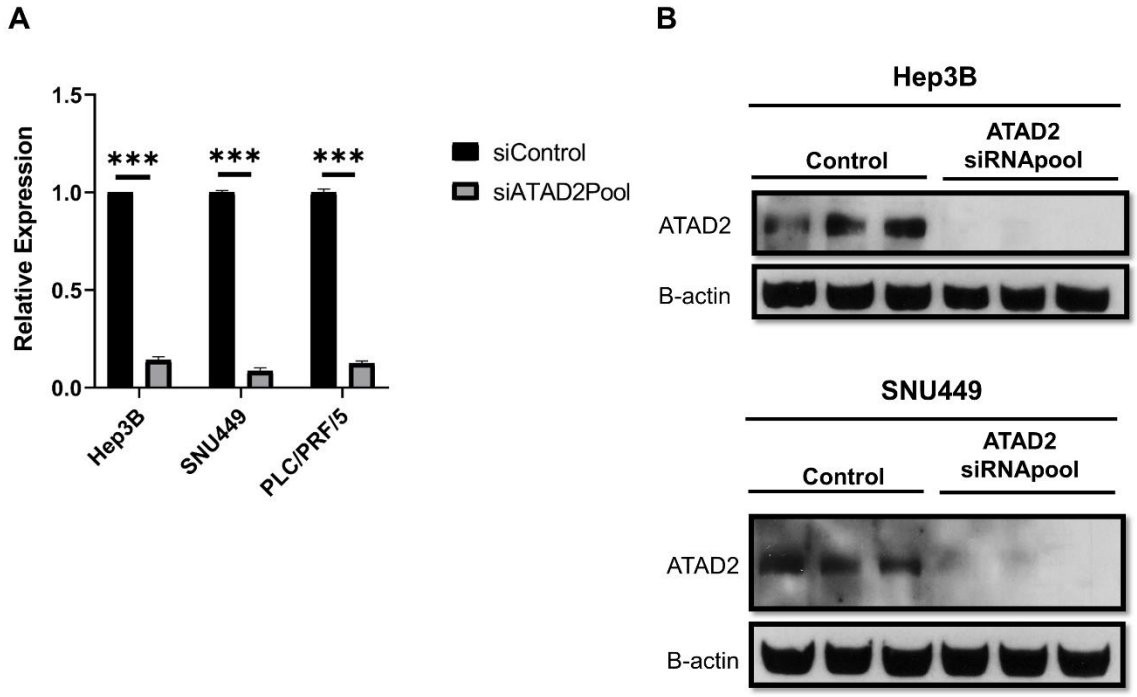

Figure 8: The efficiency of ATAD2 knock-down demonstrated by (A) real-time PCR in Hep3B, SNU449, and PLC/PRF/5, and (B) western blot analysis in Hep3B, and SNU449 before transcriptome analysis with microarray [240].

Firstly, we decided to investigate the role of ATAD2 in HCC cells by comparing expression levels of RNAs in the presence as well as under suppression of ATAD2 expression. As a first step, microarray analysis was performed with ATAD2 depleted and control samples of Hep3B, SNU449, and PLC/PRF/5 cells. Differential expression analysis was performed to determine significant changes in gene expressions across pairwise comparisons and genes have filtered with false discovery rate (FDR) ≤ 0.05 and LogFC ≥ 0.6 | LogFC ≤ -0.6 as thresholds. Interestingly, the number of differentially expressed genes (DEGs) varied in numbers based on the cell line. While Hep3B seemed the most altered cell line with 471 upregulated and 326

downregulated genes in response to ATAD2 silencing, few genes were observed in SNU449 and PLC/PRF/5 cells as given in Table 7.

Table 7: Number of deregulated genes in response to ATAD2 depletion.

	Hep3B	**SNU449**	**PLC/PRF/5**
Upregulated	471	3	6
Downregulated	326	6	36
Total	797	9	42

We further deepen the expression analysis with Gene Set Enrichment Analysis (GSEA) to associate the ATAD2 depletion and its consequences. The program analyzed 3943 gene sets and filtered in accordance with the total number of enriched and significantly enriched ($p<0.01$, $p<0.05$ or $FDR<0.25$) gene sets of each phenotype. The results of the program for each phenotype were summarized in Figure 9 for two conditions of three cell types. Based on FDR scores of ATAD2 silenced phenotype, 421 gene sets were significantly enriched in Hep3B whereas SNU449 showed 446 gene sets. Interestingly no significant gene set was provided by the program for PLC/PRF/5. At the same time, few gene sets were enriched in control groups of Hep3B and SNU449 as 2 and 14 respectively. Whereas no gene sets were significantly enriched at $FDR<0.25$ for ATAD2 silenced phenotype, 288 gene sets were enriched in control phenotype.

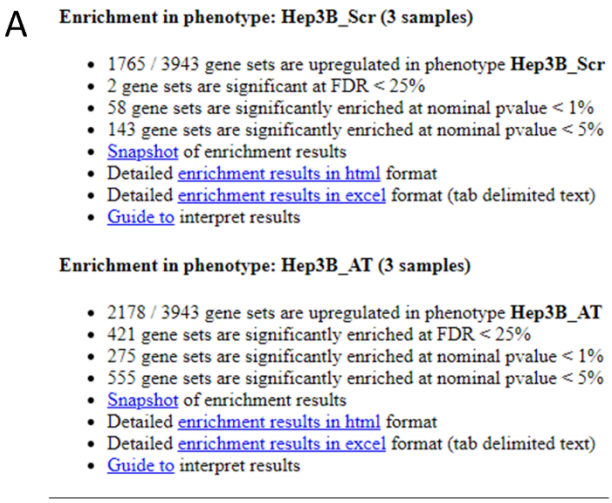

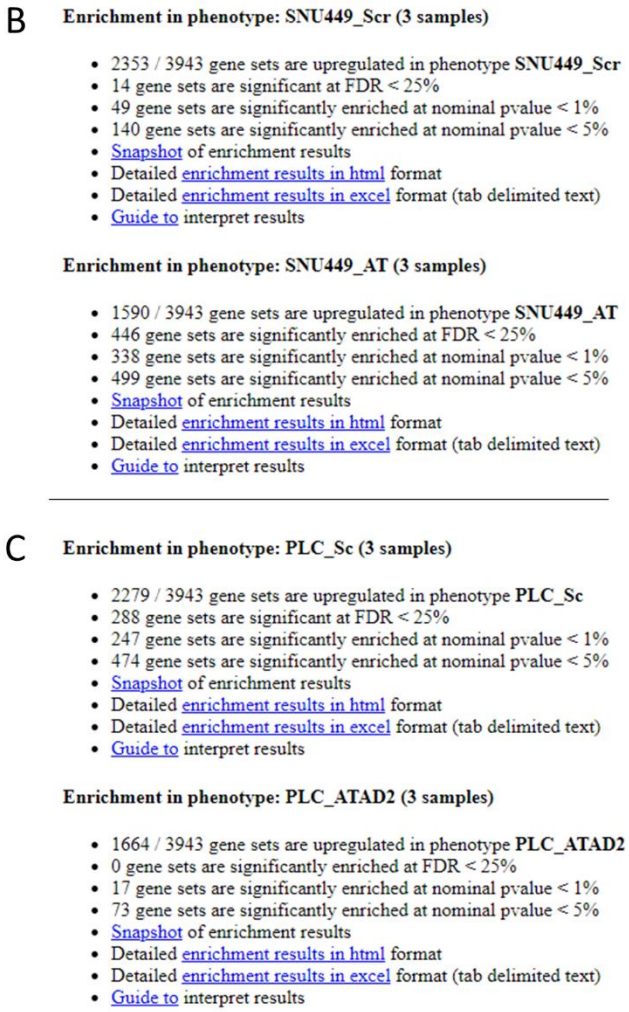

Figure 9: Summary of GSEA results for Hep3B, SNU449 and PLC/PRF/5
(A) The results of GSEA for Hep3B control and ATAD2 silenced phenotypes (B) The results of GSEA for SNU449 control and ATAD2 silenced phenotypes (C) The results of GSEA for PLC/PRF/5 control and ATAD2 silenced phenotypes.

We continued the analysis of enriched gene sets in ATAD2 silenced phenotype in details with narrowed FDR< 0.05 as listed in Figure 10. Interestingly, gene sets related to Endoplasmic-reticulum stress such as Endoplasmic-reticulum-associated protein degradation (ERAD) and Unfolded Protein Response (UPR) were enriched in Hep3B cell line. Whereas gene sets associated with cell division, especially cytokinesis were enriched in SNU449.

A

NAME	SIZE	ES	NES	NOM p-val	FDR q-val	FWER p-val
GO_RECEPTOR_CATABOLIC_PROCESS	33	-0.71556	-2.41092	0	0	0
GO_IRE1_MEDIATED_UNFOLDED_PROTEIN_RESPONSE	60	-0.57097	-2.18684	0	0.01907299	0.023
GO_PROTEIN_EXIT_FROM_ENDOPLASMIC_RETICULUM	44	-0.56722	-2.06175	0	0.021632412	0.149
GO_RESPONSE_TO_ENDOPLASMIC_RETICULUM_STRESS	260	-0.43404	-2.10661	0	0.021917682	0.076
GO_NUCLEOTIDE_SUGAR_BIOSYNTHETIC_PROCESS	22	-0.70673	-2.15444	0	0.023266364	0.041
GO_NEGATIVE_REGULATION_OF_MACROAUTOPHAGY	28	-0.62827	-2.07022	0	0.023417687	0.135
GO_RETROGRADE_TRANSPORT_ENDOSOME_TO_GOLGI	76	-0.51245	-2.09671	0	0.023531357	0.094
GO_UBIQUITIN_DEPENDENT_ERAD_PATHWAY	70	-0.51406	-2.06198	0	0.023598995	0.149
GO_ERAD_PATHWAY	92	-0.50433	-2.11302	0	0.023783516	0.068
GO_LYSOSOMAL_TRANSPORT	101	-0.48899	-2.07238	0	0.025320042	0.131
GO_AMINO_ACID_ACTIVATION	48	-0.56362	-2.11843	0	0.027755514	0.063
GO_REGULATION_OF_AUTOPHAGOSOME_ASSEMBLY	32	-0.61233	-2.07383	0	0.027880196	0.129
GO_CYTOSOLIC_TRANSPORT	146	-0.45237	-2.02884	0	0.030400146	0.236
GO_NLS_BEARING_PROTEIN_IMPORT_INTO_NUCLEUS	17	-0.69743	-2.02892	0	0.03273862	0.236
GO_ENDOPLASMIC_RETICULUM_UNFOLDED_PROTEIN_RESPONSE	108	-0.46929	-2.0186	0	0.033756074	0.275
GO_VACUOLAR_TRANSPORT	133	-0.44632	-2.00104	0	0.039647315	0.327
GO_VASCULAR_ENDOTHELIAL_GROWTH_FACTOR_PRODUCTION	33	-0.57415	-1.98291	0	0.044154376	0.402
GO_NEGATIVE_REGULATION_OF_EXTRINSIC_APOPTOTIC_SIGNALING_PATHWAY_VIA_DEATH_DOMAIN_RECEPTORS	35	-0.57551	-1.97799	0	0.04415771	0.42
GO_AMINOGLYCAN_BIOSYNTHETIC_PROCESS	109	-0.46306	-1.98677	0	0.04444247	0.381
GO_PROTEIN_LOCALIZATION_TO_VACUOLE	60	-0.5099	-1.97339	0	0.045039304	0.44
GO_REGULATION_OF_VACUOLE_ORGANIZATION	38	-0.55995	-1.96556	0	0.046952955	0.471

B

NAME	SIZE	ES	NES	NOM p-val	FDR q-val	FWER p-val
GO_MRNA_3_END_PROCESSING	94	-0.53384	-2.45006	0	0	0
GO_NCRNA_PROCESSING	352	-0.42689	-2.40658	0	0	0
GO_RNA_3_END_PROCESSING	133	-0.47584	-2.35243	0	4.20E-04	0.004
GO_MITOTIC_CYTOKINESIS	66	-0.54033	-2.2647	0	0.00111	0.011
GO_DNA_TEMPLATED_TRANSCRIPTION_TERMINATION	71	-0.50383	-2.23553	0	0.001357	0.014
GO_REGULATION_OF_CENTRIOLE_REPLICATION	21	-0.68561	-2.23022	0	0.001503	0.016
GO_MICROTUBULE_NUCLEATION	26	-0.62839	-2.20257	0	0.002285	0.025
GO_RIBOSOMAL_SMALL_SUBUNIT_BIOGENESIS	55	-0.52924	-2.20269	0	0.002357	0.025
GO_NUCLEOTIDE_EXCISION_REPAIR	105	-0.47458	-2.19562	0	0.0024	0.027
GO_NUCLEOTIDE_BINDING_DOMAIN_LEUCINE_RICH_REPEAT_CONTAINING_RECEPTOR_SIGNALING_PATHWAY	35	-0.57602	-2.18866	0	0.002573	0.03
GO_PROTEIN_LOCALIZATION_TO_CHROMOSOME	84	-0.48217	-2.15689	0	0.003872	0.047
GO_SPINDLE_ASSEMBLY	97	-0.47542	-2.15886	0	0.003888	0.046
GO_RNA_POLYADENYLATION	46	-0.53579	-2.14434	0	0.004916	0.061
GO_VESICLE_MEDIATED_TRANSPORT_BETWEEN_ENDOSOMAL_COMPARTMENTS	40	-0.55874	-2.13509	0	0.00517	0.066
GO_MATURATION_OF_SSU_RRNA	40	-0.54825	-2.13182	0	0.005402	0.07
GO_TRNA_METABOLIC_PROCESS	173	-0.40814	-2.12197	0	0.005775	0.08
GO_RRNA_METABOLIC_PROCESS	192	-0.41867	-2.11672	0	0.005902	0.083
GO_MITOTIC_SPINDLE_ASSEMBLY	52	-0.51548	-2.12203	0	0.005912	0.08
GO_POSITIVE_REGULATION_OF_CELLULAR_RESPONSE_TO_TRANSFORMING_GROWTH_FACTOR_BETA_STIMULUS	27	-0.59983	-2.12224	0	0.006056	0.08
GO_REGULATION_OF_CENTROSOME_DUPLICATION	41	-0.5428	-2.11114	0	0.006166	0.089
GO_RESPONSE_TO_ARSENIC_CONTAINING_SUBSTANCE	30	-0.58796	-2.09406	0	0.007534	0.112

Figure 10**:** Lists of significantly enriched gene sets in ATAD2 silenced phenotype of A) Hep3B and B) SNU449.

The results of GSEAs showed different pathway alterations in a cell line-dependent manner. The deeper analysis in gene sets in Hep3B, especially ER stress, showed that altered genes in gene sets were not increased considerably in terms of fold changes.

Next, we identified the differentially expressed genes which displayed more than 2-fold changes. The ATAD2 gene levels were the most downregulated gene with 11, 11 and 4-fold in Hep3B, PLC/PRF/5, and SNU449 respectively as expected. In Hep3B, the silencing of ATAD2 resulted in the downregulation of 57 and upregulation of 54 genes. The deregulated genes with ATAD2 silencing were found much lower numbers in PLC/PRF/5 cells. Interestingly, no genes were determined with altered regulation in SNU449 (Table 8).

To understand the association between ATAD2 silencing and gene functions alterations, Gene Ontology (GO) term cluster analysis was performed with FDR ≤ 0.05. The genes in up- and down-regulated gene lists were combined and analyzed.

Table 8: List of genes affected by ATAD2 knockdown in different HCC cell lines[240]

Cell	Up	Down	Total
Hep3B	54	57	111
PLC/PRF/5	9	7	16
SNU449	0	0	0

Not only the number of genes but also the associated gene ontologies have differed in cluster analysis. For PLC/PRF/5 cells, 11 GO terms were found ($p<0.05$), all of which were connected to three different functions: lipoprotein particle remodeling, positive modulation of the Wnt signaling pathway, and receptor-mediated endocytosis. In Hep3B cells, 33 GO terms with $p<0.02$ significance was identified which grouped into 17 gene functions. These functional groups were heterogeneous, some of them namely: responses to calcium or metal ions, ketone, glucocorticoid and cAMP, positive regulation of protein kinase B signaling, negative regulation of blood coagulation, Negative regulation of ion transport, zymogen activation, and apoptosis pathway (Table 9). The above-named GO function lists showed that the response against ATAD2 depletion has no commonality in Hep3B and PLC/PRF/5 cells based on GO term functions.

Table 9**:** Collapsed gene ontology functions affected by ATAD2 in two HCC cell lines*[240]

Hep3B (p Adj. <0.02)

GO term-based functions	GO terms
Response to calcium ion	1
Response to metal ion	1
Pos. regulation of protein kinase B sig.	3
Response to ketone	1
Neg. regulation of blood coagulation	11
Response to glucocorticoid	3
Neg. regulation of ion transport	1
Response to cAMP	1
Zymogen activation	1
Regulation of apoptotic signaling**	1

Regulation of response to wounding	1
Organic hydroxy compound transport	1
Reg. of heterotypic cell-cell adhesion	2
Glomerulus vasculature development.	1
Kidney vasculature development	2
Pos. regulation of hormone secretion	1
Response to organophosphorus	1

PLC/PRF/5 (p adj. <0.05)

GO term-based functions	GO terms
High-density lipoprotein particle remodeling	7
Pos. reg. of canonical Wnt signaling pw.	4
Receptor-mediated endocytosis.	1

*****Full list of related GO terms was presented in Appendix 1.

******Regulation of extrinsic apoptotic signaling pathway
via death domain receptors

4.1.5 ATAD2 expression in response to the treatment of Tunicamycin, Adriamycin, and Thapsigargin

4.1.5.1 ATAD2 expression is downregulated following Tunicamycin-induced Unfolded Protein Response

The exit from the cell cycle caused by the downregulation of Cyclin D1 levels is one of the biological repercussions of the Unfolded Protein Response (UPR) [241]. Based on this observation, we wanted to see if ATAD2 levels were also reduced during UPR triggered by Tunicamycin, a protein glycosylation inhibitor that triggers UPR. In the determination of ATAD2 levels, 12h and 24h time points were used with treatment doses of 5 µg/ml or 10 µg/ml in Hep3B and HepG2 cells. After treatments, cell lysates were tested for CHOP, an indicator of Endoplasmic Reticulum (ER) stress induced by Tunicamycin and PARP, an indicator of apoptosis, together with ATAD2 (Figure 11A and 11B). The western blot analysis showed that both HCC cell lines responded to tunicamycin with CHOP induction at the early stage (12h) as expected. While it diminished in Hep3B at 24h, the expression of CHOP was still detectable in HepG2. In parallel, cleaved PARP accumulation was identified in Hep3B cells at 12 hours, with

strong elevation at 24 hours. In HepG2 cells, cleaved PARP levels were slightly detected at 12 hours and moderate expression was detected at 24h. We also tested SKBR3, a breast cancer cell line with high basal ATAD2 expression. Interestingly, treatment of tunicamycin on this cell line also resulted in decreased ATAD2 levels in parallel with CHOP and cleaved PARP accumulation at 12h. The dramatic decrease of ATAD2 was also observed at 24hr (Figure 11C). Another ER stress agent with a different mode of action (Calcium pump inhibitor) Thapsigargin that also tested with two different doses on cell lines. However, no consistent change in ATAD2 levels was detected in Hep3B, HepG2, or SKBR3.

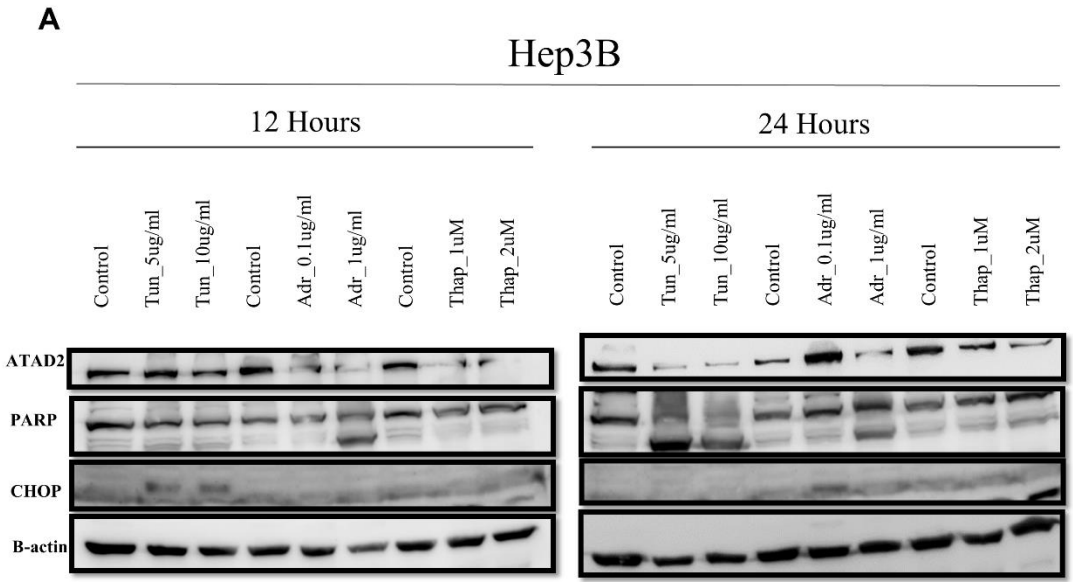

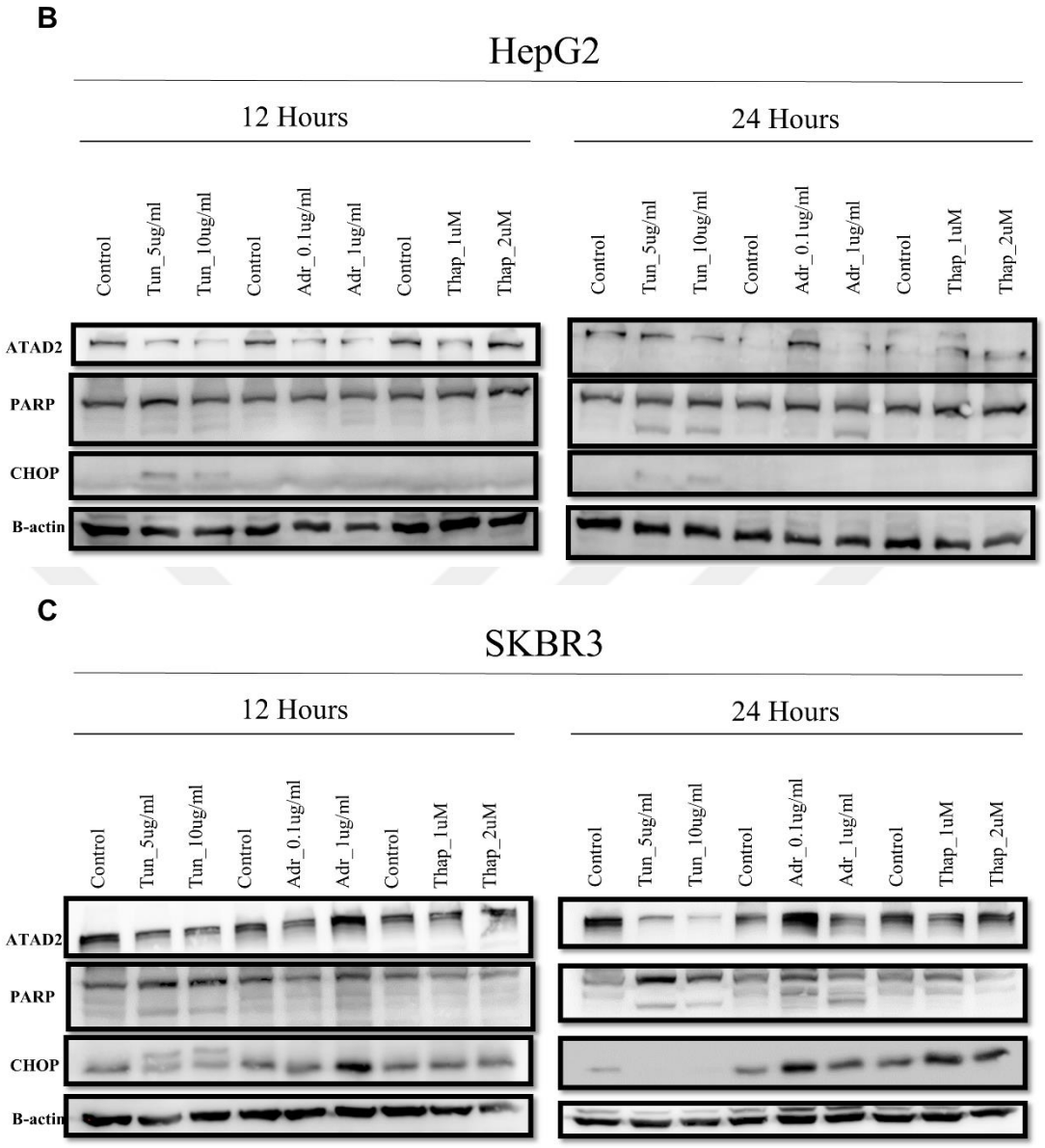

Figure 11: Western blot analysis of Hep3B, HepG2, and SKBR3 cell lines in response to different doses of Tunicamycin (Tun), Adriamycin (Adr), and Thapsigargin (Thap). Expression levels of ATAD2, cleaved PARP (apoptosis indicator), and CHOP (ER stress indicator) were demonstrated in response to drug treatments with controls in (A) Hep3B, (B) HepG2, and (C) SKBR3 cell lines for 12 hours and 24 hours[240].

4.1.5.2 Low dose Adriamycin treatment elevates ATAD2 expression in a time-dependent manner

The western blot analysis performed above showed that a low dose (0.1ug/ml) of DNA damage agent, Adriamycin, increased the expression of ATAD2 dramatically at 24 hours in all tested cell lines (Figure 11). To confirm this observation, we performed the same treatment as

triplicates in Hep3B cells as in Figure 12. As expected, the same accumulation of ATAD2 expression in response to low-dose adriamycin occurred at 24h. Cleaved PARP expression did not occur at the low dose of adriamycin at both 12h and 24h. However, a high dose of adriamycin (1ug/ml) increased the cleaved PARP levels at both 12h and 24h.

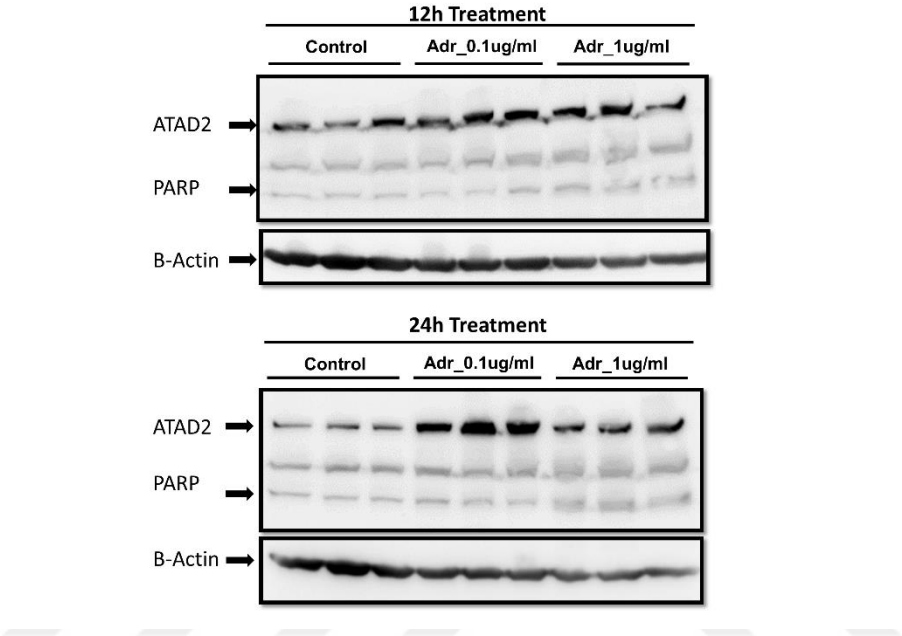

Figure 12: Western blot analysis of different doses of adriamycin treatment at different time points on Hep3B cells.

We performed cell cycle analysis in parallel to western blot to understand the cellular outcome of the accumulation of ATAD2 in response to low dose adriamycin in Hep3B at 24h. In addition, the same analysis was performed in parallel at Huh7 cells as well. As previously observed in Hep3B, ATAD2 levels were elevated in low dose treatment for 24h. Thereafter, in the cell cycle analysis for 24h, the cells in the G1 state dramatically increased from 31% to 84% with 0.1ug/ml Adriamycin treatment in Hep3B while cells in S state decreased from 23.8% to 6.5%. Accumulation of cells in the S phase and increased cleaved-PARP were observed with 1ug/ml adriamycin treatment in Hep3B cells. Unlike Hep3B, the low dose treatment of Adriamycin did not increase the ATAD2 protein expression and G1 cell distribution in Huh7. A high dose of Adriamycin affected neither ATAD2 nor cleaved-PARP levels while increased G2 phase cell distribution in Huh7 (Figure 13).

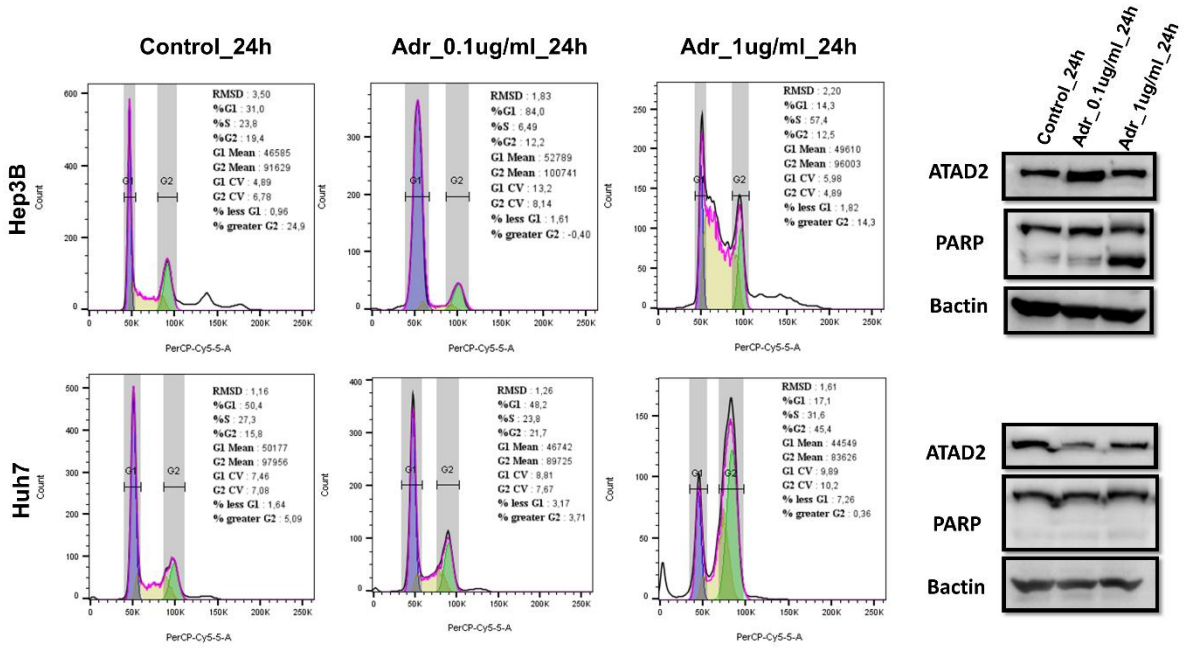

Figure 13: Flow cytometry and western blot analysis of Hep3B and Huh7 cells in response to different doses of Adriamycin (Adr) for 24h.

To sum up, ATAD2 is highly expressed in HCC tumors compared to non-tumor patient liver samples. The expression of ATAD2 is highly correlated with proliferation marker Ki-67 in HCC and rat liver regeneration samples. Moreover, ATAD2 expression changes in response to drug treatments which have a different mode of action, in dose- and cell-dependant manner. The bioinformatics analyses showed that the knockout of ATAD2 in HCC cell lines showed different cellular outcomes based on gene ontology functions.

4.2 The Determination of GPR133 in HCC

4.2.1 Determination of GPR133 as a candidate target

In order to determine potential therapeutic targets in HCC, we planned to hunt genes from microarray data that were previously generated by our group using Huh7 cell line clones which showed pre-senescence or immortal phenotype [7]. RMA normalized expression profiles were compared, and 507 genes were found to be increased 2 fold or more in the immortal group compared to controls.

We further analyzed these genes to narrow the list and understand the clinical significance. First, the list was ordered according to the geometric mean of intensities, and the first 200 genes were selected for further patient survival analysis (Appendix Table 2). These genes were analyzed individually in a web-based tool called SurvExpress [242]. Among six

databases under the liver cancer section, five of them were used for further analysis. One of them was removed from the analysis because of the small sample size of the database. Based on the significance ($p<0.05$) in patients' survival analysis among databases, 63 genes of 200 showed one or more significant correlation. Among these, 18 genes showed significant correlation within 2 or more datasets as in Table 10. These significantly correlated genes were further examined for their cellular location and functions in GeneCards [243] and Human Protein Atlas portal (www.proteinatlas.org) databases.

Table 10: The list of 18 genes upregulated in immortal phenotype.
The list of upregulated genes that are significantly correlated with patient survival within two or more liver databases of SurvExpress online tool. DS:Dataset, FC: Fold Change, IMM: Immortal, PS: Pre-senescence

Probe Set	Symbol	Name	Cellular Location (GENECARD /PROTEINATLAS)	pVal. DS1	pVal. DS2	pVal. DS3	pVal. DS5	pVal. DS6	# Of Sig.Data base	Parametric p-value	FC (IMM/PS)
201833_at	HDAC2	Histone deacetylase 2	Nucleus	0.05	0.015		0.05	0.009	4	0.0103662	2.0
220892_s_at	PSAT1	Phosphoserine aminotransferase 1	Cytosol	0.02			0.019	0.02	3	3.21E-05	2.8
202627_s_at	***SERPINE1***	Serpin Family E Member 1	Plasma Membrane /Extracellular Space			0.049	0.016	0.002	3	0.0004297	2.1
204987_at	ITIH2	Inter-alpha-trypsin inhibitor heavy chain 2	Golgi				0.018	0.05	2	0.0054188	2.0
212048_s_at	YARS	Tyrosyl-tRNA synthetase	Cytoplasm				0.0001	0.0007	2	1.94E-05	2.0
233878_s_at	XRN2	5'-3' exoribonuclease 2	Nucleolus/Nucleus				0.006	0.012	2	0.0009256	2.1
200755_s_at	CALU	Calumenin	ER/Golgi/Membrane				0.04	0.03	2	3.00E-07	2.0
212698_s_at	SEPT10	Septin 10	Cytoplasm/Actin Filaments				0.049	0.033	2	7.00E-07	2.1
203706_s_at	**FZD7**	Frizzled class receptor 7	Nucleoplasm/Plasma membrane				0.001	0.018	2	0.0000761	2
217127_at	CTH	Cystathionase (cystathionine gamma-lyase)	Cytoplasm	0.03		0.01			2	2.28E-05	3.3
209937_at	**TM4SF4**	Transmembrane 4 L six family member 4	Plasma Membrane/Cytoplasm		0.037	0.04			2	0.003809	2.7
212514_x_at	DDX3X	DEAD-Box Helicase 3, X-Linked	Nucleus/Cytosol/Extracellular Space				0.034	0.007	2	0.0058079	2.0
204993_at	GNAZ	G Protein Subunit Alpha Z	Nucleus/Plasma Membrane /Extracellular Space		0.002	0.05			2	< 1e-07	3.7
206535_at	**SLC2A2**	Solute Carrier Family 2 Member 2	Plasma Membrane				0.04	0.03	2	0.0009753	3.2
212233_at	MAP1B	Microtubule Associated Protein 1B	Cytosol/Cytoskeleton				0.02	0.017	2	1.00E-05	3.3
225396_at	RBBP4	RB Binding Protein 4	Nucleus/Cytosol				0.05	0.017	2	3.00E-07	2.3
218013_x_at	DCTN4	Dynactin Subunit 4	Nucleus/Cytosol/Cytoskeleton				0.001	0.001	2	3.60E-06	2.1
232267_at	**GPR133**	Adh. G Protein-Coupled Receptor D1	Plasma Membrane				0.002	0.008	2	0.0000002	3.2

To further narrow down the list, we evaluated the genes based on three main criteria. Selected genes: *I.* should be receptor and located on the cell surface that can make them easily targetable using antibody-based approaches, *II.* should not be expressed in critical organs since the absence of protein results in vital consequences for organism and *III.* how promising is the protein in literature among listed genes. Based on these, *GPR133* (*ADGRD1)* was selected as a candidate target for further analysis. We preferred *GPR133* for further analysis because it fits into the three main criteria as being a receptor on the plasma membrane, expressing low levels in the critical organs, and relatively less characterized.

Detailed analysis of *GPR133* from clinical perspective performed and illustrated in two different databases in Figure 14. In both databases, the risk group analysis graphs were plotted with expression values based on the prognostic index expression. It indicated the association of GPR133 expression difference between risk groups. The expression levels are higher in the high-risk group in comparison to the low-risk group. In addition, Kaplan-Meier survival plots showed the correlation of GPR133 expression with the survival of patients. High-risk group patients showed poor survival compared to the low-risk group.

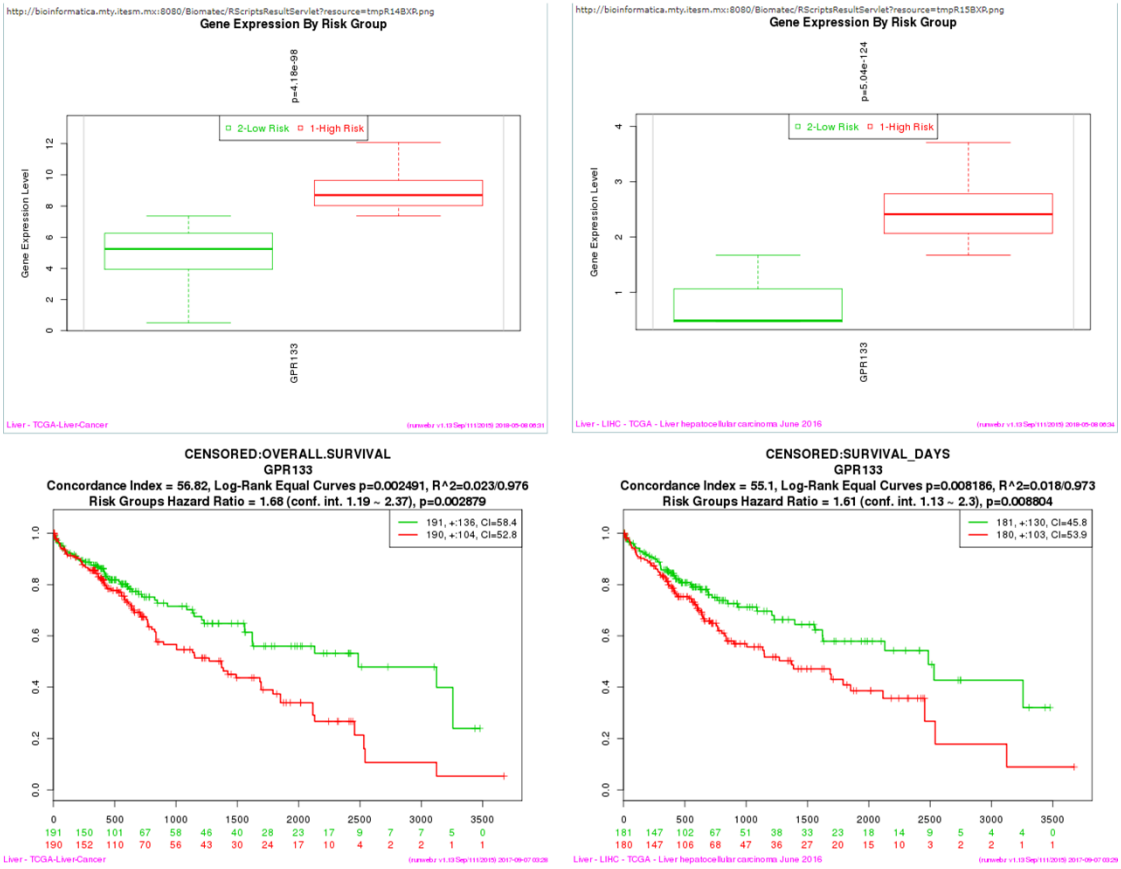

Figure 14: Gene expression and survival plots generated with SurvExpress in Liver TCGA datasets.

In the upper panel, the expression of GPR133 is significantly higher in the high-risk (Red) group than in the low-risk (Green) group. The Kaplan–Meier survival curves indicate poor survival of the high-risk group of patients (red) in respect to the low-risk group (green) at the lower panel. The x-axis indicates the monitored days of patients.

4.2.2 Transcriptional expression of GPR133 in HCC cell lines and patient samples.

The array data collected from the previous analysis were needed to be strengthened. Accordingly, we further checked the levels of GPR133 in liver cancer cell lines at the transcript level by RT-PCR. We detected mRNA expression of GPR133 with the primers designed against exon 21 and 22. These regions were conserved within most of the isoforms based on the conserved coding sequence information of Human GPR133 at USCS Genome Browser. In the analysis, besides 13 HCC cell lines, A542 (human pulmonary carcinoma cells) and HEK293 (human embryonic kidney) were also used. After RNA isolation, 1ug of each RNA sample was converted to cDNA and equal amounts of cDNA were used in RT-PCR.

The RT-PCR analysis showed different expression levels of GPR133/ADGRD1 among the HCC cell lines. Huh7 and PLC cell lines showed the highest expression among all cell lines tested. Hep40, Hep3B, and Mahlavu (MV) showed moderate expression, whereas HepG2, SKHEP1, SNU 182, 387, 398, 423, and 449 cell lines showed hardly any expression (Figure 15).

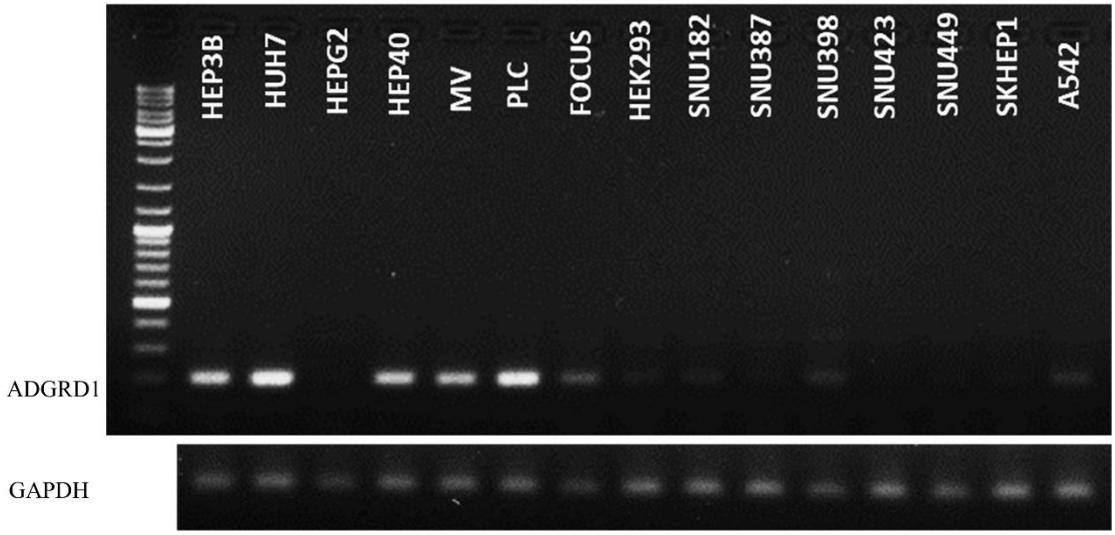

Figure 15: Expression analysis of GPR133/ADGRD1 in 13 HCC cell lines, HEK293, and A542.

An equal amount of total RNAs from cell lines were converted to cDNA and used to detect gene expression by RT-PCR. GAPDH was used as a control for expression analysis.

The same primer set was used to analyze cDNAs of the patient samples cohort that was kindly provided by Prof. Neşe Atabey. In the cohort, we tested 3 normal liver tissues, 10 pairs of cirrhosis and HCC tissue samples, and two additional cirrhotic samples. The RT-PCR results

showed GPR133/ADGRD1 was barely or not expressed in 3 normal liver samples. However, elevated expression of GPR133/ADGRD1 levels was detected almost in all cirrhosis and HCC samples. In addition, in some cases, there was an increase in GPR133/ADGRD1 expression when HCC samples compared with its cirrhotic pairs such as in patient 4, 10, and 13. However, the expression difference between all pairs of cirrhosis and HCC samples did not show an absolute correlation in the direction of increase or decrease (Figure 16).

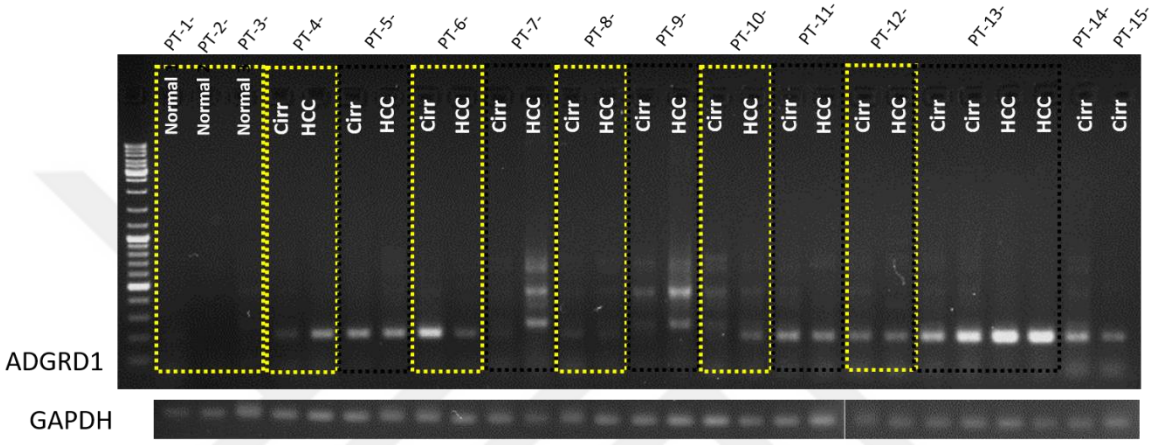

Figure 16: Expression analysis of GPR133/ADGRD1 by RT-PCR in patient sample cohort that consists of 3 normal liver tissue (Normal), 10 pairs of cirrhosis (Cirr), and HCC tissue samples, and two additional cirrhotic samples without their HCC pairs. Cirrhosis and HCC tissue sample pairs were grouped in a rectangle for each patient (PT).

4.2.3 The expression of two main isoforms of GPR133/ADGRD1 differs among cancers

To evaluate the expression of GPR133/ADGRD1 isoforms at the transcriptional level in different cancers, we collected tumor and normal patient samples of five cancers from TCGA database. The phenotypes: “Primary Solid Tumor" and "Solid Tissue Normal" groups were collected for further analysis and other patient samples like recurrence or metastatic phenotypes were discarded from datasets. We mainly compared the expression of two major isoforms of GPR133/ADGRD1 from five of which were isoform 1: “isoform_uc001uit” and isoform 2: “isoform_uc010tbm”. These two isoforms were analyzed among five cancers with high sample-sized cancers such as Liver Hepatocellular Carcinoma (LIHC), Breast Invasive carcinoma (BRCA), Lung Adenocarcinoma (LUAD), Prostate Adenocarcinoma (PRAD), and Colon Adenocarcinoma (COAD). Isoform 2, known as alternative form with additional exon at N terminal position 3rd was compared with main isoform 1. The Log2 values of transcript per

million (TPM) for each patient and significance in comparison of normal and tumor data were given in Figure 17. In contrast to our expectation, isoform 1 of GPR133/ADGRD1 decreased significantly in tumors of all cancers. Moreover, a decline of isoform 2 in tumors, was also observed in BRCA, LUAD, and PRAD. The statistical analysis listed in Appendix Table 3.

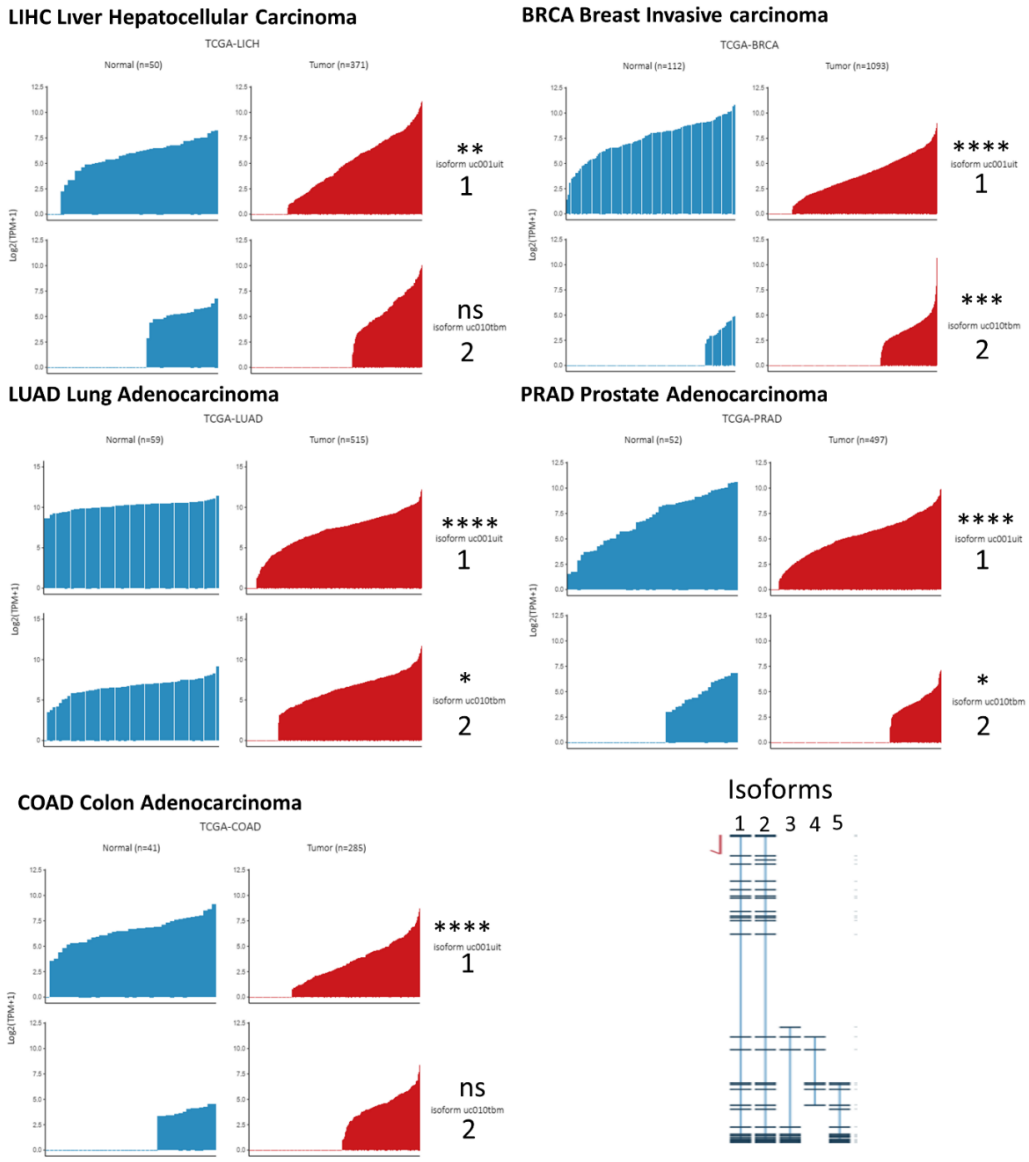

Figure 17: Comparative expression of two GPR133/ADGRD1 isoforms in normal and tumor samples.

Bar plots of isoform 1 (1) and isoform 2 (2) with log2 values of each patient in normal (blue) and tumor (red) tissues of cancers. The significance in comparison between normal and tumor samples indicated as ns: $p > 0.05$, *$p \leq 0.05$,** $p \leq 0.01$,*** $p \leq 0.001$, and **** $p \leq 0.0001$. The presence of exons in five isoforms (1-5) were illustrated as dashed lines at the right bottom corner of the figure.

4.2.4 Confirmation of rabbit polyclonal amino and carboxyl GPR133 antibodies

Our previous investigations showed the differential expression of GPR133 in cancers including HCC at the transcriptional level. In order to test the expression of GPR133 and further analysis for functional analysis at protein levels in HCC, we tested commercially available antibodies against both native and ectopic GPR133 protein but could not succeed. Thus, inadequate performance of commercial antibodies against GPR133 forced us to generate new antibodies against GPR133. Antibodies against both N and C terminal epitopes of GPR133 were generated by the company called Covalab. After immunization of animals, the affinities were followed up by ELISA tests for each intermediate bleedings of animals at days 0, 53, and 74 as in Figure 18. The immunoreactivity of serum was considered very good when the optical density (OD) reading at 450nm is above one after dilution 8000. In both cases, the immunoreactivities against antigens showed good performance. The final sera of each rabbit were collected and purified in respective columns as Amino (N-terminal) and Carboxy (C-terminal) antibodies.

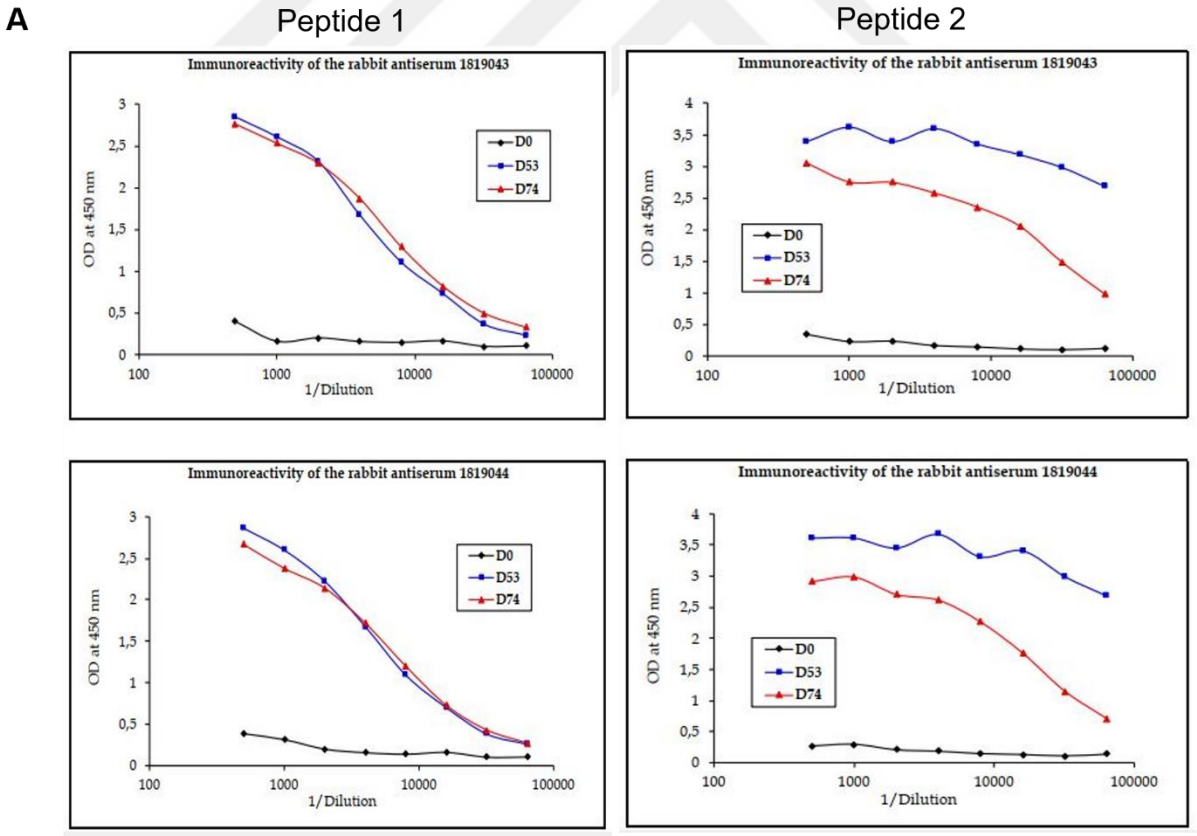

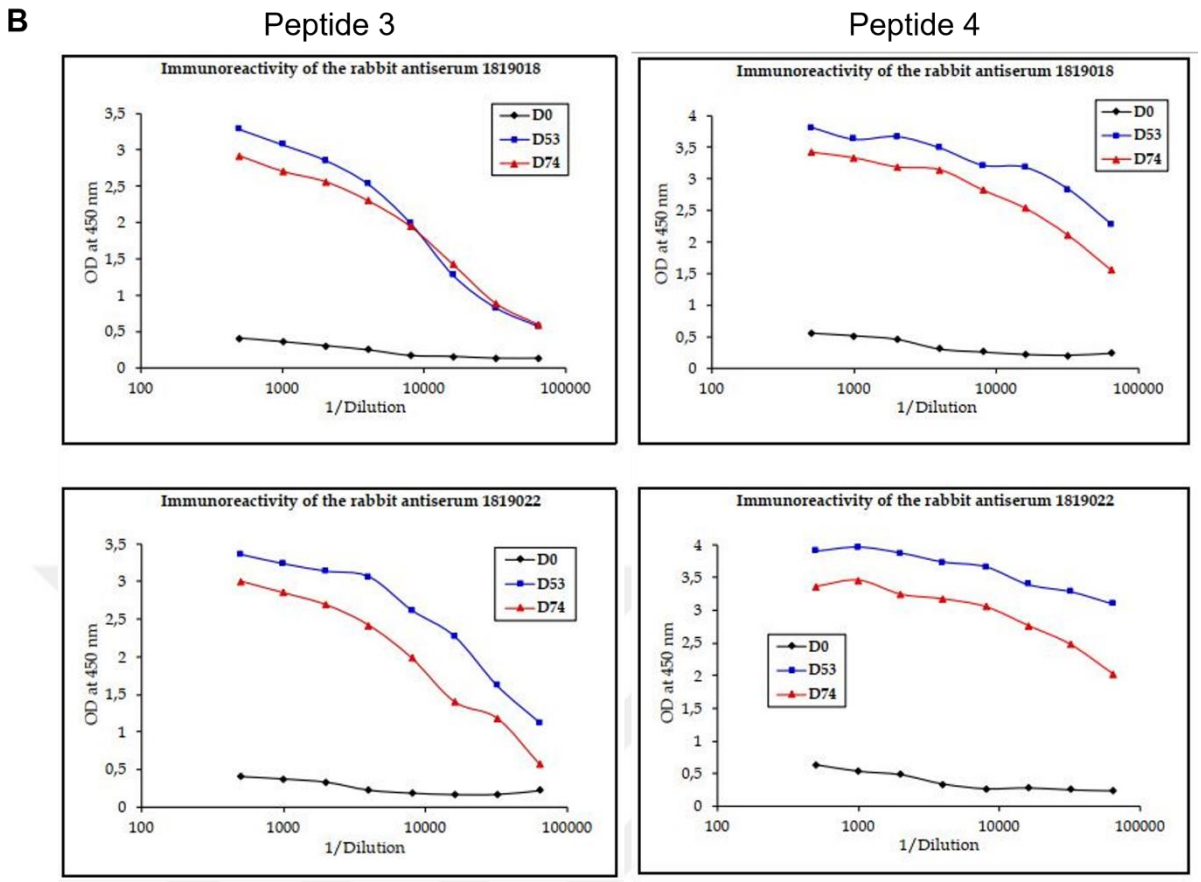

Figure 18: ELISA analysis of rabbit serum samples collected at different days against their antigen peptides.

Absorbance at 450nm against 1/dilution was plotted in corresponding animals for Days 0, 53, and 74. A) The plots generated for 2 rabbits (1819043 and 1819044) corresponds to N-terminal epitopes: peptide 1 and 2 B) The plots generated for 2 rabbits (1819018 and 1819022) corresponds to C-terminal epitopes: peptides 3 and 4.

Before the applications of antibodies generated by Covalab, we constructed a C-terminal flag tagged GPR133 plasmid to use as the positive control with ectopic expression. To test the construct, expression was detected with flag antibody firstly. HEK293T cells were transfected with the plasmid for 48 hours and visualized with confocal microscopy. As expected, transiently transfected cells were flag positive, and the expression was localized at the cell membrane (Figure 19A).

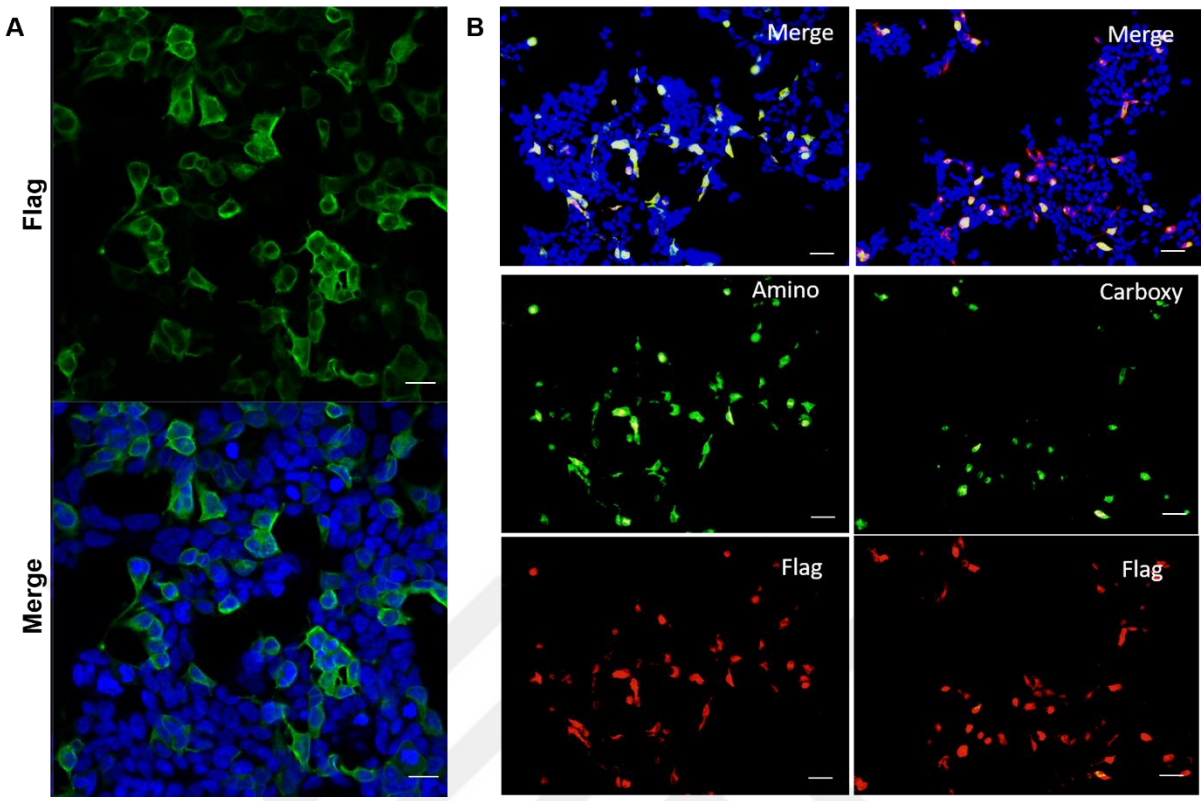

Figure 19: The confirmation of flag tagged GPR133 plasmid in HEK293 cells.
A) Detection of transient expression of flag tagged GPR133 in HEK293 cells with flag antibody. Flag antibody with green fluorescence was localized at the membrane of the cells. DAPI with blue fluorescence counterstained for nucleus. Cells visualized with confocal microscopy at 25x magnification B) Transiently transfected HEK293 cells co-stained with flag and GPR133 Amino (N-Terminal) or Carboxy (C-Terminal) antibodies. Both Flag (Red) and GPR133 (Green) signals overlapped. Detection was performed with fluorescence microscopy at 10x magnification.

After confirmation of the plasmid, we further analyzed the new N and C terminal antibodies against GPR133 with the same approach. HEK293 cells were transiently transfected with the C terminal flag tagged GPR133 vector. Cells were co-incubated with the flag (Red) and amino N or carboxy C terminal antibodies of GPR133 (Green). In both cases, flag and GPR133 antibodies were overlapped in Figure 19B as expected. Undoubtedly, the antibodies generated against GPR133 epitopes specifically recognized the GPR133 protein in immunofluorescence application.

Further, we analyzed the antibodies of GPR133 for western blot applications. HEK293T cells were transiently transfected with confirmed flag tagged GPR133 plasmid or not for

control. Total protein lysates were subjected to incubation with capture antibodies: mouse Flag, N-Terminal GPR133, and C-Terminal GPR133 for immunoprecipitation (IP). Captured proteins with different primary antibodies and their remaining total proteins called flow-through, were detected with rabbit secondary HRP-conjugated antibody as in Figure 20.

At first, we performed immunoprecipitation analysis to confirm the specificity of the antibodies and band size of the protein. Detection was performed with rabbit secondary HRP-conjugated antibody. We detected two specific bands around 75kD and 100kD with both flag and GPR133 antibodies. Besides, the band around 55kD resulted from the recognition of rabbit primary and secondary antibodies, in other words, overlapped hosts. As a result, our ectopically expressed GPR133 protein with flag tag can be captured specifically by three antibodies and gave two major bands in western blot as in Figure 20.

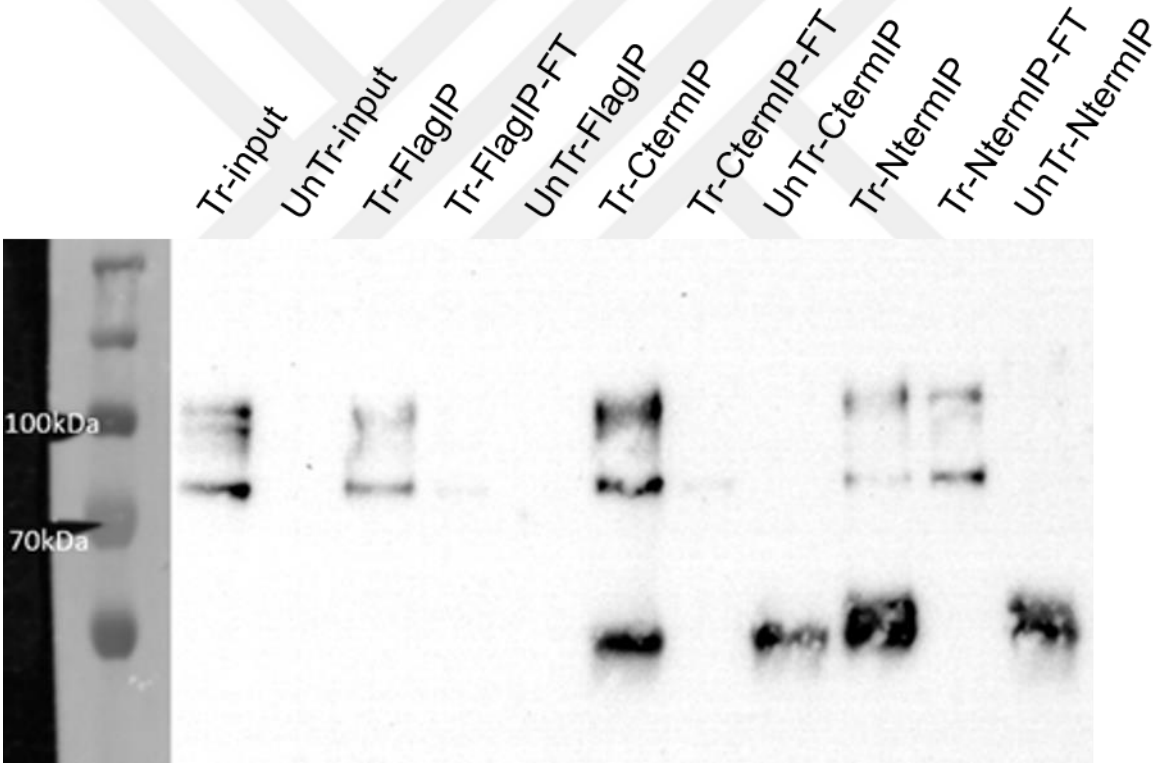

Figure 20: Westernblot analysis of ectopically expressed flag tagged GPR133 after immunoprecipitation by Flag, N-terminal, and C-terminal antibodies. Tr: Transfected, UnTr: Untransfected, IP: Immunoprecipitated, FT: Flow-through.

4.2.5 Ectopic overexpression of GPR133 with Tet-inducible system in HepG2 clones

To search for the functional outcomes of GPR133 overexpression in HCC, inducible HepG2 clones were used. HepG2 clones 15-1 and 15-10 were selected considering the GPR133

expression levels in the absence or presence of doxycycline. Clone 2-10 showing leaky expression in doxycycline response was used as the control because of its equal expression in both cases (Figure 21).

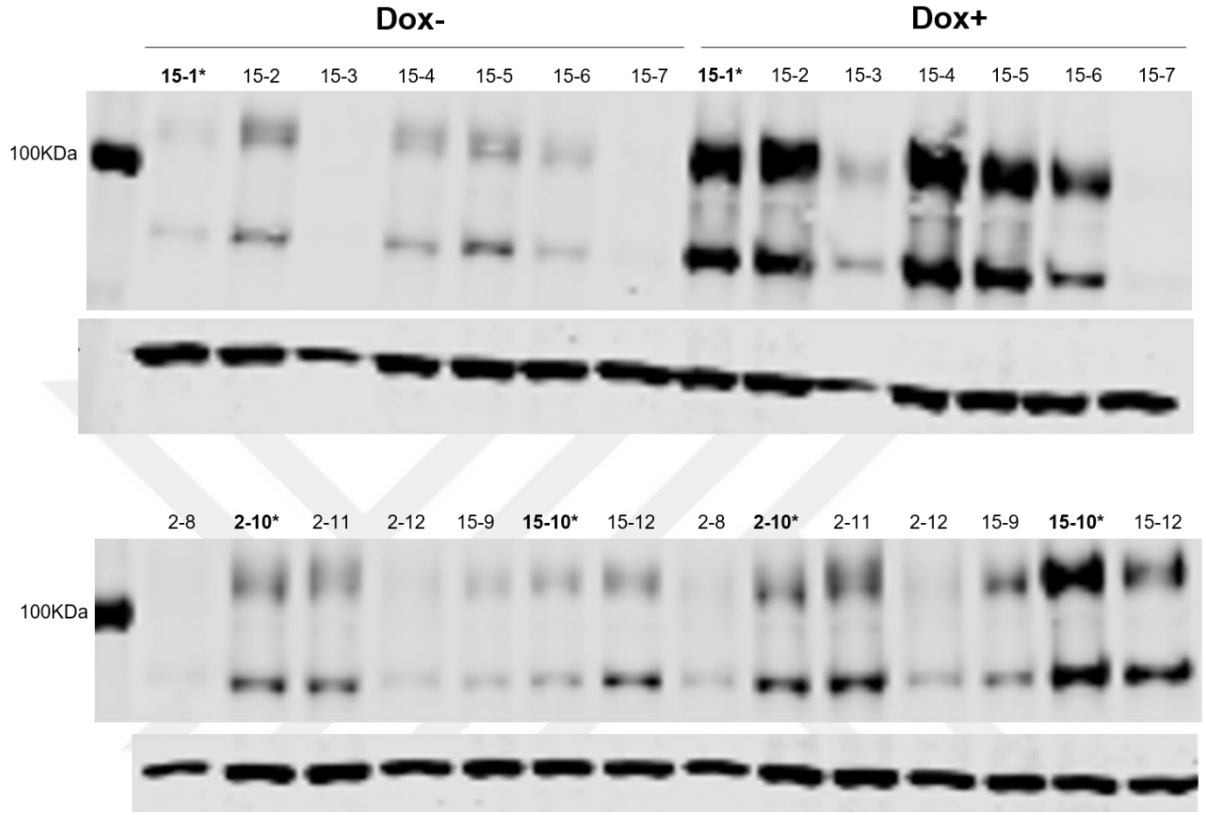

Figure 21: Western blot analysis of Tet-inducible clones for HepG2-GPR133 monoclones. The induction of GPR133 expression was generated with Doxycycline (Tetracycline analog) addition. The expression in response to doxycycline absence (Dox-) on the left and presence (Dox+) on the right were shown for every monoclones. Clones indicated bold with "*" were used in the following experiments. The 100kDa of the marker is indicated in the first well.

When we examined the results of the SRB assay, which was used to understand the effect of GPR133 overexpression on cell proliferation, we discovered that increasing GPR133 expression in both clones of HepG2 cells resulted in a substantial but minor difference in cell proliferation. There was a decrease in the control group with leaky expression, but it was not significant (Figure 22A). Further research was carried out to determine the impact of GPR133 overexpression on the ability of HepG2 clones to form colonies. The same clones were utilized in the colony formation experiment. Overexpression of GPR133 did not result in any notable changes in colony numbers (Figure 22B).

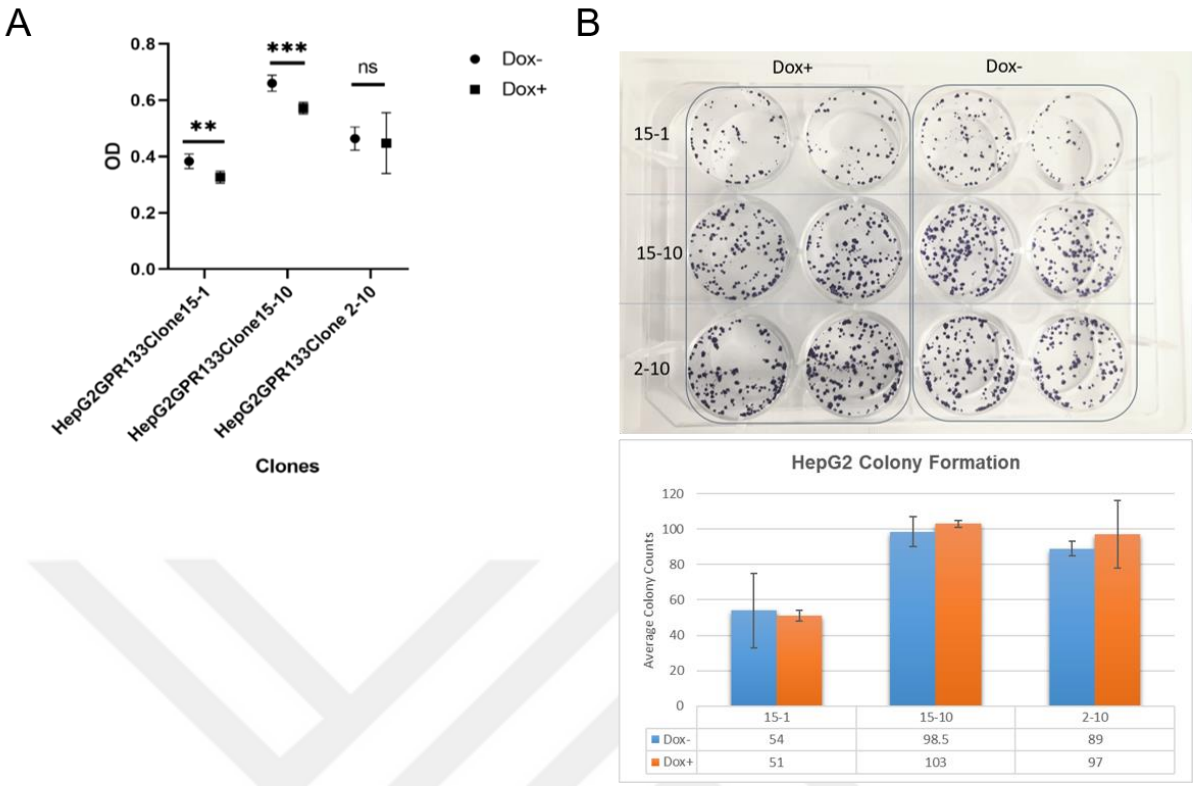

Figure 22: Analysis of HepG2 clones for proliferation and colony formation in response to GPR133 expression.

A) The SRB analysis of HepG2-GPR133 clones treated with or without doxycycline. B) Colony formation assay of HepG2-GPR133 clones treated with or without doxycycline. Picture of fixed and crystal violet-stained clones according to the presence of doxycycline. Bar plots for colony numbers of clones were also given.

To evaluate the decrease in cell proliferation with overexpression of GPR133, cell cycle analysis was performed with the same HepG2 clones. The accumulation of cells according to phases did not show any changes among clones except the slight difference in 15-1. The cell distribution of HepG2_15-1 clone in >4N phase increased from 16.2% to 25% and decreased in <2N phase from 17.4% to 8% with overexpression of GPR133, which may be an indication of obstacle in transition from G2 to M stage (Figure 23).

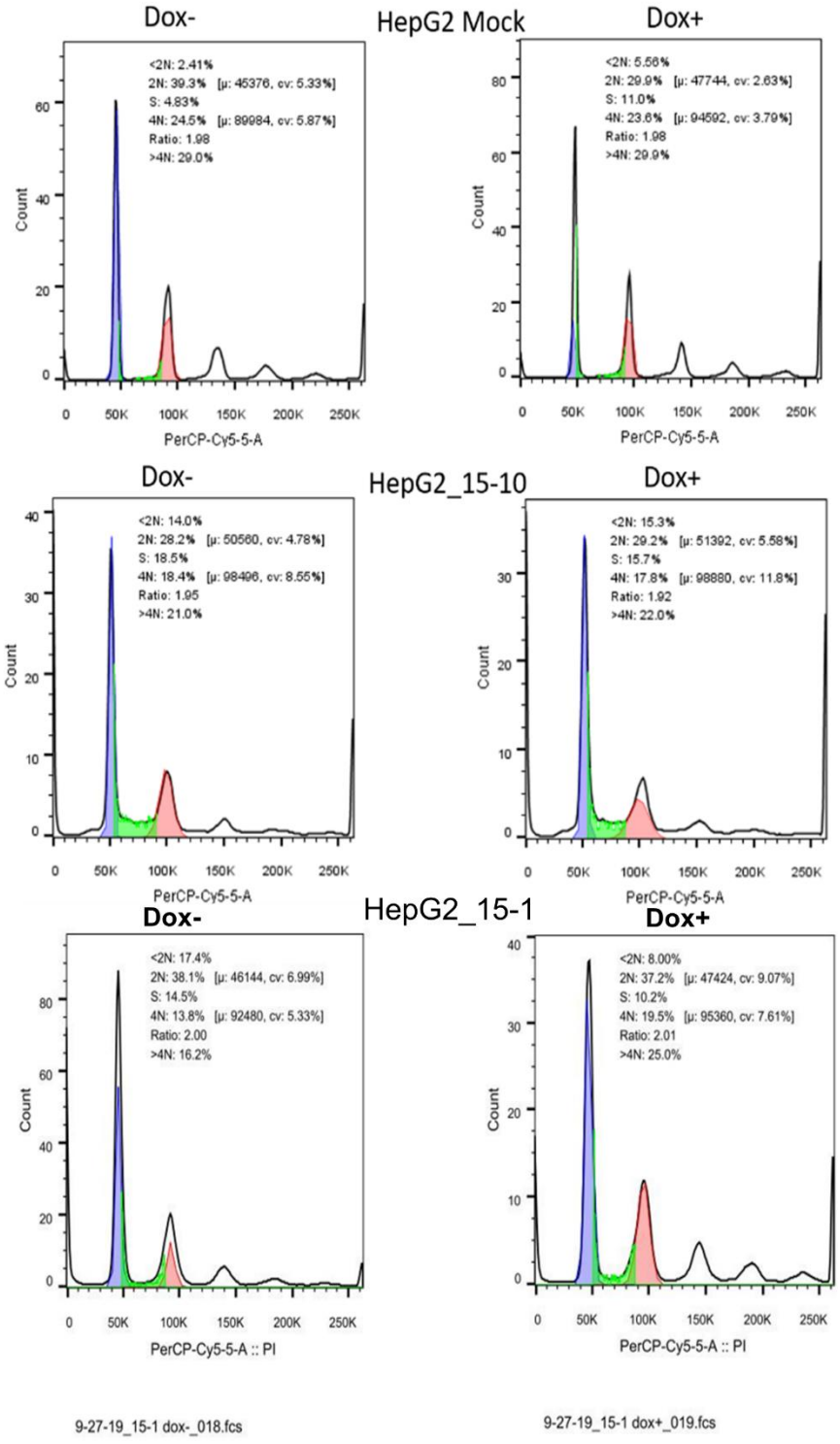

Figure 23: Flow cytometry analysis of DNA content in HepG2 clones with GPR133 expression.

As a control, HepG2 clone 2-10 (Mock) was used.

Afterward, we pushed the clone to grow as a suspension to form a spheroid whether the induction of GPR133 in HepG2 15-1 clone has an effect. In both settings, every six wells showed growth at the end of 12 days. Cells in the untreated group grew more compactly, whereas cells in the GPR133 stimulated group grew more dispersedly. Furthermore, in the untreated group, the dense spheroid formation was observed in every well while the over-expressed group showed only in two among six wells as in Figure 24.

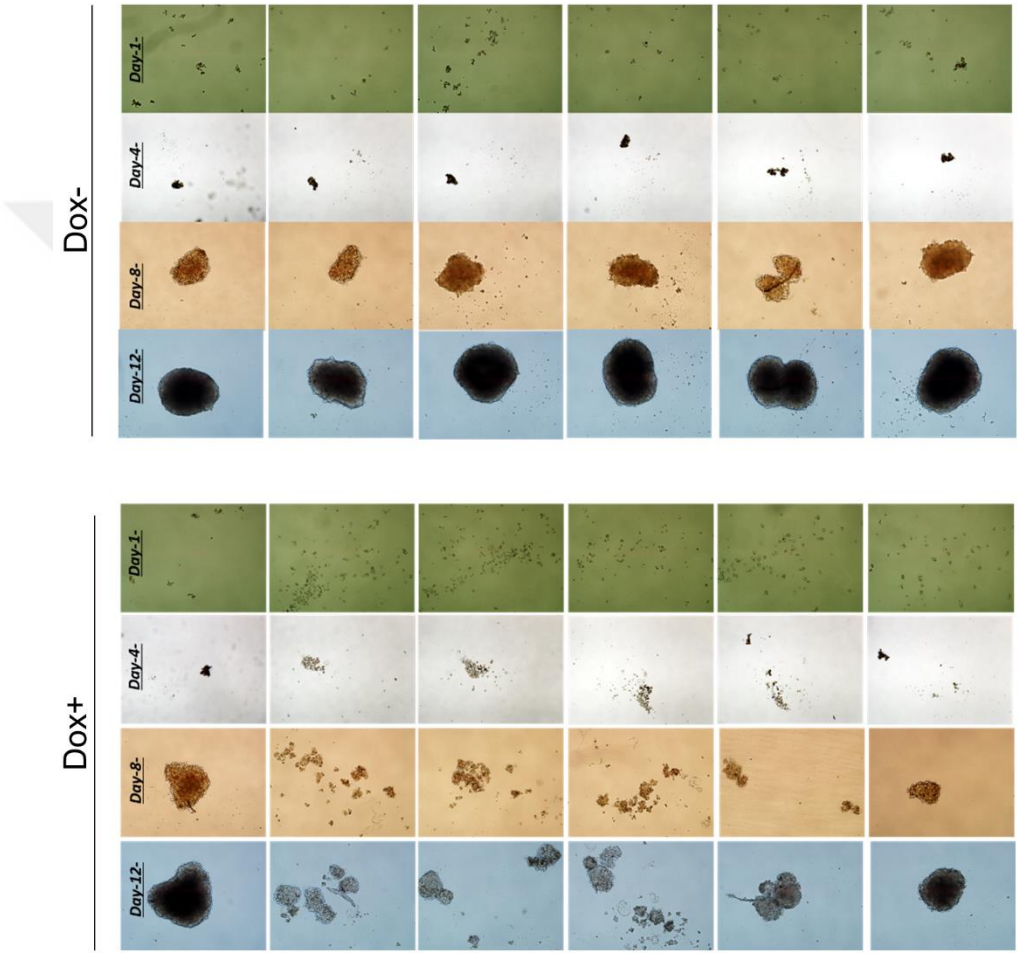

Figure 24: Images of suspension growing HepG2_15-1 clones taken on different days in response to presence and absence of doxycycline induction.

Next, spheroids were collected and embedded into paraffin for histochemical analysis. As shown in Figure 25, hematoxylin and eosin staining of spheroids that grew in the presence and absence of doxycycline were studied under a light microscope. The spheroids come from two different conditions showed different morphology. The spheroids from the un-induced group showed dense outer shell organization with a lighter and spaced core. On the contrary, spheroid in the induced group showed different morphology with a hollow structure and evident spaces between cells on the surface. The morphological changes in the structure may be due to differentiation of the cells, necrosis, or artificial defects so further histological analysis is needed.

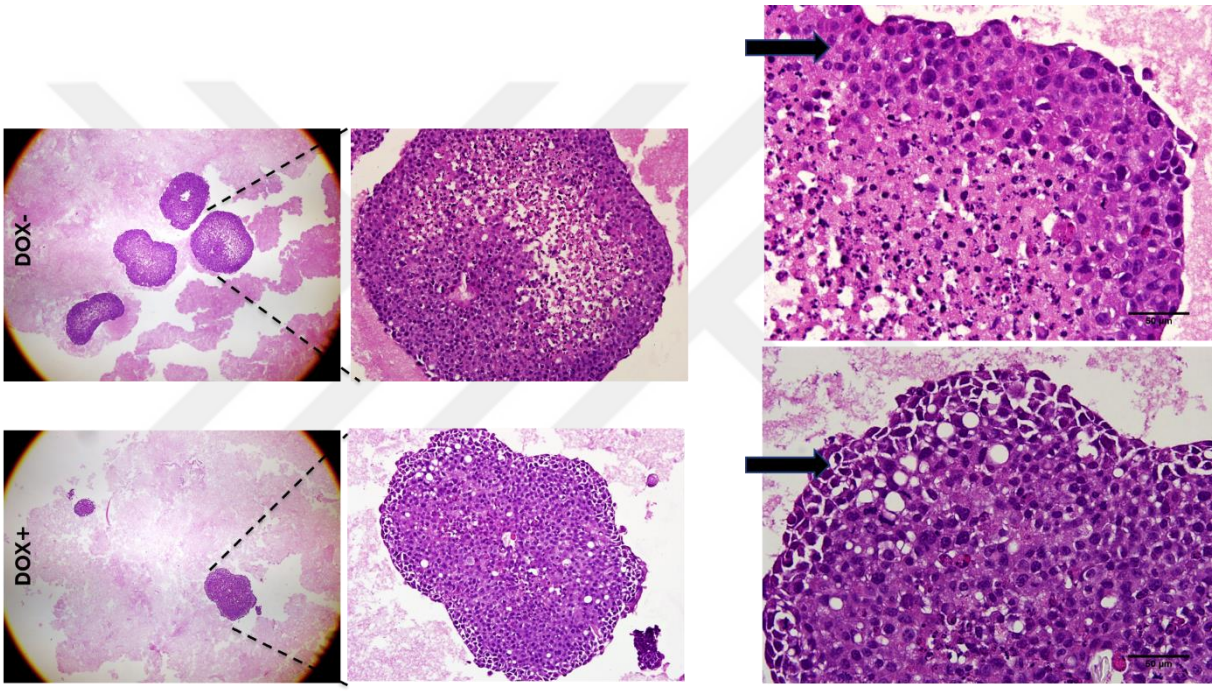

Figure 25: Hematoxylin and eosin staining of spheroids grew in the presence and absence of doxycycline with 4x, 10x and 20x magnifications.

In summary, we tried to find a novel drug-targetable protein that has significance in the survival of HCC patients. The integration of overexpressed genes in the immortal phenotype of Huh7 with survival data generated GPR133 as a candidate. We confirmed its elevated expression in cirrhosis and HCC patient samples. In addition, its expression was also observed in most HCC cell lines at the transcriptional level. The ectopic expression studies revealed reduced spheroid formation with different spherical morphology in HepG2 cells.

4.3 The association of p73 expression with Hepatocellular Carcinoma

4.3.1 The p73 isoforms differentially expressed in HCC cell lines

The expression of TAp73, TAp73Ex2, TAp73Ex2/3, DNp73, and DN'p73 isoforms at the transcriptional levels were studied in nine HCC cell lines (Huh7, HepG2, PLC/PRF/5 Hep3B, FOCUS, SNU475, Mahlavu, SNU398, SNU449) by RT-PCR (Figure 26). GAPDH was used as an internal control. The intensity of the bands corresponds to associated cell lines and isoforms summarized in Table 11.

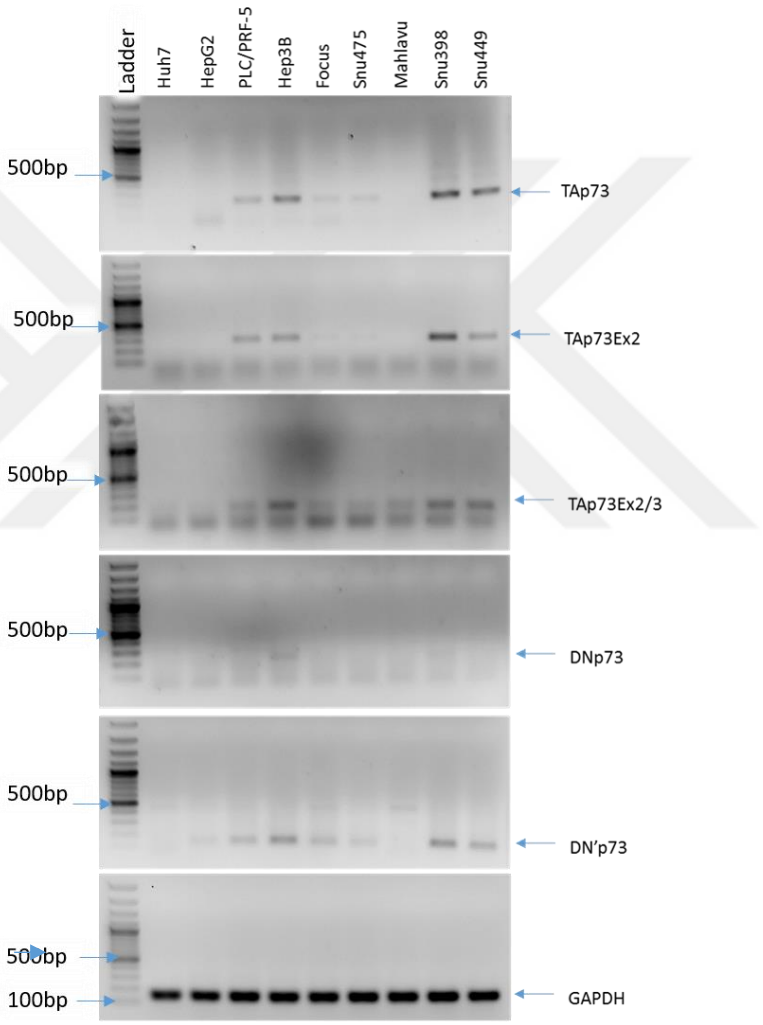

Figure 26: Expression of TAp73, TAp73Ex2, TAp73Ex2/3, DNp73, and DN'p73 isoforms in HCC cell lines.
GAPDH was used as the internal control.

HCC cell lines expressed varying levels of p73 isoforms. In particular, Hep3B and SNU398 cells strongly expressed all the isoforms of p73. Moreover, high expressions of p73 isoforms were detected in SNU449 except DNp73. The expressions of p73 isoforms were

detected weakly or not at other cell lines including Huh7, HepG2, PLC/PRF/5, Focus, SNU475, and Mahlavu.

Table 11: The expression of p73 isoforms in HCC cell lines.

Expression levels indicated as null (-), low (+), moderate (++) and high (+++)

	TAp73	TAp73Ex2	TAp73Ex2/3	DNp73	DN'p73
Huh7	-	-	-	-	-
HepG2	-	-	-	-	+
PLC/PRF/5	+	++	+	-	++
Hep3B	++	++	+++	+++	+++
Focus	+	+	+	-	++
Snu475	+	+	+	-	+
Mahlavu	-	-	+	-	-
Snu398	+++	+++	+++	++	+++
Snu449	+++	++	+++	-	++

4.3.2 The expression of p73 isoforms vary at the protein level in HCC cell lines

To determine the expression of p73 isoforms at the protein level, firstly the p73 isoforms: TAp73 -alpha, -beta, and -gamma in pTRE vector transiently expressed in Huh7 cell line respectively. Ectopically expressed p73 isoforms in Huh7 cells were used to identify endogenously expressed p73 isoforms in HCC cell lines by comparing their relative migration. The bands that correspond to different isoforms were determined as shown in Figure 27A. The HCC cell lines were analyzed by western blot for expression of isoforms. Expressions of p73 isoforms were detected with primary antibodies against full-length p73 (FLp73) and DNp73 respectively (Figure 27B-C). The western blot analysis showed that Hep3B, SNU398, and SNU449 strongly expressed TAp73 alpha. TAp73beta and TAp73gamma isoforms were only detected in SNU398 cells. The rest of the cell lines displayed low or weak expression of p73 isoforms. However, no specific signal for DNp73 expression was detected. In conclusion, high expressions of TAp73 isoforms were detected, while no specific expressions of DNp73 isoforms were observed in the same set of HCC cell lines.

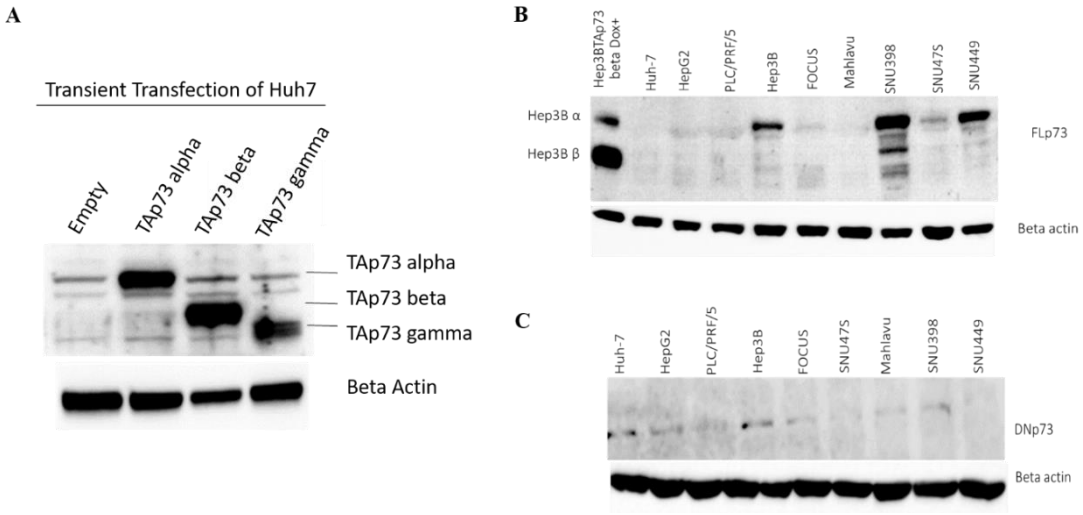

Figure 27**:** The expression of p73 isoforms in HCC cell lines.
(A) Detection of transiently expressed TAp73 -alpha, -beta, and -gamma isoforms in Huh7
(B) Detection of TAp73 isoforms in HCC cell lines by FLp73 antibody and (C) DNp73 antibody.

4.3.3 Generation of Tet-inducible TAp73beta expressing monoclones of SNU449 and HepG2

Previously generated Tet-inducible SNU449-TREx and HepG2-TREx cell lines transfected with the pT-REx-DEST30 plasmid which contains TAp73beta insert. After selection with 4µg/ml Blasticidin and 400µg/ml G418 for two weeks, inducible TAp73beta expressing clones were picked up and screened with western blot in the presence/absence of doxycycline for ectopic expression of TAp73beta. We obtained different monoclones of SNU449 and HepG2 in number which inducibly expressing TAp73beta (Figure 28).

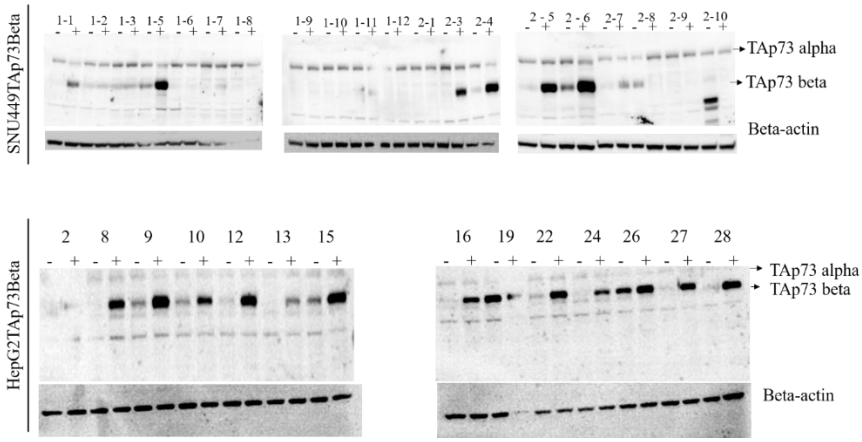

Figure 28: Western blot analysis of stable clones of HepG2 and SNU449 expressing TAp73beta in the presence (+) or absence (-) of doxycycline.

4.3.4 The TAp73beta induction decreased cell proliferation and inhibitory effect preserved despite the removal of Doxycycline

To test the effect of TAp73beta induction on cell proliferation, firstly we treated cells in the presence/absence of doxycycline for 3 days and at the end of 3 days, induction of TAp73beta decreased the cell proliferation in both inducible Hep3B and HepG2 clones. After that, these treated cells were used as seeding reserve for additional 3 days with the same treatment conditions. At the end of 6 days, results showed that the first 3 days of induction inhibited cell proliferation and subsequently, cell proliferation remained inhibited despite the absence of doxycycline for additional 3 days (Figure 29).

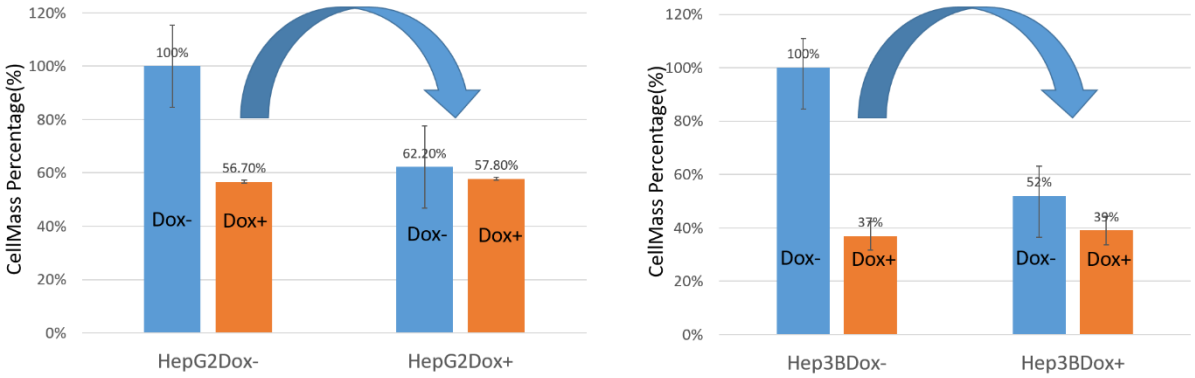

Figure 29**:** Proliferation Assay of TAp73beta induction.

The inhibition of proliferation via TAp73beta induction was preserved even with doxycycline removal.

4.3.5 Overexpression of TAp73beta inhibits colony formation in HCC cells

To investigate the effect of overexpression of TAp73beta in HCC cell lines, three inducible monoclones of HCC were tested for colony formation ability. Cells were seeded into 6 well plates in low density with or without doxycycline and checked for colony formation capacities. The crystal violet staining of fixed colonies showed that overexpression of TAp73beta convincingly decreased the numbers of colonies in both Hep3B and HepG2. However, no detectable change was observed in SNU449 (Figure 30).

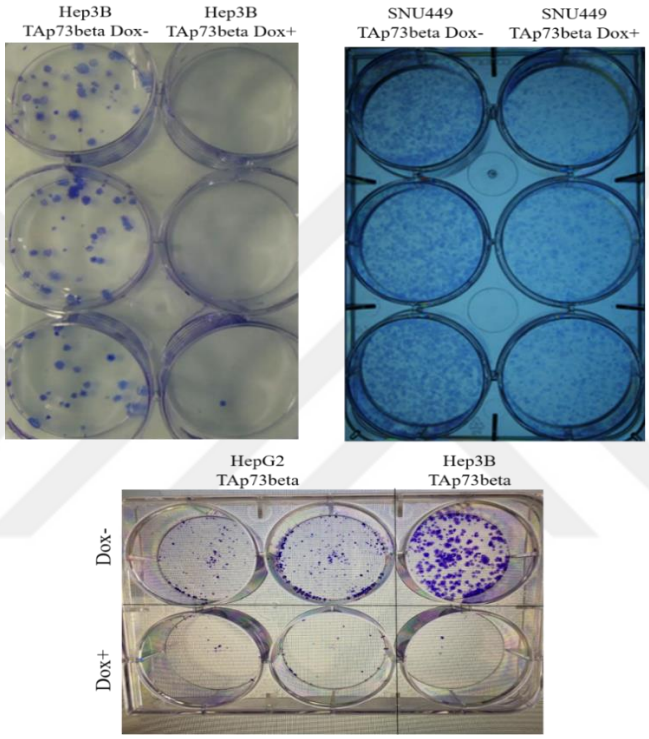

Figure 30: Colony formation capabilities of Hep3B, SNU449, and HepG2 cells after TAp73beta induction.

4.3.6 The overexpression of TAp73beta in Hep3B and SNU449 did not induce apoptosis

To understand the inhibitory mechanism behind proliferation and colony formation, firstly Hep3B and SNU449 cells were analyzed for apoptosis in response to overexpression of TAp73beta. The Annexin-V / 7-AAD stainings of Hep3B and SNU449 cells were analyzed to discriminate early and late apoptosis in response to TAp73beta overexpression. The induction of TAp73beta in Hep3B cell lines showed a 2% ($p=0.0008$) increase in early apoptosis (Q4) and 2.5% ($p=0.105$) in late apoptosis (Q2). In SNU449 cell line, the induction caused 0.5% ($p=0.31$) decrease in early apoptosis and and late apoptosis ($p=0.79$) (Q2). All in all, both cell

lines showed no significant change in apoptotic cell distributions except Hep3B in early apoptosis as in Figure 31.

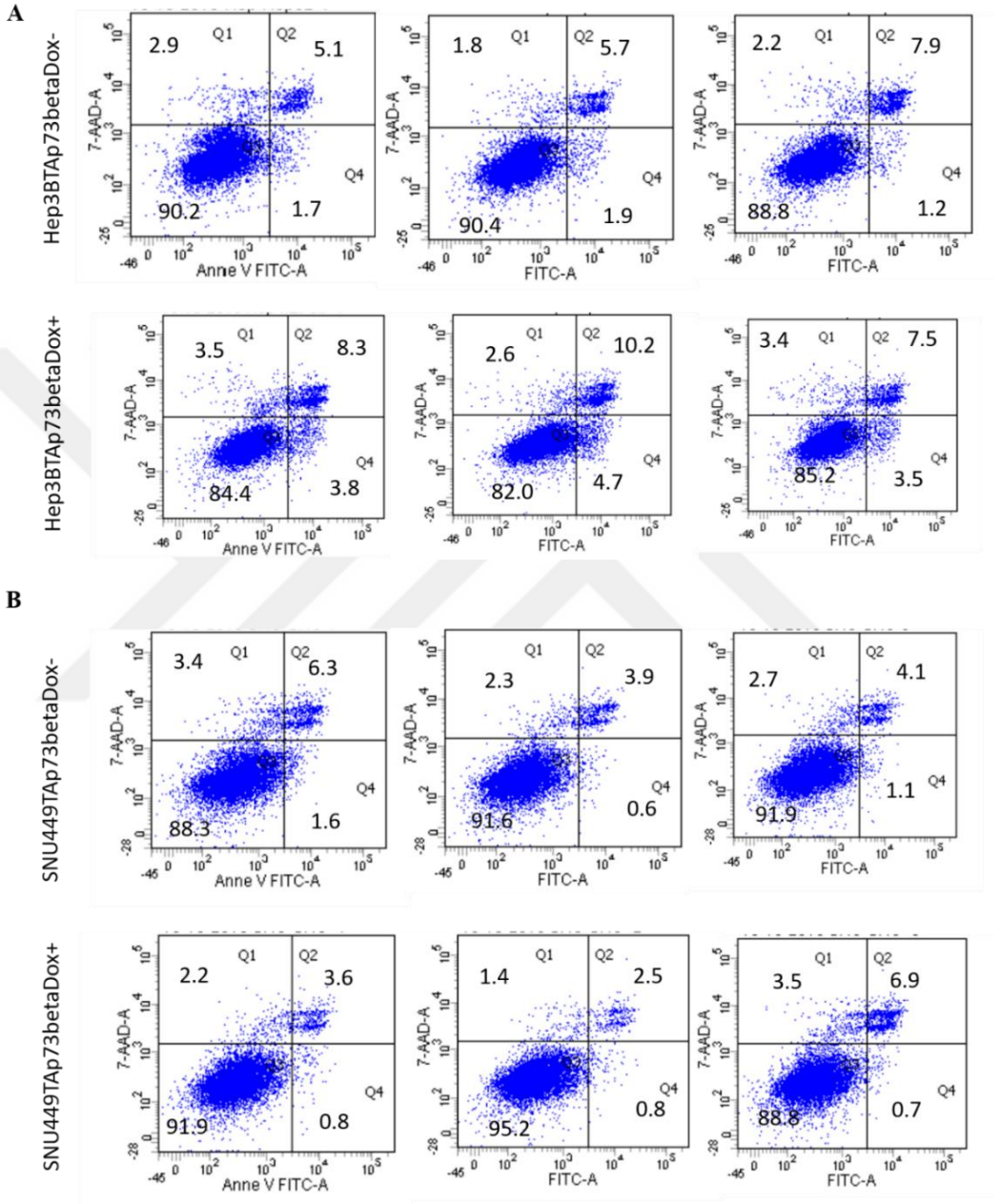

Figure 31**:** The analysis of TAp73beta induction in Hep3B and SNU449 for apoptosis. No significant early or late apoptosis observed in response to TAp73beta induction in (A) Hep3B and (B) SNU449 cells

4.3.7 The effect of TAp73beta induction on the cell cycle of Hep3B, HepG2, and SNU449 cell lines.

To test the inhibitory effect of TAp73beta induction on cell proliferation in Hep3B, HepG2, and SNU449, cell cycle analysis was performed. The overexpression of TAp73beta in Hep3B cells increased the cell accumulation in the G1 phase from 50% to 64% (p=0.0002). Likely, the percent of the cells accumulated in the G1 phase raised from 44% to 53% (p=0.0079) in HepG2. However, barely (3.5%) and not significant (p=0.0873) increase was detected in SNU449.

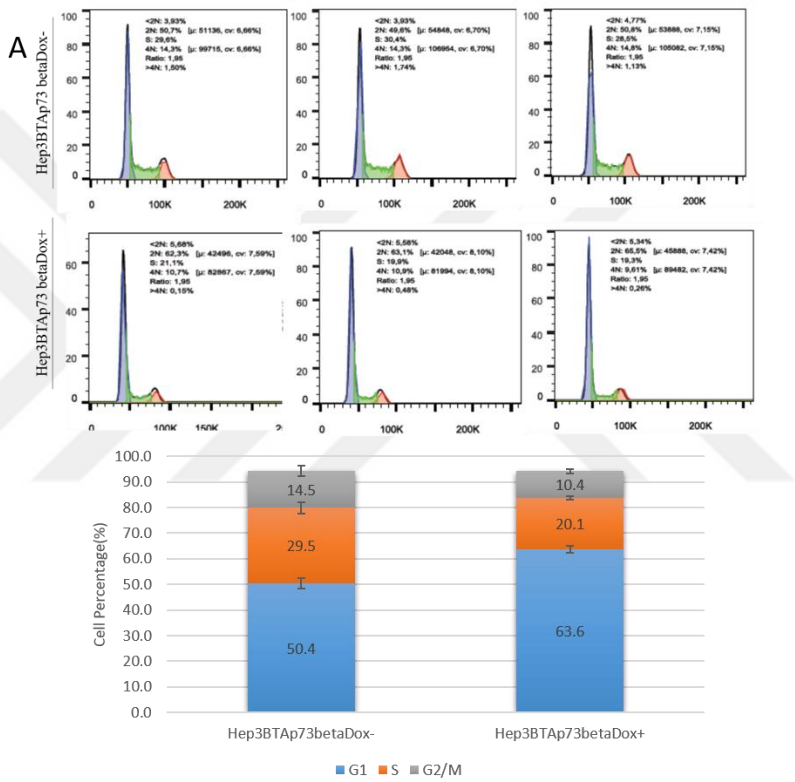

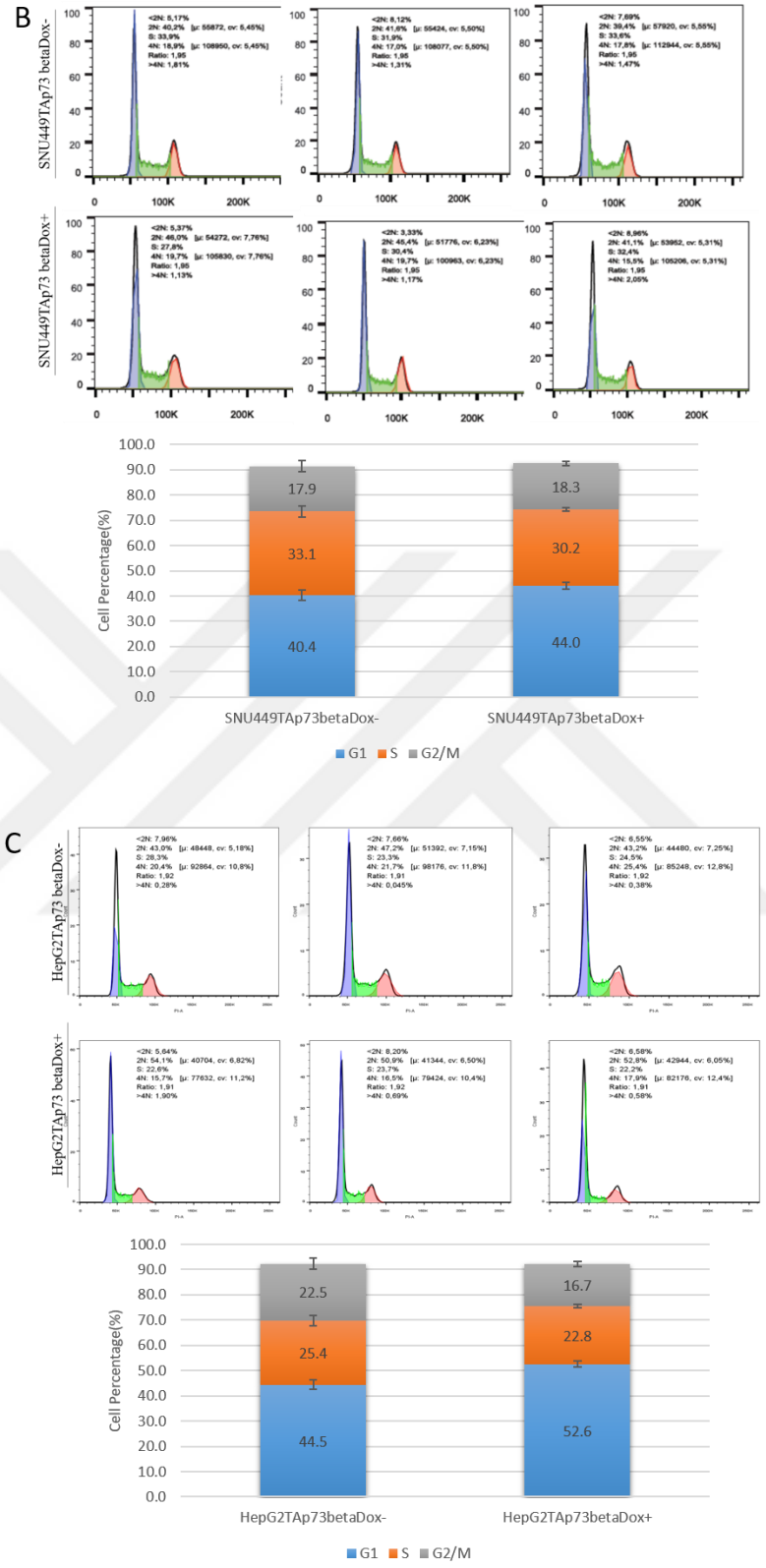

Figure 32**:** Cell cycle analysis of (A) Hep3B, (B) SNU449, and (C) HepG2 clones in response to TAp73beta induction for 72h.

4.3.8 Overexpression of TAp73beta increased p21 levels in Hep3B and HepG2

The overexpression of TAp73beta caused a decrease in cell proliferation and arrested transition from G1 to the S phase in the cell cycle. According to these previous findings, we checked the expression of p21 which is known as a key cell cycle regulator. The induction of TAp73beta for 48h and 72h resulted in the accumulation of p21 in both Hep3B and HepG2.

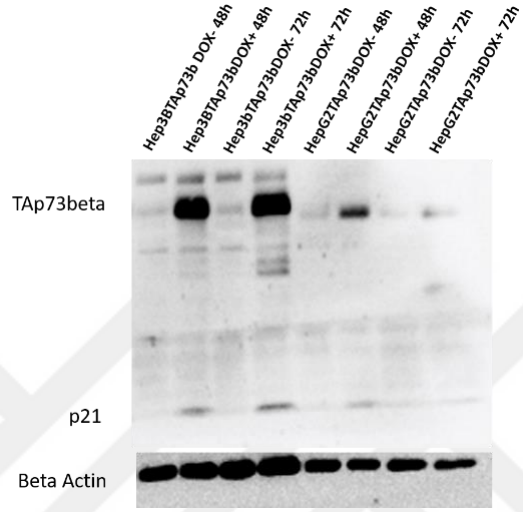

Figure 33**:** The effect of TAp73beta induction on p21 expression levels.
In both Hep3B and HepG2, overexpression of TAp73beta upregulated p21.

4.3.9 The induction of TAp73beta leads to deep changes in gene expression that affect a variety of downstream processes in Hep3B

To evaluate the mechanism behind the inhibition of proliferation in Hep3B cells with overexpression of TAp73beta, we performed microarray analysis. Hep3B cells were induced with doxycycline up to 48 h and samples were collected from induced/uninduced cells at different time points such as 12h, 24h, and 48h. The two-fold or more differentially expressed genes at least one-time point were collected. The analysis was performed in combination with array data collected from different time points and revealed 877 differentially expressed genes consisting of 578 up- and 299 down-regulated.

Next, differentially expressed genes were collected from induced and un-induced conditions of 48h subjected to GSEA. The analysis performed under “Hallmark Gene Sets” collection and nominal p values ($p<0.001$) and the false discovery rate (FDR <0.25) were used as thresholds. According to the enrichment analysis, 26 gene sets were repressed while 5 gene sets were induced in response to TAp73beta. The gene set enrichment analysis showed that

different cellular processes were affected via TAp73beta induction. As expected, genes involved in the p53 pathway and related networks induced. While it repressed growth signaling factors such as MYC targets and cell cycle associated regulators, it induced the gene sets mostly related to development, growth signaling, metabolism, immune response, and stress response (Table 12).

Table 12: Gene sets enriched in response to TAp73beta overexpression in Hep3B cells

GENE SETS	Cellular Process	Role of TAp73beta	SIZE	NOM p-val	FDR q-val
HALLMARK_ADIPOGENESIS	Development	Induction	184	0	0.13
HALLMARK_APICAL_JUNCTION	Development	Induction	193	0	0.18
HALLMARK_EPITHELIAL_MESENCHYMAL_TRANSITION	Development	Induction	192	0	0.16
HALLMARK_MYOGENESIS	Development	Induction	196	0	0.14
HALLMARK_HEDGEHOG_SIGNALING	Development	Induction	35	0	0.17
HALLMARK_ANGIOGENESIS	Development	Induction	34	0	0.15
HALLMARK_ALLOGRAFT_REJECTION	Immune response	Induction	191	0	0.15
HALLMARK_IL2_STAT5_SIGNALING	Immune response	Induction	182	0	0.17
HALLMARK_INTERFERON_ALPHA_RESPONSE	Immune response	Induction	88	0	0.14
HALLMARK_INTERFERON_GAMMA_RESPONSE	Immune response	Induction	187	0	0.19
HALLMARK_TNFA_SIGNALING_VIA_NFKB	Immune response	Induction	185	0	0.16
HALLMARK_BILE_ACID_METABOLISM	Metabolism	Induction	110	0	0.15
HALLMARK_GLYCOLYSIS	Metabolism	Induction	186	0	0.13
HALLMARK_XENOBIOTIC_METABOLISM	Metabolism	Induction	194	0	0.17
HALLMARK_E2F_TARGETS	Cell cycle	Repression	173	0	0.18
HALLMARK_G2M_CHECKPOINT	Cell cycle	Repression	178	0	0.11
HALLMARK_MITOTIC_SPINDLE	Cell cycle	Repression	185	0	0.14
HALLMARK_MYC_TARGETS_V1	Growth signaling	Repression	173	0	0.16
HALLMARK_MYC_TARGETS_V2	Growth signaling	Repression	47	0	0.19
HALLMARK_ESTROGEN_RESPONSE_EARLY	Growth signaling	Induction	183	0	0.12
HALLMARK_ESTROGEN_RESPONSE_LATE	Growth signaling	Induction	194	0	0.16
HALLMARK_KRAS_SIGNALING_UP	Growth signaling	Induction	192	0	0.19
HALLMARK_MTORC1_SIGNALING	Growth signaling	Induction	183	0	0.24
HALLMARK_P53_PATHWAY	Stress response	Induction	182	0	0.16
HALLMARK_COAGULATION	Stress response	Induction	133	0	0.17
HALLMARK_HYPOXIA	Stress response	Induction	188	0	0.15
HALLMARK_INFLAMMATORY_RESPONSE	Stress response	Induction	189	0	0.22
HALLMARK_PEROXISOME	Stress response	Induction	98	0	0.16
HALLMARK_REACTIVE_OXIGEN_SPECIES_PATHWAY	Stress response	Induction	46	0	0.16
HALLMARK_UV_RESPONSE_DN	Stress response	Induction	135	0	0.15

As a result, p73 differentially expressed among HCC cell lines and overexpression TAp73beta isoform decreased cell proliferation in Hep3B cells with increased G1 arrest. The overexpression of TAp73beta in Hep3B cells seemed in association with various cellular signaling responses.

5 DISCUSSION

Hepatocellular carcinoma is the most common kind of primary liver cancer with a poor prognosis and high recurrence rate. The diagnosis of this cancer at early stages is challenging and includes restricted curative options like resection, liver transplantation, and local ablative therapies. However, most patients miss the chance to undergo surgery when their cancer is already late stage when is diagnosed [244]. At this point, conservative chemotherapy remains an important component of a complete treatment for these patients. The treatment options advanced with the approval of sorafenib, a multikinase inhibitor that increased median survival. More recently, the approval of regorafenib and nivolumab came after, and further positive emerging studies are still on the table to cope with advanced HCC [245]. However, there is still an emerging need for new advancements in systemic therapy options for HCC to be met by identifying new drug targets. Since the chemotherapy frequently results in poor response and mostly causes relapse of the tumor in a more aggressive and less chemosensitive way [246].

In our studies, we mainly evaluated 3 different genes for their potential in HCC treatment. Their functions and significance in cancer progression and treatment, especially in HCC discussed below.

5.1 Evaluation of ATAD2 in liver malignancy

After ATAD2 was reported as being involved in tumor occurrence and development [168], relevant studies have been published, highlighting the growing interest in the prognostic impact of high ATAD2 expression in different tumor types [179]. As one of the earliest studies, our group reported ATAD2 as a member of the 15-signature gene panel for classifying hepatocellular carcinoma from cirrhosis with high accuracy [7]. Hence, ATAD2 was studied previously by Haluk Yüzügüllü in his dissertation to interpret its potential role in senescence bypass and HCC malignancy [8]. In this part of the study, ATAD2 was evaluated for its potential as a disease biomarker and therapeutic target for HCC [240].

According to previous studies of our group, ATAD2 protein expression was found low or undetectable in both normal liver and freshly isolated human hepatocytes. On the other hand, there was an upregulation of ATAD2 protein in both HCC cell lines and tumor tissue cohorts [7,8]. Thereafter, we performed comparative bioinformatics analysis in the liver dataset of The Cancer Genome Atlas (TCGA) composed of 371 HCC and 50 non-tumor liver samples. It was observed clearly that there was a significant elevation of ATAD2 transcript levels in tumor

tissues compared to normal. Our findings were consistent with other studies showing increased expression of ATAD2 in HCC compared to normal liver samples [178,181,247,248].

The further analysis with the TCGA dataset provided us the expression of ATAD2 in normal and HCC samples correlate with expression of Ki-67 which is known to express in proliferating cells at the G1, S, G2, and M stages of the cell cycle but not in resting (G0) state [249,250], and also a well-known biomarker to evaluate proliferation index in HCC tumors [249]. In line with these findings, we deemed ATAD2 as a proliferation biomarker. Following this novel correlation data, we tested to see whether ATAD2 expression is specific to liver malignancy. To test this, we analyzed the expression of *ATAD2* levels in parallel to *MKI-67* and *CCND1* in regenerating liver of rats after partial hepatectomy. When we examined the dataset of regenerating liver tissues collected at different time points from mice that had undergone partial hepatectomy, we observed that the corresponding RNA levels of these three genes showed a similar expression pattern. The expressions of three genes were steady up to 12 hours. After the initial phase of liver regeneration, which covers about the first 12 hours, ATAD2, MKI-67, and CCND1 RNA levels dramatically increased until 36h. After this pick, expressions were gradually decreased and reached initial levels at the end.

In support of previous studies, DNA synthesis peaks in rats following liver hepatectomy at 22–24 h, followed by mitosis at 28–30 h [251]. Also, in hepatocytes, the transition from G1 to S phase occurs with the help of D-type cyclins (D1, D2, and D3) whose transient expression triggers hepatocyte proliferation and liver growth *in vivo* [252]. Another equally important point is the expression of MKI-67. In parallel to our observations, MKI-67 expression increased after partial hepatectomy at early 16-17h with DNA synthesis, peaked at 36h, and kept its upsurged levels for 96 hours [253]. According to the clinical point of view of Ki-67, eight normal and ten inactive cirrhosis patients had average labeling indexes lower than 2.5, whereas higher index mean values were observed in mild and moderate-severe chronic hepatitis patients with mean index 29 and 41 respectively. With 71, the maximum mean index was obtained from eight patients with HCC [249]. Considering mentioned expression profiles of Ki-67 above, highly similar expression profiles were observed with ATAD2. Since, low expression in normal liver, whereas increased expression in regenerating rat liver, as well in the malignant liver as a function of tumor progression was also observed in ATAD2. In addition to that, our *in vitro* study with HCC cell lines confirmed that ATAD2 may be considered as a specific nuclear marker like Ki-67 for proliferating cells. Nearly all tested HCC cell lines showed positive

staining, which correlated with Ki-67 staining. Indeed, the specificity of the staining was also confirmed with siRNAs that abolished the homogenous nuclear signal of ATAD2.

In order to function properly, proteins need to be folded into the right conformations; otherwise, unfolded or misfolded proteins can be destructive to cells. ER is the place where this process occurs, and various physiological and pathological conditions may impair protein folding in the ER, which is collectively known as ER stress [254]. ER stress can be induced by tunicamycin, which activates the unfolded protein response (UPR) in response to extensive protein misfolding via preventing N-linked glycosylation of the proteins [255]. Besides, cells respond to UPR by exiting from the cell cycle by inhibiting Cyclin D1 expression [241]. In the termination of liver regeneration, hepatocytes need Cyclin D1 degradation to exit from the cell cycle in mice [256]. As a hallmark of cancer, one of the characteristics of tumor cells is to proliferate uncontrollably. Here we treated cell lines with tunicamycin to trigger UPR which exits cells from the cell cycle. The treatment of Hep3B cells with tunicamycin resulted in accumulation of CHOP at 12h with low cleaved PARP and without change in ATAD2. With the abolishment of CHOP and strong induction of PARP cleavage at 24h, ATAD2 levels were reduced dramatically. This result can be considered as cell cycle arrest as well as apoptosis induction in response to tunicamycin treatment in Hep3B. In HepG2, accumulation of CHOP was detected at both 12h and 24h with slightly increasing PARP cleavage. However, more ATAD2 downregulation was detected for 12h than 24h that suggesting slight apoptosis and obvious cell cycle exit. In SKBR3, CHOP levels increased at 12h and diminished at 24h. Cleaved PARP accumulation was observed slightly for both 12h and 24h with strong ATAD2 downregulation in both cases.

Adriamycin (Doxorubicin) is a member of anthracycline antibiotics used for cancer treatment. Different mechanisms are shown to be responsible for the mode of actions, such as DNA intercalation, DNA binding, and alkylation as well as topoisomerase II inhibition [257]. Hence, these cytotoxic effects cause DNA damage in relation to antiproliferation. Double strand DNA breaks especially with topoisomerase II inhibition, trigger DNA repair mechanisms. Failure of repair mechanism mostly concludes with apoptosis [258]. In our previous study, ATAD2 expression was downregulated with Adriamycin-induced senescence arrest in Huh7 cells [7]. Our recent finding showed that ATAD2 levels in Hep3B cells upregulated with low dose treatment of Adriamycin for 24h. Hence, this upregulation affected the distribution of cells according to cell cycle phases, substantially G0/G1 phase (Figure 10). Probably, low dose

Adriamycin delayed G1 to S transition of Hep3B cells. Considering adriamycin with various cytotoxic mechanisms, which might differ with dose and exposure time, it is not surprising that there will be different cellular responses. In support of this observation, Adriamycin can induce progression arrests at different cell cycle phases as at G0-G1 transition or during G1 [259]. Moreover, ATAD2 was appeared to be one of the significantly downregulated genes in G0 cells compared to G1 cells based on microarray analysis [260]. Our findings and other reports suggest that ATAD2 may be a biomarker of non-resting (non-G0) states.

Cellular outcomes in response to ATAD2 silencing with RNAi-based approaches indicated varying associations with tumorigenic abilities of cancer cells. Depletion of ATAD2 inhibited cell growth, colony formation as well as the invasive and migratory capacity of different cancer cell lines [172,173,181,248]. In contrast, Ciro M. et al. (2009) [170] reported that ATAD2 silencing in TIG3-T and U2OS cells did not result in a noticeable difference in proliferation rate or cell cycle profile while showing decreasing colony-forming abilities. Similarly, some HCC cell lines were also not responded to ATAD2 silencing according to our previous studies [8]. Thus, we performed comparative gene expression analysis in three different cell lines of HCC to evaluate the difference. The number of genes, in other words, cellular responses, altered with ATAD2 silencing extremely varied from few genes to hundreds among HCC cell lines. Not only gene set enrichment analysis but also cluster analysis indicated extreme heterogeneity in response to ATAD2 deficiency in tested cell lines. This heterogeneity in response to ATAD2 silencing suggested that its involvement in tumorigenic behaviors probably depends on cellular context. Thus, our comparative analysis taken together with our previous studies implied that expression of ATAD2, especially in HCC cell lines, was not essential to survive or ATAD2 was not the only responsible factor but also may need additional partners for the cellular outcomes.

5.2 The potential of GPR133 in HCC

G-protein coupled receptors modulate a wide range of biological functions via heterotrimeric guanine nucleotide-binding proteins (G proteins). GPCRs manage almost all physiological activities through G proteins, and their dysregulation is linked to a variety of human disease states like cancer [261]. Multiple aspects of GPCR-G protein signaling contribute to hallmarks of cancer including proliferation, tumor angiogenesis, invasion, metastasis, immune evasion, and deregulation of cellular energetics [262]. Thus, adhesion GPCRs, which is the second largest subfamily with 33 members and most of which are orphan

receptors with unknown physiological functions, were also in association with many cancers including lung, breast, colorectal, prostate, and gastric cancer [261,263].

Our comparative analysis in previously described Huh7 clones [7] lead us to focus on upregulated genes in immortal phenotype, and subsequent integration of clinical data revealed GPR133 as a potential drug target with significant poor prognostic impact in HCC. GPR133 can be classified as an understudied receptor in the literature. Not only its canonical function but also the ligand of the receptor is still not identified clearly. Thus, it has only been linked in just three cancer with very few studies such as glioblastoma [10,11] acute myeloid leukemia [196], and gastric cancer [197]. Here, we showed firstly in the literature that our patient survival analysis in TCGA liver datasets with SurvExpress showed GPR133 elevation may associate with poor prognosis of HCC. Our findings supported this observation with increasing transcripts of GPR133 in patient sample pairs of cirrhosis and HCC while very low expression of normal liver. In liver malignancies, chronic liver injury leads to an abnormal liver blood system, and unmet blood supply in the liver causes hypoxia. Besides blood supply, high proliferation of cells may also induce hypoxia locally in HCC [264]. Moreover, it was reported in glioblastoma that GPR133 expression was seen in the regions expressing hypoxic markers, and GPR133 was found the transcriptional target of one of these markers: hypoxia-inducible transcription factor 1 alpha (HIF-1a) [11]. Thus, the reason behind this overexpression may be due to hypoxia-driven tumor progression in HCC.

In addition, epithelial cell lines such as Hep3B, Huh7, Hep40, and PLC showed high expression while mesenchymal cells like SNU182, 387, 398, 423, 449, and SKHEP1 showed barely expression. Although HepG2 is among epithelial-like cell lines, expression was not detected. This subset expression of GPR133 in HCC cell lines needs further investigation to elucidate the potential linkage between phenotype and expression. Likewise in glioblastoma, GPR133 is selectively expressed in CD133+ cells especially in hypoxic areas [10].

Even if the GPR133 transcripts elevated in HCC cell lines and patient samples, our comparative analysis also showed that GPR133 expression levels may vary between normal and tumor samples of different cancers in terms of isoforms. Although different putative isoforms have been identified, the long isoform of GPR133 is the predominant form detected in glioblastoma [10]. In addition, GPR133 was downregulated by long non-coding RNA in gastric cancer that shows the expression of GPR133 may be regulated differently in malignancy dependent [197].

Our preliminary data with HepG2 showed the overexpression of GPR133 resulted in the decreased spheroid formation and different morphology of the sphere. However, the studies were performed with only one cell line and the receptor activation was not confirmed. All these considered, it is hard to emphasize the role of GPR133 in HCC at this level. Further extensive analysis is needed with different cell lines with additional positive controls to eliminate the bias and false positivity.

5.3 The p73 involvement in HCC

As the guardian of the cell, p53 suppresses tumor growth by regulating the expression of many genes which affect cell survival at the transcriptional level [265,266]. The p73, one of two homologs of p53, shows high structural and functional similarity to p53, especially in terms of its DNA binding site.[198,267]. Thus, cell cycle arrest, apoptosis, and cellular senescence can be induced by p73 binding to p53-responsive DNA-binding sites [199,267,268].

In many cancer types, including HCC, it has been shown that p53 has mutations, particularly in its DNA binding motif, thus making p53 unable to function [269,270]. However, p73 is rarely or not mutated in cancers [13]. Although p73 mutations have not been identified in HCC, abnormal expression of p73 has been shown in HCC patients [17,233,271].

The *in vivo* studies with p53 and its homolog p73 showed different consequences as a result of gene knockout. Mice, deficient in p53, developed normal and spontaneous tumor formation, and null mice developed tumors faster against heterozygous mice [272]. In p73 deficiency, neurological and immunological defects were observed in mice, and spontaneous tumors were not observed [219]. The difference between p53 and p73 deficiency *in vivo*, especially in tumor formation and developmental defects, shows the difference in target genes regulated by p73 and p53 despite high homology. Considering these functional different outcomes, determining the function and target genes of p73 in cancer, especially in HCC, may be important in finding new target mechanisms. Moreover, given the rarity of p73 mutations in cancer, pharmacological stimulation of p73's tumor-suppressive effects might be an appealing alternative technique for treating cancer cells, particularly those lacking or mutant p53.

In our study, we firstly determined N terminal isoforms of p73 in HCC cell lines at the transcriptional level and C terminal isoforms of full-length p73 at the protein level. We observed strong protein expression of TAp73alpha isoform in Hep3B, SNU398, and SNU449 while low or null expression in other cell lines. Thus, the determination of the presence and levels of isoforms among HCC cell lines may give clues in understanding the significance of

isoforms. Since, differential expression of p73 isoforms is in relation with different cellular outcomes that are important in cancer such as chemosensitivity [273], stemness [274], epithelial-mesenchymal transition (EMT) [275], and tumor suppression/progression [276]. We decided to ectopically express TAp73beta in cell lines lacking its basal expression like Hep3B, HepG2, and SNU449. Previous studies claimed the upregulation of TAp73beta was associated with apoptosis [17] or stimulation of apoptosis and cell cycle arrest as well [277]. In line with these, our findings suggested a decrease in cell proliferation due to cell cycle arrest at G1/S in a cell-dependent context

This cell dependency in proliferation may be stemmed from the antagonist effect of other isoforms which are already expressed at basal levels in these cells. Because, while TAp73 isoforms act as pro-apoptotic, DNp73 isoforms may inhibit the apoptotic response by competing p53 or TAp73 for their target gene activation [278,279]. In addition to this, this arrest may also be caused due to deregulation of cell cycle regulators. Since it was shown that TAp73 may contribute to genomic stability, and TAp73alpha interaction with Bub1 and Bub3 which are kinetochore proteins deregulates mitotic checkpoints and TAp73 in cancer [220,280]. Moreover, we also showed that overexpression of TAp73beta in Hep3B and HepG2 cells resulted in decreased colony formation. This anti-oncogenic effect of TAp73beta overexpression was also indicated in different cancer cell lines such as human non-small cell lung carcinoma cell line (H1299) [281] and human osteosarcoma cell (SAOS-2) [282].

To decipher the significance of TAp73beta in the malignancy of HCC, we performed microarray analysis and subsequently GSEA. The analysis performed in Hep3B cells specifically reflected the cellular consequences of TAp73beta overexpression since the effect of its homologs was eliminated in a way under p53 mutation [269] and low p63 expression in these cells [283]. The GSEA revealed that the overexpression of TAp73beta de-regulated a wide range of cellular processes, including growth control, stress response, immunological response, metabolism, and development. In support of the gene set analysis, p73 isoforms were shown to regulate the autophagy and lipid metabolism by ATG5 gene in the liver [284]. Additionally, depletion of p73 *in vivo* resulted in deregulated lysine metabolism, glycolysis, and abnormal lipid accumulation in the liver [285]. Besides, TAp73 also take a role in opposing tumor progression and angiogenesis via the recruitment of mouse double minute 2 homolog (MDM2) in HIF-1 alpha degradation and repression of pro-angiogenic and pro-inflammatory cytokines [286,287].

The presence of developmental gene sets in GSEA analysis and upregulation of yes-associated protein (YAP) as well as its target genes in response to TAp73beta overexpression in Hep3B lead us to turn our focus on the development and differentiation of the hepatocytes. The further study published by Iscan E. et. al 2021 [288] suggested the overexpression of TAp73beta in Hep3B cells may promote malignant dedifferentiation. The analysis on specific markers showed that induction of TAp73beta in Hep3B cells upregulated cholangiocyte-promoting genes (JAG1, NOTCH1, ZO-1) while inhibiting hepatocyte fate indicators (CYP3A4, AFP, HNF4, ALB) without altering hepatic stem/progenitor markers like EpCAM and LGR5. In addition to these, TAp73beta overexpression in 3D cultured Hep3B cells showed different patterns of immunohistochemical staining for CK19 and AFP which suggest the switch from hepatocyte-like phenotype to cholangiocyte-like. In the same study, we demonstrated the relevance of p73 isoforms with poor prognosis. The analysis in TCGA Splice Variant database (TSVdb) showed that no significant expression of any p73 isoform in normal liver samples. Additionally, in support of enrichment in epithelial-mesenchymal transition gene set from GSEA analysis, induction of TAp73beta increased the metastatic ability of Hep3B cells.

6 CONCLUSION AND FUTURE PERSPECTIVES

The development of HCC occurs as a multistep process with the acquisition of many genetic/molecular actors over many years. This complicated multifactorial process is mostly diagnosed at later stages and tumor resection ceases to be a solution. Until a few years ago, sorafenib was the only systemic proven drug available for patients have unresectable HCC. In the lead of clinical studies after sorafenib approval, regorafenib join the game in the second-line setting. The first- and second-line alternatives were accelerated recently with phase studies and these advancements in new drugs shifted the studies to new drug targets with combination strategies. However, the challenges with the war against advanced HCC are still present in terms of drug resistance, metastasis, and relapse. The recent developments in the field of HCC show the importance of emerging roles of new novel targets for molecular therapies.

In this study, we evaluated the potential of different genes as a therapeutic target, that may take a role at different stages of HCC progression. As a study model, different clones of Huh7 cells were used that reflect the HCC progression including premalignant, cirrhosis, and HCC phenotypes. The bioinformatics analysis in parallel with functional studies that we carried out reflected the potentially responsible genes during this transition.

One of the genes gathered from previous bioinformatics studies was ATAD2. The aberrant expression of ATAD2 was previously investigated in HCC by our group and showed elevation in HCC progression. The suppression of ATAD2 inhibited HCC progression in some of HCC cell lines *in vitro* and *in vivo*. While the inhibition of ATAD2 induced apoptosis and decreased cell proliferation, some of the cell lines did not respond to ATAD2 depletion in the same way. In this study, we confirmed that the expression of ATAD2 elevates in tumors of HCC patients compared to normal liver tissues. The heterogeneity in response to ATAD2 suppression in HCC cell lines in previous studies of our group implied that an increase in malignancy may be due to malignant proliferation. To test this, we performed the comparative analysis of ATAD2 in parallel to the well-known proliferation marker Ki-67. We realized that the correlation between ATAD2 and Ki-67 expression was not only in patient samples but also in regenerating liver, which strengthens the evidence towards elevation due to proliferation. The depletion of ATAD2 also did not change the proliferation status of tested HCC cell lines in regards to positive Ki67 staining. The microarray analysis with different HCC cell lines revealed different phenotypes as a result of ATAD2 depletion. Moreover, our drug-based studies also showed dissimilar consequences due to drug mode of actions, concentrations, and

cell lines. All together, we realized high heterogeneity in the response of HCC cell lines against ATAD2 depletion and elevation in normal cell proliferation especially in regenerating liver. This heterogeneity suggested considering ATAD2 as a proliferation biomarker rather than a therapeutic target. However, the heterogeneity in response to depletion of ATAD2 suggests that different mechanisms may be in charge. To understand the underlying mechanisms in cell lines under the control of ATAD2 expression, RNAseq and CHIP-seq analysis may be performed to understand the regulatory function. Furthermore, aberrant expression in regenerating liver also indicates that the expression of ATAD2 changes in a time-dependent manner. Thus, the regulation of ATAD2 expression should be considered, and further time course experiments are needed in the evaluation of ATAD2. The conditional knock-out system of ATAD2 may also contribute to the understanding of the mechanism and investigation of its targets. The functional analysis of ATAD2 with cell cycle regulators such as cyclins and their kinases may provide new insights in understanding the role of ATAD2 in proliferation. To evaluate its significance in cancer, it may be investigated in patient samples by immunostaining in parallel to different biomarkers for its prognostic or predictive potential.

In the scope of finding new novel drug targets in HCC, we investigated the gene sets previously collected by microarray analysis. The comparative analysis especially the genes increased in the immortal phenotype of the same cell line may give birth to new candidates. To narrow the list and increase the significance in the treatment approach, we integrated clinical datasets collected from liver patients. In parallel to significance in patient survival and increased expression in HCC, we added different filters in terms of the location and function of the protein. In our perspective, a protein in the membrane of the cell can be easily targetable especially with an antibody-based approach. Furthermore, the expression of the protein in other organs especially in essential ones should be low which suppression of the protein should not produce lethal side effects. Our literature search also added some clues in terms of the functionality of the protein with its novelty. All together, we focused on GPR133/ADGRD1 as a candidate drug target. It was a double-edged sword with high novelty that there were only a few studies restricted with glioma. In addition, GPCRs were highly popular in approved drug targets. However, functional studies were very limited. Our study was the first study that brought the GPR133/ADGRD1 and HCC together. At the first stage, we tried to confirm our hypothesis in terms of elevated expression in HCC and showed its increased expression in both patient samples and HCC cell lines at the transcriptional level. However, at the protein level,

we faced obstacles in finding positive controls and functional antibodies previously proved. Because of this insufficiency, we focused on the generation of study tools including expression vectors for ectopic expression and specific antibodies which recognizes receptor from different terminals. At this stage, we generated doxycycline-inducible GPR133 expressing HepG2 cell clones and performed some preliminary functional assays. Although, we showed the induction of GPR133 receptor protein, could not prove the functionality of the receptor in terms of elevated levels of cAMP which is the seconder messenger of the active receptor. Our preliminary data may lead to show the impact of GPR133/ADGRD1 in HCC with additional experiments. If the obstacles in the determination of basal expression of GPR133 as positive control can be overcome, the depletion studies of GPR133 with RNAseq and functional studies may shed light on new impacts of GPR133 in HCC. Moreover, *in vivo* studies with conditional expression of functional GPR133 receptor may reveal new aspects in tumorigenesis of HCC.

The importance of the tumor suppressor gene p53 is widely accepted in cancer. As a member of the p53 family, dysregulation of genes by p73 has potential oncogenic relevance in cancer progression including HCC. Our findings with p73 are important in terms of defining the transcriptional activating role of p73 and its isoforms in HCC. Our studies with HCC cell lines revealed the presence of varying N and C terminal p73 isoforms at the transcriptional level. Because of its complicated structure, translated proteins were close to each other in amino acid sequence. Thus, it is very hard to generate isoform-specific antibodies against these isoforms which makes studies tough at the protein level. In our study, we specifically focused on the TAp73beta isoform and showed that the TAp73beta isoform arrests the G1/S cell cycle in HCC cell lines, and this is performed by regulating the expression of genes that promote cell cycle progression. The microarray analysis by ectopic expression of TAp73beta also revealed the downstream signaling pathways. To elucidate these pathways in association with TAp73beta overexpression may guide further studies in terms of identification of new possible drug targets. As a transcriptional regulator, ChIP-sequencing studies may reveal the direct target genes regulated in these pathways. Besides, it may be meaningful to study isoforms that differ among HCC cells as well as consensus isoforms. From this point of view, isoform-specific deletions or over-expression studies will be meaningful in different cell lines.

In conclusion, here we evaluated and identified new candidate genes which may give some insights in terms of potentials in therapeutic targeting of HCC. Although it is obvious that no single target can meet all the requirements of therapeutic advancement in HCC treatment,

the contribution of these genes may intersect within the multistage progression of HCC. In addition to this, the potential of these genes may contribute to approved drugs in combination therapies or be considered as biomarkers that discriminate patient prognosis in terms of the progression of the disease.

7 REFERENCES

1. Llovet, J.M.; Kelley, R.K.; Villanueva, A.; Singal, A.G.; Pikarsky, E.; Roayaie, S.; Lencioni, R.; Koike, K.; Zucman-Rossi, J.; Finn, R.S. Hepatocellular carcinoma. *Nat. Rev. Dis. Prim.* **2021**, *7*, doi:10.1038/s41572-020-00240-3.

2. Golabi, P.; Fazel, S.; Otgonsuren, M.; Sayiner, M.; Locklear, C.T.; Younossi, Z.M. Mortality assessment of patients with hepatocellular carcinoma according to underlying disease and treatment modalities. *Med. (United States)* **2017**, *96*, doi:10.1097/MD.0000000000005904.

3. Kim, E.; Viatour, P. Hepatocellular carcinoma: old friends and new tricks. *Exp. Mol. Med.* **2020**, *52*, 1898–1907, doi:10.1038/s12276-020-00527-1.

4. WIEMANN, S.U.; SATYANARAYANA, A.; TSAHURIDU, M.; TILLMANN, H.L.; ZENDER, L.; KLEMPNAUER, J.; FLEMMING, P.; FRANCO, S.; BLASCO, M.A.; MANNS, M.P.; et al. Hepatocyte telomere shortening and senescence are general markers of human liver cirrhosis. *FASEB J.* **2002**, *16*, 935–942, doi:10.1096/fj.01-0977com.

5. Hanahan, D.; Weinberg, R.A. Hallmarks of cancer: The next generation. *Cell* **2011**, *144*, 646–674, doi:10.1016/j.cell.2011.02.013.

6. Ozturk, N.; Erdal, E.; Mumcuoglu, M.; Akcali, K.C.; Yalcin, O.; Senturk, S.; Arslan-Ergul, A.; Gur, B.; Yulug, I.; Cetin-Atalay, R.; et al. Reprogramming of replicative senescence in hepatocellular carcinoma-derived cells. *Proc. Natl. Acad. Sci. U. S. A.* **2006**, *103*, 2178–2183, doi:10.1073/pnas.0510877103.

7. Yildiz, G.; Arslan-Ergul, A.; Bagislar, S.; Konu, O.; Yuzugullu, H.; Gursoy-Yuzugullu, O.; Ozturk, N.; Ozen, C.; Ozdag, H.; Erdal, E.; et al. Genome-Wide Transcriptional Reorganization Associated with Senescence-to-Immortality Switch during Human Hepatocellular Carcinogenesis. *PLoS One* **2013**, *8*, doi:10.1371/journal.pone.0064016.

8. Yuzugullu, H. Genetic and Epigenetic Targets in Liver Cancer. *Bilkent Univ. PhD.Thesis* **2010**.

9. Sriram, K.; Insel, P.A. G protein-coupled receptors as targets for approved drugs: How many targets and how many drugs? *Mol. Pharmacol.* **2018**, *93*, 251–258, doi:10.1124/mol.117.111062.

10. Bayin, N.S.; Frenster, J.D.; Kane, J.R.; Rubenstein, J.; Modrek, A.S.; Baitalmal, R.; Dolgalev, I.; Rudzenski, K.; Scarabottolo, L.; Crespi, D.; et al. GPR133 (ADGRD1), an adhesion G-protein-coupled receptor, is necessary for glioblastoma growth. *Oncogenesis* **2016**, *5*, e263, doi:10.1038/oncsis.2016.63.

11. Frenster, J.D.; Inocencio, J.F.; Xu, Z.; Dhaliwal, J.; Alghamdi, A.; Zagzag, D.; Bayin, N.S.; Placantonakis, D.G. GPR133 Promotes Glioblastoma Growth in Hypoxia. *Clin. Neurosurg.* **2017**, *64*, 177–181, doi:10.1093/neuros/nyx227.

12. Stiewe, T.; Pützer, B.M. Role of p73 in malignancy: Tumor suppressor or oncogene? *Cell Death Differ.* **2002**, *9*, 237–245, doi:10.1038/sj.cdd.4400995.

13. Melino, G.; De Laurenzi, V.; Vousden, K.H. p73: Friend or foe in tumorigenesis. *Nat. Rev. Cancer* **2002**, *2*, 605–615, doi:10.1038/nrc861.

14. Rufini, A.; Agostini, M.; Grespi, F.; Tomasini, R.; Sayan, B.S.; Niklison-Chirou, M.V.; Conforti, F.; Velletri, T.; Mastino, A.; Mak, T.W.; et al. P73 in cancer. *Genes and Cancer* **2011**, *2*, 491–502, doi:10.1177/1947601911408890.

15. Murray-Zmijewski, F.; Lane, D.P.; Bourdon, J.C. p53/p63/p73 isoforms: An orchestra of isoforms to harmonise cell differentiation and response to stress. *Cell Death Differ.* **2006**, *13*, 962–972, doi:10.1038/sj.cdd.4401914.

16. Zaika, A.I.; Slade, N.; Erster, S.H.; Sansome, C.; Joseph, T.W.; Pearl, M.; Chalas, E.; Moll, U.M. δNp73, a dominant-negative inhibitor of wild-type p53 and TAp73, is up-regulated in human tumors. *J. Exp. Med.* **2002**, *196*, 765–780, doi:10.1084/jem.20020179.

17. Müller, M.; Schilling, T.; Sayan, A.E.; Kairat, A.; Lorenz, K.; Schulze-Bergkamen, H.; Oren, M.; Koch, A.; Tannapfel, A.; Stremmel, W.; et al. TAp73/ΔNp73 influences apoptotic response, chemosensitivity and prognosis in hepatocellular carcinoma. *Cell Death Differ.* **2005**, *12*, 1564–1577, doi:10.1038/sj.cdd.4401774.

18. Ozougwu, J.; Ozougwu, J.C. Physiology of the liver Cite this paper Physiology of the liver. *Int. J. Res. Pharm. Biosci.* **2017**, *4*, 13.

19. Ananthakrishnan, A.; Gogineni, V.; Saeian, K. Epidemiology of primary and secondary liver cancers. *Semin. Intervent. Radiol.* **2006**, *23*, 47–63, doi:10.1055/s-2006-939841.

20. Ogunwobi, O.O.; Harricharran, T.; Huaman, J.; Galuza, A.; Odumuwagun, O.; Tan, Y.; Ma, G.X.; Nguyen, M.T. Mechanisms of hepatocellular carcinoma progression. *World J. Gastroenterol.* **2019**, *25*, 2279–2293, doi:10.3748/wjg.v25.i19.2279.

21. Nault, J.C.; Bioulac-Sage, P.; Zucman-Rossi, J. Hepatocellular benign tumors-from molecular classification to personalized clinical care. *Gastroenterology* **2013**, *144*, 888–902, doi:10.1053/j.gastro.2013.02.032.

22. Farazi, P.A.; DePinho, R.A. Hepatocellular carcinoma pathogenesis: From genes to environment. *Nat. Rev. Cancer* **2006**, *6*, 674–687, doi:10.1038/nrc1934.

23. Zhu, R.X.; Seto, W.K.; Lai, C.L.; Yuen, M.F. Epidemiology of hepatocellular carcinoma in the Asia-Pacific region. *Gut Liver* **2016**, *10*, 332–339, doi:10.5009/gnl15257.

24. McGlynn, K.A.; Petrick, J.L.; London, W.T. Global Epidemiology of Hepatocellular Carcinoma: An Emphasis on Demographic and Regional Variability. *Clin. Liver Dis.* **2015**, *19*, 223–238, doi:10.1016/j.cld.2015.01.001.

25. El-Serag, H.B.; Rudolph, K.L. Hepatocellular Carcinoma: Epidemiology and Molecular Carcinogenesis. *Gastroenterology* **2007**, *132*, 2557–2576, doi:10.1053/j.gastro.2007.04.061.

26. Donato, F.; Tagger, A.; Gelatti, U.; Parrinello, G.; Boffetta, P.; Albertini, A.; Decarli, A.; Trevisi, P.; Ribero, M.L.; Martelli, C.; et al. Alcohol and hepatocellular carcinoma: The effect of lifetime intake and hepatitis virus infections in men and women. *Am. J. Epidemiol.* **2002**, *155*, 323–331, doi:10.1093/aje/155.4.323.

27. Dandri, M.; Burda, M.R.; Bürkle, A.; Zuckerman, D.M.; Will, H.; Rogler, C.E.; Greten, H.; Petersen, J. Increase in de novo HBV DNA integrations in response to oxidative DNA damage or inhibition of poly(ADP-ribosyl)ation. *Hepatology* **2002**, *35*, 217–223, doi:10.1053/jhep.2002.30203.

28. Neuveut, C.; Wei, Y.; Buendia, M.A. Mechanisms of HBV-related hepatocarcinogenesis. *J. Hepatol.* **2010**, *52*, 594–604, doi:10.1016/j.jhep.2009.10.033.

29. Feitelson, M.A.; Lee, J. Hepatitis B virus integration, fragile sites, and hepatocarcinogenesis. *Cancer Lett.* **2007**, *252*, 157–170, doi:10.1016/j.canlet.2006.11.010.

30. Guerrero, R.B.; Roberts, L.R. The role of hepatitis B virus integrations in the pathogenesis of human hepatocellular carcinoma. *J. Hepatol.* **2005**, *42*, 760–777, doi:10.1016/j.jhep.2005.02.005.

31. Tsai, W.L.; Chung, R.T. Viral hepatocarcinogenesis. *Oncogene* **2010**, *29*, 2309–2324, doi:10.1038/onc.2010.36.

32. Puigvehí, M.; Moctezuma-Velázquez, C.; Villanueva, A.; Llovet, J.M. The oncogenic role of hepatitis delta virus in hepatocellular carcinoma. *JHEP Reports* **2019**, *1*, 120–130, doi:10.1016/j.jhepr.2019.05.001.

33. Rowell, R.J.; Anstee, Q.M. An overview of the genetics, mechanisms and management of NAFLD and ALD. *Clin. Med. J. R. Coll. Physicians London* **2015**, *15*, s77–s82, doi:10.7861/clinmedicine.15-6-s77.

34. Seitz, H.K.; Bataller, R.; Cortez-Pinto, H.; Gao, B.; Gual, A.; Lackner, C.; Mathurin, P.; Mueller, S.; Szabo, G.; Tsukamoto, H. Alcoholic liver disease. *Nat. Rev. Dis. Prim.* **2018**, *4*, doi:10.1038/s41572-018-0014-7.

35. Yeh, M.M.; Brunt, E.M. Pathological features of fatty liver disease. *Gastroenterology* **2014**, *147*, 754–764, doi:10.1053/j.gastro.2014.07.056.

36. Siddiqui, M.S.; Harrison, S.A.; Abdelmalek, M.F.; Anstee, Q.M.; Bedossa, P.; Castera, L.; Dimick-Santos, L.; Friedman, S.L.; Greene, K.; Kleiner, D.E.; et al. Case definitions for inclusion and analysis of endpoints in clinical trials for nonalcoholic steatohepatitis through the lens of regulatory science. *Hepatology* **2018**, *67*, 2001–2012, doi:10.1002/hep.29607.

37. Friedman, S.L.; Neuschwander-Tetri, B.A.; Rinella, M.; Sanyal, A.J. *Mechanisms of NAFLD development and therapeutic strategies*; 2018; Vol. 24; ISBN 4159101801.

38. Gong, Y.Y.; Watson, S.; Routledge, M.N. Aflatoxin Exposure and Associated Human Health Effects, a Review of Epidemiological Studies. *Food Saf.* **2016**, *4*, 14–27, doi:10.14252/foodsafetyfscj.2015026.

39. Kamdem, L.K.; Meineke, I.; Gödtel-Armbrust, U.; Brockmöller, J.; Wojnowski, L. Dominant contribution of P450 3A4 to the hepatic carcinogenic activation of aflatoxin B1. *Chem. Res. Toxicol.* **2006**, *19*, 577–586, doi:10.1021/tx050358e.

40. Hussain, S.P.; Schwank, J.; Staib, F.; Wang, X.W.; Harris, C.C. TP53 mutations and hepatocellular carcinoma: Insights into the etiology and pathogenesis of liver cancer. *Oncogene* **2007**, *26*, 2166–2176, doi:10.1038/sj.onc.1210279.

41. Gouas, D.; Shi, H.; Hainaut, P. The aflatoxin-induced TP53 mutation at codon 249 (R249S): Biomarker of exposure, early detection and target for therapy. *Cancer Lett.* **2009**, *286*, 29–37, doi:10.1016/j.canlet.2009.02.057.

42. Kew, M.C. Aflatoxins as a cause of hepatocellular carcinoma. *J. Gastrointest. Liver Dis.* **2013**, *22*, 305–310.

43. Dhanasekaran, R.; Bandoh, S.; Roberts, L.R. Molecular pathogenesis of hepatocellular carcinoma and impact of therapeutic advances. *F1000Research* **2016**, *5*, 879, doi:10.12688/f1000research.6946.1.

44. Kan, Z.; Zheng, H.; Liu, X.; Li, S.; Barber, T.D.; Gong, Z.; Gao, H.; Hao, K.; Willard, M.D.; Xu, J.; et al. Whole-genome sequencing identifies recurrent mutations in hepatocellular carcinoma. *Genome Res.* **2013**, *23*, 1422–1433, doi:10.1101/gr.154492.113.

45. Nishida, N.; Kudo, M.; Nishimura, T.; Arizumi, T.; Takita, M.; Kitai, S.; Yada, N.; Hagiwara, S.; Inoue, T.; Minami, Y.; et al. Unique association between global DNA hypomethylation and chromosomal alterations in human hepatocellular carcinoma. *PLoS One* **2013**, *8*, doi:10.1371/journal.pone.0072312.

46. Roessler, S.; Long, E.L.; Budhu, A.; Chen, Y.; Zhao, X.; Ji, J.; Walker, R.; Jia, H.L.; Ye, Q.H.; Qin, L.X.; et al. Integrative genomic identification of genes on 8p associated with hepatocellular carcinoma progression and patient survival. *Gastroenterology* **2012**, *142*, 957–966, doi:10.1053/j.gastro.2011.12.039.

47. Wang, K.; Lim, H.Y.; Shi, S.; Lee, J.; Deng, S.; Xie, T.; Zhu, Z.; Wang, Y.; Pocalyko, D.; Yang, W.J.; et al. Genomic landscape of copy number aberrations enables the identification of oncogenic drivers in hepatocellular carcinoma. *Hepatology* **2013**, *58*, 706–717, doi:10.1002/hep.26402.

48. Homayounfar, K.; Schwarz, A.; Enders, C.; Cameron, S.; Baumhoer, D.; Ramadori, G.; Lorf, T.; Gunawan, B.; Sander, B. Etiologic influence on chromosomal aberrations in European hepatocellular carcinoma identified by CGH. *Pathol. Res. Pract.* **2013**, *209*,

380–387, doi:10.1016/j.prp.2013.04.004.

49. Fernandez-Banet, J.; Lee, N.P.; Chan, K.T.; Gao, H.; Liu, X.; Sung, W.K.; Tan, W.; Fan, S.T.; Poon, R.T.; Li, S.; et al. Decoding complex patterns of genomic rearrangement in hepatocellular carcinoma. *Genomics* **2014**, *103*, 189–203, doi:10.1016/j.ygeno.2014.01.003.

50. Guichard, C.; Amaddeo, G.; Imbeaud, S.; Ladeiro, Y.; Pelletier, L.; Maad, I. Ben; Calderaro, J.; Bioulac-Sage, P.; Letexier, M.; Degos, F.; et al. Integrated analysis of somatic mutations and focal copy-number changes identifies key genes and pathways in hepatocellular carcinoma. *Nat. Genet.* **2012**, *44*, 694–698, doi:10.1038/ng.2256.

51. Ma, N.F.; Hu, L.; Fung, J.M.; Xie, D.; Zheng, B.J.; Chen, L.; Tang, D.J.; Fu, L.; Wu, Z.; Chen, M.; et al. Isolation and characterization of a novel oncogene, amplified in liver cancer 1, within a commonly amplified region at 1q21 in hepatocellular carcinoma. *Hepatology* **2008**, *47*, 503–510, doi:10.1002/hep.22072.

52. Kim, T.M.; Yim, S.H.; Shin, S.H.; Xu, H.D.; Jung, Y.C.; Park, C.K.; Choi, J.Y.; Park, W.S.; Kwon, M.S.; Fiegler, H.; et al. Clinical implication of recurrent copy number alterations in hepatocellular carcinoma and putative oncogenes in recurrent gains on 1q. *Int. J. Cancer* **2008**, *123*, 2808–2815, doi:10.1002/ijc.23901.

53. Yim, S.H.; Chung, Y.J. An overview of biomarkers and molecular signatures in HCC. *Cancers (Basel).* **2010**, *2*, 809–823, doi:10.3390/cancers2020809.

54. Wang, Y.; Wu, M.C.; Sham, J.S.T.; Zhang, W.; Wu, W.Q.; Guan, X.Y. Prognostic significance of c-myc and AIB1 amplification in hepatocellular carcinoma: A broad survey using high-throughput tissue microarray. *Cancer* **2002**, *95*, 2346–2352, doi:10.1002/cncr.10963.

55. Okamoto, H.; Yasui, K.; Zhao, C.; Arii, S.; Inazawa, J. PTK2 and EIF3S3 Genes May Be Amplification Targets at 8q23-q24 and Are Associated with Large Hepatocellular Carcinomas. *Hepatology* **2003**, *38*, 1242–1249, doi:10.1053/jhep.2003.50457.

56. Iwata, N.; Yamamoto, H.; Sasaki, S.; Itoh, F.; Suzuki, H.; Kikuchi, T.; Kaneto, H.; Iku, S.; Ozeki, I.; Karino, Y.; et al. Frequent hypermethylation of CpG islands and loss of expression of the 14-3-3 σ gene in human hepatocellular carcinoma. *Oncogene* **2000**, *19*, 5298–5302, doi:10.1038/sj.onc.1203898.

57. Yuan, B.Z.; Miller, M.J.; Keck, C.L.; Zimonjic, D.B.; Thorgeirsson, S.S.; Popescu, N.C. Cloning, characterization, and chromosomal localization of a gene frequently deleted in human liver cancer (DLC-1) homologous to rat RhoGAP. *Cancer Res.* **1998**, *58*, 2196–2199.

58. Hirohashi, S. Inactivation of the E-Cadherin-Mediated Cell Adhesion System in Human Cancers. *Am. J. Pathol.* **1998**, *153*, 333–339, doi:10.1016/S0002-9440(10)65575-7.

59. Bréchot, C.; Gozuacik, D.; Murakami, Y.; Paterlini-Bréchot, P. Molecular bases for the development of hepatitis B virus (HBV)-related hepatocellular carcinoma (HCC). *Semin. Cancer Biol.* **2000**, *10*, 211–231, doi:10.1006/scbi.2000.0321.

60. Lau, C.C.; Sun, T.; Ching, A.K.K.; He, M.; Li, J.W.; Wong, A.M.; Co, N.N.; Chan, A.W.H.; Li, P.S.; Lung, R.W.M.; et al. Viral-human chimeric transcript predisposes risk to liver cancer development and progression. *Cancer Cell* **2014**, *25*, 335–349, doi:10.1016/j.ccr.2014.01.030.

61. Li, X.; Zhang, J.; Yang, Z.; Kang, J.; Jiang, S.; Zhang, T.; Chen, T.; Li, M.; Lv, Q.; Chen, X.; et al. The function of targeted host genes determines the oncogenicity of HBV integration in hepatocellular carcinoma. *J. Hepatol.* **2014**, *60*, 975–984, doi:10.1016/j.jhep.2013.12.014.

62. Zhao, L.H.; Liu, X.; Yan, H.X.; Li, W.Y.; Zeng, X.; Yang, Y.; Zhao, J.; Liu, S.P.; Zhuang, X.H.; Lin, C.; et al. Genomic and oncogenic preference of HBV integration in hepatocellular carcinoma. *Nat. Commun.* **2016**, *7*, 1–10, doi:10.1038/ncomms12992.

63. Müller, M.; Bird, T.G.; Nault, J.C. The landscape of gene mutations in cirrhosis and hepatocellular carcinoma. *J. Hepatol.* **2020**, *72*, 990–1002, doi:10.1016/j.jhep.2020.01.019.

64. Zucman-Rossi, J.; Villanueva, A.; Nault, J.C.; Llovet, J.M. Genetic Landscape and Biomarkers of Hepatocellular Carcinoma. *Gastroenterology* **2015**, *149*, 1226-1239.e4, doi:10.1053/j.gastro.2015.05.061.

65. Nahon, P.; Zucman-Rossi, J. Single nucleotide polymorphisms and risk of hepatocellular carcinoma in cirrhosis. *J. Hepatol.* **2012**, *57*, 663–674, doi:10.1016/j.jhep.2012.02.035.

66. Caruso, S.; O'Brien, D.R.; Cleary, S.P.; Roberts, L.R.; Zucman-Rossi, J. Genetics of Hepatocellular Carcinoma: Approaches to Explore Molecular Diversity. *Hepatology* **2021**, *73*, 14–26, doi:10.1002/hep.31394.

67. Ma, Z.-X.; Yang, C.-M.; Li, M.-G.; Tu, H. Telomerase reverse transcriptase promoter mutations in hepatocellular carcinogenesis. *Hepatoma Res.* **2019**, *2019*, doi:10.20517/2394-5079.2018.104.

68. Totoki, Y.; Tatsuno, K.; Covington, K.R.; Ueda, H.; Creighton, C.J.; Kato, M.; Tsuji, S.; Donehower, L.A.; Slagle, B.L.; Nakamura, H.; et al. Trans-ancestry mutational landscape of hepatocellular carcinoma genomes. *Nat. Genet.* **2014**, *46*, 1267–1273, doi:10.1038/ng.3126.

69. Schulze, K.; Imbeaud, S.; Letouzé, E.; Alexandrov, L.B.; Calderaro, J.; Rebouissou, S.; Couchy, G.; Meiller, C.; Shinde, J.; Soysouvanh, F.; et al. Exome sequencing of hepatocellular carcinomas identifies new mutational signatures and potential therapeutic targets. *Nat. Genet.* **2015**, *47*, 505–511, doi:10.1038/ng.3252.

70. Fujimoto, A.; Totoki, Y.; Abe, T.; Boroevich, K.A.; Hosoda, F.; Nguyen, H.H.; Aoki, M.; Hosono, N.; Kubo, M.; Miya, F.; et al. Whole-genome sequencing of liver cancers identifies etiological influences on mutation patterns and recurrent mutations in chromatin regulators. *Nat. Genet.* **2012**, *44*, 760–764, doi:10.1038/ng.2291.

71. Huang, J.; Deng, Q.; Wang, Q.; Li, K.Y.; Dai, J.H.; Li, N.; Zhu, Z.D.; Zhou, B.; Liu, X.Y.; Liu, R.F.; et al. Exome sequencing of hepatitis B virus-associated hepatocellular carcinoma. *Nat. Genet.* **2012**, *44*, 1117–1121, doi:10.1038/ng.2391.

72. Cleary, S.P.; Jeck, W.R.; Zhao, X.; Chen, K.; Selitsky, S.R.; Savich, G.L.; Tan, T.-X.; Wu, M.C.; Getz, G.; Lawrence, M.S.; et al. Identification of driver genes in hepatocellular carcinoma by exome sequencing. *Hepatology* **2013**, *58*, 1693–1702, doi:10.1002/hep.26540.

73. Ally, A.; Balasundaram, M.; Carlsen, R.; Chuah, E.; Clarke, A.; Dhalla, N.; Holt, R.A.; Jones, S.J.M.; Lee, D.; Ma, Y.; et al. Comprehensive and Integrative Genomic Characterization of Hepatocellular Carcinoma. *Cell* **2017**, *169*, 1327-1341.e23, doi:10.1016/j.cell.2017.05.046.

74. Nault, J.C.; Martin, Y.; Caruso, S.; Hirsch, T.Z.; Bayard, Q.; Calderaro, J.; Charpy, C.;

Copie-Bergman, C.; Ziol, M.; Bioulac-Sage, P.; et al. Clinical Impact of Genomic Diversity From Early to Advanced Hepatocellular Carcinoma. *Hepatology* **2020**, *71*, 164–182, doi:10.1002/hep.30811.

75. Weber, M.; Hellmann, I.; Stadler, M.B.; Ramos, L.; Pääbo, S.; Rebhan, M.; Schübeler, D. Distribution, silencing potential and evolutionary impact of promoter DNA methylation in the human genome. *Nat. Genet.* **2007**, *39*, 457–466, doi:10.1038/ng1990.

76. Pogribny, I.P.; Rusyn, I. Role of epigenetic aberrations in the development and progression of human hepatocellular carcinoma. *Cancer Lett.* **2014**, *342*, 223–230, doi:10.1016/j.canlet.2012.01.038.

77. Tao, R.; Li, J.; Xin, J.; Wu, J.; Guo, J.; Zhang, L.; Jiang, L.; Zhang, W.; Yang, Z.; Li, L. Methylation profile of single hepatocytes derived from hepatitis B virus-related hepatocellular carcinoma. *PLoS One* **2011**, *6*, doi:10.1371/journal.pone.0019862.

78. Shen, J.; Wang, S.; Zhang, Y.J.; Kappil, M.; Wu, H.C.; Kibriya, M.G.; Wang, Q.; Jasmine, F.; Ahsan, H.; Lee, P.H.; et al. Genome-wide DNA methylation profiles in hepatocellular carcinoma. *Hepatology* **2012**, *55*, 1799–1808, doi:10.1002/hep.25569.

79. van Attikum, H.; Gasser, S.M. Crosstalk between histone modifications during the DNA damage response. *Trends Cell Biol.* **2009**, *19*, 207–217, doi:10.1016/j.tcb.2009.03.001.

80. Bracken, A.P.; Pasini, D.; Capra, M.; Prosperini, E.; Colli, E.; Helin, K. EZH2 is downstream of the pRB-E2F pathway, essential for proliferation and amplified in cancer. *EMBO J.* **2003**, *22*, 5323–5335, doi:10.1093/emboj/cdg542.

81. Bhattacharya, S.; Reddy, D.; Ingle, A.; Khade, B.; Gupta, S. Brief Communication: Featured Article: Histone H2A mono-ubiquitination and cellular transformation are inversely related in N-nitrosodiethylamine-induced hepatocellular carcinoma. *Exp. Biol. Med.* **2016**, *241*, 1739–1744, doi:10.1177/1535370216649262.

82. Liu, C.; Liu, L.; Shan, J.; Shen, J.; Xu, Y.; Zhang, Q.; Yang, Z.; Wu, L.; Xia, F.; Bie, P.; et al. Histone deacetylase 3 participates in self-renewal of liver cancer stem cells through histone modification. *Cancer Lett.* **2013**, *339*, 60–69, doi:10.1016/j.canlet.2013.07.022.

83. Meng, F.; Henson, R.; Wehbe–Janek, H.; Ghoshal, K.; Jacob, S.T.; Patel, T. MicroRNA-21 Regulates Expression of the PTEN Tumor Suppressor Gene in Human Hepatocellular Cancer. *Gastroenterology* **2007**, *133*, 647–658, doi:10.1053/j.gastro.2007.05.022.

84. Xu, G.; Zhang, Y.; Wei, J.; Jia, W.; Ge, Z.; Zhang, Z.; Liu, X. MicroRNA-21 promotes hepatocellular carcinoma HepG2 cell proliferation through repression of mitogen-activated protein kinase-kinase 3. *BMC Cancer* **2013**, *13*, doi:10.1186/1471-2407-13-469.

85. Garofalo, M.; Di Leva, G.; Romano, G.; Nuovo, G.; Suh, S.; Ngankeu, A.; Taccioli, C.; Pichiorri, F.; Alder, H.; Secchiero, P.; et al. miR-221&222 Regulate TRAIL Resistance and Enhance Tumorigenicity through PTEN and TIMP3 Downregulation. *Cancer Cell* **2009**, *16*, 498–509, doi:10.1016/j.ccr.2009.10.014.

86. Yang, X.; Zhang, X.F.; Lu, X.; Jia, H.L.; Liang, L.; Dong, Q.Z.; Ye, Q.H.; Qin, L.X. MicroRNA-26a suppresses angiogenesis in human hepatocellular carcinoma by targeting hepatocyte growth factor-cMet pathway. *Hepatology* **2014**, *59*, 1874–1885, doi:10.1002/hep.26941.

87. Tsai, M.; Manor, O.; Wan, Y.; Mosammaparast, N.; Wang, J.K.; Lan, F.; Shi, Y.; Segal, E.; Chang, H.Y. Long Noncoding RNA as Modular Scaffold of Histone Modification Complexes. *Science (80-.).* **2010**, *329*, 689–693, doi:10.1126/science.1192002.

88. Geng, Y.J.; Xie, S.L.; Li, Q.; Ma, J.; Wang, G.Y. Large intervening non-coding RNA HOTAIR is associated with hepatocellular carcinoma progression. *J. Int. Med. Res.* **2011**, *39*, 2119–2128, doi:10.1177/147323001103900608.

89. Bataller, R.; Brenner, D.A. Liver fibrosis. *J. Clin. Invest.* **2005**, *115*, 209–218, doi:10.1172/JCI24282.

90. Zhou, W.C.; Zhang, Q.B.; Qiao, L. Pathogenesis of liver cirrhosis. *World J. Gastroenterol.* **2014**, *20*, 7312–7324, doi:10.3748/wjg.v20.i23.7312.

91. Friedman, S.L. Mechanisms of Hepatic Fibrogenesis. *Gastroenterology* **2008**, *134*, 1655–1669, doi:10.1053/j.gastro.2008.03.003.

92. Lee, U.E.; Friedman, S.L. Mechanisms of hepatic fibrogenesis. *Best Pract. Res. Clin.*

Gastroenterol. **2011**, *25*, 195–206, doi:10.1016/j.bpg.2011.02.005.

93. Seki, E.; Schwabe, R.F. Hepatic inflammation and fibrosis: Functional links and key pathways. *Hepatology* **2015**, *61*, 1066–1079, doi:10.1002/hep.27332.

94. Ying, H.Z.; Chen, Q.; Zhang, W.Y.; Zhang, H.H.; Ma, Y.; Zhang, S.Z.; Fang, J.; Yu, C.H. PDGF signaling pathway in hepatic fibrosis pathogenesis and therapeutics (Review). *Mol. Med. Rep.* **2017**, *16*, 7879–7889, doi:10.3892/mmr.2017.7641.

95. Xu, F.; Liu, C.; Zhou, D.; Zhang, L. TGF-β/SMAD Pathway and Its Regulation in Hepatic Fibrosis. *J. Histochem. Cytochem.* **2016**, *64*, 157–167, doi:10.1369/0022155415627681.

96. Nishikawa, K.; Osawa, Y.; Kimura, K. Wnt/β-catenin signaling as a potential target for the treatment of liver cirrhosis using antifibrotic drugs. *Int. J. Mol. Sci.* **2018**, *19*, doi:10.3390/ijms19103103.

97. Hazra, S.; Xiong, S.; Wang, J.; Rippe, R.A.; Chatterjee, V.K.K.; Tsukamoto, H. Peroxisome Proliferator-activated Receptor γ Induces a Phenotypic Switch from Activated to Quiescent Hepatic Stellate Cells. *J. Biol. Chem.* **2004**, *279*, 11392–11401, doi:10.1074/jbc.M310284200.

98. Affo, S.; Yu, L.X.; Schwabe, R.F. The Role of Cancer-Associated Fibroblasts and Fibrosisin Liver Cancer. *Annu. Rev. Pathol. Mech. Dis.* **2017**, *12*, 153–186, doi:10.1146/annurev-pathol-052016-100322.

99. Xie, G.; Diehl, A.M. Evidence for and against epithelial-to-mesenchymal transition in the liver. *Am. J. Physiol. - Gastrointest. Liver Physiol.* **2013**, *305*, doi:10.1152/ajpgi.00289.2013.

100. Kisseleva, T.; Cong, M.; Paik, Y.H.; Scholten, D.; Jiang, C.; Benner, C.; Iwaisako, K.; Moore-Morris, T.; Scott, B.; Tsukamoto, H.; et al. Myofibroblasts revert to an inactive phenotype during regression of liver fibrosis. *Proc. Natl. Acad. Sci. U. S. A.* **2012**, *109*, 9448–9453, doi:10.1073/pnas.1201840109.

101. Mederacke, I.; Hsu, C.C.; Troeger, J.S.; Huebener, P.; Mu, X.; Dapito, D.H.; Pradere, J.P.; Schwabe, R.F. Fate tracing reveals hepatic stellate cells as dominant contributors to liver fibrosis independent of its aetiology. *Nat. Commun.* **2013**, *4*, 1–11, doi:10.1038/ncomms3823.

102. Tacke, F.; Zimmermann, H.W. Macrophage heterogeneity in liver injury and fibrosis. *J. Hepatol.* **2014**, *60*, 1090–1096, doi:10.1016/j.jhep.2013.12.025.

103. Sahin, H.; Trautwein, C.; Wasmuth, H.E. Functional role of chemokines in liver disease models. *Nat. Rev. Gastroenterol. Hepatol.* **2010**, *7*, 682–690, doi:10.1038/nrgastro.2010.168.

104. Roehlen, N.; Crouchet, E.; Baumert, T.F. Liver Fibrosis: Mechanistic Concepts and Therapeutic Perspectives. *Cells* **2020**, *9*, 875, doi:10.3390/cells9040875.

105. Schlageter, M.; Terracciano, L.M.; D'Angelo, S.; Sorrentino, P. Histopathology of hepatocellular carcinoma. *World J. Gastroenterol.* **2014**, *20*, 15955–15964, doi:10.3748/wjg.v20.i43.15955.

106. Jiang, K.; Al-Diffhala, S.; Centeno, B.A. Primary liver cancers—part 1: Histopathology, differential diagnoses, and risk stratification. *Cancer Control* **2018**, *25*, 1–26, doi:10.1177/1073274817744625.

107. Kojiro, M. Histopathology of liver cancers. *Best Pract. Res. Clin. Gastroenterol.* **2005**, *19*, 39–62, doi:10.1016/j.bpg.2004.10.007.

108. Liu, J.; Dang, H.; Wang, X.W. The significance of intertumor and intratumor heterogeneity in liver cancer. *Exp. Mol. Med.* **2018**, *50*, e416-8, doi:10.1038/emm.2017.165.

109. Barcena-Varela, M.; Lujambio, A. The endless sources of hepatocellular carcinoma heterogeneity. *Cancers (Basel).* **2021**, *13*, 1–15, doi:10.3390/cancers13112621.

110. Torrecilla, S.; Sia, D.; Harrington, A.N.; Zhang, Z.; Cabellos, L.; Cornella, H.; Moeini, A.; Camprecios, G.; Leow, W.Q.; Fiel, M.I.; et al. Trunk mutational events present minimal intra- and inter-tumoral heterogeneity in hepatocellular carcinoma. *J. Hepatol.* **2017**, *67*, 1222–1231, doi:10.1016/j.jhep.2017.08.013.

111. Stanger, B.Z. Cellular Homeostasis and Repair in the Mammalian Liver. *Annu. Rev. Physiol.* **2015**, *77*, 179–200, doi:10.1146/annurev-physiol-021113-170255.

112. Miyajima, A.; Tanaka, M.; Itoh, T. Stem/progenitor cells in liver development, homeostasis, regeneration, and reprogramming. *Cell Stem Cell* **2014**, *14*, 561–574, doi:10.1016/j.stem.2014.04.010.

113. Peng, N.; Li, L.; Cai, X.; Tan, S.; Wu, T. Liver Stem/Progenitor Cells in the Canals of Hering: Cellular Origin of Hepatocellular Carcinoma with Bile Duct Tumor Thrombi? *Stem Cell Rev. Reports* **2010**, *6*, 579–584, doi:10.1007/s12015-010-9188-4.

114. Fausto, N.; Campbell, J.S. The role of hepatocytes and oval cells in liver regeneration and repopulation. *Mech. Dev.* **2003**, *120*, 117–130, doi:10.1016/S0925-4773(02)00338-6.

115. Sia, D.; Villanueva, A.; Friedman, S.L.; Llovet, J.M. Liver Cancer Cell of Origin, Molecular Class, and Effects on Patient Prognosis. *Gastroenterology* **2017**, *152*, 745–761, doi:10.1053/j.gastro.2016.11.048.

116. Lee, K.P.; Lee, J.H.; Kim, T.S.; Kim, T.H.; Park, H.D.; Byun, J.S.; Kim, M.C.; Jeong, W. Il; Calvisi, D.F.; Kim, J.M.; et al. The Hippo-Salvador pathway restrains hepatic oval cell proliferation, liver size, and liver tumorigenesis. *Proc. Natl. Acad. Sci. U. S. A.* **2010**, *107*, 8248–8253, doi:10.1073/pnas.0912203107.

117. Benhamouche, S.; Curto, M.; Saotome, I.; Gladden, A.B.; Liu, C.H.; Giovannini, M.; McClatchey, A.I. Nf2/Merlin controls progenitor homeostasis and tumorigenesis in the liver. *Genes Dev.* **2010**, *24*, 1718–1730, doi:10.1101/gad.1938710.

118. Mu, X.; Español-Suñer, R.; Mederacke, I.; Affò, S.; Manco, R.; Sempoux, C.; Lemaigre, F.P.; Adili, A.; Yuan, D.; Weber, A.; et al. Hepatocellular carcinoma originates from hepatocytes and not from the progenitor/biliary compartment. *J. Clin. Invest.* **2015**, *125*, 3891–3903, doi:10.1172/JCI77995.

119. Shin, S.; Wangensteen, K.J.; Teta-Bissett, M.; Wang, Y.J.; Mosleh-Shirazi, E.; Buza, E.L.; Greenbaum, L.E.; Kaestner, K.H. Genetic lineage tracing analysis of the cell of origin of hepatotoxin-induced liver tumors in mice. *Hepatology* **2016**, *64*, 1163–1177, doi:10.1002/hep.28602.

120. Umemura, A.; He, F.; Taniguchi, K.; Nakagawa, H.; Yamachika, S.; Font-Burgada, J.; Zhong, Z.; Subramaniam, S.; Raghunandan, S.; Duran, A.; et al. p62, Upregulated during Preneoplasia, Induces Hepatocellular Carcinogenesis by Maintaining Survival of Stressed HCC-Initiating Cells. *Cancer Cell* **2016**, *29*, 935–948, doi:10.1016/j.ccell.2016.04.006.

121. Tschaharganeh, D.F.; Bosbach, B.; Lowe, S.W. Coordinated Tumor Suppression by

Chromosome 8p. *Cancer Cell* **2016**, *29*, 617–619, doi:10.1016/j.ccell.2016.04.011.

122. Chen, Y.; Wong, P.P.; Sjeklocha, L.; Steer, C.J.; Sahin, M.B. Mature Hepatocytes Exhibit Unexpected Plasticity by Direct Dedifferentiation Into Liver Progenitor Cells in Culture. *Hepatology* **2011**, *55*, 563–574, doi:10.1002/hep.24712.

123. Castelli, G.; Pelosi, E.; Testa, U. Liver cancer: Molecular characterization, clonal evolution and cancer stem cells. *Cancers (Basel).* **2017**, *9*, 1–36, doi:10.3390/cancers9090127.

124. Lozano-Torres, B.; Estepa-Fernández, A.; Rovira, M.; Orzáez, M.; Serrano, M.; Martínez-Máñez, R.; Sancenón, F. The chemistry of senescence. *Nat. Rev. Chem.* **2019**, *3*, 426–441, doi:10.1038/s41570-019-0108-0.

125. Childs, B.G.; Baker, D.J.; Kirkland, J.L.; Campisi, J.; Deursen, J.M. Senescence and apoptosis: dueling or complementary cell fates? *EMBO Rep.* **2014**, *15*, 1139–1153, doi:10.15252/embr.201439245.

126. Muñoz-Espín, D.; Serrano, M. Cellular senescence: From physiology to pathology. *Nat. Rev. Mol. Cell Biol.* **2014**, *15*, 482–496, doi:10.1038/nrm3823.

127. Georgakopoulou, E.A.; Tsimaratou, K.; Evangelou, K.; Fernandez, M.P.J.; Zoumpourlis, V.; Trougakos, I.P.; Kletsas, D.; Bartek, J.; Serrano, M.; Gorgoulis, V.G. Specific lipofuscin staining as a novel biomarker to detect replicative and stress-induced senescence. A PORTA EA. 2002. Pigments in Aging: An Overview. Ann N Y Acad Sci, 959(1):57–65 DOI: 10.1111/j.1749-6632.2002.tb02083.x.method applicable in cryo-prese. *Aging (Albany. NY).* **2013**, *5*, 37–50.

128. Zhang, R.; Chen, W.; Adams, P.D. Molecular Dissection of Formation of Senescence-Associated Heterochromatin Foci. *Mol. Cell. Biol.* **2007**, *27*, 2343–2358, doi:10.1128/mcb.02019-06.

129. Victorelli, S.; Passos, J.F. Telomeres and Cell Senescence - Size Matters Not. *EBioMedicine* **2017**, *21*, 14–20, doi:10.1016/j.ebiom.2017.03.027.

130. Lopes-Paciencia, S.; Saint-Germain, E.; Rowell, M.C.; Ruiz, A.F.; Kalegari, P.; Ferbeyre, G. The senescence-associated secretory phenotype and its regulation. *Cytokine* **2019**, *117*, 15–22, doi:10.1016/j.cyto.2019.01.013.

131. Kumari, R.; Jat, P. Mechanisms of Cellular Senescence: Cell Cycle Arrest and Senescence Associated Secretory Phenotype. *Front. Cell Dev. Biol.* **2021**, *9*, 1–24, doi:10.3389/fcell.2021.645593.

132. Huda, N.; Liu, G.; Hong, H.; Yan, S.; Khambu, B.; Yin, X.M. Hepatic senescence, the good and the bad. *World J. Gastroenterol.* **2019**, *25*, 5069–5081, doi:10.3748/wjg.v25.i34.5069.

133. Blackburn, E.H. Structure and function of telomeres. *Nature* **1991**, *350*, 569–573, doi:10.1038/350569a0.

134. De Lange, T. Shelterin: The protein complex that shapes and safeguards human telomeres. *Genes Dev.* **2005**, *19*, 2100–2110, doi:10.1101/gad.1346005.

135. D'Adda Di Fagagna, F. Living on a break: Cellular senescence as a DNA-damage response. *Nat. Rev. Cancer* **2008**, *8*, 512–522, doi:10.1038/nrc2440.

136. Wade Harper, J.; Adami, G.R.; Wei, N.; Keyomarsi, K.; Elledge, S.J. The p21 Cdk-interacting protein Cip1 is a potent inhibitor of G1 cyclin-dependent kinases. *Cell* **1993**, *75*, 805–816, doi:10.1016/0092-8674(93)90499-G.

137. Serrano, M. The tumor suppressor protein p16(INK4a). *Exp. Cell Res.* **1997**, *237*, 7–13, doi:10.1006/excr.1997.3824.

138. Petti, C.; Molla, A.; Vegetti, C.; Ferrone, S.; Anichini, A.; Sensi, M. Coexpression of NRASQ61R and BRAFV600E in human melanoma cells activates senescence and increases susceptibility to cell-mediated cytotoxicity. *Cancer Res.* **2006**, *66*, 6503–6511, doi:10.1158/0008-5472.CAN-05-4671.

139. Courtois-Cox, S.; Jones, S.L.; Cichowski, K. Many roads lead to oncogene-induced senescence. *Oncogene* **2008**, *27*, 2801–2809, doi:10.1038/sj.onc.1210950.

140. Young, A.P.; Kaelin, W.G. Senescence triggered by the loss of the VHL tumor suppressor. *Cell Cycle* **2008**, *7*, 1709–1712, doi:10.4161/cc.7.12.6124.

141. Di Micco, R.; Fumagalli, M.; Cicalese, A.; Piccinin, S.; Gasparini, P.; Luise, C.; Schurra, C.; Garré, M.; Giovanni Nuciforo, P.; Bensimon, A.; et al. Oncogene-induced senescence is a DNA damage response triggered by DNA hyper-replication. *Nature* **2006**, *444*, 638–642, doi:10.1038/nature05327.

142. Bartkova, J.; Rezaei, N.; Liontos, M.; Karakaidos, P.; Kletsas, D.; Issaeva, N.; Vassiliou, L.F.; Kolettas, E.; Niforou, K.; Zoumpourlis, V.C.; et al. Oncogene-induced senescence is part of the tumorigenesis barrier imposed by DNA damage checkpoints. **2006**, *444*, 2–6, doi:10.1038/nature05268.

143. Kim, W.Y.; Sharpless, N.E. The Regulation of INK4/ARF in Cancer and Aging. *Cell* **2006**, *127*, 265–275, doi:10.1016/j.cell.2006.10.003.

144. Gil, J.; Peters, G. Regulation of the INK4b-ARF-INK4a tumour suppressor locus: All for one or one for all. *Nat. Rev. Mol. Cell Biol.* **2006**, *7*, 667–677, doi:10.1038/nrm1987.

145. Bracken, A.P.; Kleine-Kohlbrecher, D.; Dietrich, N.; Pasini, D.; Gargiulo, G.; Beekman, C.; Theilgaard-Mönch, K.; Minucci, S.; Porse, B.T.; Marine, J.C.; et al. The Polycomb group proteins bind throughout the INK4A-ARF locus and are disassociated in senescent cells. *Genes Dev.* **2007**, *21*, 525–530, doi:10.1101/gad.415507.

146. Ogrunc, M.; Di Micco, R.; Liontos, M.; Bombardelli, L.; Mione, M.; Fumagalli, M.; Gorgoulis, V.G.; D'Adda Di Fagagna, F. Oncogene-induced reactive oxygen species fuel hyperproliferation and DNA damage response activation. *Cell Death Differ.* **2014**, *21*, 998–1012, doi:10.1038/cdd.2014.16.

147. Sun, P.; Yoshizuka, N.; New, L.; Moser, B.A.; Li, Y.; Liao, R.; Xie, C.; Chen, J.; Deng, Q.; Yamout, M.; et al. PRAK Is Essential for ras-Induced Senescence and Tumor Suppression. *Cell* **2007**, *128*, 295–308, doi:10.1016/j.cell.2006.11.050.

148. Mangnall, D.; Bird, N.C.; Majeed, A.W. The molecular physiology of liver regeneration following partial hepatectomy. *Liver Int.* **2003**, *23*, 124–138, doi:10.1034/j.1600-0676.2003.00812.x.

149. Malato, Y.; Naqvi, S.; Schürmann, N.; Ng, R.; Wang, B.; Zape, J.; Kay, M.A.; Grimm, D.; Willenbring, H. Fate tracing of mature hepatocytes in mouse liver homeostasis and regeneration. *J. Clin. Invest.* **2011**, *121*, 4850–4860, doi:10.1172/JCI59261.

150. Gagliano, N.; Grizzi, F.; Annoni, G. Mechanisms of aging and liver functions. *Dig. Dis.* **2007**, *25*, 118–123, doi:10.1159/000099475.

151. Hoare, M.; Das, T.; Alexander, G. Ageing, telomeres, senescence, and liver injury. *J. Hepatol.* **2010**, *53*, 950–961, doi:10.1016/j.jhep.2010.06.009.

152. Ferreira-Gonzalez, S.; Rodrigo-Torres, D.; Gadd, V.L.; Forbes, S.J. Cellular Senescence in Liver Disease and Regeneration. *Semin. Liver Dis.* **2021**, *41*, 50–66, doi:10.1055/s-0040-1722262.

153. Baker, D.J.; Childs, B.G.; Durik, M.; Wijers, M.E.; Sieben, C.J.; Zhong, J.; Saltness, R.A.; Jeganathan, K.B.; Casaclang Verzosa, G.; Pezeshki, A.; et al. Naturally occurring p16 Ink4a-positive cells shorten healthy lifespan. *Nature* **2016**, *530*, 184–189, doi:10.1038/nature16932.

154. Childs, B.G.; Gluscevic, M.; Baker, D.J.; Laberge, R.M.; Marquess, D.; Dananberg, J.; Van Deursen, J.M. Senescent cells: An emerging target for diseases of ageing. *Nat. Rev. Drug Discov.* **2017**, *16*, 718–735, doi:10.1038/nrd.2017.116.

155. Fausto, N. Liver regeneration. *J. Hepatol.* **2000**, *32*, 19–31, doi:10.1016/s0168-8278(00)80412-2.

156. Tsukada, S.; Parsons, C.J.; Rippe, R.A. Mechanisms of liver fibrosis. *Clin. Chim. Acta* **2006**, *364*, 33–60, doi:10.1016/j.cca.2005.06.014.

157. Rudolph, K.L.; Chang, S.; Millard, M.; Schreiber-Agus, N.; DePinho, R.A. Inhibition of experimental liver cirrhosis in mice by telomerase gene delivery. *Science (80-.).* **2000**, *287*, 1253–1258, doi:10.1126/science.287.5456.1253.

158. Feng, X.X.; Luo, J.; Liu, M.; Yan, W.; Zhou, Z.Z.; Xia, Y.J.; Tu, W.; Li, P.Y.; Feng, Z.H.; Tian, D.A. Sirtuin 6 promotes transforming growth factor-β1/H2O2/HOCl-mediated enhancement of hepatocellular carcinoma cell tumorigenicity by suppressing cellular senescence. *Cancer Sci.* **2015**, *106*, 559–566, doi:10.1111/cas.12632.

159. Suh, S. Il; Pyun, H.Y.; Cho, J.W.; Baek, W.K.; Park, J.B.; Kwon, T.K.; Park, J.W.; Suh, M.H.; Carson, D.A. 5-Aza-2'-deoxycytidine leads to down-regulation of aberrant p16INK4A RNA transcripts and restores the functional retinoblastoma protein pathway in hepatocellular carcinoma cell lines. *Cancer Lett.* **2000**, *160*, 81–88, doi:10.1016/S0304-3835(00)00566-8.

160. Zhang, H.; Zheng, H.; Mu, W.; He, Z.; Yang, B.; Ji, Y.; Hui, L. DUSP16 ablation arrests the cell cycle and induces cellular senescence. **2015**, *282*, 4580–4594, doi:10.1111/febs.13518.

161. Cattaneo, M.; Morozumi, Y.; Perazza, D.; Boussouar, F.; Jamshidikia, M.; Rousseaux,

S.; Verdel, A.; Khochbin, S. Lessons from yeast on emerging roles of the ATAD2 protein family in gene regulation and genome organization. *Mol. Cells* **2014**, *37*, 851–856, doi:10.14348/molcells.2014.0258.

162. Caron, C.; Lestrat, C.; Marsal, S.; Escoffier, E.; Curtet, S.; Virolle, V.; Barbry, P.; Debernardi, A.; Brambilla, C.; Brambilla, E.; et al. Functional characterization of ATAD2 as a new cancer/testis factor and a predictor of poor prognosis in breast and lung cancers. *Oncogene* **2010**, *29*, 5171–5181, doi:10.1038/onc.2010.259.

163. Boussouar, F.; Jamshidikia, M.; Morozumi, Y.; Rousseaux, S.; Khochbin, S. Malignant genome reprogramming by ATAD2. *Biochim. Biophys. Acta - Gene Regul. Mech.* **2013**, *1829*, 1010–1014, doi:10.1016/j.bbagrm.2013.06.003.

164. Morozumi, Y.; Boussouar, F.; Tan, M.; Chaikuad, A.; Jamshidikia, M.; Colak, G.; He, H.; Nie, L.; Petosa, C.; De Dieuleveult, M.; et al. ATAD2 is a generalist facilitator of chromatin dynamics in embryonic stem cells. *J. Mol. Cell Biol.* **2016**, *8*, 349–362, doi:10.1093/jmcb/mjv060.

165. Cho, C.; Jang, J.; Kang, Y.; Watanabe, H.; Uchihashi, T.; Kim, S.J.; Kato, K.; Lee, J.Y.; Song, J.J. Structural basis of nucleosome assembly by the Abo1 AAA+ ATPase histone chaperone. *Nat. Commun.* **2019**, *10*, 1–13, doi:10.1038/s41467-019-13743-9.

166. Koo, S.J.; Fernández-Montalván, A.E.; Badock, V.; Ott, C.J.; Holton, S.J.; von Ahsen, O.; Toedling, J.; Vittori, S.; Bradner, J.E.; Gorjánácz, M. ATAD2 is an epigenetic reader of newly synthesized histone marks during DNA replication. *Oncotarget* **2016**, *7*, 70323–70335, doi:10.18632/oncotarget.11855.

167. Shahnejat-Bushehri, S.; Ehrenhofer-Murray, A.E. The ATAD2/ANCCA homolog Yta7 cooperates with Scm3HJURP to deposit Cse4CENP-A at the centromere in yeast. *Proc. Natl. Acad. Sci. U. S. A.* **2020**, *117*, 5386–5393, doi:10.1073/pnas.1917814117.

168. Zou, J.X.; Revenko, A.S.; Li, L.B.; Gemo, A.T.; Chen, H.-W.W. ANCCA, an estrogen-regulated AAA+ ATPase coactivator for ERα, is required for coregulator occupancy and chromatin modification. *Proc. Natl. Acad. Sci. U. S. A.* **2007**, *104*, 18067–18072, doi:10.1073/pnas.0705814104.

169. Revenko, A.S.; Kalashnikova, E. V.; Gemo, A.T.; Zou, J.X.; Chen, H.-W. Chromatin Loading of E2F-MLL Complex by Cancer-Associated Coregulator ANCCA via

Reading a Specific Histone Mark. *Mol. Cell. Biol.* **2010**, *30*, 5260–5272, doi:10.1128/mcb.00484-10.

170. Ciró, M.; Prosperini, E.; Quarto, M.; Grazini, U.; Walfridsson, J.; McBlane, F.; Nucifero, P.; Pacchiana, G.; Capra, M.; Christensen, J.; et al. ATAD2 is a novel cofactor for MYC, overexpressed and amplified in aggressive tumors. *Cancer Res.* **2009**, *69*, 8491–8498, doi:10.1158/0008-5472.CAN-09-2131.

171. Zhang, Y.; Sun, Y.; Li, Y.; Fang, Z.; Wang, R.; Pan, Y.; Hu, H.; Luo, X.; Ye, T.; Li, H.; et al. ANCCA protein expression is a novel independent poor prognostic marker in surgically resected lung adenocarcinoma. *Ann. Surg. Oncol.* **2013**, *20*, 577–582, doi:10.1245/s10434-013-3027-1.

172. Wan, W.N.; Zhang, Y.X.; Wang, X.M.; Liu, Y.J.; Zhang, Y.Q.; Que, Y.H.; Zhao, W.J. ATAD2 is highly expressed in ovarian carcinomas and indicates poor prognosis. *Asian Pacific J. Cancer Prev.* **2014**, *15*, 2777–2783, doi:10.7314/APJCP.2014.15.6.2777.

173. Liu, Q.; Liu, H.; Li, L.; Dong, X.; Ru, X.; Fan, X.; Wen, T.; Liu, J. ATAD2 predicts poor outcomes in patients with ovarian cancer and is a marker of proliferation. *Int. J. Oncol.* **2020**, *56*, 219–231, doi:10.3892/ijo.2019.4913.

174. Hou, M.; Huang, R.; Song, Y.; Feng, D.; Jiang, Y.; Liu, M. ATAD2 overexpression is associated with progression and prognosis in colorectal cancer. *Jpn. J. Clin. Oncol.* **2016**, *46*, 222–227, doi:10.1093/jjco/hyv195.

175. Luo, Y.; Ye, G.Y.; Qin, S.L.; Yu, M.H.; Mu, Y.F.; Zhong, M. ATAD2 Overexpression Identifies Colorectal Cancer Patients with Poor Prognosis and Drives Proliferation of Cancer Cells. *Gastroenterol. Res. Pract.* **2015**, *2015*, doi:10.1155/2015/936564.

176. Zheng, L.; Li, T.; Zhang, Y.; Guo, Y.; Yao, J.; Dou, L.; Guo, K. Oncogene ATAD2 promotes cell proliferation, invasion and migration in cervical cancer. *Oncol. Rep.* **2015**, *33*, 2337–2344, doi:10.3892/or.2015.3867.

177. Zhang, M.J.; Zhang, C.Z.; Du, W.J.; Yang, X.Z.; Chen, Z.P. ATAD2 is overexpressed in gastric cancer and serves as an independent poor prognostic biomarker. *Clin. Transl. Oncol.* **2016**, *18*, 776–781, doi:10.1007/s12094-015-1430-8.

178. Hwang, H.W.; Ha, S.Y.; Bang, H.; Park, C.K. ATAD2 as a poor prognostic marker for hepatocellular carcinoma after curative resection. *Cancer Res. Treat.* **2015**, *47*, 853–

861, doi:10.4143/crt.2014.177.

179. Han, H.J.; Huang, Q.Y.; Huang, L.J.; Chang, F.; Diao, Q.Z. Prognostic value of ATPase family, AAA+ domain containing 2 expression in human cancers: A systematic review and meta-Analysis. *Med. (United States)* **2019**, *98*, doi:10.1097/MD.0000000000017180.

180. Wu, G.; Lu, X.; Wang, Y.; He, H.; Meng, X.; Xia, S.; Zhen, K.; Liu, Y. Epigenetic high regulation of ATAD2 regulates the Hh pathway in human hepatocellular carcinoma. *Int. J. Oncol.* **2014**, *45*, 351–361, doi:10.3892/ijo.2014.2416.

181. Lu, W.J.; Chua, M.S.; So, S.K. Suppression of ATAD2 inhibits hepatocellular carcinoma progression through activation of p53-and p38-mediated apoptotic signaling. *Oncotarget* **2015**, *6*, 41722–41735, doi:10.18632/oncotarget.6152.

182. Rosenbaum, D.M.; Rasmussen, S.G.F.F.; Kobilka, B.K. The structure and function of G-protein-coupled receptors. *Nature* **2009**, *459*, 356–363, doi:10.1038/nature08144.

183. Weis, W.I.; Kobilka, B.K. The Molecular Basis of G Protein–Coupled Receptor Activation. *Annu. Rev. Biochem.* **2018**, *87*, 897–919, doi:10.1146/annurev-biochem-060614-033910.

184. Hamann, J.; Aust, G.; Araç, D.; Engel, F.B.; Formstone, C.; Fredriksson, R.; Hall, R.A.; Harty, B.L.; Kirchhoff, C.; Knapp, B.; et al. International Union of Basic and Clinical Pharmacology. XCIV. Adhesion G Protein-Coupled Receptors. *Pharmacol. Rev.* **2015**, *67*, 338–367, doi:10.1124/pr.114.009647.

185. Langenhan, T.; Aust, G.; Hamann, J. Sticky signaling - Adhesion class g protein-coupled receptors take the stage. *Sci. Signal.* **2013**, *6*, 1–22, doi:10.1126/scisignal.2003825.

186. Araç, D.; Boucard, A.A.; Bolliger, M.F.; Nguyen, J.; Soltis, S.M.; Südhof, T.C.; Brunger, A.T. A novel evolutionarily conserved domain of cell-adhesion GPCRs mediates autoproteolysis. *EMBO J.* **2012**, *31*, 1364–1378, doi:10.1038/emboj.2012.26.

187. Vizurraga, A.; Adhikari, R.; Yeung, J.; Yu, M.; Tall, G.G. Mechanisms of adhesion G protein–coupled receptor activation. *J. Biol. Chem.* **2020**, *295*, 14065–14083, doi:10.1074/jbc.REV120.007423.

188. Bjarnadóttir, T.K.; Fredriksson, R.; Höglund, P.J.; Gloriam, D.E.; Lagerström, M.C.; Schiöth, H.B. The human and mouse repertoire of the adhesion family of G-protein-coupled receptors. *Genomics* **2004**, *84*, 23–33, doi:10.1016/j.ygeno.2003.12.004.

189. Bohnekamp, J.; Schöneberg, T. Cell adhesion receptor GPR133 couples to G s protein. *J. Biol. Chem.* **2011**, *286*, 41912–41916, doi:10.1074/jbc.C111.265934.

190. Liebscher, I.; Schön, J.; Petersen, S.C.; Fischer, L.; Auerbach, N.; Demberg, L.M.; Mogha, A.; Cöster, M.; Simon, K.U.; Rothemund, S.; et al. A Tethered Agonist within the Ectodomain Activates the Adhesion G Protein-Coupled Receptors GPR126 and GPR133. *Cell Rep.* **2014**, *9*, 2018–2026, doi:10.1016/j.celrep.2014.11.036.

191. Frenster, J.D.; Stephan, G.; Ravn-Boess, N.; Bready, D.; Wilcox, J.; Kieslich, B.; Wilde, C.; Sträter, N.; Wiggin, G.R.; Liebscher, I.; et al. Functional impact of intramolecular cleavage and dissociation of adhesion G protein-coupled receptor GPR133 (ADGRD1) on canonical signaling. *J. Biol. Chem.* **2021**, *296*, 100798, doi:10.1016/j.jbc.2021.100798.

192. Tönjes, A.; Koriath, M.; Schleinitz, D.; Dietrich, K.; Böttcher, Y.; Rayner, N.W.; Almgren, P.; Enigk, B.; Richter, O.; Rohm, S.; et al. Genetic variation in GPR133 is associated with height: Genome wide association study in the self-contained population of Sorbs. *Hum. Mol. Genet.* **2009**, *18*, 4662–4668, doi:10.1093/hmg/ddp423.

193. Marroni, F.; Pfeufer, A.; Aulchenko, Y.S.; Franklin, C.S.; Isaacs, A.; Pichler, I.; Wild, S.H.; Oostra, B.A.; Wright, A.F.; Campbell, H.; et al. A Genome-Wide Association Scan of RR and QT Interval Duration in 3 European Genetically Isolated Populations. *Circ. Cardiovasc. Genet.* **2009**, *2*, 322–328, doi:10.1161/CIRCGENETICS.108.833806.

194. Chan, Y.F.; Jones, F.C.; McConnell, E.; Bryk, J.; Bünger, L.; Tautz, D. Parallel selection mapping using artificially selected mice reveals body weight control loci. *Curr. Biol.* **2012**, *22*, 794–800, doi:10.1016/j.cub.2012.03.011.

195. Bianchi, E.; Sun, Y.; Almansa-Ordonez, A.; Woods, M.; Goulding, D.; Martinez-Martin, N.; Wright, G.J. Control of oviductal fluid flow by the G-protein coupled receptor Adgrd1 is essential for murine embryo transit. *Nat. Commun.* **2021**, *12*, doi:10.1038/s41467-021-21512-w.

196. Yang, J.; Wu, S.; Alachkar, H. Characterization of upregulated adhesion GPCRs in acute myeloid leukemia. *Transl. Res.* **2019**, *212*, 26–35, doi:10.1016/j.trsl.2019.05.004.

197. Zhou, L.L.; Jiao, Y.; Chen, H.M.; Kang, L.H.; Yang, Q.; Li, J.; Guan, M.; Zhu, G.; Liu, F.Q.; Wang, S.; et al. Differentially expressed long noncoding RNAs and regulatory mechanism of LINC02407 in human gastric adenocarcinoma. *World J. Gastroenterol.* **2019**, *25*, 5973–5990, doi:10.3748/wjg.v25.i39.5973.

198. Kaghad, M.; Bonnet, H.; Yang, A.; Creancier, L.; Biscan, J.C.; Valent, A.; Minty, A.; Chalon, P.; Lelias, J.M.; Dumont, X.; et al. Monoallelically expressed gene related to p53 at 1p36, a region frequently deleted in neuroblastoma and other human cancers. *Cell* **1997**, *90*, 809–819, doi:10.1016/S0092-8674(00)80540-1.

199. Melino, G.; Lu, X.; Gasco, M.; Crook, T.; Knight, R.A. Functional regulation of p73 and p63: Development and cancer. *Trends Biochem. Sci.* **2003**, *28*, 663–670, doi:10.1016/j.tibs.2003.10.004.

200. Horvat, A.; Tadijan, A.; Vlašić, I.; Slade, N. p53/p73 Protein Network in Colorectal Cancer and Other Human Malignancies. *Cancers (Basel).* **2021**, *13*, 2885, doi:10.3390/cancers13122885.

201. Ramos, A.; Tse, P.W.; Wang, J.; Ethayathulla, A.S.; Viadiu, H. Sequence Variation in the Response Element Determines Binding by the Transcription Factor p73. *Biochemistry* **2015**, *54*, 6961–6972, doi:10.1021/acs.biochem.5b00152.

202. Coutandin, D.; Löhr, F.; Niesen, F.H.; Ikeya, T.; Weber, T.A.; Schäfer, B.; Zielonka, E.M.; Bullock, A.N.; Yang, A.; Güntert, P.; et al. Conformational stability and activity of p73 require a second helix in the tetramerization domain. *Cell Death Differ.* **2009**, *16*, 1582–1589, doi:10.1038/cdd.2009.139.

203. Vikhreva, P.; Melino, G.; Amelio, I. p73 Alternative Splicing: Exploring a Biological Role for the C-Terminal Isoforms. *J. Mol. Biol.* **2018**, *430*, 1829–1838, doi:10.1016/j.jmb.2018.04.034.

204. Chen, X.; Zheng, Y.; Zhu, J.; Jiang, J.; Wang, J. p73 is transcriptionally regulated by DNA damage, p53, and p73. *Oncogene* **2001**, *20*, 769–774, doi:10.1038/sj.onc.1204149.

205. Brooks, L.A.; Sullivan, A.; O'Nions, J.; Bell, A.; Dunne, B.; Tidy, J.A.; Evans, D.J.;

Osin, P.; Vousden, K.H.; Gusterson, B.; et al. E7 proteins from oncogenic human papillomavirus types transactivate p73: Role in cervical intraepithelial neoplasia. *Br. J. Cancer* **2002**, *86*, 263–268, doi:10.1038/sj.bjc.6600033.

206. Fontemaggi, G.; Gurtner, A.; Strano, S.; Higashi, Y.; Sacchi, A.; Piaggio, G.; Blandino, G. The Transcriptional Repressor ZEB Regulates p73 Expression at the Crossroad between Proliferation and Differentiation. *Mol. Cell. Biol.* **2001**, *21*, 8461–8470, doi:10.1128/mcb.21.24.8461-8470.2001.

207. Irwin, M.; Marin, M.C.; Phillips, A.C.; Seelan, R.S.; Smith, D.I.; Liu, W.; Flores, E.R.; Tsai, K.Y.; Jacks, T.; Vousden, K.H.; et al. Role for the p53 homologue p73 in E2F-1-induced apoptosis. *Nature* **2000**, *407*, 645–648, doi:10.1038/35036614.

208. Stiewe, T.; Putzer, B.M. Role of the p53-homologue p73 in E2F1-induced apoptosis. *Nat. Genet.* **2000**, *26*, 464–469, doi:10.1038/82617.

209. Pediconi, N.; Ianari, A.; Costanzo, A.; Belloni, L.; Gallo, R.; Cimino, L.; Porcellini, A.; Screpanti, I.; Balsano, C.; Alesse, E.; et al. Differential regulation of E2F1 apoptotic target genes in response to DNA damage. *Nat. Cell Biol.* **2003**, *5*, 552–558, doi:10.1038/ncb998.

210. Marabese, M.; Vikhanskaya, F.; Rainelli, C.; Sakai, T.; Broggini, M. DNA damage induces transcriptional activation of p73 by removing C-EBPα repression on E2F1. *Nucleic Acids Res.* **2003**, *31*, 6624–6632, doi:10.1093/nar/gkg869.

211. Lee, S.W.; Kim, E.J.; Um, S.J. Transcriptional regulation of the p73 gene, a member of the p53 family, by early growth response-1 (Egr-1). *Biochem. Biophys. Res. Commun.* **2007**, *362*, 1044–1050, doi:10.1016/j.bbrc.2007.08.128.

212. Lalioti, M.-E.; Arbi, M.; Loukas, I.; Kaplani, K.; Kalogeropoulou, A.; Lokka, G.; Kyrousi, C.; Mizi, A.; Georgomanolis, T.; Josipovic, N.; et al. GemC1 governs multiciliogenesis through direct interaction and transcriptional regulation of p73. *J. Cell Sci.* **2019**, 2017, doi:10.1242/jcs.228684.

213. Lai, J.; Nie, W.; Zhang, W.; Wang, Y.; Xie, R.; Wang, Y.; Gu, J.; Xu, J.; Song, W.; Yang, F.; et al. Transcriptional regulation of the p73 gene by Nrf-2 and promoter CpG methylation in human breast cancer. *Oncotarget* **2014**, *5*, 6909–6922, doi:10.18632/oncotarget.2230.

214. Yuan, Z.M.; Shioya, H.; Ishiko, T.; Sun, X.; Gu, J.; Huang, Y.; Lu, H.; Kharbanda, S.; Weichselbaum, R.; Kufe, D. p73 is regulated by tyrosine kinase c-Abl in the apoptotic response to DNA damage. *Nature* **1999**, *399*, 814–817, doi:10.1038/21704.

215. Gaiddon, C.; Lokshin, M.; Gross, I.; Levasseur, D.; Taya, Y.; Loeffler, J.P.; Prives, C. Cyclin-dependent kinases phosphorylate p73 at Threonine 86 in a cell cycle-dependent manner and negatively regulate p73. *J. Biol. Chem.* **2003**, *278*, 27421–27431, doi:10.1074/jbc.M300251200.

216. Bang, S.; Kaur, S.; Kurokawa, M. Regulation of the p53 family proteins by the ubiquitin proteasomal pathway. *Int. J. Mol. Sci.* **2020**, *21*, doi:10.3390/ijms21010261.

217. Oberst, A.; Malatesta, M.; Aqeilan, R.I.; Rossi, M.; Salomoni, P.; Murillas, R.; Sharma, P.; Kuehn, M.R.; Oren, M.; Croce, C.M.; et al. The Nedd4-binding partner 1 (N4BP1) protein is an inhibitor of the E3 ligase Itch. *Proc. Natl. Acad. Sci. U. S. A.* **2007**, *104*, 11280–11285, doi:10.1073/pnas.0701773104.

218. Levy, D.; Adamovich, Y.; Reuven, N.; Shaul, Y. The Yes-associated protein 1 stabilizes p73 by preventing Itch-mediated ubiquitination of p73. *Cell Death Differ.* **2007**, *14*, 743–751, doi:10.1038/sj.cdd.4402063.

219. Yang, A.; Walker, N.; Bronson, R.; Kaghad, M.; Oosterwegel, M.; Bonnin, J.; Vagner, C.; Bonnet, H.; Dikkes, P.; Sharpe, A.; et al. p73-Deficient mice have neurological, pheromonal and inflammatory defects but lack spontaneous tumours. *Nature* **2000**, *404*, 99–103, doi:10.1038/35003607.

220. Tomasini, R.; Tsuchihara, K.; Wilhelm, M.; Fujitani, M.; Rufini, A.; Cheung, C.C.; Khan, F.; Itie-Youten, A.; Wakeham, A.; Tsao, M.S.; et al. TAp73 knockout shows genomic instability with infertility and tumor suppressor functions. *Genes Dev.* **2008**, *22*, 2677–2691, doi:10.1101/gad.1695308.

221. Talos, F.; Nemajerova, A.; Flores, E.R.; Petrenko, O.; Moll, U.M. p73 Suppresses Polyploidy and Aneuploidy in the Absence of Functional p53. *Mol. Cell* **2007**, *27*, 647–659, doi:10.1016/j.molcel.2007.06.036.

222. Allocati, N.; Di Ilio, C.; De Laurenzi, V. P63/P73 in the Control of Cell Cycle and Cell Death. *Exp. Cell Res.* **2012**, *318*, 1285–90, doi:10.1016/j.yexcr.2012.01.023.

223. Lefkimmiatis, K.; Caratozzolo, M.F.; Merlo, P.; D'Erchia, A.M.; Navarro, B.; Levrero,

M.; Sbisa', E.; Tullo, A. P73 and P63 Sustain Cellular Growth By Transcriptional Activation of Cell Cycle Progression Genes. *Cancer Res.* **2009**, *69*, 8563–8571, doi:10.1158/0008-5472.CAN-09-0259.

224. Lin, Y.L.; Sengupta, S.; Gurdziel, K.; Bell, G.W.; Jacks, T.; Flores, E.R. p63 and p73 transcriptionally regulate genes involved in DNA repair. *PLoS Genet.* **2009**, *5*, 1–13, doi:10.1371/journal.pgen.1000680.

225. Zaika, E.; Wei, J.; Yin, D.; Andl, C.; Moll, U.; El-Rifai, W.; Zaika, A.I. p73 protein regulates DNA damage repair. *FASEB J.* **2011**, *25*, 4406–4414, doi:10.1096/fj.11-192815.

226. Yoon, M.K.; Ha, J.H.; Lee, M.S.; Chi, S.W. Structure and apoptotic function of p73. *BMB Rep.* **2015**, *48*, 81–90, doi:10.5483/BMBRep.2015.48.2.255.

227. Wilhelm, M.T.; Rufini, A.; Wetzel, M.K.; Tsuchihara, K.; Inoue, S.; Tomasini, R.; Itie-Youten, A.; Wakeham, A.; Arsenian-Henriksson, M.; Melino, G.; et al. Isoform-specific p73 knockout mice reveal a novel role for ΔNp73 in the DNA damage response pathway. *Genes Dev.* **2010**, *24*, 549–560, doi:10.1101/gad.1873910.

228. Sakil, H.A.M.; Stantic, M.; Wolfsberger, J.; Brage, S.E.; Hansson, J.; Wilhelm, M.T. ΔNp73 regulates the expression of the multidrug-resistance genes ABCB1 and ABCB5 in breast cancer and melanoma cells - a short report. *Cell. Oncol.* **2017**, *40*, 631–638, doi:10.1007/s13402-017-0340-x.

229. Stiewe, T.; Stanelle, J.; Theseling, C.C.; Pollmeier, B.; Beitzinger, M.; Pützer, B.M. Inactivation of retinoblastoma (RB) tumor suppressor by oncogenic isoforms of the p53 family member p73. *J. Biol. Chem.* **2003**, *278*, 14230–14236, doi:10.1074/jbc.M300357200.

230. Petrenko, O.; Zaika, A.; Moll, U.M. ΔNp73 Facilitates Cell Immortalization and Cooperates with Oncogenic Ras in Cellular Transformation In Vivo. *Mol. Cell. Biol.* **2003**, *23*, 5540–5555, doi:10.1128/mcb.23.16.5540-5555.2003.

231. Dulloo, I.; Hooi, P.B.; Sabapathy, K. Hypoxia-induced DNp73 stabilization regulates Vegf-A expression and tumor angiogenesis similar to TAp73. *Cell Cycle* **2015**, *14*, 3533–3539, doi:10.1080/15384101.2015.1078038.

232. Rodríguez, N.; Peláez, A.; Barderas, R.; Domínguez, G. Clinical implications of the

deregulated TP73 isoforms expression in cancer. *Clin. Transl. Oncol.* **2018**, *20*, 827–836, doi:10.1007/s12094-017-1802-3.

233. Sayan, A.E.; Sayan, B.S.; Findikli, N.; Ozturk, M. Acquired expression of transcriptionally active p73 in hepatocellular carcinoma cells. *Oncogene* **2001**, *20*, 5111–5117, doi:10.1038/sj.onc.1204669.

234. Augello, G.; Emma, M.R.; Azzolina, A.; Puleio, R.; Condorelli, L.; Cusimano, A.; Giannitrapani, L.; McCubrey, J.A.; Iovanna, J.L.; Cervello, M. The NUPR1/p73 axis contributes to sorafenib resistance in hepatocellular carcinoma. *Cancer Lett.* **2021**, *519*, 250–262, doi:10.1016/j.canlet.2021.07.026.

235. Gautier, L.; Cope, L.; Bolstad, B.M.; Irizarry, R.A. Affy - Analysis of Affymetrix GeneChip data at the probe level. *Bioinformatics* **2004**, *20*, 307–315, doi:10.1093/bioinformatics/btg405.

236. Ritchie, M.E.; Phipson, B.; Wu, D.; Hu, Y.; Law, C.W.; Shi, W.; Smyth, G.K. Limma powers differential expression analyses for RNA-sequencing and microarray studies. *Nucleic Acids Res.* **2015**, *43*, e47, doi:10.1093/nar/gkv007.

237. Yu, G.; Wang, L.G.; Han, Y.; He, Q.Y. ClusterProfiler: An R package for comparing biological themes among gene clusters. *Omi. A J. Integr. Biol.* **2012**, *16*, 284–287, doi:10.1089/omi.2011.0118.

238. Subramanian, A.; Tamayo, P.; Mootha, V.K.; Mukherjee, S.; Ebert, B.L.; Gillette, M.A.; Paulovich, A.; Pomeroy, S.L.; Golub, T.R.; Lander, E.S.; et al. Gene set enrichment analysis: A knowledge-based approach for interpreting genome-wide expression profiles. *Proc. Natl. Acad. Sci.* **2005**, *102*, 15545–15550, doi:10.1073/pnas.0506580102.

239. Goldman, M.J.; Craft, B.; Hastie, M.; Repečka, K.; McDade, F.; Kamath, A.; Banerjee, A.; Luo, Y.; Rogers, D.; Brooks, A.N.; et al. Visualizing and interpreting cancer genomics data via the Xena platform. *Nat. Biotechnol.* **2020**, *38*, 675–678, doi:10.1038/s41587-020-0546-8.

240. Ekin, U.; Yuzugullu, H.; Ozen, C.; Korhan, P.; Bagirsakci, E.; Yilmaz, F.; Yuzugullu, O.G.; Uzuner, H.; Alotaibi, H.; Kirmizibayrak, P.B.; et al. Evaluation of ATAD2 as a Potential Target in Hepatocellular Carcinoma. *J. Gastrointest. Cancer* **2021**,

doi:10.1007/S12029-021-00732-9.

241. Brewer, J.W.; Hendershot, L.M.; Sherr, C.J.; Diehl, J.A. Mammalian unfolded protein response inhibits cyclin D1 translation and cell-cycle progression. *Proc. Natl. Acad. Sci. U. S. A.* **1999**, *96*, 8505–8510, doi:10.1073/pnas.96.15.8505.

242. Aguirre-Gamboa, R.; Gomez-Rueda, H.; Martínez-Ledesma, E.; Martínez-Torteya, A.; Chacolla-Huaringa, R.; Rodriguez-Barrientos, A.; Tamez-Peña, J.G.; Treviño, V. SurvExpress: An Online Biomarker Validation Tool and Database for Cancer Gene Expression Data Using Survival Analysis. *PLoS One* **2013**, *8*, 1–9, doi:10.1371/journal.pone.0074250.

243. Stelzer, G.; Rosen, N.; Plaschkes, I.; Zimmerman, S.; Twik, M.; Fishilevich, S.; Iny Stein, T.; Nudel, R.; Lieder, I.; Mazor, Y.; et al. The GeneCards suite: From gene data mining to disease genome sequence analyses. *Curr. Protoc. Bioinforma.* **2016**, *2016*, 1.30.1-1.30.33, doi:10.1002/cpbi.5.

244. Kumari, R.; Sahu, M.K.; Tripathy, A.; Uthansingh, K.; Behera, M. Hepatocellular carcinoma treatment: hurdles, advances and prospects. *Hepatic Oncol.* **2018**, *5*, HEP08, doi:10.2217/hep-2018-0002.

245. Raoul, J.L.; Kudo, M.; Finn, R.S.; Edeline, J.; Reig, M.; Galle, P.R. Systemic therapy for intermediate and advanced hepatocellular carcinoma: Sorafenib and beyond. *Cancer Treat. Rev.* **2018**, *68*, 16–24, doi:10.1016/j.ctrv.2018.05.006.

246. Marin, J.J.G.; Briz, O.; Herraez, E.; Lozano, E.; Asensio, M.; Di Giacomo, S.; Romero, M.R.; Osorio-Padilla, L.M.; Santos-Llamas, A.I.; Serrano, M.A.; et al. Molecular bases of the poor response of liver cancer to chemotherapy. *Clin. Res. Hepatol. Gastroenterol.* **2018**, *42*, 182–192, doi:10.1016/j.clinre.2017.12.006.

247. Huang, J.; Yang, J.; Lei, Y.; Gao, H.; Wei, T.; Luo, L.; Zhang, F.; Chen, H.; Zeng, Q.; Guo, L. An ANCCA/PRO2000-miR-520a-E2F2 regulatory loop as a driving force for the development of hepatocellular carcinoma. *Oncogenesis* **2016**, *5*, e229–e229, doi:10.1038/oncsis.2016.22.

248. Wu, G.; Liu, H.; He, H.; Wang, Y.; Lu, X.; Yu, Y.; Xia, S.; Meng, X.; Liu, Y. MiR-372 down-regulates the oncogene ATAD2 to influence hepatocellular carcinoma proliferation and metastasis. *BMC Cancer* **2014**, *14*, 1–11, doi:10.1186/1471-2407-14-

107.

249. Kaita, K.D.E.; Pettigrew, N.; Minuk, G.Y. Hepatic regeneration in humans with various liver disease as assessed by Ki-67 staining of formalin-fixed paraffin-embedded liver tissue. *Liver* **1997**, *17*, 13–16, doi:10.1111/j.1600-0676.1997.tb00772.x.

250. Gerdes, J.; Schwab, U.; Lemke, H.; Stein, H. Production of a mouse monoclonal antibody reactive with a human nuclear antigen associated with cell proliferation. *Int. J. Cancer* **1983**, *31*, 13–20, doi:10.1002/ijc.2910310104.

251. Corlu, A.; Loyer, P. Culture Conditions Promoting Hepatocyte Proliferation and Cell Cycle Synchronization. In *Protocols in In Vitro Hepatocyte Research*; 2015; Vol. 1250, pp. 27–51 ISBN 9781493920747.

252. Mullany, L.K.; White, P.; Hanse, E.A.; Nelsen, C.J.; Goggin, M.M.; Mullany, J.E.; Anttila, C.K.; Greenbaum, L.E.; Kaestner, K.H.; Albrecht, J.H. Distinct proliferative and transcriptional effects of the D-type cyclins in vivo. *Cell Cycle* **2008**, *7*, 2215–2224, doi:10.4161/cc.7.14.6274.

253. Gerlach, C.; Sakkab, D.Y.; Scholzen, T.; Daßler, R.; Alison, M.R.; Gerdes, J. Ki-67 expression during rat liver regeneration after partial hepatectomy. *Hepatology* **1997**, *26*, 573–578, doi:10.1053/jhep.1997.v26.pm0009303485.

254. Lin, J.H.; Walter, P.; Yen, T.S.B. Endoplasmic reticulum stress in disease pathogenesis. *Annu. Rev. Pathol. Mech. Dis.* **2008**, *3*, 399–425, doi:10.1146/annurev.pathmechdis.3.121806.151434.

255. Bassik, M.C.; Kampmann, M. Knocking out the door to tunicamycin entry. *Proc. Natl. Acad. Sci. U. S. A.* **2011**, *108*, 11731–11732, doi:10.1073/pnas.1109035108.

256. Lai, S.S.; Zhao, D.D.; Cao, P.; Lu, K.; Luo, O.Y.; Chen, W.B.; Liu, J.; Jiang, E.Z.; Yu, Z.-H.H.; Lee, G.; et al. PP2Acα positively regulates the termination of liver regeneration in mice through the AKT/GSK3β/Cyclin D1 pathway. *J. Hepatol.* **2016**, *64*, 352–360, doi:10.1016/j.jhep.2015.09.025.

257. Doultsinos, D.; Avril, T.; Lhomond, S.; Dejeans, N.; Guédat, P.; Chevet, E. Control of the Unfolded Protein Response in Health and Disease. *SLAS Discov.* **2017**, *22*, 787–800, doi:10.1177/2472555217701685.

258. Tacar, O.; Sriamornsak, P.; Dass, C.R. Doxorubicin: An update on anticancer molecular action, toxicity and novel drug delivery systems. *J. Pharm. Pharmacol.* **2013**, *65*, 157–170, doi:10.1111/j.2042-7158.2012.01567.x.

259. Siu, W.Y.; Yam, C.H.; Poon, R.Y.C. G1 versus G2 cell cycle arrest after adriamycin-induced damage in mouse Swiss3T3 cells. *FEBS Lett.* **1999**, *461*, 299–305, doi:10.1016/S0014-5793(99)01481-7.

260. Oki, T.; Nishimura, K.; Kitaura, J.; Togami, K.; Maehara, A.; Izawa, K.; Sakaue-Sawano, A.; Niida, A.; Miyano, S.; Aburatani, H.; et al. A novel cell-cycle-indicator, mVenus-p27K -, identifies quiescent cells and visualizes G0-G1 transition. *Sci. Rep.* **2014**, *4*, doi:10.1038/srep04012.

261. Gad, A.A.; Balenga, N. The Emerging Role of Adhesion GPCRs in Cancer. *ACS Pharmacol. Transl. Sci.* **2020**, *3*, 29–42, doi:10.1021/acsptsci.9b00093.

262. Arang, N.; Gutkind, J.S. G Protein-Coupled receptors and heterotrimeric G proteins as cancer drivers. *FEBS Lett.* **2020**, *594*, 4201–4232, doi:10.1002/1873-3468.14017.

263. Aust, G.; Zhu, D.; Van Meir, E.G.; Xu, L. Adhesion GPCRs in Tumorigenesis. In *Definitions*; 2016; pp. 369–396 ISBN 3319415239.

264. Wu, X.Z.; Xie, G.R.; Chen, D. Hypoxia and hepatocellular carcinoma: The therapeutic target for hepatocellular carcinoma. *J. Gastroenterol. Hepatol.* **2007**, *22*, 1178–1182, doi:10.1111/j.1440-1746.2007.04997.x.

265. El-Deiry, W.S. p21/p53, Cellular Growth Control and Genomic Integrity. In *Cell Cycle*; 1998; Vol. 7, pp. 121–137.

266. Sharpless, N.E.; DePinho, R.A. p53: Good cop/bad cop. *Cell* **2002**, *110*, 9–12, doi:10.1016/S0092-8674(02)00818-8.

267. Jost, C.A.; Marin, M.C.; Kaelin, W.G. P73 Is a Human P53-Related Protein That Can Induce Apoptosis. *Nature* **1997**, *389*, 191–194, doi:10.1038/38298.

268. De Laurenzi, V.; Costanzo, A.; Barcaroli, D.; Terrinoni, A.; Falco, M.; Annicchiarico-Petruzzelli, M.; Levrero, M.; Melino, G. Two New p73 Splice Variants, γ and δ, with Different Transcriptional Activity. *J. Exp. Med.* **1998**, *188*, 1763–1768, doi:10.1084/jem.188.9.1763.

269. Bressac, B.; Kew, M.; Wands, J.; Ozturk, M. Selective G to T mutations of p53 gene in hepatocellular carcinoma from southern Africa. *Nature* **1991**, *350*, 429–431, doi:10.1038/350429a0.

270. Hollstein, M.; Hergenhahn, M.; Yang, Q.; Bartsch, H.; Wang, Z.Q.; Hainaut, P. New approaches to understanding p53 gene tumor mutation spectra. *Mutat. Res. - Fundam. Mol. Mech. Mutagen.* **1999**, *431*, 199–209, doi:10.1016/S0027-5107(99)00162-1.

271. Pan, H.; Liao, S.J.; Lai, W.Y.; Lu, H.C.; Hsiao, K.M. Overexpression but lack of mutation and methylation of p73 in hepatocellular carcinoma. *Acta Oncol. (Madr).* **2002**, *41*, 550–555, doi:10.1080/02841860214968.

272. Donehower, L.A.; Harvey, M.; Slagle, B.L.; McArthur, M.J.; Montgomery, C.A.; Butel, J.S.; Bradley, A. Mice deficient for p53 are developmentally normal but susceptible to spontaneous tumours. *Nature* 1992, *356*, 215–221.

273. Lunghi, P.; Costanzo, A.; Mazzera, L.; Rizzoli, V.; Levrero, M.; Bonati, A. The p53 family protein p73 provides new insights into cancer chemosensitivity and targeting. *Clin. Cancer Res.* **2009**, *15*, 6495–6502, doi:10.1158/1078-0432.CCR-09-1229.

274. Sharif, T.; Martell, E.; Dai, C.; Singh, S.K.; Gujar, S. Regulation of the proline regulatory axis and autophagy modulates stemness in TP73/p73 deficient cancer stem-like cells. *Autophagy* **2019**, *15*, 934–936, doi:10.1080/15548627.2019.1586321.

275. Thakur, A.K.; Nigri, J.; Lac, S.; Leca, J.; Bressy, C.; Berthezene, P.; Bartholin, L.; Chan, P.; Calvo, E.; Iovanna, J.L.; et al. TAp73 loss favors Smad-independent TGF-β signaling that drives EMT in pancreatic ductal adenocarcinoma. *Cell Death Differ.* **2016**, *23*, 1358–1370, doi:10.1038/cdd.2016.18.

276. Engelmann, D.; Meier, C.; Alla, V.; Pützer, B.M. A balancing act: Orchestrating amino-truncated and full-length p73 variants as decisive factors in cancer progression. *Oncogene* **2015**, *34*, 4287–4299, doi:10.1038/onc.2014.365.

277. Das, S.; Nama, S.; Antony, S.; Somasundaram, K. p73β-expressing recombinant adenovirus: A potential anticancer agent. *Cancer Gene Ther.* **2005**, *12*, 417–426, doi:10.1038/sj.cgt.7700803.

278. Stiewe, T.; Theseling, C.C.; Pützer, B.M. Transactivation-deficient ΔTA-p73 inhibits p53 by direct competition for DNA binding. Implications for tumorigenesis. *J. Biol.*

Chem. **2002**, *277*, 14177–14185, doi:10.1074/jbc.M200480200.

279. Marabese, M.; Vikhanskaya, F.; Broggini, M. p73: A chiaroscuro gene in cancer. *Eur. J. Cancer* **2007**, *43*, 1361–1372, doi:10.1016/j.ejca.2007.01.042.

280. Vernole, P.; Neale, M.H.; Barcaroli, D.; Munarriz, E.; Knight, R.A.; Tomasini, R.; Mak, T.W.; Melino, G.; De Laurenzi, V. TAp73α binds the kinetochore proteins Bub1 and Bub3 resulting in polyploidy. *Cell Cycle* **2009**, *8*, 421–429, doi:10.4161/cc.8.3.7623.

281. Nguyen, D.; Yang, K.; Chiao, L.; Deng, Y.; Zhou, X.; Zhang, Z.; Zeng, S.X.; Lu, H. Inhibition of tumor suppressor p73 by nerve growth factor receptor via chaperone-mediated autophagy. *J. Mol. Cell Biol.* **2020**, *12*, 700–712, doi:10.1093/jmcb/mjaa017.

282. Naka, M.; Ozaki, T.; Takada, N.; Takahashi, M.; Shishikura, T.; Sakiyama, S.; Tada, M.; Todo, S.; Nakagawara, A. Functional characterization of naturally occurring mutants (P405R and P425L) of p73α and p73β found in neuroblastoma and lung cancer. *Oncogene* **2001**, *20*, 3568–3572, doi:10.1038/sj.onc.1204470.

283. Petitjean, A.; Ruptier, C.; Tribollet, V.; Hautefeuille, A.; Chardon, F.; Cavard, C.; Puisieux, A.; Hainaut, P.; De Fromentel, C.C. Properties of the six isoforms of p63: P53-like regulation in response to genotoxic stress and cross talk with δNp73. *Carcinogenesis* **2008**, *29*, 273–281, doi:10.1093/carcin/bgm258.

284. He, Z.; Liu, H.; Agostini, M.; Yousefi, S.; Perren, A.; Tschan, M.P.; Mak, T.W.; Melino, G.; Simon, H.U. P73 regulates autophagy and hepatocellular lipid metabolism through a transcriptional activation of the ATG5 gene. *Cell Death Differ.* **2013**, *20*, 1415–1424, doi:10.1038/cdd.2013.104.

285. He, Z.; Agostini, M.; Liu, H.; Melino, G.; Simon, H.U. P73 Regulates Basal and Starvation-Induced Liver Metabolism in Vivo. *Oncotarget* **2015**, *6*, 33178–33190, doi:10.18632/oncotarget.5090.

286. Amelio, I.; Melino, G. The p53 family and the hypoxia-inducible factors (HIFs): Determinants of cancer progression. *Trends Biochem. Sci.* **2015**, *40*, 425–434, doi:10.1016/j.tibs.2015.04.007.

287. Stantic, M.; Sakil, H.A.M.; Zirath, H.; Fang, T.; Sanz, G.; Fernandez-Woodbridge, A.; Marin, A.; Susanto, E.; Mak, T.W.; Henriksson, M.A.; et al. TAp73 suppresses tumor

angiogenesis through repression of proangiogenic cytokines and HIF-1α activity. *Proc. Natl. Acad. Sci. U. S. A.* **2015**, *112*, 220–225, doi:10.1073/pnas.1421697112.

288. Iscan, E.; Ekin, U.; Yildiz, G.; Oz, O.; Keles, U.; Suner, A.; Cakan-Akdogan, G.; Ozhan, G.; Nekulova, M.; Vojtesek, B.; et al. TAp73β can promote hepatocellular carcinoma dedifferentiation. *Cancers (Basel).* **2021**, *13*, 1–19, doi:10.3390/cancers13040783.

8 APPENDIX

8.1 Appendix Tables

Appendix Table 1: Full list of related GO terms for Hep3B

ID	Description	GeneRa	BgRatio	pvalue	p.adju	qvalue	geneID
GO:0051592	response to calcium ion	8/80	148/18670	2E-07	5E-04	0.00044	FOS/THBS1/DUSP1/CAV1/SYT15/FGA/NEDD4/FGG
GO:0010038	response to metal ion	10/80	364/18670	3E-06	0.004	0.00325	FOS/THBS1/DUSP1/CAV1/SYT15/SLC30A1/FGA/ABAT/NEDD4/FGG
GO:0051896	regulation of protein kinase B signaling	8/80	244/18670	1E-05	0.006	0.00494	THBS1/IGFBP5/IAPP/AREG/KLF4/AKR1C2/FGF1/EREG
GO:0051897	positive regulation of protein kinase B signaling	7/80	176/18670	1E-05	0.006	0.00494	THBS1/IGFBP5/IAPP/AREG/AKR1C2/FGF1/EREG
GO:1901654	response to ketone	7/80	193/18670	2E-05	0.007	0.00562	GLB1/FOS/THBS1/DUSP1/CAV1/KLF4/AKR1C2
GO:0043491	protein kinase B signaling	8/80	269/18670	2E-05	0.007	0.00562	THBS1/IGFBP5/IAPP/AREG/KLF4/AKR1C2/FGF1/EREG
GO:0030193	regulation of blood coagulation	5/80	79/18670	2E-05	0.007	0.00562	THBS1/CAV1/FGA/ABAT/FGG
GO:1900046	regulation of hemostasis	5/80	80/18670	2E-05	0.007	0.00562	THBS1/CAV1/FGA/ABAT/FGG
GO:0050818	regulation of coagulation	5/80	84/18670	3E-05	0.008	0.00633	THBS1/CAV1/FGA/ABAT/FGG
GO:0051384	response to glucocorticoid	6/80	146/18670	4E-05	0.008	0.00673	GLB1/FOS/DUSP1/PAPPA/STC1/AREG
GO:0048545	response to steroid hormone	9/80	385/18670	4E-05	0.008	0.00673	GLB1/FOS/THBS1/DUSP1/CAV1/PAPPA/STC1/NEDD4/AREG
GO:0043271	negative regulation of ion transport	6/80	157/18670	6E-05	0.011	0.00876	THBS1/CAV1/SLC30A1/STC1/ABAT/NEDD4
GO:0051591	response to cAMP	5/80	97/18670	6E-05	0.011	0.00876	FOS/IGFBP5/DUSP1/STC1/AREG
GO:0031960	response to corticosteroid	6/80	162/18670	7E-05	0.011	0.00921	GLB1/FOS/DUSP1/PAPPA/STC1/AREG
GO:0030195	negative regulation of blood coagulation	4/80	53/18670	8E-05	0.011	0.00921	THBS1/FGA/ABAT/FGG
GO:0031638	zymogen activation	4/80	53/18670	8E-05	0.011	0.00921	THBS1/ASPH/FGA/FGG
GO:1900047	negative regulation of hemostasis	4/80	54/18670	8E-05	0.011	0.00933	THBS1/FGA/ABAT/FGG
GO:0007596	blood coagulation	8/80	336/18670	1E-04	0.012	0.00955	THBS1/VAV3/CAV1/LMAN1/FGA/ABAT/TFPI2/FGG
GO:0050819	negative regulation of coagulation	4/80	57/18670	0.0001	0.012	0.00955	THBS1/FGA/ABAT/FGG
GO:0007599	hemostasis	8/80	341/18670	0.0001	0.012	0.00955	THBS1/VAV3/CAV1/LMAN1/FGA/ABAT/TFPI2/FGG
GO:0050817	coagulation	8/80	342/18670	0.0001	0.012	0.00955	THBS1/VAV3/CAV1/LMAN1/FGA/ABAT/TFPI2/FGG
GO:1902041	regulation of extrinsic apoptotic signaling pathway via death domain recep	4/80	58/18670	0.0001	0.012	0.00955	THBS1/ATF3/FGA/FGG
GO:1903034	regulation of response to wounding	6/80	179/18670	0.0001	0.012	0.0098	THBS1/CAV1/FGA/ABAT/FGG/KLF4
GO:0015850	organic hydroxy compound transport	7/80	262/18670	0.0001	0.012	0.01024	TMF1/SCP2/CAV1/SYT15/SLC16A1/SLC22A3/ABAT
GO:0034113	heterotypic cell-cell adhesion	4/80	61/18670	0.0001	0.012	0.01024	DSC2/FGA/FGG/KLF4
GO:0031639	plasminogen activation	3/80	25/18670	0.0002	0.014	0.01139	THBS1/FGA/FGG
GO:0072012	glomerulus vasculature development	3/80	25/18670	0.0002	0.014	0.01139	EGR1/HES1/IL6R
GO:0034114	regulation of heterotypic cell-cell adhesion	3/80	26/18670	0.0002	0.015	0.01238	FGA/FGG/KLF4
GO:0061437	renal system vasculature development	3/80	27/18670	0.0002	0.016	0.01296	EGR1/HES1/IL6R
GO:0061440	kidney vasculature development	3/80	27/18670	0.0002	0.016	0.01296	EGR1/HES1/IL6R
GO:0042730	fibrinolysis	3/80	28/18670	0.0002	0.017	0.014	THBS1/FGA/FGG
GO:0046887	positive regulation of hormone secretion	5/80	131/18670	0.0002	0.018	0.01467	TMF1/TM7SF3/FGA/ABAT/FGG
GO:0046683	response to organophosphorus	5/80	134/18670	0.0003	0.019	0.01572	FOS/IGFBP5/DUSP1/STC1/AREG
GO:1903522	regulation of blood circulation	7/80	297/18670	0.0003	0.019	0.01572	CACNA2D3/ASPH/CAV1/DSC2/FGA/STC1/FGG
GO:0061045	negative regulation of wound healing	4/80	76/18670	0.0003	0.021	0.01713	THBS1/FGA/ABAT/FGG
GO:0022407	regulation of cell-cell adhesion	8/80	403/18670	0.0003	0.021	0.01723	HES1/CAV1/FGA/ABAT/SOX2/IL6R/FGG/KLF4
GO:0045907	positive regulation of vasoconstriction	3/80	32/18670	0.0003	0.021	0.01754	CAV1/FGA/FGG
GO:0046879	hormone secretion	7/80	312/18670	0.0004	0.023	0.01894	TMF1/SLC16A1/TM7SF3/MYO5A/FGA/ABAT/FGG
GO:0097191	extrinsic apoptotic signaling pathway	6/80	224/18670	0.0004	0.023	0.01912	THBS1/CAV1/ATF3/FGA/IL6R/FGG
GO:0034109	homotypic cell-cell adhesion	4/80	81/18670	0.0004	0.023	0.01912	DSC2/FGA/ABAT/FGG
GO:0032642	regulation of chemokine production	4/80	82/18670	0.0004	0.024	0.01955	EGR1/CXCL6/IL6R/KLF4
GO:0061041	regulation of wound healing	5/80	148/18670	0.0004	0.024	0.01962	THBS1/CAV1/FGA/ABAT/FGG
GO:0014074	response to purine-containing compound	5/80	149/18670	0.0004	0.024	0.01975	FOS/IGFBP5/DUSP1/STC1/AREG
GO:0009914	hormone transport	7/80	322/18670	0.0005	0.024	0.01975	TMF1/SLC16A1/TM7SF3/MYO5A/FGA/ABAT/FGG
GO:0008625	extrinsic apoptotic signaling pathway via death domain receptors	4/80	86/18670	0.0005	0.026	0.02109	THBS1/ATF3/FGA/FGG
GO:0016485	protein processing	7/80	328/18670	0.0005	0.026	0.02109	THBS1/ASPH/SNX12/ADAMTS3/FGA/CPM/FGG
GO:0050673	epithelial cell proliferation	8/80	434/18670	0.0005	0.026	0.0212	THBS1/HES1/IGFBP5/CAV1/SOX2/AREG/FGF1/EREG
GO:2001236	regulation of extrinsic apoptotic signaling pathway	5/80	155/18670	0.0005	0.026	0.0212	THBS1/CAV1/ATF3/FGA/FGG
GO:0032602	chemokine production	4/80	89/18670	0.0006	0.027	0.02232	EGR1/CXCL6/IL6R/KLF4
GO:1903035	negative regulation of response to wounding	4/80	90/18670	0.0006	0.028	0.02282	THBS1/FGA/ABAT/FGG
GO:0030072	peptide hormone secretion	6/80	250/18670	0.0007	0.032	0.02643	SLC16A1/TM7SF3/MYO5A/FGA/ABAT/FGG
GO:0090277	positive regulation of peptide hormone secretion	4/80	96/18670	0.0008	0.033	0.02676	TM7SF3/FGA/ABAT/FGG
GO:0021983	pituitary gland development	3/80	42/18670	0.0008	0.033	0.02676	HES1/TBX19/SOX2
GO:0022409	positive regulation of cell-cell adhesion	6/80	255/18670	0.0008	0.033	0.02676	HES1/CAV1/FGA/SOX2/IL6R/FGG
GO:0048660	regulation of smooth muscle cell proliferation	5/80	169/18670	0.0008	0.033	0.02676	THBS1/IGFBP5/IL6R/KLF4/EREG
GO:0072124	regulation of glomerular mesangial cell proliferation	2/80	10/18670	0.0008	0.033	0.02676	EGR1/IL6R
GO:0023061	signal release	8/80	462/18670	0.0008	0.033	0.02676	TMF1/SLC16A1/SLC30A1/TM7SF3/MYO5A/FGA/ABAT/FGG

GO:0023061	signal release	6/80	482/18670	0.0008	0.033	0.02689	TMF1/SLC16A1/SLC30A1/TM7SF3/FGA/ABAT/FGG
GO:0086004	regulation of cardiac muscle cell contraction	3/80	43/18670	0.0008	0.033	0.02689	CAV1/DSC2/STC1
GO:0048659	smooth muscle cell proliferation	5/80	171/18670	0.0008	0.033	0.02689	THBS1/IGFBP5/IL6R/KLF4/EREG
GO:0090257	regulation of muscle system process	6/80	259/18670	0.0009	0.033	0.027	IGFBP5/CAV1/DSC2/STC1/ABAT/KLF4
GO:0048661	positive regulation of smooth muscle cell proliferation	4/80	101/18670	0.0009	0.034	0.02765	THBS1/IGFBP5/IL6R/EREG
GO:0032570	response to progesterone	3/80	45/18670	0.0009	0.034	0.02765	FOS/THBS1/CAV1
GO:0032102	negative regulation of response to external stimulus	7/80	365/18670	0.001	0.034	0.02765	THBS1/DUSP1/FGA/ABAT/FGG/KLF4/NT5E
GO:0072110	glomerular mesangial cell proliferation	2/80	11/18670	0.001	0.034	0.02765	EGR1/IL6R
GO:0090193	positive regulation of glomerulus development	2/80	11/18670	0.001	0.034	0.02765	EGR1/IL6R
GO:0046883	regulation of hormone secretion	6/80	266/18670	0.001	0.034	0.02765	TMF1/SLC16A1/TM7SF3/FGA/ABAT/FGG
GO:0034766	negative regulation of ion transmembrane transport	4/80	103/18670	0.001	0.034	0.02765	THBS1/CAV1/SLC30A1/NEDD4
GO:0060443	mammary gland morphogenesis	3/80	46/18670	0.001	0.034	0.02765	IGFBP5/CAV1/AREG
GO:0030198	extracellular matrix organization	7/80	368/18670	0.001	0.034	0.02765	THBS1/MATN3/ADAMTS3/FGA/FGG/HAS3/PTX3
GO:1903115	regulation of actin filament-based movement	3/80	47/18670	0.0011	0.035	0.02895	CAV1/DSC2/STC1
GO:0042136	neurotransmitter biosynthetic process	4/80	106/18670	0.0011	0.036	0.02967	CAV1/ABAT/KLF4/PTX3
GO:0090331	negative regulation of platelet aggregation	2/80	12/18670	0.0012	0.037	0.03052	ABAT/FGG
GO:0050678	regulation of epithelial cell proliferation	7/80	378/18670	0.0012	0.037	0.03052	THBS1/HES1/CAV1/SOX2/AREG/FGF1/EREG
GO:2001238	positive regulation of extrinsic apoptotic signaling pathway	3/80	49/18670	0.0012	0.038	0.03092	THBS1/CAV1/ATF3
GO:0006012	galactose metabolic process	2/80	13/18670	0.0014	0.041	0.03366	GLB1/PGM2L1
GO:0014745	negative regulation of muscle adaptation	2/80	13/18670	0.0014	0.041	0.03366	IGFBP5/KLF4
GO:0021984	adenohypophysis development	2/80	13/18670	0.0014	0.041	0.03366	HES1/SOX2
GO:0015872	dopamine transport	3/80	52/18670	0.0014	0.042	0.03487	SYT15/SLC22A3/ABAT
GO:0042035	regulation of cytokine biosynthetic process	4/80	114/18670	0.0015	0.043	0.0349	EGR1/THBS1/KLF4/EREG
GO:0051604	protein maturation	7/80	397/18670	0.0016	0.044	0.03633	THBS1/ASPH/SNX12/ADAMTS3/FGA/CPM/FGG
GO:0090287	regulation of cellular response to growth factor stimulus	6/80	292/18670	0.0016	0.044	0.03633	THBS1/HES1/CAV1/ADAMTS3/NEDD4/FGF1
GO:1901722	regulation of cell proliferation involved in kidney development	2/80	14/18670	0.0016	0.044	0.03633	EGR1/IL6R
GO:1902043	positive regulation of extrinsic apoptotic signaling pathway via death dom	2/80	14/18670	0.0016	0.044	0.03633	THBS1/ATF3
GO:0045785	positive regulation of cell adhesion	7/80	403/18670	0.0017	0.047	0.03826	VAV3/HES1/CAV1/FGA/SOX2/IL6R/FGG
GO:0034111	negative regulation of homotypic cell-cell adhesion	2/80	15/18670	0.0018	0.049	0.04034	ABAT/FGG
GO:0090192	regulation of glomerulus development	2/80	15/18670	0.0018	0.049	0.04034	EGR1/IL6R
GO:0042089	cytokine biosynthetic process	4/80	123/18670	0.0019	0.049	0.0406	EGR1/THBS1/KLF4/EREG
GO:0060326	cell chemotaxis	6/80	304/18670	0.0019	0.049	0.0406	THBS1/VAV3/DUSP1/CXCL6/IL6R/FGF1
GO:0019229	regulation of vasoconstriction	3/80	58/18670	0.002	0.049	0.0406	CAV1/FGA/FGG
GO:0042107	cytokine metabolic process	4/80	124/18670	0.002	0.049	0.0406	EGR1/THBS1/KLF4/EREG
GO:0090276	regulation of peptide hormone secretion	5/80	208/18670	0.002	0.049	0.0406	SLC16A1/TM7SF3/FGA/ABAT/FGG
GO:0070527	platelet aggregation	3/80	59/18670	0.0021	0.049	0.0406	FGA/ABAT/FGG
GO:2000351	regulation of endothelial cell apoptotic process	3/80	59/18670	0.0021	0.049	0.0406	THBS1/FGA/FGG
GO:0097529	myeloid leukocyte migration	5/80	210/18670	0.0021	0.049	0.0406	THBS1/VAV3/DUSP1/CXCL6/IL6R
GO:0034116	positive regulation of heterotypic cell-cell adhesion	2/80	16/18670	0.0021	0.049	0.0406	FGA/FGG
GO:0042448	progesterone metabolic process	2/80	16/18670	0.0021	0.049	0.0406	EGR1/AKR1C2
GO:0072109	glomerular mesangium development	2/80	16/18670	0.0021	0.049	0.0406	EGR1/IL6R
GO:0045667	regulation of osteoblast differentiation	4/80	126/18670	0.0021	0.049	0.0406	IGFBP5/CEBPD/IL6R/AREG

Appendix Table 2: Fırst 200 genes upregulated in immortal phenotype ordered according to the geometric mean of intensities (GMI)

ProbeSet	Symbol	GMI in IMMORTAL	GMI in PRESENESCENT	Fold-change (IMM/PS)	Parametric p-value	FDR
204987_at	ITIH2	5038.9	2491.64	2.02	0.0054188	0.0434
208693_s_at	GARS	2702.37	1347.97	2	0.0000814	0.00245
205047_s_at	ASNS	2633.39	752.82	3.5	0.0000077	0.00053
220892_s_at	PSAT1	2453.47	892.91	2.75	0.0000321	0.00133
205040_at	ORM1	1901.67	781.39	2.43	0.0000799	0.00242
205719_s_at	PAH	1799.32	880.22	2.04	< 1e-07	< 1e-07
200692_s_at	HSPA9	1519.37	678.93	2.24	0.0000196	0.000965
223579_s_at	APOB	1397.03	288.7	4.84	0.000253	0.00527
225285_at	BCAT1	1317.57	454.19	2.9	0.0031533	0.03
212160_at	XPOT	1200.72	604.94	1.98	0.0001692	0.00403
201014_s_at	PAICS	1186.48	607.87	1.95	0.0000307	0.0013
200946_x_at	GLUD1	1150.71	490.02	2.35	0.0000004	0.000079
208815_x_at	HSPA4	1138.41	572.66	1.99	0.000002	0.000224
212048_s_at	YARS	1121.14	554.51	2.02	0.0000194	0.000961
1554375_a_at	NR1H4	1012.8	458.54	2.21	< 1e-07	< 1e-07
204602_at	DKK1	993.86	476.3	2.09	0.0099938	0.0655
233878_s_at	XRN2	906	441.62	2.05	0.0009256	0.0129
218782_s_at	ATAD2	872.91	382.61	2.28	0.0000002	0.000048
204551_s_at	AHSG	869.25	348.85	2.49	0.0113836	0.0709
200755_s_at	CALU	865.65	428.72	2.02	0.0000003	6.38E-05
211955_at	IPO5	852.23	429.1	1.99	0.0000071	0.000505
202887_s_at	DDIT4	806.14	223.36	3.61	0.000082	0.00246
225424_at	GPAM	761.89	360.24	2.11	0.0000035	0.000323
210529_s_at	TCAF1	741.39	316.53	2.34	0.0188427	0.1
202847_at	PCK2	714.08	348.78	2.05	0.0031296	0.0298
212698_s_at	SEPT10	705.23	332.52	2.12	0.0000007	0.000117
204143_s_at	ENOSF1	692.93	292.94	2.37	0.0000002	0.000048
215794_x_at	GLUD2	631.36	238.22	2.65	< 1e-07	< 1e-07
201139_s_at	SSB	596.1	269.35	2.21	0.0002485	0.0052
201833_at	HDAC2	589.79	301.42	1.96	0.0103662	0.067
222559_s_at	RPRD1A	574.53	288.34	1.99	0.0000128	0.000741
203358_s_at	EZH2	565.05	224.97	2.51	0.0000003	6.38E-05
216320_x_at	MST1	560.77	267.36	2.1	0.0000407	0.00154
213380_x_at	MST1P9	555.21	211.76	2.62	0.000001	0.000144
205105_at	MAN2A1	554.7	273.7	2.03	0.000047	0.0017
203706_s_at	FZD7	547.83	273.32	2	0.0000761	0.00234
212295_s_at	SLC7A1	542.25	263.48	2.06	0.0001609	0.00389
210139_s_at	PMP22	542.05	191.4	2.83	< 1e-07	< 1e-07
201195_s_at	SLC7A5	520.65	155.15	3.36	0.0000032	0.000306
202174_s_at	PCM1	519.99	250	2.08	0.0003892	0.00702
204033_at	TRIP13	518.27	244.37	2.12	0.0000005	9.27E-05
222427_s_at	LARS	516.62	184.01	2.81	< 1e-07	< 1e-07
201635_s_at	FXR1	516.48	240.43	2.15	0.0037798	0.0339
209990_s_at	GABBR2	515.87	112.54	4.58	0.0003832	0.00693
1555788_a_at	TRIB3	513.23	182.41	2.81	0.0014447	0.0175
210049_at	SERPINC1	512.34	184.1	2.78	0.000004	0.000352
227059_at	GPC6	507.24	259.99	1.95	0.0042885	0.0371
201617_x_at	CALD1	501.84	194.94	2.57	0.0004456	0.0077
236140_at	GCLM	496.96	206.35	2.41	0.0001804	0.00418
210587_at	INHBE	462.44	98.76	4.68	0.0000017	0.000201
220651_s_at	MCM10	461.42	211.94	2.18	0.0000002	0.000048
227752_at	SPTLC3	457.2	217.45	2.1	0.0000015	0.000186
211450_s_at	MSH6	443.83	209.95	2.11	0.0063894	0.0484
215177_s_at	ITGA6	437.74	149.05	2.94	0.0000466	0.00169
203095_at	MTIF2	430.56	218.5	1.97	0.0000014	0.000179
214323_s_at	UPF3A	422.4	192.31	2.2	0.0001462	0.00364
48808_at	DHFR	417.54	201.32	2.07	0.0000142	0.000794
205672_at	XPA	414.49	179.87	2.3	0.000028	0.00123
226438_at	SNTB1	413.12	207.29	1.99	0.0000002	0.000048
202447_at	DECR1	403.98	159.28	2.54	< 1e-07	< 1e-07
203196_at	ABCC4	402.96	170.05	2.37	< 1e-07	< 1e-07
221781_s_at	DNAJC10	399.71	200.27	2	0.000522	0.00863
217127_at	CTH	399.29	122.51	3.26	0.0000228	0.00106
203344_s_at	RBBP8	399.09	192.41	2.07	0.0000016	0.000193
202444_s_at	ERLIN1	392.86	194.17	2.02	0.0147724	0.0848
242093_at	SYTL5	391.52	199.81	1.96	0.0000162	0.000857
204162_at	NDC80	384.01	177.48	2.16	0.0001189	0.00317
218663_at	NCAPG	379.9	176.98	2.15	0.000118	0.00315
214701_s_at	FN1	379.24	88.92	4.26	0.000092	0.00266
212454_x_at	HNRPDL	375.61	132.74	2.83	0.0000609	0.00203
201711_x_at	RANBP2	373.03	186.63	2	0.0116407	0.0721
233827_s_at	SUPT16H	372.3	140.32	2.65	0.0100364	0.0656
208931_s_at	ILF3	369.84	182.66	2.02	0.0000478	0.00172
200665_s_at	SPARC	368.47	153.43	2.4	0.0000003	6.38E-05
227759_at	PCSK9	365.93	173.7	2.11	0.0000335	0.00137
205774_at	F12	364.48	163.92	2.22	0.0104269	0.0673
205822_s_at	HMGCS1	362.2	171.86	2.11	0.0402048	0.165
201450_s_at	TIA1	358.76	170.33	2.11	0.0001698	0.00404
212093_s_at	MTUS1	355.34	145.96	2.43	0.0000722	0.00226
226329_s_at	MITD1	355.24	137.76	2.58	0.0000002	0.000048
216733_s_at	GATM	354.34	112.29	3.16	0.0000006	0.000106
222846_at	RAB8B	350.78	164.33	2.13	0.0020048	0.022
1554878_a_at	ABCD3	348.98	125.12	2.79	0.0000002	0.000048
212008_at	UBXN4	347.19	172.49	2.01	0.0016142	0.0189
204646_at	DPYD	345.55	143.02	2.42	0.0000054	0.000425
202976_s_at	RHOBTB3	344.67	132.56	2.6	0.000096	0.00273
238021_s_at	CRNDE	339.47	121.9	2.78	0.0001098	0.003
225855_at	EPB41L5	338.88	104.9	3.23	0.0000002	0.000048
222728_s_at	TAF1D	336.6	161.74	2.08	0.0001631	0.00393
200841_s_at	EPRS	336.14	147.31	2.28	0.0047664	0.0398
230029_x_at	UBR3	326.66	165.78	1.97	0.000089	0.0026
209421_at	MSH2	319.84	160.32	2	0.0000012	0.000162
203438_at	STC2	318.45	138	2.31	0.0007654	0.0112
222122_s_at	THOC2	312.79	156.82	1.99	0.0028728	0.0281
201911_s_at	FARP1	311.42	145.5	2.14	0.0028355	0.0279
209937_at	TM4SF4	309.64	115.99	2.67	0.003809	0.0341
213092_x_at	DNAJC9	309.06	158.12	1.95	0.0000015	0.000186
225610_at	UHRF2	304.55	154.85	1.97	0.0028412	0.0279
222754_at	TRNT1	302.75	147.82	2.05	0.0000021	0.000232

1569106_s_at	SETD5	299.85	87.61	3.42	0.0000018	0.000209
221760_at	MAN1A1	299.43	62.15	4.82	0.0022816	0.024
241682_at	KLHL23	297.78	107.27	2.78	0.0011991	0.0154
225107_at	INRNPA2B	289.55	146	1.98	0.0000047	0.000389
219525_at	SLC47A1	289.26	93.27	3.1	0.0000062	0.000466
212406_s_at	PCMTD2	288.23	136.11	2.12	0.0000076	0.000527
217678_at	SLC7A11	286.03	92.01	3.11	0.0000784	0.00239
201559_s_at	CLIC4	285.16	136.49	2.09	0.0033681	0.0314
212690_at	DDHD2	284.78	139.5	2.04	0.0000509	0.00179
227198_at	AFF3	282.96	114.61	2.47	0.0003219	0.00617
203492_x_at	CEP57	282.6	141.46	2	0.0000021	0.000232
215037_s_at	BCL2L1	281.76	140.34	2.01	0.0258752	0.124
212298_at	NRP1	281.45	139.39	2.02	0.0103235	0.0668
212514_x_at	DDX3X	281.35	144.45	1.95	0.0058079	0.0455
209337_at	PSIP1	280.58	142.05	1.98	0.0000797	0.00242
221039_s_at	ASAP1	280.18	132.06	2.12	0.0000184	0.00093
1558093_s_at	MATR3	280.01	115.83	2.42	0.0017643	0.0201
230078_at	RAPGEF6	280	128.11	2.19	0.0000006	0.000106
1555434_a_at	SLC39A14	277.71	111.85	2.48	0.0052301	0.0424
218842_at	RPAP3	276.27	133.95	2.06	0.0023488	0.0245
218645_at	ZNF277	272.91	133.69	2.04	0.0000012	0.000162
228329_at	DAB1	268.95	133.91	2.01	0.0009071	0.0127
203428_s_at	ASF1A	266.6	131.44	2.03	0.0011254	0.0147
218781_at	SMC6	265.39	126.29	2.1	0.0000001	3.05E-05
204993_at	GNAZ	265.11	71.7	3.7	< 1e-07	3.05E-05
200935_at	CALR	262.08	113.06	2.32	0.0064498	0.0487
205227_at	IL1RAP	252.5	127.81	1.98	0.0005092	0.00848
222848_at	CENPK	252.44	90.7	2.78	0.0000036	0.000327
204128_s_at	RFC3	252.24	109.03	2.31	< 1e-07	< 1e-07
229905_at	RAP1GDS1	246.61	118.96	2.07	0.0023173	0.0243
219972_s_at	PCNX4	246.18	94.18	2.61	0.0001154	0.00311
218397_at	FANCL	245.83	96.41	2.55	0.0000321	0.00133
225144_at	BMPR2	245.72	125.29	1.96	0.0006339	0.00987
209209_s_at	FERMT2	244.95	122.74	2	0.0000186	0.000936
202627_s_at	SERPINE1	242.43	117.2	2.07	0.0004297	0.00752
202906_s_at	NBN	242.04	81.04	2.99	< 1e-07	< 1e-07
242517_at	KISS1R	241	114.51	2.1	0.0000152	0.000821
213346_at	TEX30	240.8	121.14	1.99	0.0000002	0.000048
203712_at	PUM3	240	114.92	2.09	0.0000001	3.05E-05
213677_s_at	PMS1	239.54	106.38	2.25	0.0000088	0.000574
229061_s_at	SLC25A13	230.15	107.87	2.13	0.0110079	0.0694
207098_s_at	MFN1	230.08	108.78	2.12	0.000211	0.00468
226881_at	GRPEL2	229.69	89.87	2.56	0.0000016	0.000193
206535_at	SLC2A2	228.77	72.42	3.16	0.0009753	0.0133
203584_at	EMC2	227.59	94.56	2.41	0.0000024	0.000254
212233_at	MAP1B	225.9	68.2	3.31	0.00001	0.000624
214499_s_at	BCLAF1	225.58	112.56	2	0.0228767	0.114
228841_at	LYRM7	224.77	112.01	2.01	0.000036	0.00142
209310_s_at	CASP4	224.63	111.89	2.01	0.0000014	0.000179
237215_s_at	TFRC	223.52	61.78	3.62	0.0107584	0.0685
225396_at	RBBP4	221.53	95.38	2.32	0.0000003	6.38E-05
1559954_s_at	DDX42	220.88	94.55	2.34	0.0045788	0.0388
206204_at	GRB14	219.09	112.25	1.95	0.0017835	0.0203
209654_at	ICE1	217.63	108.65	2	0.0000008	0.000126
209055_s_at	CDC5L	217.59	103.11	2.11	0.0001254	0.00328
205394_at	CHEK1	217.46	99.25	2.19	0.0000064	0.000475
212785_s_at	LARP7	216.11	107.66	2.01	0.0000002	0.000048
1558214_s_at	CTNNA1	214.99	68.8	3.13	0.0054116	0.0434
205112_at	PLCE1	213.17	98.03	2.17	0.0010411	0.0139
210892_s_at	GTF2I	210.35	88.99	2.36	0.0099802	0.0654
213374_x_at	HIBCH	206.13	75.82	2.72	0.0000307	0.0013
218013_x_at	DCTN4	204.93	97.44	2.1	0.0000036	0.000327
232267_at	ADGRD1	202.37	64.19	3.15	0.0000002	0.000048
227105_at	CSPP1	201.8	100.57	2.01	0.0012469	0.0158
203049_s_at	TTC37	201.59	91.34	2.21	0.0003839	0.00694
201624_at	DARS	200.5	102.24	1.96	0.000334	0.00631
224589_at	XIST	199.36	78.36	2.54	0.0004412	0.00766
211563_s_at	URI1	197.93	66.81	2.96	0.0000053	0.000422
219306_at	KIF15	197.77	95.97	2.06	0.0000682	0.00218
214934_at	ATP9B	197.07	96.67	2.04	0.0005883	0.00939
234915_s_at	DENR	196.96	96.6	2.04	0.0041713	0.0364
207819_s_at	ABCB4	196.48	83.64	2.35	0.0000017	0.000201
216205_s_at	MFN2	194.65	74.67	2.61	0.0048747	0.0404
225782_at	MSRB3	193.43	72.19	2.68	0.0002102	0.00467
218893_at	ISOC2	191.62	96.22	1.99	0.0002986	0.00585
202717_s_at	CDC16	191.07	90.52	2.11	0.0028471	0.0279
219558_at	ATP13A3	189.47	76.82	2.47	0.003045	0.0293
233924_s_at	EXOC6	189.38	91.05	2.08	0.000012	0.000706
214336_s_at	COPA	186.99	84.19	2.22	0.0242838	0.119
212179_at	SFRS18	186.86	89.12	2.1	0.0000027	0.000273
1555564_a_at	CFI	185.54	89.36	2.08	0.0000002	0.000048
205042_at	GNE	183.79	91.76	2	0.0000425	0.00158
203310_at	STXBP3	181.92	89.68	2.03	0.0004754	0.00808
225633_at	DPY19L3	181.52	86.65	2.09	0.0000777	0.00237
212512_s_at	CARM1	180.38	80.77	2.23	0.0021978	0.0234
212142_at	MCM4	179.03	83.78	2.14	0.0022067	0.0235
203355_s_at	PSD3	178.48	59.31	3.01	0.000045	0.00165
229229_at	AGXT2	178.33	48.99	3.64	0.000001	0.000144
209822_s_at	VLDLR	178.23	53.54	3.33	0.0004035	0.00721
1554433_a_at	ZNF146	177.67	79.81	2.23	0.0000994	0.0028
226654_at	MUC12	176.77	64.16	2.76	0.0000026	0.000268
213022_s_at	UTRN	176.46	83.87	2.1	0.0002355	0.00501
211300_s_at	TP53	176.14	84.8	2.08	0.0110369	0.0695
219270_at	CHAC1	174.83	85.35	2.05	0.0123273	0.075
34031_i_at	KRIT1	173.54	85.52	2.03	0.0101924	0.0663
202422_s_at	ACSL4	172.84	84.97	2.03	0.0097745	0.0645
234660_s_at	DIS3	169.85	81.9	2.07	0.000007	0.000502
223805_at	OSBPL6	169.47	58.58	2.89	0.0000008	0.000126
212579_at	SMCHD1	169.29	86.6	1.95	0.0001012	0.00284
221989_at	RPL10	168.65	83.15	2.03	0.0001456	0.00362

Appendix Table 3 Statistical analyses of differential expression of two GPR133 isoforms in different cancers

Cancer type	ADGRD1 isoform	Normal Median (IQR)	Tumor Median (IQR)	Mean Rank(N-T)	*p* value
LICH	isoform_uc001uit	62.2 (78)	16.04 (119.2)	253.16-205.32	*0.009
	isoform_uc010tbm	0.0 (36)	0.0 (30.2)	208.45-211.34	0.86
BLCA	isoform_uc001uit	412.0 (1806.9)	2.1 (12.4)	395.3-205.5	*0.00000000002463
	isoform_uc010tbm	8.4 (40.5)	0.0 (3.2)	272.0-211.3	*0.01
BRCA	isoform_uc001uit	247.4 (369.9)	10.1 (32.7)	1048.9-557.3	*4.1323E-46
	isoform_uc010tbm	0.0 (0.0)	0.0 (6.5)	515.9-611.9	*0.001
PRAD	isoform_uc001uit	151.8 (494.2)	38.4 (81.9)	376.87-264.34	*0.000001
	isoform_uc010tbm	0.0 (19.8)	0.0 (7.2)	317.33-270.57	*0.014
STAD	isoform_uc001uit	168.8 (523.1)	33.1 (145.1)	329.17-216.76	*0.00000088324
	isoform_uc010tbm	0.0 (11.7)	14.4 (63.9)	158.4-231.16	*0.000837
LUAD	isoform_uc001uit	1246.1 (517.3)	166.5 (369.9)	509.00-262.12	*2.4464E-27
	isoform_uc010tbm	109.5 (79.3)	70.1 (179.8)	329.67-282.67	*0.039
LUSC	isoform_uc001uit	1388.9 (740.8)	16.4 (42.7)	526.84-251.02	*4.9694E-32
	isoform_uc010tbm	172.8 (120.3)	6.0 (24.3)	503.34-253.41	*1.9991E-28
COAD	isoform_uc001uit	100.4 (137.5)	5.4 (22.5)	276.0-147.31	*2.0159E-16
	isoform_uc010tbm	0.0 (10.0)	0.0 (19.3)	139.33-166.98	0.053
ESCA	isoform_uc001uit	715.9 (1209.6)	8.9 (40.6)	181.09-93.03	*0.0000004676
	isoform_uc010tbm	235.5 (683.0)	0 (18.4)	148.36-94.99	*0.000431

M:Median, IQR: Interquartile Range, Mean-Rank: Normal vs Tumor, *p≤0.05

isoform_uc001uit Isoform 1

isoform_uc010tbm Isoform 2 Alternative form with additional Exon at N term position 3rd

8.2 Journal Publications

1. **Ekin, U**.; Yuzugullu, H.; Ozen, C.; Korhan, P.; Bagirsakci, E.; Yilmaz, F.; Yuzugullu, O.G.; Uzuner, H.; Alotaibi, H.; Kirmizibayrak, P.B.; et al. Evaluation of ATAD2 as a Potential Target in Hepatocellular Carcinoma. *J. Gastrointest. Cancer* **2021**, doi:10.1007/S12029-021-00732-9.

2. Iscan, E.; **Ekin, U**.; Yildiz, G.; Oz, O.; Keles, U.; Suner, A.; Cakan-Akdogan, G.; Ozhan, G.; Nekulova, M.; Vojtesek, B.; et al. TAp73β can promote hepatocellular carcinoma dedifferentiation. *Cancers (Basel).* **2021**, *13*, 1–19, doi:10.3390/cancers13040783.

3. Iscan, E., Karakülah, G., **Ekin, U**. et al. TAp73α is Upregulated in the Most Common Human Cancers. Mol Biol (2022). https://doi.org/10.1134/S0026893322020066.

4. Ozturk, M.; Batur, T.; **Ekin, U**.; Erdogan, A.; İscan, E.; Keles, U.; Oz, O.; Ozen, C. Molecular Pathogenesis of Liver Cancer. *J. Gastrointest. Cancer* **2017**, *48*, 222–224, doi:10.1007/s12029-017-9957-2.

5. Ferroudj, S.; Yildiz, G.; Bouras, M.; Iscan, E.; **Ekin, U**.; Ozturk, M. Role of Fanconi anemia/BRCA pathway genes in hepatocellular carcinoma chemoresistance. *Hepatol. Res.* **2016**, *46*, 1264–1274, doi:10.1111/HEPR.12675.

6. Keles, U.; Iscan, E.; Yilmaz, H.E.; Karakülah, G.; Suner, A.; Bal, E.; Tasdemir, N.; Cavga, A.D.; **Ekin, U**.; Mutlu, Z.; et al. Differential expression of full-length and NH2 terminally truncated FAM134B isoforms in normal physiology and cancer. *Am. J. Physiol. Liver Physiol.* **2020**, *319*, G733–G747, doi:10.1152/ajpgi.00094.2020.

Journal of Gastrointestinal Cancer (2021) 52:1356–1369
https://doi.org/10.1007/s12029-021-00732-9

INVITED ARTICLE

Evaluation of ATAD2 as a Potential Target in Hepatocellular Carcinoma

Umut Ekin[1,2] · Haluk Yuzugullu[3,4] · Cigdem Ozen[1,3,8] · Peyda Korhan[1] · Ezgi Bagirsakci[1,2] · Funda Yilmaz[5] · Ozge Gursoy Yuzugullu[3,4] · Hamdiye Uzuner[1,2] · Hani Alotaibi[1,2] · Petek Ballar Kirmizibayrak[6] · Nese Atabey[1,7] · Gökhan Karakülah[1,2] · Mehmet Ozturk[1,3,4,7]

Accepted: 7 October 2021 / Published online: 5 November 2021

Abstract

Purpose Hepatocellular carcinoma (HCC) is one of the leading causes of cancer-related death worldwide with lack of effective systemic chemotherapy. In this study, we aimed to evaluate the value of ATPase family AAA domain-containing protein 2 (ATAD2) as a biomarker and potential therapeutic target for HCC.

Methods The expression of ATAD2 was tested in different HCC patient cohorts by immunohistochemistry and comparative transcriptional analysis. The co-expression of ATAD2 and proliferation markers was compared during liver regeneration and malignancy with different bioinformatics tools. The cellular effects of ATAD2 inactivation in liver malignancy was tested on cell cycle, apoptosis, and colony formation ability as well as tumor formation using RNA interference. The genes affected by ATAD2 inactivation in three different HCC cell lines were identified by global gene expression profiling and bioinformatics tools.

Results ATAD2 overexpression is closely correlated with HCC tumor stage. There was gradual increase from dysplasia, well-differentiated and poorly-differentiated HCC, respectively. We also observed transient upregulation of ATAD2 expression during rat liver regeneration in parallel to changes in Ki-67 expression. ATAD2 knockdown resulted in apoptosis and decreased cell survival in vitro and decreased tumor formation in some HCC cell lines. However, three other HCC cell lines tested were not affected. Similarly, gene expression response to ATAD2 inactivation in different HCC cell lines was highly heterogeneous.

Conclusions ATAD2 is a potential proliferation marker for liver regeneration and HCC. It may also serve as a therapeutic target despite heterogeneous response of malignant cells.

Keywords Liver cancer · ATAD2 · Proliferation · Apoptosis · Gene expression profiles · Gene knock down

✉ Mehmet Ozturk
mehmet.ozturk@ibg.edu.tr

1 Izmir Biomedicine and Genome Center, Izmir, Turkey

2 Izmir International Biomedicine and Genome Institute, Dokuz Eylul University, Izmir, Turkey

3 Department of Molecular Biology and Genetics, Bilkent University, Ankara, Turkey

4 Institut Albert Bonniot, Grenoble, France

5 Department of Pathology, Faculty of Medicine, Ege University, Izmir, Turkey

6 Department of Biochemistry, Faculty of Pharmacy, Ege University, Izmir, Turkey

7 Faculty of Medicine, Izmir Tinaztepe University, Izmir, Turkey

8 Present Address: Center for Molecular and Cellular Bioengineering, Technische Universität Dresden, Bioinformatics group, Dresden, Germany

Introduction

The AAA + ATPase and bromodomain factor ATAD2/ANCCA (ATAD2) is composed of two AAA + domains and a bromodomain that recognizes acetylated histones [1]. As a nucleosomal protein present on active genes, its functions are closely associated with chromatin remodeling, DNA replication, and DNA repair. ATAD2 has been referred to as a "generalist facilitator of chromatin dynamics" based on demonstrations where histone acetylation guides ATAD2 to chromatin, resulting in an overall increase of chromatin accessibility and histone dynamics [2]. ATAD2 bromodomain was shown to recognize di-acetylated histones, and it associates with H4K5acK12ac modifications found on newly synthesized histones following DNA replication, suggesting a critical role for ATAD2 following DNA replication [3].

Based on structural studies with its yeast homolog, ATAD2 was proposed to form a hexameric complex and to facilitate H3-H4 loading by binding to histone tails [4]. Recently, Shahnejat-Bushehri and Ehrenhofer-Murray [5] reported that the yeast homolog of ATAD2 is a deposition factor for CENP-A homolog with help from HJURP homolog, thus acting as a co-chaperon for centrosome assembly.

ATAD2 has been described initially as a co-activator of the estrogen receptor overexpressed in breast cancer [6], and several other cancers [7], as well as a cancer/testis antigen [8]. Shortly after, we reported *ATAD2* as a component of 15-hepatocellular immortality signature gene panel that discriminates hepatocellular carcinoma (HCC) from cirrhosis with high accuracy [9]. ATAD2 has now been implicated in a large set of cancer and been considered a therapeutic target [10].

Here, we studied the expression and functional implications of ATAD2 in liver malignancy in order to evaluate its potential as a potential target for HCC treatment. A series of investigations using gene and protein expression in normal and malignant tissues and cells, gene inactivation techniques, as well as in vitro and in vivo cell survival and tumorigenicity assays allowed us to draw critical conclusions about the value of ATAD2 as a therapeutic target for HCC with some implications that could be expanded to other cancer types overexpressing this particular epigenetic regulator.

Material and Methods

Cell Lines and Hepatocytes

Cell lines used in the study were obtained and cultivated as previously described [11]. Cell lines were maintained in RPMI medium supplemented with 10% Fetal Bovine Serum, 100 IU/ml penicillin, 100 µg/ml streptomycin and 1 × non-essential amino acid (ThermoFisher) under humidified 5% CO_2 and 37 °C conditions. Routine cell passages were performed when cell confluency reached to 70–80%. Freshly isolated human hepatocytes were obtained commercially (hNHEPSTM-Human Hepatocytes, Lonza Group, Basel, Switzerland), as reported previously [9].

Generation of Polyclonal Anti-human ATAD2 Antibody

An anti-human ATAD2 antibody was generated in rabbits. The DNA fragment containing amino acids 2 to 251 at the N-terminus of the ATAD2 protein (Online Resource 1) was cloned into pET28 MHL plasmid vector. Briefly, the sequence to be cloned was amplified by polymerase chain reaction from a pCDNA3.1-HA-C plasmid carrying the human ATAD2 cDNA. Primers used for this PCR: 5′ TTG TATTTCCAGGGCGTGGTTCTCCGCAGCAGCTTG-3′ and 5′-CAAGCTTCGTCATCATTGGTCTTCACCCTC TTCAGATGAC-3′.

In-Fusion kit (Clontech) was used for cloning. pET28 MHL vector was cut with BseRI (R0581L, NEB) and purified with Nucleospin gel cleaning kit (Macherey–Nagel). Linear vector DNA and PCR-amplified ATAD2 DNA were mixed in the reaction medium at a ratio of 2:1. After ligation, the reaction solution was transformed into *E. coli* DH5α strain. The plasmid was transformed to *E. coli* T7 expression bacterial strain. Recombinant protein produced in bacteria was purified by Ni NTA agarose affinity chromatography using the non-soluble protein purification method. Rabbits were immunized with recombinant ATAD2 protein and rabbit sera were collected by CovalAb S.A.S. (Villeurbanne, France). Polyclonal antibody was purified using HiTrap Protein G HP ÄKTA FPLC system (GE Healthcare).

Other Antibodies

The list of other antibodies used here was shown in Online Resource 2.

Western Blotting

Harvested cell pellets were lysed in RIPA lysis buffer containing 150 mM NaCl, 1% Nonidet P–40, 0.5% Sodium deoxycholate, 0.1% SDS, 25 mM pH7.4 Tris, 1 × protease inhibitor cocktail (cOmplete, ROCHE), 1 mM Na_3OV_4 and 1 mM NaF. Total protein amounts were measured and equalized according to BSA standard linear regression method. Equal amounts of denatured total protein samples were loaded to 10% SDS–polyacrylamide gels for electrophoresis. Transfers were performed to polyvinylidene difluoride membranes (immobilon-P, Millipore) and blocked with 5% non-fat milk. Membranes were probed with primary antibodies of targeted proteins and subsequently incubated with appropriate HRP-conjugated secondary antibodies. Detection of membranes was performed with enhanced chemiluminescence.

siRNAs and Transfections

Different ATAD2-targeting siRNAs were used. The effects of ATAD2 knock-down on cell proliferation and apoptosis were tested using following siRNAs generated by Eurogentec (France). ATAD2 siRNA1: ACUAACACUGCUGAA GCUG; ATAD2 siRNA2: GGUUGUAGCUCCUCCAAA U; ATAD2 siRNA3: GCUAAGGA UUUCGAGGUAG; ATAD2 siRNA4 UCUUCUGCUGUCAGUGAUC. Control siRNA (siCTRL); GGCCUUUCACUACUCCUAC. For transfections, cells were seeded in 6 well plates. After 24 h,

cells transfected with 100 pmol ATAD2 siRNAs and 4 µl of oligofectamine transfection reagent (Invitrogen) for 6 h without serum and antibiotics. At the end of 6 h, media was changed and experiments continued as indicated for each test. The effects of ATAD2 knock-down on gene expression profiles were studied with transfection of ON-TARGETplus siRNAs (Dharmacon): S2: siRNA J-017603–06, Target Sequence: GUAAUCAGCCAAUGUAUUU, S3: siRNA J-017603–07, Target Sequence: CGUCGAAGUUGUAGG AUUA, S4: siRNA J-017603–08, Target Sequence: CUG AUGAGGUUCCUGAUUA, Control Luciferase Duplex, Target Sequence: CAUUCUAUCCUCUAGAGGAUG. Transfections were carried out according to supplier's instructions. Briefly, 500 µl OptiMem (Thermofisher) and pool of 20 nM ATAD2 siRNAs 2, 3 and 4 were added to each well of 6-well plates and mixed gently. 5 µl of Lipofectamine RNAiMax solution (Thermofisher) was added to each well and left to incubate for 20 min at room temperature by gently mixing again. Suspension of 1×10^5 cells in 2.5 ml antibiotic-free medium was added to each well. At 48 h, cells were collected. ATAD2 knock-down was confirmed by real-time PCR of transfected cell RNAs using the following primers: ATAD2_F-5′-TGAAAAGGCTTT GGCAATTC-3′, ATAD2_R-5′-TGCGATGCCGATAAA TACA-3′, GAPDH_F-5′-GGCTGAGAACGGGAAGCT TGTCAT-3′, and GAPDH_R-5′-CAGCCTTCTCCATGG TGGTGAAGA-3′ were used for control experiments. Total Hep3B, SNU449, and PLC/PRF/5 RNAs used in microarray analysis were isolated with NucleoSpin RNA II Kit (MN Macherey–Nagel, Duren, Germany) and cDNA synthesis was performed using RevertAid First Strand cDNA synthesis kit (MBI Fermantas, Germany). Quantitative expression analyses were carried up with DyNAmo HS SYBR Green qPCR Kit F410 (Finnzymes). The reaction mix per well contained 10 µl Sybergreen, 0.8 µl of 10 pmol forward and reverse primers, 7.4 µl ddH_2O and 1 µl cDNA. After adding mineral oil onto each well as 1:1, reaction carried out in Mx3005p PCR machine (Stratagene). The housekeeping gene, glyceraldehyde-3-phosphate dehydrogenase (GAPDH), was used as the internal control.

Cell Proliferation, Colony Formation, and Apoptosis Studies

HCC cells were seeded in 6 well plates. After 24 h, cells transfected with 100 pmol ATAD2 siRNAs and 4 µl of oligofectamine (Invitrogen) transfection reagent for 6 h without serum and antibiotics. At the end of 6 h, media with 3 × serum added on. Cells were monitored for 96 h and stained with Coomassie blue at the end of the experiment. For colony formation studies, Hep3B and HepG2 cells were seeded at 72 h following transfection, and grown for 10 days for colony formation. Colonies were stained with crystal violet and quantified. Similarly, Hep3B, HepG2, Huh7 and Hep40 cells were treated with siRNAs of ATAD2 and cultured for 3 days. Cells suspended and pelleted by centrifugation. Cells washed with PBS and fixed with ice cold ethanol. Ethanol discarded and cells washed with PBS. Cells treated with RNase A (Fermentas) and stained with propidium iodide (Sigma). In Annexin V staining, Hep3B and HepG2 cell pellets resuspended with Annexin V binding buffer and stained with Annexin V-Cy3 dyes (Sigma Aldrich). After 5 min incubation at dark, FACS scan (Beckton Dickonson) with FL2 channel was used for analysis.

Clinical Tissue Specimens and Immunohistochemistry

Normal liver and HCC tumor samples were collected and analyzed at Ege University Department of Pathology under the ethical approval. In total, 7 normal liver, 9 low grade dysplastic nodules (LGDN), 18 high grade dysplastic nodules (HGDN), and 27 HCC samples were identified. The diagnosis of dysplatic nodules and HCC, as well as HCC grading, was made according to previously defined criteria [12]. Immunohistochemical analyses were performed on 5 µm-thick sections taken on positively charged slides. Sections were deparaffinized in xylene and then rehydrated. Immunohistochemical staining for anti-ATAD2 antibody (HPA029424, Sigma, 1:150 dilution) was performed using an automated immunohistochemical stainer according to the manufacturer's guidelines (streptavidin-peroxidase protocol; BenchMark, Ventana, PA, USA). The immunoreactivity was revealed by 3, 3-diaminobenzidine tetrahydrochloride (DAB) staining and the sections were counterstained with hematoxylin. The intensity and extent of staining were evaluated semi-quantitatively.

Immunofluorescence

First, a pool of ATAD2 siRNAs or control siRNAs were mixed with Lipofectamine RNAiMax solution (Thermofisher) in serum-free RPMI and left for 10 min at room temperature. Transfection media was mixed with cell suspension (5000 cells/well in RPMI) in 24-well plates containing coverslips. Cells were then incubated for 48 h. To stop the experiment, cell wells were washed with PBS and fixed with ice-cold Acetone-Methanol mixture (1:1) for 10 min at −20 °C. Fixative was discarded and coverslips washed with PBS. Cells blocked for 30 min with PBS-T (PBS and 0.1% Triton-X) complemented with 1% BSA. Cells were co-incubated with primary antibodies to Ki-67 and ATAD2 diluted in PBS-T containing 0.5% BSA for 2 h at room temperature with gentle agitation. Cells were then washed and co-probed with fluorescence tagged anti-mouse and anti-rabbit secondary antibodies diluted in PBS-T containing

0.5% BSA for 90 min. Cells were washed, incubated with DAPI, rinsed with dH_2O and mounted on slides with mounting media.

Study of ATAD2 Response to Cell Stress

Hep3B and HepG2 cells were seeded on 60 mm dishes and incubated for 48 h. When they reached a confluence of 60–70% at 48 h, media were changed with fresh media containing tunicamycin (5 µg/ml and 10 µg/ml) per vehicle. Tunicamycin stock solution was dissolved in DMSO. After 12 h and 24 h treatments, cells were collected, and used for total protein extraction using RIPA buffer.

Comparative Analysis of ATAD2 and Ki-67 Expression

We analyzed the relationship between ATAD2 and Ki-67 expression in rat liver with publicly available microarray gene expression data (GEO Accession: GSE63742) generated from rat liver during regeneration following partial hepatectomy. To analyze the expression data, we used GEO2R (https://www.ncbi.nlm.nih.gov/geo/geo2r/) web based interactive tool. The highest expression values with the "Probe Set 1374775_at" for Mki-67, the "Probe Set 1376599_at" for Atad2 genes were used respectively. Means and Standard Deviations (SD) of expression data for each time points were used for reporting. The correlation between ATAD2 and Ki67 expression in hepatocellular carcinoma was analyzed using TCGA LIHC tumor dataset available at UCSC Xena Browser [13]. Data of recurrent tumor samples were excluded from downstream analysis steps. The expression of ATAD2 and MKi67 was analyzed in 50 normal solid tissue and 371 primary solid tumors of liver. The correlation between ATAD2 and MKi67 is determined with Pearson's correlation method. The following R packages were used in analysis of expression data and generating graphs are dplyr (v1.0.4), ggplot2 (v3.3.3) and ggpubr (v0.4.0).

Generation of Doxycycline-Induced shATAD2 Expression Clones

The lentiviral constructs, pTRIPz shRNAmir lentiviral vector targeting ATAD2 or shControl were used (Open Biosystems company, Huntsville, USA) in the generation of Hep3B stable clones. The sequences in the constructs used as: Targeting shRNA: pTRIPz-tet-shRNA-ATAD2, 5′-ATTACAGTGACATAATCAG-3′ and NonTargeting Control RNA: pTRIPz-tet-shRNA-nontargeting control, 5′-AATTCTCCGAACGTGTCACGT-3′. These doxycycline-inducible constructs also include Red Fluorescent Protein (RFP) cassette that led to track cells. The lentiviral constructs transfected with Arrest-in transfection reagents (Open-biosystems Company, Huntsville, USA) to HEK293TA cells. Cells treated with reagent-construct complex in media for 6 h and media refreshed. After 48 h, virus-containing supernatants collected and filtered by 0.45 µM PVDF filters for use. Hep3B cells seeded on 24 well plates before the day of transduction. At the day of transduction, media refreshed with virus containing media with Hexadimethrine Bromide Sigma (St. Louis, MO, USA). After 6 h incubation, virus containing media refreshed with fresh media. After 24 h, cells cultured with media containing 1 µg/ml puromycin (Sigma, St. Louis, MO, USA) to generate stable clones.

Tumorigenicity Assays

In the generation of xenograft models, shControl and shATAD2 clones of 10×10^6 Hep3B cells resuspended in phosphate-buffered saline and injected to both sides of 6 Female athymic NMRI nude mice (Janvier, Le Genest-Isle, France). Doxycycline (Sigma, St. Louis, MO, USA) dissolved in drinking water of 3 mice to induce expression of shControl and shATAD2. Size of the tumors measured every 3 or 4 days and graphed using Graphpad Prism V8. RFP expressing tumors were visualized by IVIS Kinetic device (Caliper Life Sciences) in vivo imaging system before mice sacrificed. Tumors of mice extracted for western blot analysis.

Gene Expression Profiling by Microarrays

Total RNAs of siRNA-transfected cells were first tested with the Agilent Bioanalyzer 2100 for quality control. Only samples with RNA integrity number values (RIN) greater than 9 were used in microarray experiments. Affymetrix microarray system was used as described in our previous study [9]. Briefly, Affymetrix platform with GeneChip Human Genome U133 Plus 2.0 arrays were used for microarray analysis according to manufacturer instructions. In order to collect and store data, Operating Software (Affymetrix) was used. Bioinformatic analysis of microarray data was performed with R statistical computing environment (v3.6.1). Raw probe intensities in CEL files were subjected to robust multichip average normalization (RMA) using expresso function of Bioconductor affy package (v1.68.0) [14]. Differential expression analysis was performed with Limma package (v3.46.0) [15] to measure significant changes in gene expressions across pairwise comparisons. In this step, lmFit function was utilized to fit a linear model, and estimated coefficients and standard errors were then computed with contrasts.fit function. Empirical Bayes statistics were obtained using eBayes function. We considered differentially expressed genes using a fold change cutoff ≥ 2. The Gene Ontology (GO) enrichment analysis of differentially expressed genes was performed with clusterProfiler package

(v3.14.3) [16] and the GO terms with FDR ≤ 0.05 were considered significant.

Statistical Analysis

Graphs were generated with Prism 8 (Graphpad Software, La Jolla California, USA) and Microsoft Office Excel (2016). Group comparisons were analyzed with t tests. The differences between groups were considered statistically significant as $*p \leq 0.05$, $**p \leq 0.01$, and $***p \leq 0.001$.

Results

ATAD2 is Over-expressed in HCC Tumors in a Tumor Grade Dependent Manner

To assess the clinical relevance of ATAD2 in HCC, we surveyed its expression by immunohistochemistry in 7 normal liver tissues, 9 low-grade dysplastic nodules (LGDN), 18 high-grade dysplastic nodules (HGDN) and 27 HCC cases. ATAD2 was expressed in 3 (16.7%) HGDN, and 14 (51.9%) HCC cases. There was no detectable ATAD2 expression in normal liver and LGDN. Thereafter, we observed a gradual increase in the percent of ATAD2-positive cells according to HCC grade. ATAD2 expressions in well-, moderate-, and poorly differentiated HCC were 25.0%, 66.7%, and 83.3%, respectively (Fig. 1a and Table 1).

Strong Correlation Between ATAD2 and Ki-67 Expression in HCC as well as in Regenerating Liver

Next, we compared *ATAD2* expression at RNA levels with that of Ki-67 transcripts encoded by *MKI-67* gene using The Cancer Genome Atlas (TCGA) data available at UCSC Xena Browser [13]. As shown in Fig. 1b, both transcripts were upregulated significantly ($p < 0.001$) in HCC samples ($n = 371$) as compared to non-tumor liver samples ($n = 50$). Based on expression similarities between *ATAD2* and *MKI-67*, we also performed Pearson correlation analysis for their co-expression in normal liver and HCC samples (Fig. 1c). We observed a significant correlation between *ATAD2* and *MKI-67* expression ($R = 0.61$, $p < 2.2e\text{-}16$). The data we obtained with clinical tissue samples strongly suggested that *ATAD2* expression in liver is related to cell proliferation, similarly to *MKI-67* expression. To further explore this correlation, we compared *ATAD2* expression with the expression of two cell proliferation markers namely *CCND1* (encoding for Cyclin D1 protein) and *MKI-67* during experimental liver regeneration induced in rats by partial hepatectomy using a microarray expression dataset (GEO Accession: GSE63742) available at GEO database [17]. As shown in Fig. 1d, all three transcripts were low at the beginning of the regeneration process and all of them displayed a peak of expression between 24 and 36 h. *CCND1* showed another increase at 72 h. Thereafter there was slow but progressive decrease in the levels of *ATAD2*, *MKI-67*, and *CCND1* transcripts, which came down to initial levels at 168 h or 7 days. Thus, there was a perfect correlation in the dynamic expression patterns of *ATAD2* and cell proliferation markers *CCND1* and *MKI-67* in regenerating liver.

Differential Expression of ATAD2 in Hepatocytes and HCC Cell Lines

We reported previously that ATAD2 protein was not detectable by Western blotting in freshly isolated human hepatocytes, in contrast to consistent expression in HCC cell lines [9]. Here we confirmed and complemented these data by immunocytochemistry (Fig. 2a) and immunofluorescence studies (Fig. 2b). Non-proliferating hepatocytes lacked ATAD2 expression whereas HCC cell lines in culture displayed almost 100% positive nuclear staining. As demonstrated with SNU449 cell line, this nuclear positivity was specific to ATAD2 because of its attenuation under ATAD2 siRNA treatment (Fig. 2b left panels).

ATAD2 staining showed a good correlation with nuclear Ki-67 staining, a proliferation marker largely used for tumor pathology (Fig. 2b—middle panel). Taken together, in vivo and in vitro studies reported here clearly demonstrated that ATAD2 expression in liver is not specifically related to liver malignancy and correlated directly with the proliferation state of this tissue.

ATAD2 Expression Is Downregulated Following Tunicamycin-Induced Unfolded Protein Response

One of the cellular consequences of Endoplasmic Reticulum (ER) stress is Unfolded Protein Response (UPR) which leads to the exit from the cell cycle through downregulation of Cyclin D1 levels [18]. Based on this finding, we aimed to test whether ATAD2 levels are also downregulated during UPR induced by tunicamycin, an inhibitor of protein glycosylation, triggering ER stress [19]. Hep3B and HepG2 cells were treated with 5 µg/ml or 10 µg/ml tunicamycin for 12 h or 24 h and cell lysates were tested for expression of CHOP, an indicator of Endoplasmic Reticulum (ER) stress induced by tunicamycin and PARP cleavage, an indicator of apoptosis together with ATAD2 abundance (Fig. 3). Both Hep3B and HepG2 cells responded to tunicamycin with early (12 h) induction of CHOP as expected. The accumulation of cleaved PARP was detected at 12 h in Hep3B cells with a strong increase at 24 h. HepG2 cell response was less pronounced with detectable PARP cleavage at 24 h only. ATAD2 levels showed a late decrease (24 h) in Hep3B, but early response (12 h) in HepG2 cells. These results suggest

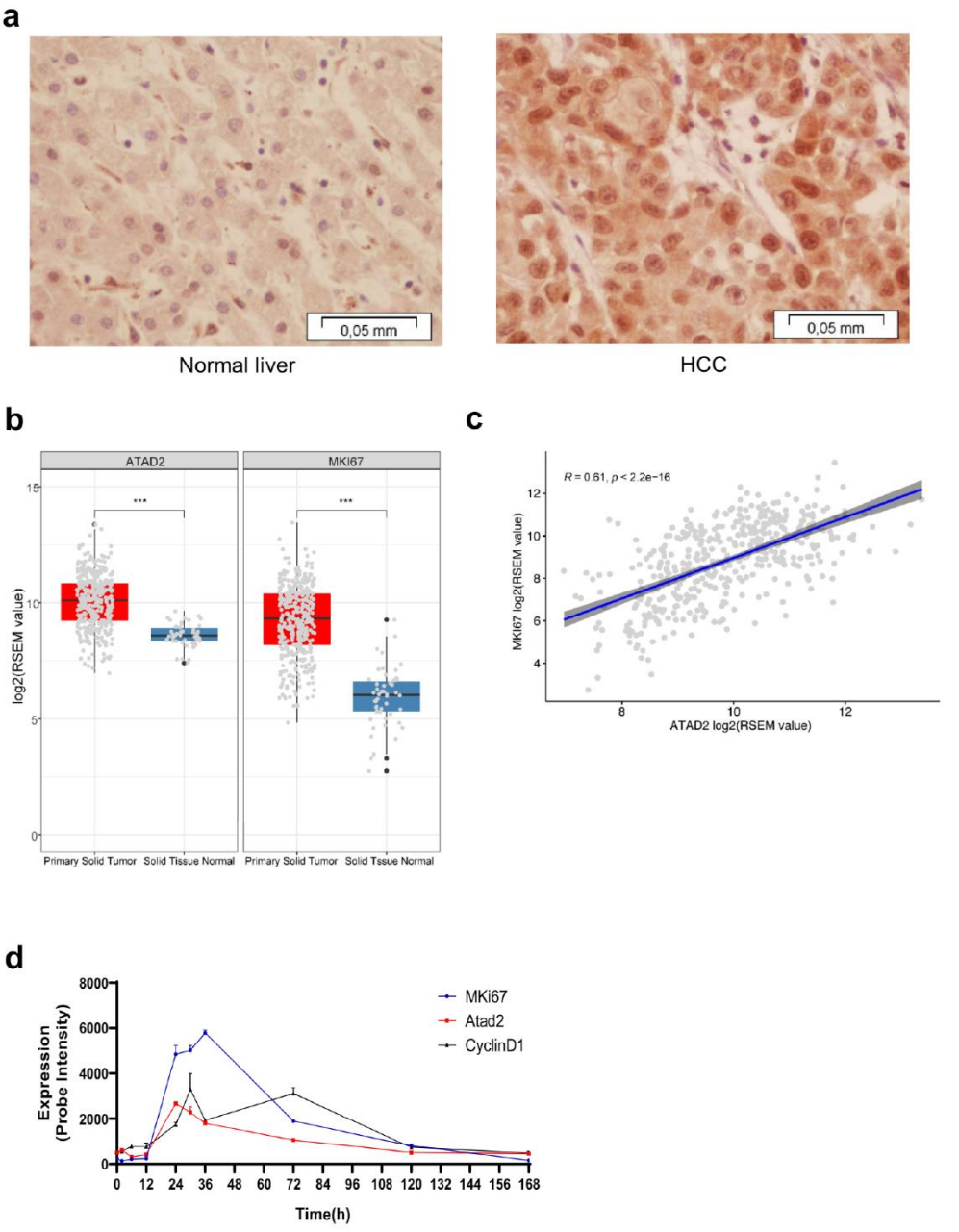
a
0,05 mm
Normal liver
0,05 mm
HCC
b
ATAD2
MKI67
log2(RSEM value)
***
***
Primary Solid Tumor
Solid Tissue Normal
Primary Solid Tumor
Solid Tssue Normal
c
R = 0.61, p < 2.2e−16
MKI67 log2(RSEM value)
ATAD2 log2(RSEM value)
d
Expression (Probe Intensity)
MKi67
Atad2
CyclinD1
Time(h)

◂**Fig. 1** ATAD2 expression is induced in human HCC and during liver regeneration in correlation with Ki-67. **a** Representative immunohistochemical images of ATAD2 expression in human normal liver (left) and HCC (Right). **b** Both ATAD2 and Ki-67 transcripts are induced significantly in normal liver and HCC samples in TCGA collection. **c** Highly significant correlation between ATAD2 and Ki-67 expression in HCC. MKI67: Human gene encoding Ki-67. **d** ATAD2 expression during rat liver regeneration display similar profile with the profile of proliferation biomarkers Cyclin D1 and Ki-67, as shown by transcript analysis. MKi67: Rat gene encoding Ki-67

that when cell cycle arrest/apoptosis is triggered, ATAD2 levels are going down.

ATAD2 siRNA Treatment Inhibits HCC Cell Survival in Some but not All HCC Cell Lines

Based on close association between ATAD2 expression and hepatocellular proliferation, we sought to know whether ATAD2 is essential to HCC cell survival. We transfected a set of HCC cell lines with *ATAD2* siRNAs and followed their growth and survival. Out of five cell lines tested, Hep3B and HepG2 showed strong growth inhibition. SNU449 displayed only weak growth inhibition, whereas Huh7 and PLC/PRF/5 showed no noticeable change (Online Resource 3).

To investigate the functional consequences of *ATAD2* depletion, we transfected Hep3B and HepG2 cells with two different siRNAs. ATAD2 immunoblotting confirmed successful knock-down of *ATAD2* (Fig. 4a). Western blot analysis of cleaved caspase-3 protein (Fig. 4a) and detection of up to 30% Annexin V positive cells by flow cytometry suggested ATAD2 depletion induces apoptosis (Fig. 4b). These cell lines also reacted to *ATAD2* suppression with drastic changes in cell cycle phase distribution with accumulation of subG1 cells, supporting our previous observation (Fig. 4c). As a result, survival of Hep3B and HepG2 decreased significantly as assessed by colony formation assays (Fig. 4d).

Next, we expanded our investigations on in vivo effects of ATAD2 silencing using Hep3B cells, which responded strongly to *ATAD2* depletion. Due to the deleterious effects of *ATAD2* silencing, we chose a Doxycycline-inducible shRNA expression technique. Hep3B cells were first marked with stable expression of red fluorescent protein (RFP); then, we generated ATAD2 shRNA and control shRNA stable cell lines. shCTRL- and shATAD2-expressing Hep3B cells injected subcutaneously into the right and left sides of mice, allowed the tumors to grow for 2 weeks and shRNA expression triggered by including Doxycycline into drinking water (Fig. 5a). Tumor samples isolated at the end of the study validated successful ATAD2 knock-down (Fig. 5b). Doxycycline-treatment of mice led to significant tumor growth inhibition in shATAD2 tumors with respect to shCTRL ($p = 0.0064$, Fig. 5c). This effect was further demonstrated by reduced RFP signals from ATAD2shRNA-expressing tumors using live imaging (Fig. 5a).

We selected Huh7 as a representative of HCC cell line whose survival did not show robust change upon ATAD2 siRNA treatment (Online Resource 3). As shown in Fig. 6, despite effective decrease of ATAD2 levels by ATAD2 siRNAs (Fig. 6a), there was no consistent change in cell cycle distribution. Of particular interest, subG1 signal, representing apoptotic cells, did not show any indication of increase (Fig. 6b, c).

Gene Expression Response of HCC cells to ATAD2 Is Highly Heterogeneous

Phenotypic heterogeneity of different HCC cell lines in their response to ATAD2 depletion warranted further investigation. Therefore, we decided to compare global gene expression profiles of three different HCC cell lines in the presence as well as under suppression of ATAD2 expression. We chose Hep3B (high response), PLC/PRF/5 (medium/no response) and SNU449 (medium/no response) cell lines and used Affymetrix microarray technology. All cell lines were analyzed after 48 h of ATAD2 siRNA treatment as compared to control siRNAs. Effective downregulation of ATAD2 levels by siRNAs were demonstrated by real-time PCR (Fig. 7).

Expression levels of RNAs were compared between ATAD2 siRNA- and control siRNA-treated cells, and genes displaying more than twofold changes were identified. As expected, ATAD2 mRNA levels decreased 11, 11, and fourfold in Hep3B, PLC/PRF/5 and SNU449 respectively. ATAD2 knock-down resulted in the downregulation for 57 genes, while 54 displayed upregulation in Hep3B. The number of affected genes was much lower in PLC/PRF/5 cells (9 up and 7 downregulated respectively, while it was nil in SNU449 cells (Table 2). In order to find out what gene functions are affected by these changes, GSEA was utilized using gene ontology (GO) terms. As shown in Table 3, 11 GO terms all related to three diverse functions, namely lipoprotein particle remodeling, positive regulation of Wnt signaling pathway and Receptor-mediated endocytosis were identified for PLC/PRF/5 cells ($p < 0.05$). Much higher number of gene functions were identified in Hep3B cells (33 GO terms with $p < 0.02$). These functions were highly heterogeneous and grouped into 17 gene functions. Top affected functions were response to calcium ions, metal ions, ketone, glucocorticoid and cAMP, positive regulation of protein kinase B signaling, negative regulation of blood coagulation, negative regulation of ion transport, zymogen activation, and apoptosis pathway (Table 3). There was no commonality between the GO terms identified in Hep3B and PLC/PRF/5 cells.

Table 1 Immunohistochemistry staining analysis of ATAD2 protein in normal liver, dysplastic nodules and HCC

Differentiation	Total	Positive	% positive
Normal liver	7	0	0.0
LGDN	9	0	0.0
HGDN	18	3	16.7
WD HCC	12	3	25.0
MD HCC	9	6	66.7
PD HCC	6	5	83.3

Discussion

We identified ATAD2 several years ago as a member of senescence-related 15-gene signature set providing high confidence prediction of HCC patients with 97.5% accuracy [9]. In the same report, we also showed that freshly isolated human hepatocytes lack detectable ATAD2 protein in contrast to nine different HCC cell lines all expressing it. Here we evaluated the value of ATAD2 as a disease biomarker and potential therapeutic target for HCC. Our observations clearly indicate that this protein is a good disease progression marker, but a conditional therapeutic target.

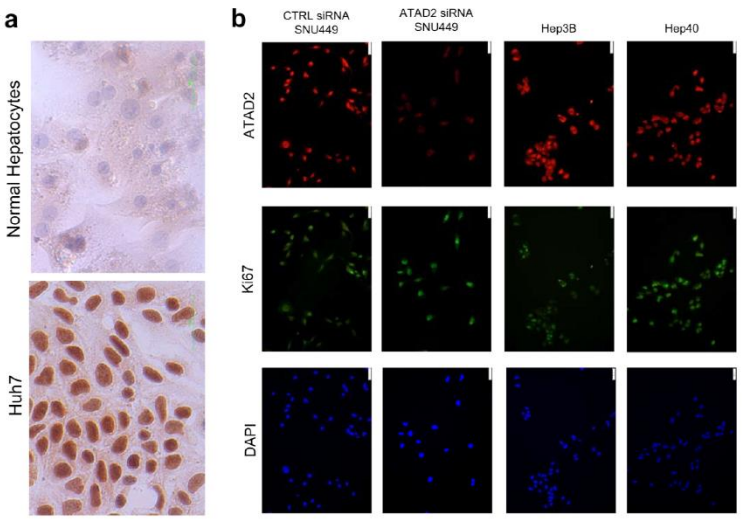

Fig. 2 ATAD2 is highly expressed in proliferating HCC cells, but not in non-proliferating hepatocytes. **a** Immunohistochemistry images show the absence of detectable ATAD2 protein in non-proliferating hepatocytes in contrast to Huh7 cells. **b** Immunofluorescence imaging of HCC cells indicating nuclear staining of ATAD2 mirroring Ki-67 staining

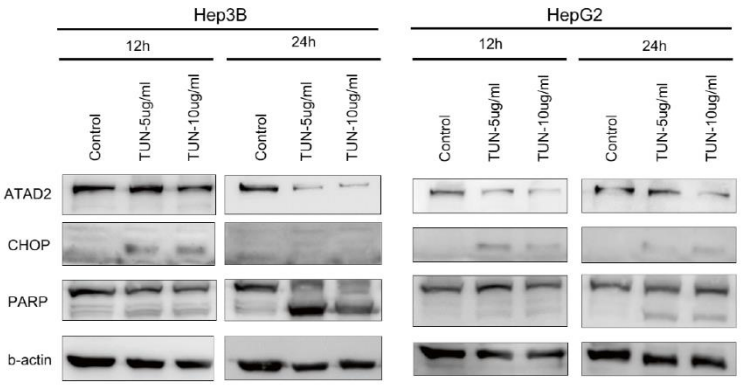

Fig. 3 Western blot analysis of Hep3B and HepG2 cells under UPR induced by tunicamycin treatment. Note the decreased expression of ATAD2 in late phase (24 h) coinciding with strong apoptosis in Hep3B cells. In contrast HepG2 cells responded to tunicamycin with less apoptosis but early (12 h) inhibition of ATAD2 expression

The value as a tumor marker was evaluated using a set of tissues representing normal liver, dysplastic nodules and well-, moderate-, and poorly differentiated HCCs. We observed almost a perfect correlation between ATAD2-positive staining cell numbers and disease progression. Accordingly, ATAD2 was not detected in LGDNs but was positive in 17% of HGDNs. This positivity progressively increased up to 83% in poorly differentiated HCCs. Our observations correlate with data reported previously [20–22]. Here we provide novel data showing that ATAD2 expression in normal liver and HCC is closely correlated with Ki-67 expression, a well-known biomarker used to evaluate proliferation index in tumors [23]. This led us to consider ATAD2 as a proliferation biomarker. Next, we tested whether *ATAD2* expression in liver is specific to malignancy. Thus, we analyzed the status of its expression following induction of liver regeneration by partial hepatectomy in rats. This analysis was done in parallel to *MKI-67* and *CCND1* expression. *ATAD2*, *MKI-67*, and *CCND1* RNA levels were low in the initial phase of the liver regeneration and all three showed strong induction between 24 and 36 h, followed by a gradual decrease until the end of proliferation process. The absence of *ATAD2* expression in normal liver together with its increased expression in regenerating rat liver, as well as in malignant liver lesions as a function of tumor progression is reminiscent of Ki67 expression in these situations. Indeed, Ki67 labelling index (LI) is less than 5% in normal liver and inactive cirrhosis, but higher in chronic hepatitis (LI: 29–41) and very high (LI: 71) in HCC [23]. In confirmation of our observations, MKI-67 expression during rat liver regeneration is induced and remained high for at least 4 days [24]. Ki-67 is a nuclear protein expressed in proliferating (G1, S, G2 and M phases) cells, but not in resting (G0 phase) cells including hepatocytes [25].

Our in vitro studies confirmed that ATAD2 is indeed a specific nuclear marker for proliferating cells like Ki-67. As shown in Fig. 2, normal hepatocytes did not express ATAD2, but all tested HCC cell lines displayed nearly 100% positive staining which paralleled Ki-67 staining. Indeed, ATAD2 immunostaining performs better than Ki-67 staining because of its homogenous nuclear staining pattern. The presence of nuclear ATAD2 in all proliferating cells despite its role in "co-chaperon" role in the organization of newly loaded histones during DNA synthesis [3] is not necessarily contradictory. Ki-67, a well-known marker for cells in proliferation (G1, S, G2, M phases) serves as a biological surfactant to disperse mitotic chromosomes during M phase [26].

Tunicamycin which causes extensive protein misfolding and activation of the unfolded protein response (UPR) is an ER-stress inducer [19, 27]. One of the cellular responses to UPR is to exit from the cell cycle by downregulation of Cyclin D1 levels [18]. Cyclin D1 degradation is also necessary for exit of hepatocytes from cell cycle and termination of liver regeneration [28]. HCC cell lines like many cancer cell lines display uncontrolled cell proliferation. In order to force HCC cell lines to exit cell cycle by UPR, we treated them with tunicamycin and tested ATAD2 protein levels. As shown in Fig. 3, following 12 h and 24 h treatment with tunicamycin, Hep3B cells displayed early accumulation of CHOP and strong induction of PARP cleavage, as well as downregulation of ATAD2 levels particularly at 24 h. This suggested that tunicamycin treatment caused a cell cycle arrest as well as apoptosis induction. The response of HepG2 cells was milder in terms of PARP cleavage but ATAD2 downregulation was evident at 12 h and strong at 24 h, suggesting minor apoptosis and more pronounced cell cycle exit. In support of our conclusion, we noticed that ATAD2 was one of the significantly downregulated genes in G0 as compared to G1 cells [29]. Taken together our observations supported by other reports are in favor of ATAD2 being a biomarker for a non-resting (non G0) state independent of cell cycle phases.

Next, we examined HCC cell response to *ATAD2* downregulation. Out of five HCC cell lines tested, only two displayed clear and objective survival response (Online Resource 3). Detailed phenotypic analysis of *ATAD2* knockdown effects in four representative cell lines clearly demonstrated that ATAD2 dependency is highly heterogeneous. Although a few HCC cell lines experience decreased survival and cell death, many others do not show any severe survival defect. Our compared global gene expression analysis also indicates extreme heterogeneity in response to ATAD2 deficiency. Cellular response varied between no detectable alterations in gene expression to more than 100 genes affected. Thus, our observations lead us to conclude that ATAD2 expression is not absolutely necessary for survival of HCC cell lines or its effects are dependent on other factors. In other words, the effects of ATAD2 deficiency appear unpredictable in the contexts we analyzed. In accordance with our previous studies we concluded that ATAD2 depletion related survival outcomes do not associate with metastatic (EMT) status of HCC cells, as well as mutations in p53 or Rb pathway. Two out of 4 epithelial cells (Hep3B and HepG2) responded to ATAD2 depletion but the other 2 epithelial lines (PLC/PRF/5 and Huh7) and SNU449, as the only EMT cell line in our panel, did not [30]. Among the responders HepG2 is p53wt, whereas Hep3B is p53 null. Also, all the cell lines used in this study, responders and non-responders, are Rb pathway deficient [31]. Therefore, additional studies are necessary to identify markers of response to ATAD2 depletion.

In support of this conclusion, ATAD2 has been qualified previously as a global "helper" which in growing cells can be compensated for by other factors [2]. When compared to previous reports on the effects of ATAD2 suppression on HCC cell lines, our observations correlate only partially. Indeed, similar

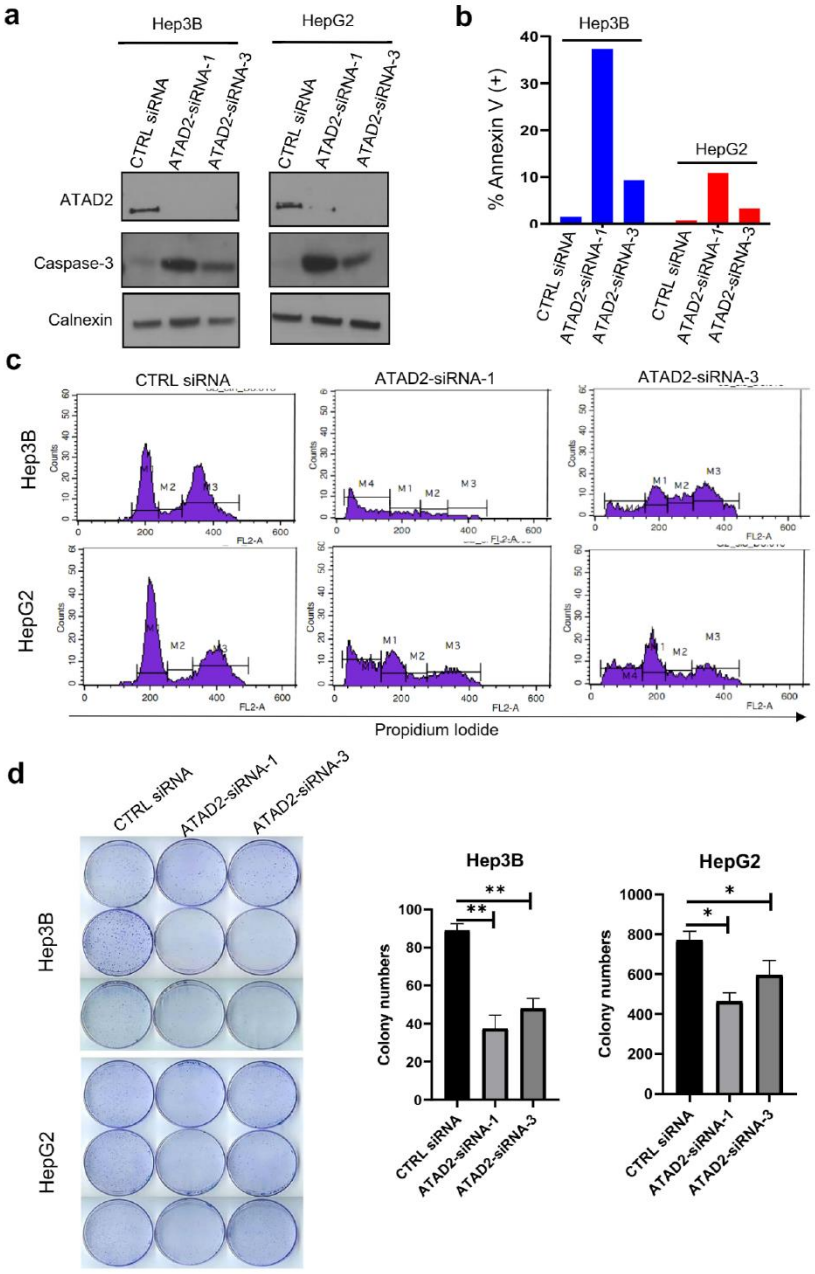
a
Hep3B
HepG2
CTRL siRNA
ATAD2-siRNA-1
ATAD2-siRNA-3
ATAD2
Caspase-3
Calnexin
b
Hep3B
HepG2
% Annexin V (+)
c
CTRL siRNA
ATAD2-siRNA-1
ATAD2-siRNA-3
Hep3B
HepG2
Counts
FL2-A
Propidium Iodide
d
Hep3B
HepG2
Colony numbers

◂**Fig. 4** Suppression of ATAD2 by siRNAs inhibits cell growth and induces apoptosis. **a** Western blot analysis of ATAD2 protein expression in Hep3B and HepG2 cell lines after transfection of control siRNA, ATAD2 siRNA1 and ATAD2 siRNA3 demonstrates ATAD2 knock-down accompanied by increased expression of active Caspase-3. **b** Annexin V FACS analysis of ATAD2-suppressed Hep3B and HepG2 cells at day 2 shows abundant apoptosis in Hep3B and less but evident apoptosis in HepG2 cells. **c** Cell cycle analysis by flow cytometry at day 3 following siRNA treatment showed strong perturbation of cell cycle phase distribution with increase in SubG1 cells. **d** ATAD2 siRNA-treated cells displayed significant decrease in colony formation ability as shown by Coomassie blue staining (left) and colony number counting (right). or control siRNA transfected Hep3B and HepG2 cell colonies

observations were reported for Hep3B and HepG2 cells [21, 32]. But we could not confirm earlier reports on ATAD2 dependency of Huh7 and PLC/PRF/5 cell lines [21, 32, 33]. The reasons of this discrepancy are not known. Cell lines used in these studies may have undergone drifts during their long-term maintenance between different laboratories. Alternatively, experimental conditions may have affected the phenotypic outcomes. Nevertheless, it is of interest that ATAD2-independent HCC cell survival has not been noticed in previous reports [21, 32, 33]. Here we show that ATAD2 is not a critical gene for the survival of many different HCC cell lines. These findings strongly suggest that this gene is not a preferable target for development of new targeted therapy approaches for HCC unless its function is further characterized. Indeed, as a gene associated with both normal and malignant cell proliferation, even if successful results can be achieved, such therapies might present undesirable side effects. Altogether, here we show that ATAD2 is an excellent proliferation marker for liver diseases including HCC. However, currently, it is not a preferable therapeutic target.

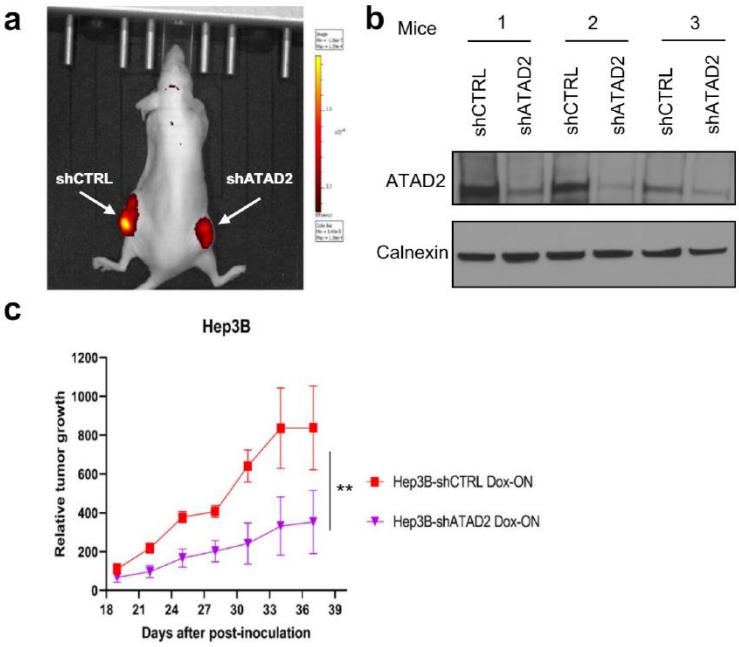

Fig. 5 ATAD2 knock-down by doxycycline-induced shRNA expression inhibits Hep3B tumor development in immunodeficient mice. **a** Representative in vivo image of tumors formed by control and ATAD2-deficient Hep3B cells in immunodeficient mice. Hep3B-derived RFP-expressing clones with Doxycycline-induced shATAD2 and shCTRL expression were inoculated into opposite sides of mice ($n=3$) and tumor formation in doxycycline-fed mice were followed up to 37 days. **b** Western blot analysis of ATAD2 protein levels in shCTRL- and shATAD2-expressing tumors demonstrating efficient inhibition of ATAD2. **c** Tumor growth curves of shCTRL and shATAD2 Hep3B cells based on doxycycline treatment that showed significant inhibition by ATAD2 knock-down ($p=0.0064$)

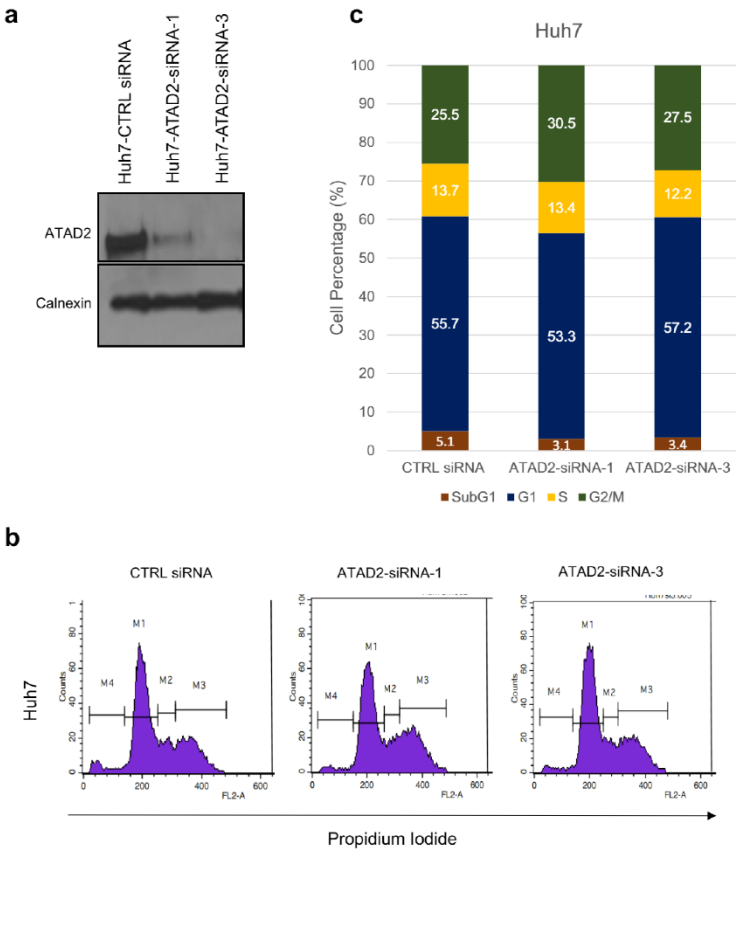

Fig. 6 Suppression of ATAD2 by siRNAs did not affect cell cycle distribution in Huh7 cell line. **a** Detection of ATAD2 protein expression in Huh7 cell line transfected with control siRNA, ATAD2 siRNA1 or ATAD2 siRNA3 at day 2 by Western blotting. **b** Cell cycle analysis with propidium iodide staining of control siRNA, ATAD2 siRNA1 and ATAD2 siRNA3 transfected Huh7 cell line at day 3. **c** Quantification of cells at different phases of cell cycle showing that there is no consistent change under ATAD2 silencing

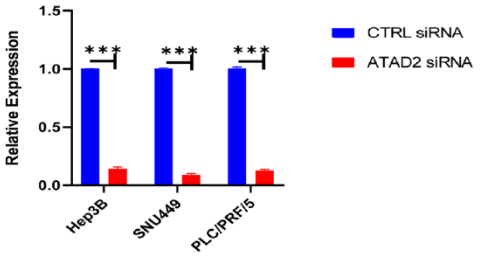

Fig. 7 Demonstration of ATAD2 knock-down by real-time PCR in Hep3B, SNU449, and PLC/PRF/5 prior to transcriptome analysis by microarray

Table 2 Distribution of genes affected by ATAD2 knockdown in different HCC cell lines

Cell	Up	Down	Total
Hep3B	54	57	111
PLC/PRF/5	9	7	16
SNU449	0	0	0

Table 3 Collapsed gene ontology functions affected by ATAD2 in two HCC cell lines*

GO term-based functions	GO terms
Hep3B (p Adj. < 0.02)	
Response to calcium ion	1
Response to metal ion	1
Pos. regulation of protein kinase B sig	3
Response to ketone	1
Neg. regulation of blood coagulation	11
Response to glucocorticoid	3
Neg. regulation of ion transport	1
Response to cAMP	1
Zymogen activation	1
Regulation of apoptotic signaling**	1
Regulation of response to wounding	1
Organic hydroxy compound transport	1
Reg. of heterotypic cell–cell adhesion	2
Glomerulus vasculature development	1
Kidney vasculature development	2
Pos. regulation of hormone secretion	1
Response to organophosphorus	1
PLC/PRF/5 (p adj. < 0.05)	
High-density lipoprotein particle remodeling	7
Pos. reg. of canonical Wnt signaling pw	4
Receptor-mediated endocytosis	1

*Full list of related GO terms where presented in Online Resource 4; **Regulation of extrinsic apoptotic signaling pathway via death domain receptors

Conclusions

In the study, the comparative analysis based on TCGA and immunochemistry strongly indicated that ATAD2 expression increases in HCC tumor samples. The expression of ATAD2 showed a strong correlation with Ki-67 expression in normal liver and HCC. At the cellular level, ATAD2 depletion showed decreased survival in some but not all of HCC cell lines, indicating ATAD2 is not a crucial gene for survival. In addition, comparative gene expression analysis in ATAD2 depleted HCC cell lines showed different types of cellular responses resulted in a cell line dependent manner. The randomness in cellular fate with ATAD2 depletion, and its correlative expression with proliferation markers in regenerating liver, shows ATAD2 needs further explorations as a proliferation biomarker or preferential therapeutic target in clinical use.

Supplementary Information The online version contains supplementary material available at https://doi.org/10.1007/s12029-021-00732-9.

Acknowledgements This work was part of PhD theses of H.Y. (Bilkent University, Ankara, Turkey). We would like to thank Izmir Biomedicine and Genome Center's core facilities especially Optical Imaging and IBG Bioinformatics Platform (IBG-BIP) for their support during data collection and analysis.

Author Contribution Study conception and design: MO; experiments: UE, HY, CO, OY, PK, and EB. Bioinformatics and statistical analyses: GK, HU, and UE; evaluation of the data: MO, NA, HA, FY, and PBK; drafting of the manuscript: MO and UE. All authors were involved in finalization of the manuscript and approved the submitted version.

Funding This study was supported by the funds from TUBITAK (109S191, 111T558), Turkish Academy of Sciences, Dokuz Eylul University, and İzmir Biomedicine and Genome Center.

Availability of Data and Material The contributions for the study are included in the article/Online Resources. Raw microarray data that support the findings of this study and further information are available upon request from corresponding author.

Declarations

Ethics Approval Study with clinical samples was approved by Ege University Ethics Committee. Animal experiments were approved by Bilkent University Animal Ethics Committee. (Decision No: 2006/1; Decision date: 10/5/2006).

Conflict of Interest The authors declare no competing interests.

References

1. Cattaneo M, Morozumi Y, Perazza D, Boussouar F, Jamshidikia M, Rousseaux S, Verdel A, Khochbin S. Lessons from yeast on emerging roles of the ATAD2 protein family in gene regulation and genome organization. Mol Cells. 2014;37:851–6. https://doi.org/10.14348/molcells.2014.0258.
2. Morozumi Y, Boussouar F, Tan M, Chaikuad A, Jamshidikia M, Colak G, He H, Nie L, Petosa C, De Dieuleveult M, et al. ATAD2 is a generalist facilitator of chromatin dynamics in embryonic stem cells. J Mol Cell Biol. 2016;8:349–62. https://doi.org/10.1093/jmcb/mjv060.
3. Koo SJ, Fernández-Montalván AE, Badock V, Ott CJ, Holton SJ, von Ahsen O, Toedling J, Vittori S, Bradner JE, Gorjánácz M. ATAD2 is an epigenetic reader of newly synthesized histone marks during DNA replication. Oncotarget. 2016;7:70323–35. https://doi.org/10.18632/oncotarget.11855.
4. Cho C, Jang J, Kang Y, Watanabe H, Uchihashi T, Kim SJ, Kato K, Lee JY, Song JJ. Structural basis of nucleosome assembly by the Abo1 AAA+ ATPase histone chaperone. Nat Commun. 2019;10:1–13. https://doi.org/10.1038/s41467-019-13743-9.
5. Shahnejat-Bushehri S, Ehrenhofer-Murray AE. The ATAD2/ANCCA homolog Yta7 cooperates with Scm3HJURP to deposit Cse4CENP-A at the centromere in yeast. Proc Natl Acad Sci U S A. 2020;117:5386–93. https://doi.org/10.1073/pnas.1917814117.
6. Zou JX, Revenko AS, Li LB, Gemo AT, Chen HW. ANCCA, an estrogen-regulated AAA+ ATPase coactivator for ERα, is required for coregulator occupancy and chromatin modification. Proc Natl Acad Sci U S A. 2007;104:18067–72. https://doi.org/10.1073/pnas.0705814104.
7. Ciró M, Prosperini E, Quarto M, Grazini U, Walfridsson J, McBlane F, Nucifero P, Pacchiana G, Capra M, Christensen J, et al. ATAD2 is a novel cofactor for MYC, overexpressed and amplified in aggressive tumors. Cancer Res. 2009;69:8491–8. https://doi.org/10.1158/0008-5472.CAN-09-2131.
8. Caron C, Lestrat C, Marsal S, Escoffier E, Curtet S, Virolle V, Barbry P, Debernardi A, Brambilla C, Brambilla E, et al.

Functional characterization of ATAD2 as a new cancer/testis factor and a predictor of poor prognosis in breast and lung cancers. Oncogene. 2010;29:5171–81. https://doi.org/10.1038/onc.2010.259.
9. Yildiz G, Arslan-Ergul A, Bagislar S, Konu O, Yuzugullu H, Gursoy-Yuzugullu O, Ozturk N, Ozen C, Ozdag H, Erdal E, Karademir S, et al. Genome-wide transcriptional reorganization associated with senescence-to-immortality switch during human hepatocellular carcinogenesis. PLoS One. 2013;8. https://doi.org/10.1371/journal.pone.0064016.
10. Hussain M, Zhou Y, Song Y, Hameed HMA, Jiang H, Tu Y, Zhang J. ATAD2 in cancer: a pharmacologically challenging but tractable target. Expert Opin Ther Targets. 2018;22:85–96. https://doi.org/10.1080/14728222.2018.1406921.
11. Yuzugullu H, Benhaj K, Ozturk N, Senturk S, Celik E, Toylu A, Tasdemir N, Yilmaz M, Erdal E, Akcali KC, et al. Canonical Wnt signaling is antagonized by noncanonical Wnt5a in hepatocellular carcinoma cells. Mol Cancer. 2009;8:90. https://doi.org/10.1186/1476-4598-8-90.
12. Torbenson MS, Ng IOL, Park YN, Roncalli M, Sakamoto M. Hepatocellular carcinoma. In: WHO Classification of Tumors Editorial Board. Digestive system tumours. WHO classification of tumours series. 5th ed. Lyon: Int Agen Res Cancer. 2019:229–39.
13. Goldman MJ, Craft B, Hastie M, Repečka K, McDade F, Kamath A, Banerjee A, Luo Y, Rogers D, Brooks AN, et al. Visualizing and interpreting cancer genomics data via the Xena platform. Nat Biotechnol. 2020;38:675–8. https://doi.org/10.1038/s41587-020-0546-8.
14. Gautier L, Cope L, Bolstad BM, Irizarry RA. Affy-analysis of Affymetrix GeneChip data at the probe level. Bioinformatics. 2004;20:307–15. https://doi.org/10.1093/bioinformatics/btg405.
15. Ritchie ME, Phipson B, Wu D, Hu Y, Law CW, Shi W, Smyth GK. Limma powers differential expression analyses for RNA-sequencing and microarray studies. Nucleic Acids Res. 2015;43:e47. https://doi.org/10.1093/nar/gkv007.
16. Yu G, Wang LG, Han Y, He QY. ClusterProfiler: an R package for comparing biological themes among gene clusters. Omi A J Integr Biol. 2012;16:284–7. https://doi.org/10.1089/omi.2011.0118.
17. Edgar R, Domrachev M, Lash AE. Gene Expression Omnibus: NCBI gene expression and hybridization array data repository. Nucleic Acids Res. 2002;30:207–10. https://doi.org/10.1093/nar/30.1.207.
18. Brewer JW, Hendershot LM, Sherr CJ, Diehl JA. Mammalian unfolded protein response inhibits cyclin D1 translation and cell-cycle progression. Proc Natl Acad Sci U S A. 1999;96:8505–10. https://doi.org/10.1073/pnas.96.15.8505.
19. Banerjee A, Lang JY, Hung MC, Sengupta K, Banerjee SK, Baksi K, Banerjee DK. Unfolded protein response is required in nu/nu mice microvasculature for treating breast tumor with tunicamycin. J Biol Chem. 2011;286:29127–38. https://doi.org/10.1074/jbc.M110.169771.
20. Yang J, Huang J, Luo L, Chen Z, Guo Y, Guo L. Significance of PRO2000/ANCCA expression, a novel proliferation-associated protein in hepatocellular carcinoma. Cancer Cell Int. 2014;14:1–7. https://doi.org/10.1186/1475-2867-14-33.
21. Huang J, Yang J, Lei Y, Gao H, Wei T, Luo L, Zhang F, Chen H, Zeng Q, Guo L. An ANCCA/PRO2000-miR-520a-E2F2 regulatory loop as a driving force for the development of hepatocellular carcinoma. Oncogenesis. 2016;5:e229. https://doi.org/10.1038/oncsis.2016.22.
22. Hwang HW, Ha SY, Bang H, Park CK. ATAD2 as a poor prognostic marker for hepatocellular carcinoma after curative resection. Cancer Res Treat. 2015;47:853–61. https://doi.org/10.4143/crt.2014.177.
23. Kaita KDE, Pettigrew N, Minuk GY. Hepatic regeneration in humans with various liver disease as assessed by Ki-67 staining of formalin-fixed paraffin-embedded liver tissue. Liver. 1997;17:13–6. https://doi.org/10.1111/j.1600-0676.1997.tb00772.x.
24. Gerlach C, Sakkab DY, Scholzen T, Daßler R, Alison MR, Gerdes J. Ki-67 expression during rat liver regeneration after partial hepatectomy. Hepatology. 1997;26:573–8. https://doi.org/10.1053/jhep.1997.v26.pm0009303485.
25. Gerdes J, Schwab U, Lemke H, Stein H. Production of a mouse monoclonal antibody reactive with a human nuclear antigen associated with cell proliferation. Int J Cancer. 1983;31:13–20. https://doi.org/10.1002/ijc.2910310104.
26. Cuylen S, Blaukopf C, Politi AZ, Muller-Reichert T, Neumann B, Poser I, Ellenberg J, Hyman AA, Gerlich DW. Ki-67 acts as a biological surfactant to disperse mitotic chromosomes. Nature. 2016;535:308–12. https://doi.org/10.1038/nature18610.
27. Bassik MC, Kampmann M. Knocking out the door to tunicamycin entry. Proc Natl Acad Sci U S A. 2011;108:11731–2. https://doi.org/10.1073/pnas.1109035108.
28. Lai S-S, Zhao D-D, Cao P, Lu K, Luo O-Y, Chen W-B, Liu J, Jiang E-Z, Yu Z-H, Lee G, et al. PP2Acα positively regulates the termination of liver regeneration in mice through the AKT/GSK3β/Cyclin D1 pathway. J Hepatol. 2016;64:352–60. https://doi.org/10.1016/j.jhep.2015.09.025.
29. Oki T, Nishimura K, Kitaura J, Togami K, Maehara A, Izawa K, Sakaue-Sawano A, Niida A, Miyano S, Aburatani H, Kiyonari H, et al. A novel cell-cycle-indicator, mVenus-p27K -, identifies quiescent cells and visualizes G0-G1 transition. Sci Rep. 2014;4. https://doi.org/10.1038/srep04012.
30. Sreekumar R, Emaduddin M, Al-Saihati H, Moutasim K, Chan J, Spampinato M, Bhome R, Yuen HM, Mescoli C, Vitale A, Cillo U, et al. Protein kinase C inhibitors override ZEB1-induced chemoresistance in HCC. Cell Death Dis. 2019;10. https://doi.org/10.1038/s41419-019-1885-6.
31. Sayan AE, Sayan BS, Findikli N, Ozturk M. Acquired expression of transcriptionally active p73 in hepatocellular carcinoma cells. Oncogene. 2001;20:5111–7. https://doi.org/10.1038/sj.onc.1204669.
32. Lu WJ, Chua MS, So SK. Suppression of ATAD2 inhibits hepatocellular carcinoma progression through activation of p53-and p38-mediated apoptotic signaling. Oncotarget. 2015;6:41722–35. https://doi.org/10.18632/oncotarget.6152.
33. Wu G, Liu H, He H, Wang Y, Lu X, Yu Y, Xia S, Meng X, Liu Y. MiR-372 down-regulates the oncogene ATAD2 to influence hepatocellular carcinoma proliferation and metastasis. BMC Cancer. 2014;14:1–11. https://doi.org/10.1186/1471-2407-14-107.

8.3 Curriculum Vitae in ARBIS format

UMUT EKİN

Personal Information

Contact Information

Contact Address	[redacted]
Telephone	[redacted]
Email	[redacted]
Web Page	

Education Information

01 March 2017 - Now (5 Year)
Doktora, Doktora, DOKUZ EYLÜL ÜNİVERSİTESİ, TÜRKİYE
İZMİR ULUSLARARASI BİYOTIP VE GENOM ENSTİTÜSÜ, MOLEKÜLER BİYOLOJİ VE GENETİK (DR) (İNGİLİZCE)
Cumulative Grade Point Average: 3.72 / 4.0

02 September 2010 - 04 September 2013 (3 Year 1 Month)
Yüksek Lisans, Tezli Program, İZMİR YÜKSEK TEKNOLOJİ ENSTİTÜSÜ, TÜRKİYE
MÜHENDİSLİK VE FEN BİLİMLERİ ENSTİTÜSÜ, MOLEKÜLER BİYOLOJİ VE GENETİK (YL) (TEZLİ)
Diploma Number: LU1334
Cumulative Grade Point Average: 3.25 / 4.0

06 September 2004 - 20 July 2010 (5 Year 11 Month)
Lisans, Anadal/Normal Öğretim, İZMİR YÜKSEK TEKNOLOJİ ENSTİTÜSÜ, TÜRKİYE
FEN FAKÜLTESİ, MOLEKÜLER BİYOLOJİ VE GENETİK PR. (İNGİLİZCE)
Diploma Number: 1391
Cumulative Grade Point Average: 2.41 / 4.0

Foreign Language Information

İNGİLİZCE (Reading: İyi, Writing: İyi, Speaking: İyi)

Scientific Technological Activity Fields

Scientific Technological Activity Field Information

Temel Bilimler -- Yaşam Bilimleri -- Moleküler Biyoloji ve Genetik -- Kanser Moleküler Biyoloj si

Temel Bilimler -- Yaşam Bilimleri -- Moleküler Biyoloji ve Genetik -- Genetik Mühendisliği

Temel Bilimler -- Yaşam Bilimleri -- Biyoteknoloji -- Endüstriyel Biyoteknoloji

Keywords

Karaciğer Kanseri

Hepatoselüler Karsinoma

Kanser Genetiği

Moleküler Klonlama

Gen Transfeksiyonu

Hücre Kültürü Teknikleri

Biyobenzer

Antikor Üretimi

R&D Competency

Articles

E. ISCAN, G. KARAKULAH, U. EKİN, M. OZTURK, H. UZUNER & A. SUNER, TAp73 alpha is Upregulated in the Most Common Human Cancers, MOLECULAR BIOLOGY, 2022, 0026-8933.

U. EKİN, H. YUZUGULLU, C. OZEN, P. KORHAN, E. BAGİRSAKCİ, F. YİLMAZ, O. G. YUZUGULLU, H. UZUNER, H. ALOTAİBİ, P. B. KİRMİZİBAYRAK, N. ATABEY, G. KARAKULAH & M. OZTURK, Evaluation of ATAD2 as a Potential Target in Hepatocellular Carcinoma, JOURNAL OF GASTROINTESTINAL CANCER, 2021, 1941-6628.

E. ISCAN, U. EKİN, G. YİLDİZ, O. OZ, U. KELES, A. SUNER, G. CAKAN-AKDOGAN, G. OZHAN, M. NEKULOVA, B. VOJTESEK, H. UZUNER, G. KARAKULAH, H. ALOTAİBİ & M. OZTURK, TAp73 beta Can Promote Hepatocellular Carcinoma Dedifferentiation, CANCERS, 2021, 2072-6694, 13, 4.

U. KELES, E. ISCAN, H. E. YİLMAZ, G. KARAKULAH, A. SUNER, E. BAL, N. TASDEMİR, A. D. CAVGA, U. EKİN, Z. MUTLU, S. KAHYAOGLU, M. A. SERDAR, N. ATABEY & M. OZTURK, Differential expression of full-length and NH2 terminally truncated FAM134B isoforms in normal physiology and cancer, AMERICAN JOURNAL OF PHYSIOLOGY-GASTROINTESTINAL AND LIVER PHYSIOLOGY, 2020, 0193-1857, 319, 6, G733-G747.

M. OZTURK, T. BATUR, U. EKİN, A. ERDOGAN, E. ISCAN, U. KELES, O. OZ & C. OZEN, Molecular Pathogenesis of Liver Cancer, JOURNAL OF GASTROINTESTINAL CANCER, 2017, 1941-6628, 48, 3, 222-224.

S. FERROUDJ, G. YİLDİZ, M. BOURAS, E. ISCAN, U. EKİN & M. OZTURK, Role of Fanconi anemia/BRCA pathway genes in hepatocellular carcinoma chemoresistance, HEPATOLOGY RESEARCH, 2016, 1386-6346, 46, 12, 1264-1274.

Conference Papers

G. Y. A. S. G. K. M. Ö. UMUT EKİN, HEPATOSELÜLER KARSİNOMADA ADGRD1 GENİNİN OLASI İLAÇ HEDEFİ OLARAK BELİRLENMESİ, Sözlü Sunum, ONKOLOJİDE İZ BIRAKANLAR ZİRVESİ 2019, 14 November 2019, 17 November 2019.

G. Y. M. Ö. UMUT EKİN, HEPATOSELÜLER KARSİNOMADA ADGRD1'İN OLASI İLAÇ HEDEFİ OLARAK IN-SLICO YÖNTEMLE BELİRLENMESİ, Sözlü Sunum, 3. Çukurova Hepatoselüler Karsinoma Kongresi, 21 February 2019, 23 February 2019.

Projects

1007 - KAMU, BURSİYER, Kanser Ve Osteoporoz Tedavisi İçin Monoklonal Antikor Etkin Maddeli Biyobenzer İlaç Geliştirilmesi Ve Üretilmesi, Enforcing Institution: İZMİR BİYOTIP VE GENOM MERKEZİ (Still continues) .

YUNAN, BURSİYER, p73 ve mikroRNA Hedeflerinin Karaciğer Kanserinin Kemosensibilitesindeki Rolü, Enforcing Institution: İZMİR BİYOTIP VE GENOM MERKEZİ, 01 February 2014, 01 February 2016.

TÜBİTAK Scholarships and Fundings

Project Info

1135389, p73 ve mikroRNA Hedeflerinin Karaciğer Kanserinin Kemosensibilitesindeki Rolü, Uluslararası, Burslu, Sonuçlandı, ARDEB, SBAG - Sağlık Bilimleri Araştırma Destek Grubu, Project Participation/Leave Dates: 2/14/14 - 2/1/16, Project Start/End Dates: 2/1/14 - 2/1/16.
115G073, Kanser Ve Osteoporoz Tedavisi İçin Monoklonal Antikor Etkin Maddeli Biyobenzer İlaç Geliştirilmesi Ve Üretilmesi, 1007 - Kamu, Burslu, Yürürlükte, ARDEB, KAMAG - Kamu Araştırmaları Destek Grubu, Project Participation/Leave Dates: 1/6/17 - 4/30/18, Project Start/End Dates: 11/15/16 - 1/1/22.

Number of Panelist/Observer/Reporter Jobs

Refereeing/Panelist/Outer Consultant Count	ARDEB/BİDEB 0	TEYDEB 0	Total 0
Number of Observer/Consultant Jobs	ARDEB/BİDEB 0	TEYDEB 0	Total 0
Number of Reporter Jobs	ARDEB/BİDEB 0	TEYDEB 0	Total 0